Multireference Approaches for Excited States of Molecules

Hans Lischka, Dana Nachtigallova, Adélia J A Aquino, Peter G. Szalay, Felix Plasser, Francisco B C Machado, Mario Barbatti

Multireference Approaches for Excited States of Molecules †

Hans Lischka[a,b,c]*, Dana Nachtigallová[d,e], Adélia J. A. Aquino[a,b,f], Péter G. Szalay[g],

Felix Plasser[c,h], Francisco B. C. Machado[i], Mario Barbatti[h]

[a]*School of Pharmaceutical Sciences and Technology, Tianjin University, Tianjin 300072, P.R. China*

[b]*Department of Chemistry and Biochemistry, Texas Tech University, Lubbock, Texas 79409, United States*

[c]*Institute of Theoretical Chemistry, Faculty of Chemistry, University of Vienna, Währinger Straße 17, 1090 Vienna, Austria*

ORCID: 0000-0002-5656-3975

[d]*Institute of Organic Chemistry and Biochemistry v.v.i., The Czech Academy of Sciences, Flemingovo nám. 2, 160610 Prague 6, Czech Republic*

[e]*Regional Centre of Advanced Technologies and Materials, Palacký University, 77146 Olomouc, Czech Republic*

ORCID: 0000-0002-9588-8625

[f]*Institute for Soil Research, University of Natural Resources and Life Sciences Vienna, Peter-Jordan-Strasse 82, A-1190 Vienna, Austria*

ORCID: 0000-0003-4891-6512

[g]*ELTE Eötvös Loránd University, Laboratory of Theoretical Chemistry, Pázmány Péter sétány 1/A, 1117 Budapest, Hungary*

ORCID: 0000-0003-1885-3557

[h]*Department of Chemistry, Loughborough University, LE11 3TU, United Kingdom*

ORCID: 0000-0003-0751-148X

[i]*Departamento de Química, Instituto Tecnológico de Aeronáutica, São José dos Campos 12228-900, São Paulo, Brazil*

ORCID: 0000-0002-2064-3463

[h]*Aix Marseille Univ, CNRS, ICR, Marseille, France*

ORCID: 0000-0001-9336-6607; ResearchID: F-5647-2014

† Cite this paper as: Lischka, H.; Nachtigallová, D.; Aquino, A. J. A.; Szalay, P. G.; Plasser, F.; Machado, F. B. C.; Barbatti, M. Multireference Approaches for Excited States of Molecules. *Chem. Rev.* **2018**, DOI: 10.1021/acs.chemrev.8b00244. This document is the unedited Author's version of a Submitted Work that was subsequently accepted for publication in Chemical Reviews, copyright © American Chemical Society after peer review. To access the final edited and published work see dx.doi.org/10.1021/acs.chemrev.8b00244
* Corresponding author: hans.lischka@univie.ac.at

ABSTRACT

Obtaining an understanding of the properties of electronically excited states is a challenging task that becomes increasingly important for numerous applications in Chemistry, Molecular Physics, Molecular Biology, and Materials Science. A substantial impact is exerted by the fascinating progress in time-resolved spectroscopy, which leads to a strongly growing demand for theoretical methods to describe the characteristic features of excited states accurately. Whereas for electronic ground state problems of stable molecules the quantum chemical methodology is now so well developed that informed non-experts can use it efficiently, the situation is entirely different concerning the investigation of excited states. This review is devoted to a specific class of approaches, usually denoted as multireference (MR) methods, the generality of which is needed for solving many spectroscopic or photodynamical problems. However, the understanding and proper application of these MR methods is often found to be difficult due to their complexity and their computational cost. The purpose of this review is to provide an overview of the most important facts about the different theoretical approaches available and to present by means of a collection of characteristic examples useful information, which can guide the reader in performing their own applications.

1. Introduction

The knowledge and understanding of the behavior of molecules in excited states is an intriguing challenge both for experimentalists and theoreticians who want to predict spectroscopic and photodynamical properties that can lead, depending on the situation, to quite different outcomes than for the ground state. Photoinduced molecular processes play a prominent role in many scientific and technological areas of biology, physics, and chemistry, such as photostability of DNA,[1] photosynthesis and light-harvesting,[2] photocatalysis,[3] organic photovoltaics, and photodevices.[4] The experimental methods used include conventional, stationary spectroscopy[5] and, as an attractive extension, time-resolved spectroscopy.[6] The fascination of observing so many different facets of electronic properties is derived from the fact that actually two types of processes are involved, a usually fast electronic motion and a slower nuclear motion, which may, however, become strongly coupled in case of potential energy surfaces (PES) approaching each other energetically.

The Born-Oppenheimer approximation,[7,8] one of the major foundations of our understanding of molecules, in conjunction with the Franck-Condon approximation, forms the fundament for the calculation of electronic spectra,[9–11] allowing the separate investigation of different electronic states. In ground-state calculations, a vast selection of methods and extensive experience is available for choosing appropriate procedures, depending on the size of the molecules to be investigated and the accuracy to be achieved. The situation is not as straightforward, though, for the calculation of electronically excited states. Within the range of the Franck-Condon excitations, i.e., starting from a region on the PES close to the ground state minimum, computational methods can still rely in many cases on the validity of the closed shell Hartree-Fock method as a good starting point; and high accuracy can be obtained in calculations

at least of the lowest excited states. But even in these cases, strong variations in the character of the electronic states, whether they are valence or Rydberg states, or whether they have local, delocalized or charge transfer character, are encountered. These questions have considerable influence on the choice of the appropriate computational method and basis set used. The situation will become even more involved when the model of single excitations breaks down.

The just-discussed range of states characterized as single excitations in the Franck-Condon region constitutes a key area of electronic excitations in the ultraviolet (UV) and visible region of the electromagnetic spectrum. As already mentioned, these methods rely mostly on the dominance of a single reference (SR) configuration (closed shell Hartree-Fock) used as reference in the ground state for considering electronic excitation and electron correlation processes. In the simplest case, this classification leads to the method of configuration interaction with single excitations (CIS),[12] but will extend to the highly accurate equation of motion coupled cluster theory (EOM-CC),[13–15] and to time-dependent density functional theory (TDDFT).[16,17] Nevertheless, in spite of the great success of these approaches, they will not be able to cover the whole range of excited states.

The framework of multireference (MR) theory aims at a generalization of the construction of the electronic wavefunction beyond the SR case. In principle, the concept is simple and consists of two steps: (i) the MR character is taken into account by considering a set of configurations as references, and (ii) orbital excitations from those references are constructed to improve the flexibility of the wavefunction. The first step aims primarily at the resolution of quasi-degeneracies regarding orbitals and strongly coupled configuration (usually termed nondynamic, static or strong electron correlation) and the second step is meant to include the remaining electron correlation as is done in the SR case (dynamic electron correlation). This procedure - dating back to early work of Shavitt[18,19] and Buenker and Peyerimhoff[20,21] - has been continuously improved over the time,

resulting in impressive progress in computational methods based on variational techniques, leading to MR configuration interaction (MRCI). For a comprehensive review of MRCI theory see, e.g., Ref.[22] Three major variants of MRCI in the form of uncontracted (*uc*),[23] internally contracted (*ic*),[24–26] and selected MRCI[27] will be discussed below. Truncation of the orbital excitation level, which has to be introduced for practical reasons, leads to size-extensivity errors (for definition and discussion see Sec. 2.1.3).[28,29] It can be corrected *a-posteriori* using several versions of the Davidson correction[22,30,31] or, preferentially, in an internally consistent way, by means of the variational MR averaged coupled pair functional (MR-ACPF)[32] and MR averaged quadratic coupled cluster (MR-AQCC)[33,34] methods.

MRCI methods are, of course, not the only class of methods available for computing excited states in a general way. MR coupled cluster (MRCC) methods form another important theoretical framework for accurate quantum chemical calculations. In this review, the current status of different approaches will be described. As one of the most powerful approaches for computing excited states nowadays, MR perturbation theory has proven to be at the forefront of the methods of choice. The second-order complete active space (CAS) perturbation theory (CASPT2)[35–38] and many other MRPT approaches[39,40] derive their vast popularity from a successful balance of computational efficiency and good accuracy, which makes them attractive candidates especially to the calculation of exited states of large molecular systems. In the attempt of reducing the large computational effort required in MRCI calculations, semiempirical Hamiltonians have been introduced which alleviate the computational burden considerably and are being used successfully in many challenging photodynamical simulations. MR DFT is another approach which has been developed into different directions and will be discussed extensively here. Not the least, a number of interesting new algorithms have been developed in recent years,

among them the density matrix renormalization group (DMRG) method and full configuration interaction quantum Monte Carlo (FCIQMC), for which we want to describe the current status of this rapidly evolving field.

The discussion of excited states would not be complete if it was not extended beyond the Franck-Condon region. This leads to the broader topic of photoinduced processes,[41] nonadiabatic photodynamics,[42] and nonadiabatic interactions.[43,44] Most critical is the computation of intersections with the ground state since, in this case, strong mixing between different configurations will occur for both states involved, which will prohibit the use of SR calculations or at least make them more problematic. MR methods provide especially in this case, but also for the description of entire excited-states surfaces, the appropriate tools.

Because of the broad topic of the review, it will not be possible to cover all relevant methods and the large range of applications in detail. An overview covering single- and multireference methods until the year 2005 by Serrano-Andrés and Merchán can be found in Ref.[45] Single reference methods have been reviewed by Dreuw and Head-Gordon,[46] EOM-CC methods by Bartlett,[14] and the spin-flip equation-of-motion coupled cluster method has been summarized by Krylov.[47] The plan of this review is to describe in its first part the main features of the most important MR methods relevant in the present context and to provide in the second part by means of representative classes of applications insight into the potential of these methods in terms of their accuracy and predictive capabilities.

2. Theory and Methods

2.1. Configuration Interaction

2.1.1. Basic concepts

The most straightforward general version of variational methods for computing approximate solutions for the Schrödinger equation is the configuration interaction (CI) method in which the wavefunction Ψ^I of an electronic state I is written as a linear expansion of a set of many-electron basis functions $\left|\Phi_j\right\rangle$, $j = 1 \ldots N_{\mathrm{CI}}$

$$\left|\Psi^I\right\rangle = \sum_{j=1}^{N_{\mathrm{CI}}} c_j^I \left|\Phi_j\right\rangle . \tag{1}$$

The many-electron functions Φ_j are constructed from molecular orbitals (MOs) either by means of individual determinants or as configuration state functions (CSFs). The latter are eigenfunctions of the spin operators $\hat{S}^2$ and $\hat{S}_z$ by construction. The MOs must be computed before performing a CI calculation, either through an SCF or MCSCF calculation or by any other appropriate method (see below, Section 2.2).

Eq. (1) is used as a trial function to define the expectation value

$$E^I = \frac{\left\langle \Psi^I \left| \hat{H} \right| \Psi^I \right\rangle}{\left\langle \Psi^I \middle| \Psi^I \right\rangle} \tag{2}$$

$\hat{H}$ is here the clamped nucleus nonrelativistic electronic Hamiltonian operator

$$\hat{H} = -\frac{1}{2}\sum_l \nabla_l^2 - \sum_{l,A} \frac{Z_A}{r_{lA}} + \sum_{l>m} \frac{1}{r_{lm}} \tag{3}$$

written in atomic units as the sum of the electron kinetic energy, the electron-nuclear attraction, and the electron-electron repulsion. The indices l and m number the electrons and the index A labels the nuclei. The constant nuclear-nuclear repulsion term can be added if needed. The CI

energies E^I and the expansion coefficients c_j^I are determined from the stationarity condition of Eq. (2), which leads to the standard matrix eigenvalue equation

$$\mathbf{H}\mathbf{c}^I = E^I\mathbf{c}^I \tag{4}$$

where the matrix elements of **H** are given by $H_{jk} = \left\langle \Phi_j \middle| \hat{H} \middle| \Phi_k \right\rangle$ and $\mathbf{c}^I$ collects the CI coefficients c_j^I for state I in a column vector. Several electronic states can be computed by finding the respective roots of **H**. For more information on the basics of the CI method, see Refs.[18,22,48]. If all configurations are included in the CI expansion, then this procedure is called a Full-CI (FCI), which corresponds to the exact solutions of the Schrödinger equation in a given orbital basis. Extrapolation of the FCI results to the complete orbital set will lead to the complete CI limit. In an attempt to exploit these systematic properties of CI, one should not forget the dramatic increase of the size of the FCI of approximately n^N for n orbitals and N electrons. Thus, FCI (and even more so complete CI) limits can be reached only in rather exceptional cases for small molecules.

2.1.2. Single- and Multireference Spaces

In the development of practical approaches to construct configuration spaces, the concepts of a reference space and reference configurations play a crucial role. In the simplest case, one can choose a Hartree-Fock (HF) determinant as a single reference (SR). In Figure 1 the orbital and excitation schemes are shown for the case of a closed shell singlet. This scheme shows electron excitations from the reference doubly-occupied orbitals into the space of virtual orbitals. Frozen core orbitals are not involved at all and remain doubly occupied all the time.

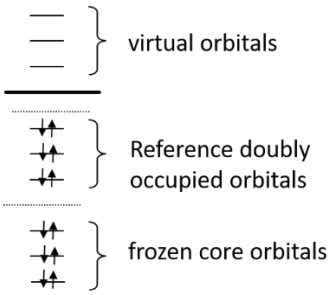

Figure 1. Orbital scheme used for the construction of SR wavefunctions.

According to this scheme, the configuration space $\left\{\left|\Phi_j\right\rangle\right\}$ is composed of the HF determinant Φ_0 itself plus configurations that are created by hierarchies of excitations from occupied to virtual orbitals:

$$\left\{\left|\Phi_j\right\rangle, j=1\ldots N_{\mathrm{CI}}\right\}=\left\{\left|\Phi_0\right\rangle,\left|\Phi_i^a\right\rangle,\left|\Phi_{ij}^{ab}\right\rangle,\left|\Phi_{ijk}^{abc}\right\rangle,\ldots\right\} \tag{5}$$

$\left|\Phi_i^a\right\rangle$ denotes a single (S) excitation from an occupied orbital *i* to a virtual orbital *a*, $\left|\Phi_{ij}^{ab}\right\rangle$ stands for a double (D) excitation from occupied orbitals *i*,*j* to virtual orbitals *a*,*b*; triple (T) and higher excitations follow in Eq. (5). Thus, dropping the state index *I* for convenience here, the wavefunction defined in Eq. (1) will be expanded as

$$\left|\Psi\right\rangle=c_0\left|\psi_0\right\rangle+\sum_{i,a}c_i^a\left|\Phi_i^a\right\rangle+\sum_{i>j,a>b}c_{ij}^{ab}\left|\Phi_{ij}^{ab}\right\rangle+\sum_{i>j>k,a>b>c}c_{ijk}^{abc}\left|\Phi_{ijk}^{abc}\right\rangle+\ldots \tag{6}$$

Truncation of the expansion space on the excitation level leads to SR-CIS, SR-CISD, SR-CISDT, etc. The label SR is usually omitted when the character of single reference is evident. CIS is the simplest case in the expansion, followed by CISD. Considering full triples (CISDT) will lead in most cases to computationally expensive calculations and is not routinely done. It should be noted that in the SR case, the linear CI expansion has been replaced mostly by the exponential expansion

of coupled cluster (CC) theory[49] because of the need to consider size-extensivity effects (see 2.1.3) properly. Only the CIS approach is in still in use, mostly for calculations on excited states.

The validity of the SR approach depends on the assumption that the HF determinant is a good starting point or, in other words, that C_0 dominates in the expansion of Eq. (6). For a discussion on this point in the case of increasingly larger systems see Ref.[50] and the analysis of NO occupations and unpaired electrons of Eq. (52). The dominance of one configuration will certainly not be found for bond breaking processes or the description of many excited states, especially if the nuclear coordinates are moved away from the Franck-Condon region. In these cases, one single configuration cannot be defined since several quasi-degenerate orbitals will have open-shell character with similar non-integer occupations. For such situations, the MRCI and related methods have been developed, providing a flexible tool for constructing different classes of wavefunctions. To take into account quasi-degeneracies, a set of reference configurations $\left\{\left|\Phi_m;\mathrm{ref}\right\rangle, m=1\ldots N_{\mathrm{ref}}\right\}$ is defined. It is chosen such that it contains all terms that are considered as important to describe the main characteristics of the wavefunction, especially regarding quasi-degeneracies. Figure 2 shows an orbital and electron excitation scheme which is extended by a set of active orbitals in comparison to the SR case. The active space is set up such that it allows the construction of more than one reference configuration. A great variety of choices for the reference space are in use. If all possible configurations within the active space are included, this space is termed complete active space (CAS).[51] This space is straightforward but can be computationally expensive because of its factorial increase with the number of orbitals. Less expensive alternatives will be discussed in the sections 2.1.6, 2.1.8 and 2.2. The doubly occupied and active orbitals taken together are called internal orbitals and the corresponding space internal space.

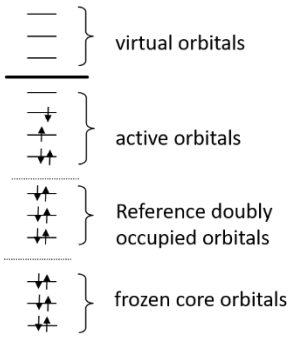

Figure 2. Orbital scheme used for the construction of MR wavefunctions.

The expansion space of the MRCI wavefunction is constructed by orbital excitation for each member of the reference set $|\Phi_m;\mathrm{ref}\rangle$ individually. The union of all the configurations created in this way up to a certain excitation limit constitutes the MRCI expansion space. For practical reasons, excitations up to doubles only are considered in all practical cases; the respective expansion is then denoted MR-CISD. It can be written in the following general form:[52]

$$|\Psi_{\mathrm{MRCI}}\rangle = \sum_I c_I |\Phi_I\rangle + \sum_{S,a} c_S^a |\Phi_S^a\rangle + \sum_{D,a,b} c_D^{ab} |\Phi_D^{ab}\rangle + \ldots \qquad (7)$$

where the functions $|\Phi_I\rangle$ represent internal configurations (all *N* electrons in the internal space), the $|\Phi_S^a\rangle$'*s* comprise single excitations with *N*-1 electrons in the internal space and the $|\Phi_D^{ab}\rangle$ configurations describe double excitations into the virtual space (assuming appropriate spin coupling in all cases).

In some cases, an excitation from one reference function leads to the same final configuration as a different excitation from another reference function. This situation will lead to linear dependencies in the expansion space, which must be removed. As an alternative, these redundancies can be avoided by using an occupation-based approach, scanning through a unique list of configurations created, e.g., by means of the Unitary Group Approach[53] or using the

Symmetric Group.[54] A possible configuration either conforms with or violates the chosen occupation restrictions, which determines its acceptance or rejection.

The MRCI expansion is usually truncated to single and double excitations (singles and doubles) resulting in the MRCISD approach. The construction of the MRCI wavefunction by performing excitations from each of the N_{ref} reference configurations individually leads to a procedure that is called "uncontracted" (*uc*-MRCI)[22,55] as opposed to the "internally contracted" MRCI (ic-MRCI),[24–26] which will be introduced further below (Section 2.1.4). In this review, the denomination MRCI will be used for an uncontracted approach. The labels *uc* and *ic* will be used only in case the distinction is needed.

The solution of the CI eigenvalue problem is usually performed iteratively by means of the Davidson subspace method,[56] which is based on computing the matrix-vector product **Hx** of the Hamiltonian matrix **H** and an arbitrary expansion vector **x**. For an extended discussion of the Davidson method, including improvement suggested by Olsen et al.,[57] see Ref.[22]. This procedure can be profitably combined with the idea of a direct CI,[58] where **Hx** is computed directly from the list of one- and two-electron integrals. The **Hx** matrix-vector product is the most expensive step of the MRCI calculation. A discussion of its efficient treatment including parallelization can be found in Refs.[59] and [60]. Efficient uc-MRCISD calculations can be performed, *e.g.*, with the COLUMBUS program.[55]

2.1.3. Size-extensivity Problem

Size-extensivity refers to the property of a computational method of scaling properly with the size of a molecule,[61,29] or, in the special case of independent particles, the sum of the energies of monomers equals that of the entire system (the latter property is often termed as size-

consistency). One of the major challenges in applying truncated SRCI and MRCI is that both contain size-extensivity errors deriving from the absence of disconnected higher excitations, i.e., excitations obtained as products of lower excitations.[28] Size-extensivity errors can be accounted for in several ways. One popular and simple class of approaches are collected under the name Davidson correction. These corrections are applied *a-posteriori*, i.e., after the CI calculation has finished. In Eq. (8), the original version E_{DC} is shown[30,62]

$$E_{\mathrm{DC}} = \left(1 - c_0^2\right) \Delta E \,. \tag{8}$$

This equation gives the correction as a product of the correlation energy ΔE and the squared norm of the correlation part of the wavefunction. In the SR case, c_0^2 refers to the weight of the HF reference whereas in the MR case it refers to the weight of all references combined. A comparison of several popular variations of the Davidson correction can be found in Ref.[22] Options for extending the Davidson corrections to the multireference case are reviewed there also. The application of the Davidson correction is usually indicated by adding the label +Q to the method used, such as MRCI+Q.

An internally consistent way of calculating size-extensivity effects was suggested by Gdanitz and Ahlrichs[32] in the form of their MR averaged coupled pair functional (MR-ACPF) method. The derivation is based on a variational approach and, therefore, could be directly related to MRCI. Overestimation of higher excitations in MR-ACPF led Szalay and Bartlett to suggest a modified version; the MR averaged quadratic coupled cluster (MR-AQCC) method.[63,34] Both approaches offer good possibilities of calculating size-extensivity effects in the framework of MR approaches and are available in several quantum chemical program packages. A linear-response theory (LRT) version of these methods available in the form of MR-AQCC-LRT[64] allows the computation of transition moments also.

2.1.4. Contracted CI

Contracted MRCI methods have been developed to reduce the often exceedingly high computational costs of the uncontracted MRCI of Eq. (7). The internal contraction scheme as introduced independently by Meyer[24,26] and Siegbahn,[25] is probably the most popular one in which the reference wavefunction is contracted as

$$\left|\tilde{\Phi}_0\right\rangle = \sum_{m=1}^{N_{\text{ref}}} c_m^{\text{ref}} \left|\Phi_m^{\text{ref}}\right\rangle . \tag{9}$$

Single and double excitations are then constructed by application of single- and double excitation operators to $\left|\tilde{\Phi}_0\right\rangle$ as a whole, keeping the coefficients c_m^{ref} fixed as computed from a preceding multiconfiguration self-consistent field (MCSCF) calculation resulting in the following expansion[52]

$$\left|\tilde{\Psi}\right\rangle = \tilde{c}_0 \left|\tilde{\Phi}_0\right\rangle + \sum_{ij}^{\text{int}} \sum_{pq}^{\text{act+virt}} \tilde{c}_{ij}^{pq} \left|\tilde{\Phi}_{ij}^{pq}\right\rangle \tag{10}$$

where *i*,*j* runs over internal orbitals and *p*,*q* over active plus virtual orbitals. The functions $\left|\tilde{\Phi}_{ij}^{pq}\right\rangle$ are obtained by the action of spin-free excitation operators $\hat{E}_{ij}^{pq}$ as[52]

$$\left|\Phi_{ij}^{pq}\right\rangle = \hat{E}_{ij}^{pq} \left|\tilde{\Phi}_0\right\rangle . \tag{11}$$

The main advantage of the internal contraction scheme is that the total number of configurations is independent of the number of reference configurations. Following the notation introduced in Ref. [65], this contraction scheme is termed “fully internally contracted” (FIC) to distinguish it from other contraction schemes to be discussed below.

In practice, the expansion will be truncated after the double excitations. The number of variational parameters is comparable to an SR expansion, which explains the computational efficiency of this approach. However, one must note that this approach is an approximation to the

uncontracted MRCI and a contraction error will occur. The *ic*-MRCISD has been successfully developed by Werner and Knowles[66,67] as a popular approach available in the MOLPRO program package[68] for performing large-scale MRCI calculations. In their approach, only the double excitations were contracted (WK scheme or partially contracted scheme (PC)) in order to avoid diagonalization of reduced density matrices of orders higher than two. Partial contraction in the context of MRCI has also been used in their PC-MRCI method by Shamasundar et al.[52] A FIC-MRCI based on the density matrix renormalization group (DMRG) method has been reported by Saitow et al.[69,70] A strong contraction (SC) scheme has been introduced by Angeli et al.[40,71] in their second-order N-electron valence state perturbation theory (NEVPT2) to be discussed in more detail in Sec. 2.4. FIC-MRCI, PC-MRCI and SC-MRCI methods have been implemented recently into the ORCA suite of programs[72] and extensive comparisons have been made with uc-MRCI.[65] The error introduced by the internal contraction was reported to be about 2-3% of the total electron correlation energy. FIC-MRCI is found as a fairly good approximation to PC-MRCI and is obtained at a significantly reduced computational cost. The SC-MRCI, which represents an even more compact representation of the wavefunction, shows significantly enhanced errors of up to 6% relative to the uncontracted MRCI. Furthermore, the non-invariance of the energy concerning orbital rotations in invariant subspaces (e.g., due to orbital localization) creates problems and is not acceptable for local multireference correlation approaches. It is concluded that the strong contractions work well for NEVPT2 in a canonical basis, but that it does not do so for MRCI.

Special care has to be taken with contracted MRCI approaches in case of avoided crossings as described in Ref. [65] for the case of covalent/ionic curves for LiF. A state-averaged CASSCF(2,2) reference wavefunction has been used. It gives an avoided crossing at 4.1 Å, which is a very unfavorable starting point in comparison with the full CI result of 6.6 Å obtained by Bauschlicher

and Langhoff.[73] The uc-MRCI curve shows an improved avoided crossing distance of 5.2 Å. The different contracted MRCI variants investigated in Ref. [65] produce potential curves that are too close to each other and also show unphysical narrow double crossings. Multistate approaches within contracted MRCI as those described by Werner and Knowles[74] are needed for the proper description of these cases. Differences between internally contracted and uncontracted calculations have been reported for the long-range potential for the reaction H + O_2[75] where internally contracted MRCI gave a small barrier as opposed to a monotonically attractive potential obtained with uncontracted MRCI. A similar case concerning the asymptotic behavior of the potential for the reaction O + O_2 in the electronic ground state will be discussed in Sec. 3.1.

It is also noted that the complexity of the derivation of the elements of the Hamiltonian matrix in internally contracted wavefunctions is considerable requiring density matrices up to fifth order for MRCI. Both for MOLPRO[52] and ORCA[65] automatization techniques were used to cope with this problem.

2.1.5. Calculation of Excited States

The calculation of excited states is straightforward in the uncontracted scheme since the many-electron expansion basis (Eq. (7)) does not depend explicitly on the electronic states. If a balanced set of references has been chosen, all states of interest can be calculated by diagonalizing the same Hamiltonian (Eq. (4)). For the internally contracted scheme, a state-specific optimization procedure has been developed[74] for computing the wavefunction Ψ^I for each state *I* separately and finally, diagonalizing the Hamiltonian matrix $\left\langle \Psi^I \left| \hat{H} \right| \Psi^J \right\rangle$ in the space of these functions (multistate approach).

Most simply, the afore-mentioned Davidson subspace method (Section 2.1.2) can be used to compute all lower roots including the desired one. However, it is also possible with this method to converge to selected roots by root-homing and vector-following, respectively, according to certain conditions, avoiding the computation of unwanted roots. In the root-following method, for example, during the Davidson iteration, the approximate vector with the largest overlap with a predefined reference vector can be chosen for improvement.[22]

2.1.6. Individual Selection Schemes

In the previous presentation of ic- and uc-MRCI, it was implicitly assumed that after setting up the active space and the corresponding set of reference configurations, all configurations according to a certain truncation scheme (usually up to singles and doubles) were included in the expansion of the wavefunction to be used in the construction and solution of the eigenvalue problem of Eq. (4). In the individual selection scheme proposed by Buenker and Peyerimhoff in their multi-reference double-excitation (MRD-CI) program,[20,76] the CI expansion space is divided into two sets: the first one is considered to contain the important configurations to be treated explicitly, while for the second set the configurations are considered only by means of perturbation theory. Extrapolation methods are used to estimate FCI limits. Advanced algorithms for selected CI have been presented by Hanrath and Engels[77] and in terms of massive parallelization by Stampfuß et al.[78,79] For reviews see Refs.[22]and [80]. An adaptive, systematically improvable selection scheme (adaptive configuration interaction (ACI)) applicable also to MR cases has been developed by Evangelista[81] and also applied to the calculation of excited states.[82]

2.1.7. Local MRCI Approaches

Another way of reducing the cost of MRCI calculations is the introduction of a local correlation (LC) treatment, i.e., by localizing the orbitals in space and restricting the excitations to

occur only between orbitals in spatial proximity. Applications have been mostly implemented for closed shell SR cases (see, e.g., Refs. [83–85]). The introduction of LC into MRCI has been successfully achieved by the group of Carter[86–89] within the framework of their TIGERCI program[90] using the weak pairs (WP) approximation developed by Sæbo and Pulay.[84,85] The WP approximation procedure of TIGERCI has also been implemented into the COLUMBUS code based on a localization and WP selection scheme considering reference doubly occupied orbitals only.[91] The method has been applied to the biradicaloid character in singlet and triplet states of triangular non-Kekulé structures and zethrenes[91] and to the calculation of the reaction barrier of the strain-promoted oxidation-controlled cycloalkyne-1,2-quinone cycloaddition (SPOCQ) reaction.[92] A linear scaling local MRCI version has been developed by the Carter group[93–95] with application to excited states.[96]

2.1.8. Natural Orbitals for Use in MRCI

The most common approach to create orbitals to be used in the MRCI and also in other MR methods is the multiconfigurational self-consistent field (MCSCF) method discussed in Sec. 2.2 below. However, this method can be costly especially for large active spaces and can also show other problems such as with convergence and the existence of multiple solutions. Therefore, as an alternative, the use of natural orbitals (NOs),[97] which are the eigenvectors of the one-electron density matrix, has been suggested. The idea is to compute the NOs based on a correlated, but computationally cheaper method such as is discussed below. Besides the motivation of replacing the sometimes inconvenient MCSCF step by a simpler procedure, another benefit of using NOs is the possibility of introducing systematic truncation schemes for the weakly occupied NOs in MRCI and other highly-correlated methods. Such schemes can lead to significant savings in computational cost while influencing the desired accuracy to a rather minor extent.[98] Frozen

natural orbitals (FNOs)[99] are beneficial for this purpose and can be obtained by diagonalizing the virtual density block independently. They are well suited for the mentioned truncation schemes as has been shown by Landau et al.[100] in equation-of-motion- coupled cluster calculations on ionized states. Many of the NO usages have been performed for the ground state (see, e.g., Refs. [101] and [102]). Application of NO schemes to excited states has been performed by Neese[103] in his "spectroscopy oriented configuration interaction" (SORCI) procedure and by Aquilante et al.[104] in the context of multiconfigurational perturbation theory. Related to these approaches is the improved virtual orbital-complete active space configuration interaction (IVO-CASCI) method by Potts et al.[105] An interesting method to construct NOs for several excited states in a balanced way has been suggested by Lu and Matsika[98,106] based on high-multiplicity NOs (HMNOs). In this approach, the HMNOs are computed at single reference CISD level followed by high-level MR-CISD calculation. It is shown that this approach reproduces vertical excitation energies computed with standard MRCI calculations based on CASSCF orbitals well and that it is also applicable to the investigation of potential energy surfaces for valence excited states.

2.2. Multiconfiguration Self-Consistent Field Method

The MCSCF method is a variational procedure, which is based on the expansion of the wavefunction shown in Eq. (1). Whereas in the CI approach the focus was laid on the optimization of the linear expansion coefficients c_j^I, in the MCSCF approach both the CI coefficients and the MOs are optimized. Thus, the MCSCF method shares many features with the CI approach resulting in a matrix eigenvalue problem but also requires non-linear optimization steps for the orbital part of the wavefunction. Several efficient solutions for these optimizations have been developed in the past decades leading to linearly, quadratically, or higher-order convergent formalisms. The different formalisms and numerical procedures have been worked out in detail. We refer the reader

to extensive reviews on this topic in the literature.[107–109] The situation is more difficult when several electronic states should be described at the same time. In this case, state averaging (SA) is usually performed[110,111] in which the average energy of several states is optimized to obtain a balanced description of these states.

The MCSCF approach can be used as a method of its own for calculating several electronic states of a molecule, but also as a procedure that serves only to create the MOs needed in the correlated multireference calculations for defining the many-electron expansion functions $\left|\Phi_j\right\rangle$ used in Eq. (1) and to compute the Hamiltonian matrix **H** (Eq. (4)).

A popular choice for the wavefunction used in the MCSCF method is, because of its conceptual simplicity, the complete active space (CAS) wavefunction,[51] leading to the CASSCF approach. In it, all possible configurations in a given orbital space and for a given number of electrons are constructed. It is essentially an FCI approach in the restricted space of active orbitals and electrons. Because of this construction, the CAS is invariant under purely active orbital rotations. This space is usually characterized as CAS(*n* el., *m* orb.). Because of the factorial increase of the size of the CAS with the number of active orbitals (see Weyl's dimension formula[112]), occupation restrictions have been introduced[113] in the form of restricted active spaces (RAS), which are usually divided into a set of subspaces RAS1/RAS2/RAS3. RAS1 contains a given maximum of holes, in RAS2 all possible occupations are allowed (corresponding to a CAS) and RAS3 contains up to a given number of electrons. Generalizations are available in the form of the occupation-restricted-multiple-active-space (ORMAS)[114] and the generalized active space, (GAS).[115] Unfortunately, there are no straightforward rules on how to determine the actual sizes of these spaces.[116] In the simplest case, choices are made based on experience with previous calculations, which can be tested empirically by investigating the sensitivity of computed results

to different choices of active spaces. The first attempts toward systematic determination of active space sizes have been made by Pulay and Hamilton,[117] based on the natural orbital (NO) occupation of an unrestricted Hartree-Fock (UHF) calculation. Recommended NO occupation numbers for including orbitals into the active space lie in the range between 0.02 and 1.98 *e*. The method has been termed UNO-CAS later on[101] and has been tested extensively by means of comparison with results obtained from Density Matrix Renormalization Group (DMRG) methods.[118] NOs determined from a second order Møller-Plesset perturbation calculation have been used with the same goal of determining efficient active spaces for CASSCF calculations.[119] Other strategies for reducing the CAS for systematic scans of energy surfaces and for direct dynamics has been investigated by Boggio-Pasqua and Groenhof[120] for selected photochemical pathways. Also, NO occupations derived from averaged SCF density matrices have been used[121] to obtain a balanced description of multiple electronic states in RASSCF calculations. A simple, but useful MCSCF version is the two-configuration self-consistent-field (TCSCF) method[122] which has found an interesting application in connection with the TCSCF-CI method.[123]

In recent years, impressive progress has been made in the technical possibilities for the sizes of CASSCF calculations using the density matrix renormalization group (DMRG) method to be discussed in Sec. 2.7.1.[124,125] For example, DMRG-CASSCF(22,27) calculations with 3000 basis functions have been reported recently.[124] As alternative speed-up of CASSCF calculations, GPU-accelerated state-averaged (SA)-CASSCF combined with ab initio multiple spawning (AIMS) photodynamical simulations have been reported by Snyder et al.[126] The floating occupation molecular orbitals (FOMOs)-CASCI method[127] has been developed in combination with semiempirical Hamiltonians and has also been successfully extended to ab initio

applications.[128] It has been found that it often represents a good approximation to SA-CASSCF calculations.

2.2.1. Multiple MCSCF Solutions and Symmetry Breaking

In many cases, the MCSCF calculations can be performed without problems. It should, however, not be forgotten that due to the nonlinear orbital optimization process multiple solutions can occur, which can manifest themselves by convergence problems, root-flipping between close-lying states and symmetry breaking. A detailed general analysis can be found, e.g., in the work by Shepard[107,129] and a discussion of specific problems is given in Ref.[116].

The phenomenon of symmetry breaking of the wavefunction at a symmetric structure is an interesting phenomenon and has been discussed in many cases, such as HCO_2,[130–133] NO_2,[134,135] BNB,[136–144] NO_3.[145,146] and the allyl radical.[147] In this section we concentrate on the aspects of symmetry breaking in the sense that at a high-symmetry molecular structure the symmetry of the wavefunction is broken. At Hartree-Fock level, this situation has been formulated in the well-known symmetry dilemma by Löwdin.[148] A general discussion of the consequence of artificial symmetry breaking due to inappropriate wavefunctions, which leads further on to wrong predictions about symmetry-broken molecular structures has been given by Davidson and Borden.[149] The purpose of the subsequent discussion is to show for two examples how appropriate wavefunctions can be constructed in the framework of MR theory to provide reliable adiabatic energy surfaces, which can be further used on, e.g., calculations of Jahn-Teller or pseudo Jahn-Teller effects (see Refs. [141,144,149] related to the present discussion). The construction of these wavefunctions, which do not show symmetry breaking, can often be tedious. In this context, we also want to mention the singly excited active space complete active space configuration interaction (SEAS-CASCI) method developed by Shu and Levine[150] where the orbitals to be used

in a CASCI calculation are optimized based on an energy expression in which off-diagonal Hamiltonian matrix elements driving the symmetry breaking are neglected.

The first example for symmetry breaking was discussed many years ago by McLean et al.[130] for the formyloxyl radical HCO_2. In case of the σ radical, two valence bond structures can be drawn (Figure 3). In one there is a lone pair on O_1 and a radical center on O_2 and in the second one, the role of the two oxygen atoms is reversed. It is noted that the orbitals describing the lone pair and the radical do not have the same size. The doubly occupied orbital is significantly expanded in comparison to the radical one. A balanced wavefunction must contain both types of orbitals on each O atom, a requirement that has been named orbital doubling. The other critical effect is the stabilizing resonance effect between the two VB structures shown in Figure 3. It has been argued in Ref. [130] that the strong bias of symmetry broken solutions at MCSCF level does not make them suitable for subsequent CI calculations. Thus, an MCSCF wavefunction should be constructed, such as it does not show symmetry breaking at the C_{2v} structure where the two CO bond lengths are equal. In fact, it has been shown in Ref. [130] how to systematically construct wavefunctions by means of orbital doubling in order to obtain the full molecular symmetry in the wavefunction and to use these wavefunctions in subsequent MRCI calculations for including dynamic electron correlation effects.

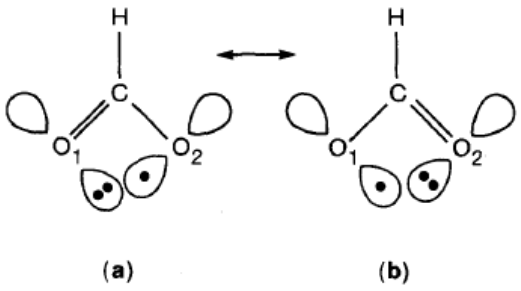

Figure 3. Valence bond structures of HCO_2. Reproduced with permission from Ref. [130]. Copyright 1985 AIP Publishing.

The linear $\tilde{X}^2\Sigma_u^+$ state of BNB is another convenient benchmark system for studying symmetry breaking because of its relatively small number of valence electrons. The symmetry breaking in unrestricted Hartree-Fock and coupled cluster calculations has been well discussed by Gwaltney and Head-Gordon.[138] We want to focus here on the behavior of the CASSCF and MRCI methods. It has been shown by full valence CASSCF(11,12) calculations on the symmetric $D_{\infty h}$ structure of BNB by Kalemos et al.[139] that in single-state CASSCF calculations a symmetry breaking occurs with one B in the ^{2}P state and the other one in the excited ^{4}P state. Since the two B atoms need to be equivalent in the $D_{\infty h}$ structure, the wavefunction has to be represented by the two equivalent VB structures shown in Figure 4. The inclusion of dynamic electron correlation via single-state CASSCF in combination with second-order perturbation theory (PT2) is not able to correct for this deficiency of symmetry breaking. However, state-averaging describes both B atoms equivalently.

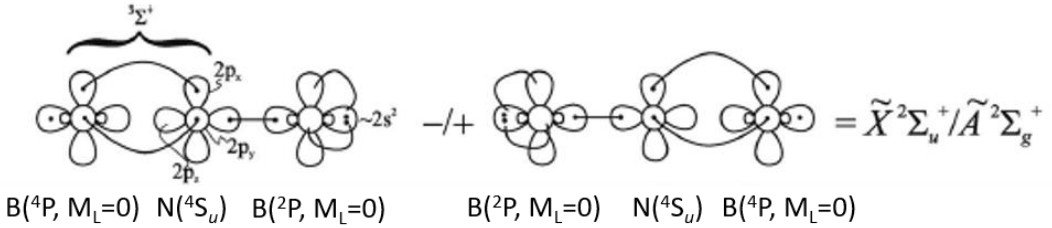

Figure 4. VB structures for the $\tilde{X}^2\Sigma_u^+$ and $A^2\Sigma_g^+$ states of BNB. Adapted with permission from Ref. [143]. Copyright 2013 AIP Publishing.

Based on the experience gained with these SA-CASSCF calculations, single-state and state-averaged (over two states, $\tilde{X}^2\Sigma_u^+$ and $A^2\Sigma_g^+$) CASSCF calculations were performed at the high-symmetry $D_{\infty h}$ geometry using C_{2v} symmetry[143] and improved by MRCI and MRCI+Q approaches. Different active spaces were used to study the extent of symmetry breaking: (i) a CAS(9,11) space ($(2s + 2p)_B + (2p)_N$), (ii) including the $2s_N$ into the CAS led to a CAS(11,12) ($(2s + 2p)_B + (2s + 2p)_N$) and (iii) adding an additional correlating orbital for $2s_N$ gave the (CAS(11,13), ($(2s + 2p)_B + (2s + 2p + s')_N$). In all three cases, single-state CASSCF leads to symmetry breaking in the wavefunction at the $D_{\infty h}$ geometry, whereas the SA-CASSCF calculations resulted in symmetry correct results. In the SA-CASSCF calculations (i) and (iii) also a single high-symmetry energy minimum geometry was found whereas in case (ii) a double minimum geometry was obtained. These results were always confirmed by subsequent MRCI calculations. They illustrate the possibilities of obtaining symmetry correct results at CASSCF level for the high-symmetry structure, which have to be regarded as a pre-requisite for balanced calculations. However, they also show that, nevertheless, energy minima at unsymmetric structures can be obtained because of subtle further balances of different electron correlation effects favoring in case (ii) an unsymmetric structure. The origin of the double minimum occurring in the CAS(11,12) (case (ii)) was traced back to a missing correlating orbital for $2s_N$. Its addition also gave a symmetric $D_{\infty h}$ geometry, which has to be regarded as the most accurate result of this set of calculations. In the afore-mentioned coupled cluster investigations[138] an unsymmetric $C_{\infty v}$ structure had been obtained with a barrier of ~160 cm^{-1} to the symmetric $D_{\infty h}$ one. A similar barrier height of ~140 cm^{-1} has been reported by Stanton[141] in his equation-of motion coupled-cluster method for ionization (EOMIP-CCSDT), starting in this case from well-behaved closed shell orbitals of the anion. In both cases, the barriers are located well below the zero-point energy level. No potential energy curves or

barriers were given in the work by Kalemos[151] so that no further comparisons between the two seemingly contradictory results of the coupled cluster and MRCI results can be made.

2.3. Coupled cluster methods:

Coupled cluster (CC) methods represent a robust toolset for quantum chemistry. Its power manifests itself a) in the exponential parametrization of the wavefunction, which allows inclusion of the most important higher excitations in an efficient way, b) in the size-extensivity of the results, and c) in the hierarchical way of truncation, which allows control of accuracy. CC methods have been reviewed in several papers[49,152–155] and even the multireference versions — the focus of this work — have been recently reviewed by Lyak, Musiał, and Bartlett[156] (see also Ref. [157]). In this section, we summarize the multireference CC methods capable of describing excited states and highlight the most promising recent developments.

The formalism of multireference CC methods is rather complicated. Therefore, for better understanding, we first shortly introduce the concept of excitation energy calculation by CC methods in the single reference case. This is also not off-topic for the present review since these methods, although based on a single-reference ground-state wavefunction, provide a well-balanced multiconfigurational description of the excited states essentially.[14]

2.3.1. Single reference coupled cluster methods to describe excited states

In CC theory, the ground state wavefunction is parametrized in an exponential way:

$$\Psi_{CC} = \exp\left(\hat{T}\right)\Phi_0 \tag{12}$$

with Φ_0 the reference determinant usually built from Hartree-Fock orbitals and the cluster operator

$$\hat{T} = \hat{T}_1 + \hat{T}_2 + \hat{T}_3 + \ldots \tag{13}$$

Here, $\hat{T}_n$ is the *n*-fold excitation operator including the wavefunction parameters. Since the expectation value with the above exponential wavefunction gives an expression with an infinite number of terms for the energy (and even the stationary equations are infinite[33]), projected Schrödinger equations are used to solve for the amplitudes:

$$\left\langle \Phi_{ijk\ldots}^{abc\ldots} \middle| \exp\left(-\hat{T}\right) \hat{H} \exp\left(\hat{T}\right) \middle| \Phi_0 \right\rangle = 0 \tag{14}$$

with $\Phi_{ijk\ldots}^{abc\ldots}$ representing excited determinants. A hierarchical set of approximate methods can be defined by truncating the cluster operator: CCD includes just double-,[158] CCSD includes single- and double-,[159] CCSDT includes single-, double-, and triple excitations,[160] and so forth. Using also perturbation theory arguments, methods in between these can be defined: CC2[161] and CCSD(2)[162] are approximations to CCSD, while, CCSD(T),[163] CCSDT-n,[164–166] and CC3[167] are methods above CCSD including the effect of connected triple excitations approximately. Most of these approximate methods have the advantage that the highest-level amplitudes (e.g., doubles for CC2 or triples for CCSD(T)) do not need to be stored, introducing a substantial computational advantage.

Since the wavefunction in the above form must be dominated by a single determinant, as in case of SRCI, it is in general not suited for excited states. A further complication comes from the fact that the amplitudes are not obtained variationally but from the projected Schrödinger equations, and these usually cannot be solved for higher roots. There are two ways to generalize the CC methods for excited states: one is the Equation of Motion[168,169] (EOM), the other one is the Linear Response[170] formalism. In case of the truncated methods, the two routes give the same excitation energy, but slightly different oscillator strength and other transition properties.[171] For a numerical comparison of oscillator strengths obtained by the EOM and LR ways, see Ref. [172].

Essentially, solving either EOM-CC or CC-LR equations means the diagonalization of a transformed Hamiltonian in the proper space of the excited determinants:[14]

$$\begin{aligned} \bar{H} &= \exp\left(-\hat{T}\right)\hat{H}\exp\left(\hat{T}\right) \\ \bar{H}\hat{R}_i &= E_i\hat{R}_i \end{aligned} \tag{15}$$

Here $\hat{R}_i$ is again an excitation operator. This means that the excited states are described as linear combinations of single, double, and higher excitations out of the ground state wavefunction, i.e. a) it is not necessary for the wavefunction to be dominated by a single function (determinant); and b) excitations of the same class (e.g., singles) are treated equivalently. Therefore, several excited states can be handled at the same time, and the description is clearly *multideterminantal*. The power of the method lies in the fact that the excited state wavefunction is not just a linear combination of the determinants of the expansion space, instead it has an exponential part obtained for the ground state:

$$\Psi_i = \hat{R}_i \exp\left(\hat{T}\right)\Phi_0 \tag{16}$$

i.e. essentially treating differential correlation with respect to the ground state.[13]

Hierarchical truncation is again possible. EOM-CCSD[13,173] or CCSD-LR[174] is based on a CCSD ground state and includes single and double excitations in the diagonalization of $\bar{H}$ as well. EOM-CCSDT[175] also includes triple excitations for both the ground and the excited state. Note that states dominated by excitation level one less than that in the expansion space can be described properly by the method.[176] Perturbative treatment of the highest excitation level is also possible, although several possibilities exist here, and EOM and LR formalisms do not necessarily lead to the same equations. To approximate doubles iteratively, CC2-LR[161], EOM-CCSD(2)[162] (also known as EOM-MBPT(2)[177]) or the Algebraic-Diagrammatic Construction (ADC) family of methods[178–180] can be used, while CIS(D)[181] can be considered as a non-iterative variant.

Closer analysis of the equations shows that only states dominated by single excitations can correctly be described if the expansion space is limited (either directly or approximately) to double excitations. At the next level, to approximate triple excitations, methods like CC3-LR,[182,] EOM-CCSDT-3[183] should be mentioned as the most often used variants. Non-iterative versions can follow two strategies. The LR framework suggests an approximate ground state at the desired level and then a correction also to the excitation energy is applied. CCSDR(3) by Christiansen et al.[184] and the recent CCSD(T)(a)* method by Matthews and Stanton[185] can be mentioned here. Another strategy is to use the perturbative expansion of the excitation energy based on the CCSD ground state (e.g., EOM-CCSD(T) by Watts and Bartlett[186]). The LR approach is slightly more expensive since already the ground state is treated by the corrected method, but, according to a recent test,[187] this effort is rewarded by higher accuracy.

There is a large number of applications where EOM-CC/CC-LR calculations have been used, molecules as large as nucleotide dimers can be routinely calculated even at the triples level.[188] Recently, several papers have reported benchmark data on CC excited state methods,[172,187,189–192] establishing a good knowledge base for the reliability of different approximations. For more details on EOM-CC methods, the interested reader may consult the recent review by Bartlett.[14]

In summary, CC methods for excited states based on single reference ground states represent a powerful tool in quantum chemistry, which have been used to solve many chemical problems, in particular for cases where the potential energy surface around the equilibrium geometry of the ground state was needed.[14] However, these methods fundamentally fail if the ground state cannot be properly described by the single reference CC wavefunction. This failure includes the description of conical intersection between the ground and excited state, an important

event in many photochemical processes. Note, however, that with some additional effort, conical intersections between the excited states can indeed be handled by SR-CC methods as shown by Köhn and Tajti.[193] Description of Conical intersections based on SR-CC has also been discussed in Refs. [194,195]

2.3.2. Multireference coupled cluster Methods

Unlike the case of CI, the generalization of CC theory for more than one reference determinant is not straightforward. The basic problem is that a genuine CC formalism requires a proper "*vacuum,*" i.e., a reference occupation where orbitals can be classified either as "occupied" or "virtual." Without this, the excitation operators will not commute, and many complications arise in forming the exponential wave operator and deriving the equations, including non-terminating commutator expansion, redundancy, intruder states, non-invariance to internal rotation of orbitals.

Many attempts have been made to overcome these difficulties. Two classes can be distinguished, depending on whether the exponential operator acts on the reference function or on the individual determinants of the reference space:

$$\begin{aligned}\Psi_{JM} &= d_1 \exp\left(\hat{T}^{(1)}\right)\Phi_1 + d_2 \exp\left(\hat{T}^{(2)}\right)\Phi_2 + d_3 \exp\left(\hat{T}^{(3)}\right)\Phi_3 + ... \\ &= \sum_{\mu \in ref} d_\mu \exp\left(\hat{T}^{(\mu)}\right)\Phi_\mu\end{aligned} \tag{17}$$

$$\begin{aligned}\Psi_{IC} &= \exp\left(\hat{T}\right)\left(c_1\Phi_1 + c_2\Phi_2 + c_3\Phi_3 + ...\right) \\ &= \exp\left(\hat{T}\right)\Psi_0\end{aligned} \tag{18}$$

Here Φ_1, Φ_2, … are reference determinants, $\hat{T}, \hat{T}^{(1)}, \hat{T}^{(2)}, \hat{T}^{(3)}, ..., \hat{T}^{(\mu)}$ are cluster operators, c_1, c_2, … and d_1, d_2, … are coefficients. The first ansatz was suggested by Jeziorski and Monkhorst (JM)[196] and named after these two pioneers. For many decades, it was considered as the most rewarding, and theoretically most justified solution for the problem ("*genuine MRCC*"). Several

methods based on the JM ansatz have been worked out, including multistate approaches ("*state universal*," by the CC nomenclature) and also state-specific versions. State-universal versions treat excited states together with the ground state, while in state specific-version, some special formulation (e.g., EOM or LR) is required for general excited states.

The second ansatz is essentially an internal contraction (IC) scheme, as discussed above in case of MRCI (Section 2.1.4). Although used earlier as well (Mukherjee et al.[197], Simons and Banerjee[198,199]), it has become popular in the recent years, mostly thanks to the general normal ordering concept by Mukherjee and Kutzelnigg.[200,201] By construction, this is a state-specific formulation, and either EOM or LR extension is required for excited states.

A third possibility to define MRCC methods is offered by the use of SR techniques with the inclusion of specific higher excitation components. This group includes methods based on ground state ansatz[202], or excited state EOM ansätze.[155,203,204] The advantage of these methods is that formal properties, like size-extensivity, are automatically maintained, and the well-developed toolset of SR-CC theory can be used. The disadvantage is that only a certain class of excited states can be reached.

A detailed analysis of MRCC methods of all three categories can be found in the excellent review by Lyakh and Bartlett.[156] The state-specific versions have also been reviewed separately.[205] Historical reviews by Jeziorski[206] and by Szalay[207] have also appeared on the occasion of 50 years of Quantum Theory Project,[208] where many of the CC developments had their root. Here, we shortly summarize the most important features of these methods, concentrating on those versions that can handle or can be extended for excited states. The goal is to provide orientation among the proliferation of methods developed over the years.

2.3.2.1. MRCC methods based on the Jeziorski-Monkhorst ansatz

According to the original formulation by Jeziorski and Monkhorst (JM),[196] the method targets on as many electronic states as the dimension of the reference space (often called the *model space* in CC literature). Therefore, such methods are termed "*State-Universal*" (SU)-MRCC and trivially deliver not just the ground but also some excited states. (As a separate approach, a so-called *Valence-Universal* (VU) formulation is also possible,[156] but this does not form the scope of the present paper.)

The working equations are obtained after introducing an effective Hamiltonian ($\hat{H}_{eff}$) defined in the reference space

$$\hat{H}_{eff} = \sum_{\mu}\sum_{\nu} \left|\Phi_\mu\right\rangle \left\langle\Phi_\mu\right| \hat{H}\hat{\Omega} \left|\Phi_\nu\right\rangle \left\langle\Phi_\nu\right| \tag{19}$$

with the Jeziorski-Monkhorst wave operator

$$\hat{\Omega} = \sum_{\mu\in ref} \exp\left(\hat{T}^{(\mu)}\right) \left|\Phi_\mu\right\rangle \left\langle\Phi_\mu\right| \tag{20}$$

The wave operator is used to obtain the final wave function from the reference wave function, i.e.

$$\Psi = \hat{\Omega}\Phi_0 \tag{21}$$

where the reference function Φ_0 is a combination of the reference determinants.

The advantage of this form is that essentially each reference determinant (Φ_μ) forms the vacuum for its own cluster operator $\hat{T}^{(\mu)}$. Diagonalization of $\hat{H}_{eff}$ in the reference space will yield the targeted ground and excited state energies in the entire expansion space, not just the reference energies. The amplitudes are obtained by projection of the Schrödinger equation. The most straightforward way is to project against the same determinants that the $\hat{T}^{(\mu)}$ produce. In this way, one obtains equations for all the reference determinants (Φ_μ), which are similar to the single

reference ones, except that these are coupled.[209] For this reason, one simultaneously needs to solve for all the eigenstates corresponding to all the reference functions, i.e., certain excited states are automatically delivered.

For a proper normalization (an essential issue in CC theory), a CAS must be used as reference space. This choice often leads to the so-called *intruder state problem*, which appears whenever the model space also includes high-lying states, e.g., when the CAS space includes many orbitals. Intruder states slow down the convergence, hampering the applicability of the method seriously. The attempt to cure this problem leads to the introduction of the so-called *incomplete model space* formulation of SU-MRCC: here only a subset of CAS functions is involved in the reference space. Those left out need to be included in the wave operator, which, in turn, introduces redundancies into the equations. The redundancies can be removed by applying the so-called C-conditions.[210] This problem is discussed in detail in the review by Lyakh, Musiał, and Bartlett.[156]

For both complete and incomplete model spaces, the truncation of the cluster operator defines practical methods: SU-MRCCSD includes singles and doubles,[196,209,211–215] while in SU-MRCCSDT also triples are included.[216] To our knowledge, no production code exists for the SU-MRCC method.

In the literature, one may only find applications of SU-MRCC methods on excited states of small molecules: LiH,[211] water,[217] methylene,[218] cyclobutadiene,[219] and alkali-metal dimers.[220] Recently, Li and Paldus presented SU-MRCC results on various states of ethylene and p-benzyne,[221] furan, and pyrrole[222] as well as of BN, formaldehyde, trans-butadiene, formamide, and benzene.[223] Detailed conclusions on the accuracy and applicability of SU-MRCC variants are delivered in these papers.[221,223]

To overcome the intruder state problem, Hubač and coworkers,[224,225] Mukherjee and coworkers,[226,227] as well as Mahapatra and coworkers[228,229] introduced *state specific* (SS) versions based on the Jeziorski-Monkhorst ansatz, where only one state — usually the ground state — is obtained from the reference space. Like the incomplete model space case, redundancy between the equations appears, which must be treated. Appropriate sufficiency conditions need to be defined, which make the number of equations equal to the number of variables. Details about the possibilities have been discussed by Pittner[230] and Kong,[231] but also the review by Lyakh, Musiał, and Bartlett[156] includes a thorough analysis. Three variants have been identified:[156] Brilluoin-Wigner (BW)-MRCC,[224,225,230] the single root (sr)-MRCC,[228,229] and the Mukherjee (Mk)-MRCC.[226,227,232,233] It is the latter version where full size-extensivity is preserved. Therefore, it has been considered as the most promising variant.

It was Hanrath[234] who investigated the so-called *proper residual problem* and was able to eliminate redundant cluster amplitudes from the ansatz completely. The resulting MRexpT method can be considered as a Jeziorski-Monkhorst state-specific approach, where amplitudes associated with the same excited determinant are grouped together.

All BW-MRCC, Mk-MRCC, sr-MRCC, and MRexpT methods are essentially designed for the ground state; excited states can only be calculated as lowest states of an irreducible representation of the molecular point group or spin. The disadvantage is that separate calculations converging to different roots of the effective Hamiltonian are required, while in SU-MRCC all roots are obtained in a single calculation. The MRexpT method was tested for the first excited state (2^1A_1) of H_8,[235] CH_2 singlet-triplet splitting,[234] Σ^+ and Π states (singlet and triplet) of HF,[236] but we are not aware of any realistic applications. Using sr-SS-MRCC, Mahapatra calculated H_4, H_8, N_2H_2, and CH_2.[229] Singlet-triplet gap of oxyallyl radical was calculated by Simsa et al.,[237] who

concluded that the triples correction is required for accurate results, and in this case Mk-MRCC is somewhat better than BW-MRCC.

For general excited states, either EOM or LR extension is necessary. Mk-MRCCSD-LR has been presented by Jagau and Gauss.[238] The method was very promising for problems with strong multireference character (ozone and benzynes), but unfortunately, here too, a severe problem appears due to redundancy: some of the excited states will appear multiple times. Even worse, not all of these roots give a correct description of the states and their assignment is not straightforward.[238,239] The problem can be attributed to the general shortcomings of the Jeziorski-Monkhorst state-specific formulation,[240] i.e. the already mentioned over-parametrization. Therefore, Mk-MRCCSD-LR does not seem to be ready for routine applications.[238] An implementation for the two-determinantal case is available in the CFOUR program system.[241]

One should also mention that already for the ground state serious convergence problems have been observed which could be attributed to the lack of orbital invariance of the Jeziorski-Monkhorst ansatz.[241] . For details see the papers by Das, Mukerjee, and Kállay[233] and Evangelista and Gauss[242]

2.3.2.2. Using multideterminantal vacuum state: internally contracted MRCC methods

The concept of a multideterminantal vacuum state (ansatz Eq. (18) above) has been introduced long ago; see, e.g., Mukherjee et al.[197,243] and Banerjee and Simons.[198,199] The complication here is twofold: first, the multideterminantal reference state is not a proper vacuum for the CC formalism, causing non-commuting excitation operators and consequently non-terminating commutator expansions. The second problem is again over-parametrization, i.e., redundancies among the equations, which is also present in case of ic-MRCI but with less severe

consequences.[66,67] Therefore, the above mentioned pioneering applications excluded excitation to and from the active orbitals (internal excitations) or used truncation of the commutator expansion.

This ansatz came into the frontiers of MRCC research in the recent years for two reasons: first, as discussed above (Section 2.3.2.1), it became apparent that the state-specific JM ansatz has substantial problems. Second, Mukherjee, and Kutzelnigg[200,201] presented a generalized Wick's theorem for multideterminantal vacuum states, allowing a more straightforward derivation of the equations. It was clear that new developments should consider internal excitations and the resulting overparameterization needed to be addressed. The increasing interest is well represented by the fact that in 2011, three new formulations appeared in the literature. Evangelista and Gauss,[244] as well as Hanauer and Köhn[245] presented their versions of the ic-MRCC methods, while Datta, Kong, and Nooijen[246] introduced a partially internally contracted version (pIC-MRCC). The approaches by Evangelista and Gauss[244] and by Hanauer and Köhn[245] are similar, with the main difference being how the redundancies are handled: while Evangelista and Gauss[244] use Löwdin canonical orthogonalization, Hanauer and Köhn[245] apply singular value decomposition. Handling of higher order commutators become possible by automated derivation and programming, and luckily these expansions seem to converge rapidly.[245] The size-extensivity lost by eliminating redundancy could be restored recently by Hanauer et al.[247]

A somewhat different route has been suggested by Datta, Kong, and Nooijen.[246] In their pIC-MRCC approach, they discard the internal excitations from the cluster ansatz $\hat{T}$. Therefore, the non-commutation problem is resolved. Unlike the old formulation by Banerjee and Simons,[198,199] internal excitations are also considered in a second step in an uncontracted fashion (origin of the name), when a transformed Hamiltonian ($\exp\left(-\hat{T}\right)\hat{H}\exp\left(\hat{T}\right)$, with $\hat{T}$ being the cluster operator) is diagonalized in the MRCIS space (note that internal doubles are still not

considered). To solve for the cluster amplitudes, Datta et al.[246] considered several ways to define equations. This procedure is similar to the EOM-CC idea, where the eigenproblem of a transformed Hamiltonian is also solved, and that exact size-extensivity is sacrificed in the diagonalization step.

For completeness, we also mention the somewhat related method by Yanai and Chen (Canonical Transformation Theory for MR problem)[248,249] and a Unitary group based version by Chen and Hoffman.[250]

As state-specific methods, general excited states cannot be treated by either the ic-MRCC or pIC-MRCC methods. Naturally, the first tests included some excited states of different symmetry than that of the ground state. For these benchmarks, the methods worked as good as for the ground state.[245]

For general access of excited states, LR formulation of the ic-MRCC method has been presented by Samanta et al.[239] It turned out that EOM and LR formulations are not equivalent but the former seems to be more practical due to the presence of some difficult couplings in the latter. Test examples included methylene, p-benzene, and trans-oligoenes. These results showed that for single-excitation-dominated states vertical excitation energies calculated by ic-MRCCSD-LR are as accurate as CC3-LR results, and that the former method outperforms it for double-excitation-dominated states. It was also found that the accuracy of ic-MRCCSD-LR does not deteriorate when the reference state shows significant multireference character. For those states that can be obtained by the ic-MRCCSD as well, the two results are very close. However, as in the SR-CCSD case, ic-MRCC formalism is still not suited to access conical intersections between the reference state and the excited states.

Another possibility to access excited states is the multistate version of the ic-MRCC method, which has been presented recently by Aoto and Köhn.[251] Not too much experience is available yet, but it is hoped that in this way it will be possible to describe state crossing (also with the ground state). Promising results have been presented for LiF and BeF.[251]

The relation of pIC-MRCC to EOM-CC led to its straightforward generalization for multiple states. In the so-called MR-EOMCC method of Nooijen and coworkers,[252–254] instead of diagonalizing $\bar{H}$ in the MRCIS space as in pIC-MRCC, the space is now extended by the inclusion of up to double excitations into the active space. Therefore, MR-EOMCC can be considered as an EOM-CC style extension of pIC-MRCC to excited states, although the equations for the amplitudes are somewhat different.[255] Again, there are different options for defining equations for the cluster amplitudes, leading to different versions of the method.[256] Initial applications show that the method is, in particular, applicable for the description of transition metal atoms.[252–256] Successful benchmark numbers have been presented for the potential energy surfaces of C_2 and O_2 and for organic molecules,[252] as well. In a recent paper, Huntington et al.[257] also benchmarked this method against the Mülheim set of excited states,[189] and accuracy of 0.1 eV has been observed with respect to CC3-LR results on vertical excitation energies. It is also stated[255] that MR-EOMCC shows comparable accuracy to EOM-CCSD(T) without the need of triple excitations. However, as underlined by Hutington et al.[257], MR-EOMCC is not an ideal method for calculating potential energy surfaces, and also not suited for conical intersections with the ground state.[252] Implementation of MR-EOMCCSD is available in ACESII,[258] and ORCA[72] codes.

There are not enough data in the literature to make a comparison between ic-MRCC-LR and MR-EOMCC in detail. Formally the two methods seem to be complementary: ic-MRCC will provide accurate energies for states with no occupation change in the active space. These states

are not accessible at all in MR-EOMCC.[257] However, the latter gives a more compact description and is therefore well suited for complicated problems, such as transition metals.[257] Although ic-MRCC is more expensive, both ic-MRCC and MR-EOM are limited to small active spaces (such as CAS(10,10)).

The comparison of ic-MRCC-LR and Mk-MRCC-LR has been presented by Samanta et al.[239] For states dominated by double occupied to virtual excitations, both results agree with each other and with the corresponding single reference CC-LR results.[239] For states dominated by excitations to or from active orbitals, however, Mk-MRCC-LR and ic-MRCC-LR results differ considerably, the latter being up to 0.9 eV lower.[239]

2.3.2.3. MRCC based on SR formalism

In 1991, Oliphant and Adamowitz[202] suggested an MRCC ansatz that is based on the traditional single reference CC formalism. The reference space is multi-determinantal, but one of them is chosen as vacuum state to define second quantization. The cluster operator is truncated considering the excitation level with respect to all reference functions. This cluster operator is essentially very similar to the excitation operator of MRCI, e.g., in case of SD approximation all excitations are included in the wavefunction, which are single or double in regard to any of the reference functions. This means that certain higher excitation operators concerning the vacuum state are also considered. However, the challenge comes into play once disconnected higher excitations are taken into account. These higher excitations and, thus, the resulting wavefunction depend on the choice of the "vacuum", and the optimal choice might change along the potential energy surface.[259] The problem becomes especially severe if two or more of the reference determinants are (nearly) degenerate. A related method is the Active Space EOM-CC method by Piecuch et al.[260,261] and the tailored CCSD (TCCSD) by Bartlett et al.[262]

The method has been used to calculate excited states with different symmetry and spin than the ground state by Adamowitz, Ivanov, and Lyakh.[263,264] Systems like water, FH, C_2, and formaldehyde were studied for calibration. An LR response version for excited states has also been presented by Kállay and Gauss,[265] but only benchmark calculations for some small systems, such as the $^2B_1$ and $^2A_1$ states of NH_2, stationary points on the S_1 surface of NH_3, have been reported. Also Köhn and Olsen[266] presented an LR generalization of excited states and studied N_2, C_2, H_2O, and CH_2.

Special forms of single reference EOM-CC methods can also be used for MR treatment of several states. The spin-flip (SF) EOM-CC method by Krylov and coworkers[203,204] employs a triplet state as reference, while the subsequent EOM calculation restores the required spin states. In their double-ionization(DI)/double-attachment(DA)-MRCC scheme, Bartlett and coworkers[155,267,268] used doubly ionized/attached systems as vacuum, and the states of interest were obtained by a single EOM calculation adding/removing two electrons. By this, the requested states will appear as roots of an EOM matrix. Thus, all of them, including the ground state, are handled at the same footing. While these methods can provide a correct wavefunction for certain systems, their use is limited by the complicated relationship between the vacuum state and the target states.

2.3.2.4. Outlook on MRCC for excited states

As a conclusion on the CC methods, it can be stated that multireference CC methods offer several ways of calculating excited states. The different models represent different parametrization of the wavefunction with advantages and disadvantages for specific systems. The main appealing property of CC theory is size-extensivity, which is not easy to maintain for MR methods, in particular for excited states. If size-extensivity is kept, like in case of Mk-MRCC, other problems arise, like non-invariance to orbital rotation or artificial splitting of states. Nevertheless, the

methods discussed here, if at all, only slightly violate size-extensivity, and it is not expected that this would bias the results. An appealing feature of MRCC methods is that triples extensions are readily available, since derivation and implementation can be performed by automated processes.[269–273]

Despite many efforts put recently into this topic, it seems that MRCC methods are not yet ready for routine applications, as well shown by the sparsity of applications to realistic chemical problems. Our opinion is that ic-MRCC-LR[239] seems to be the best candidate from the purely theoretical point of view. The MR-EOMCC by Nooijen and coworkers[252–254] is very promising, in particular for transition metals. The problem with MR-EOMCC is its quite complicated concept and its large number of variants. In short, presently MR-CC methods do not seem to replace either MR-CI and variants like MR-AQCC nor SR-EOMCC in routine applications, but this conclusion might change in the near future.

2.4. Mutireference perturbation theory

In the previous sections, we have discussed how excited states can be calculated in multireference situations either in the configuration interaction (Section 2.1) on in the coupled cluster (Section 2.3) frameworks. Now, we turn to a third framework, the many-body perturbation theory (MBPT). In MBPT, nondynamical electron correlation is recovered as the result of a perturbation to a zeroth-order Hamiltonian. The challenge in the field has been to extend the non-degenerate MBPT, successfully developed for the ground state, into a quasi-degenerate version, to allow the treatment of multireference problems.

A large number of multireference perturbation theory (MRPT) variants have been implemented over the years (see Refs.[22,274,275]). Some of the most well-known is the second-order complete active space perturbation theory (CASPT2) developed by Roos and coworkers,[35,36] the

second-order multireference Møller-Plesset perturbation theory (MRMP2) developed by Hirao,[39,276,277] and the *N*-electron valence state perturbation theory (NEVPT) developed by Angeli, Cimiraglia, and collaborators.[40,71,278,279] All these methods have proven to be efficient and effective approaches to deal with excited states.

The major difference between the various MRPT approaches is in the definition of the zeroth-order wavefunction $\Psi^{(0)}$ and zeroth-order Hamiltonian H_0. In the popular CASPT2 approach,[35,36] which is following the Møller-Plesset partitioning, a pure mono-electronic (Fock-like) Hamiltonian is used. In the derivation by Andersson, Malmqvist, and Roos,[36] the CASSCF wavefunction Φ^{CAS} is adopted as the zeroth-order reference wavefunction

$$\left|\Psi^{(0)}\right\rangle = \left|\Phi^{CAS}\right\rangle . \tag{22}$$

The first-order interacting wavefunction is then expanded by means of excitation operators applied to $\left|\Psi^{(0)}\right\rangle$. Note that this approach represents an internal contraction scheme similar to what is described for *ic*-MRCI (Sec. 2.1.4). Without going into details (for more information see Ref. [36]), the configuration space, is divided into four subspaces: (1) V_0, the space spanned by $\left|\Phi^{CAS}\right\rangle$, (2) V_K, the space spanned by the orthogonal complement to $\left|\Phi^{CAS}\right\rangle$ in the restricted full CI space of the CAS; (3) V_{SD}, the space spanned by all single and double excitations from $\left|\Phi^{CAS}\right\rangle$ (not contained in V_K), and (4) $V_{TQ\ldots}$, the space containing all higher-order excitations (not included V_K and V_{SD}). Since the functions contained in the spaces V_K and V_{TQ} do not interact with $\left|\Psi^{(0)}\right\rangle$ via H, the *first-order interacting space* (FOIS) is given by V_{SD} and the first-order perturbed wavefunction $\left|\Psi^{(1)}\right\rangle$ is expanded into the functions $\left|\Phi_j^{SD}\right\rangle$ of V_{SD} as follows:

$$\left|\Psi^{(1)}\right\rangle = \sum_j C_j \left|\Phi_j^{SD}\right\rangle. \tag{23}$$

The expansion coefficients are given by the set of linear equations

$$\sum_j C_j \left\langle \Phi_i^{SD} \left| \hat{H}_0 - E^{(0)} \right| \Phi_j^{SD} \right\rangle = -\left\langle \Phi_i^{SD} \left| \hat{H} \right| \Phi^{CAS} \right\rangle. \tag{24}$$

$\hat{H}_0$ is the zeroth-order Hamiltonian, and $E^{(0)} = \left\langle \Phi^{CAS} \left| \hat{H}_0 \right| \Phi^{CAS} \right\rangle$ is the zeroth-order energy. The second-order energy $E^{(2)}$ is then computed from the expression

$$E^{(2)} = \left\langle \Phi^{CAS} \left| \hat{H} \right| \Psi^{(1)} \right\rangle. \tag{25}$$

The definition of the zeroth-order Hamiltonian is of crucial relevance. Anderson, Malmqvist, and Roos[36] defined as requirements that its formulation should lead to a rapidly converging perturbation expansion, equivalence to the Møller-Plesset Hamiltonian in the limiting case of a closed-shell reference wavefunction, and efficient computational implementation.

Defining a generalized Fock operator $\hat{F}$ [36] and rewriting Eq. (24) leads to the following expression

$$\left(\mathbf{F} - E_0 \mathbf{S}\right)\mathbf{C} = -\mathbf{V} \tag{26}$$

where $F_{ij} = \left\langle \Phi_i^{SD} \left| \hat{F} \right| \Phi_j^{SD} \right\rangle$, $S_{ij} = \left\langle \Phi_i^{SD} \middle| \Phi_j^{SD} \right\rangle$ and $V_i = \left\langle \Phi_i^{SD} \left| \hat{H} \right| \Phi^{CAS} \right\rangle$. Since the number of configurations created by double excitations from $\left|\Psi^{(0)}\right\rangle$ is larger than the space V_{SD}, linear dependencies will occur which are removed by diagonalizing **S** and deleting the eigenvectors corersponding to zero (or close to zero) eigenvalues.

Despite successful applications of the CASPT2//CASSCF protocol (CASPT2 energies on CASSCF-optimized geometries)[280,281] to study spectroscopy and photochemistry of small- to medium-sized molecules (see, e.g., Refs. [189] and [282]) the method has, however, several drawbacks.

Extensions to cope with these difficulties are discussed in the following paragraphs. For their review see, e.g., Refs. [283,282]

Using the standard Fock-matrix formulation of the zeroth-order Hamiltonian, a systematic error has been noticed in the description of processes that involve an alteration in the number of unpaired electrons.[284] To overcome this problem, a shifted zeroth-order Hamiltonian has been introduced[284] with modified diagonal elements of the Fock matrix, which are used to construct $\hat{H}_0$. The argument is that the physically correct diagonal Fock matrix elements should always resemble -IP (ionization potential) for an excitation out of an orbital and -EA (electron affinity) for an excitation into an orbital. This condition is naturally fulfilled for inactive and virtual orbitals whereas the Fock matrix element corresponding to an active orbital is a weighted average between -IP and -EA. Ghigo et al.[284] have proposed to remove this problem by modifying the Fock matrix elements depending on whether an excitation comes out of or goes into an active orbital. Practically, this procedure requires one empirical shift parameter, the IPEA shift. The benchmark studies on the excitation energies of nitrogen dimer have shown that the use of an IPEA of 0.25 a.u. reduces the average error of two lowest singlet and triplet excitation energies from 0.31 eV to 0.11 eV.[284] Recently, Zobel *et al.*[282] have performed extended studies on the performance of the CASPT2 to calculate the excitation energies of a large set (several hundreds) of organic molecules, including also the results of the benchmark set of more than 220 excited states of Schreiber *et al.*,[189] discussing the effect of IPEA shift. They have found that the IPEA corrections depended on the size of the system and on the basis set, which contrasts with the idea of using a universal empirical IPEA shift to correct for systematic CASPT2 error in the excited state calculations. Furthermore, comparisons of (i) previously reported CASPT2 (IPEA = 0.0 a.u.) and experimentally observed excitation energies of more than 50 medium-size organic molecules (356

excited states) and (ii) CASPT2 (IPEA = 0.0 a.u.) and benchmark full CI excitation energies of 13 di- and triatomic molecules (137 excited states) have resulted in the negligible errors of 0.02 and 0.05 eV, respectively. Based on these results, the authors have questioned the justification of the use IPEA shift for moderate-size organic chromophores and considered the CASPT2 (IPEA = 0.0 a.u.) as the method of choice to study excited states.[282]

The calculation of excited states with CASPT2 often leads to situations in which some of the expectation values of doubly excited configurations $E_i^{(0)} = \left\langle \Phi_i^{SD} \middle| \hat{H}_0 \middle| \Phi_i^{SD} \right\rangle$ are near the expectation value of the zeroth-order wavefunction $E^{(0)} = \left\langle \Phi^{CAS} \middle| \hat{H}_0 \middle| \Phi^{CAS} \right\rangle$. When this situation occurs, the second-order energy diverges and $\left| \Phi_i^{SD} \right\rangle$ is said to be an intruder state. The straightforward way to get rid of intruder states is to include $\left| \Phi_i^{SD} \right\rangle$ in the CAS wavefunction. This procedure, however, quickly makes the calculation unfeasible. Additional improvement of the CASPT2 method has been made by introducing an energy shift to remove singularities to handle intruder states in the perturbative scheme.[285–287] This shift removes the problem of too small energy differences. The originally implemented use of the level shift correction scheme (LS-CASPT2)[285] does not guarantee to find suitable values of the shift that removes singularities from all states of interest. The results of higher excited states may be significantly influenced by the choice of the shift value. In the *imaginary-shift* modification of LS-CASPT2[287] a formal imaginary shift is used in the denominators, which has the effect of replacing the singularities with a small distortion of the potential energy function. Another possibility to avoid the intruder state problem combines the MRPT approach with an improved virtual orbital complete active space configuration interaction (IVO-CASCI) reference function (IVOSSMRPT).[275]

The originally implemented perturbation theory of Roos and collaborators described above is formulated as state-specific perturbation theory, referred to in the literature as the single-state CASPT2 (SS-CASPT2), and also called "diagonalize then perturb." In this version, the zeroth-order wavefunction is first constructed by diagonalizing the Hamiltonian over the reference space, followed by the perturbation expansion over this zeroth-order function. Such an approach leads to serious problems when the perturbation (i.e. including the full two-electron interaction) mixes two states, *e.g.*, valence and Rydberg or covalent and ionic states, strongly. (see Ref [37] for discussion). In addition, the relative contributions of particular states often depend sensitively on the molecular geometry, *e.g.*, at the avoided crossing. In the multireference treatment, the relative contributions of the reference configurations in the reference and correlated wavefunctions differ significantly. To overcome this problem, the multistate formalism has been implemented in the CASPT2 method (MS-CASPT2).[37] In the MS-CASPT2 formalism, the energies of the perturbed states and the couplings between them are evaluated in a first step. In the second step, the resulting Hamiltonian matrix is diagonalized. An important consequence of this procedure is that intersections between states of the same multiplicity possess a proper conical shape, which is not the case of SS-CASPT2.[288,289] A further refinement of MS-CASPT2 is given through its extended version XMS-CASPT2.[290,291] For more detailed discussion on multistate versions of the perturbative treatment, including the use of Rayleigh–Schrödinger partitioning, see Refs.[292,293]

An important extension has been made by implementation of second-order perturbation theory restricted active space (RASPT2) method,[294] in which high excitation levels within the active space method are restricted.[113] As shown by Sauri *et al.*[295] the RASPT2 method provides the excitation energies with similar accuracy as the CASPT2 method. Thus, it extends the

applicability of the multiconfigurational perturbation theory to calculate excited state properties of much larger systems, not affordable with the CASPT2 method.

Other developments include implementation of (i) the third-order CASSCF-based perturbative approach CASPT3,[296] providing the excitation energies almost independent on the IPEA shift parameter;[297] (ii) CIPT2 method,[298] which combines MRCI and CASPT2 methods; (iii) analytical gradients;[299] and (iv) CASPT2-F12[300] method, which uses explicit R12-dependent correlation functions accelerating the basis-set convergence of the second-order energies. An additional problem not mentioned so far is the size-consistency of the multireference perturbation theory as discussed by Rintelman *et al.*[301] based on fully uncontracted MRMP2. Recently, the size-consistent multireference perturbation theory (SMRPT) based on the Rayleigh–Schrödinger approach[302] has been developed. Its performance has been tested mainly for dissociation processes, more examinations on the suitability for excited state calculations need still to be done.

An alternative approach to cope with some drawbacks of the CASPT2 method, including the size-consistency, has been introduced with the n-electron valence state perturbation theory (NEVPT), developed by Angeli, Cimiraglia, and collaborators.[40,71,278,279] Unlike the CASPT2 method, NEVPT uses the Dyall Hamiltonian,[303] which introduces two-electron terms in the zeroth-order Hamiltonian. The zero-order energies and the perturbed functions are obtained by partitioning of the first-order interacting space (FOIS) into subspaces, which are defined by the type of excited electrons (excited from the core or active spaces) and orbitals characterizing the excitation (active or virtual orbitals). The Hamiltonian is then diagonalized in these subspaces. The degree of contraction of the FOIS distinguishes between the strongly and partially contracted versions of NEVPT. This method has several advantages. Like CASPT2, it is spin pure due to its spinless formulation and invariant with respect to the orbital rotation. Moreover, it is size-

consistent and free from intruder-states , providing excellent results for excited state energies.[304–306] Since its implementation, several extensions have been made (see Ref [307] for recent updates), including the multistate version known as quasi-degenerate second order n-electron valence state perturbation theory (QD-NEVPT2).[308]

Recently, its time-dependent version, called time-dependent *n*-electron valence second-order perturbation theory (t-NEVPT2) for a CASSCF[309] and matrix product space (MPS)[310] wavefunctions, has been implemented. The t-NEVPT2 approach is equivalent to the fully uncontracted version (NEVPT), at lower computational scaling as compared to other contracted NEVPT approximations.

In developments alternative to the CASPT2 and NEVPT methods, a simplified multireference second-order Møller-Plesset (MRMP2) approach has been implemented. It includes versions that rely on the restricted active space configuration interaction (RAS-CI),[311,312] the quasi-complete active space (QCAS),[313,314] and complete active space configuration interaction (CASCI)[315] reference wavefunctions. Note that the multistate version of MRMP2[316,276,277] has long been known as the multi-configuration quasi-degenerate perturbation theory (MCQDPT).[317–321] Extension to the MCDQPT2 method, called extended multiconfiguration quasi-degenerate perturbation theory (XMCQDPT2), has been formulated by Granovski.[290] The difference between these two methods is the choice of the zeroth-order Hamiltonian, which is, in contrast to, *e.g.*, MS-CASPT2, invariant concerning unitary transformations within the model space. As a result, the XMCQDPT2 method is also invariant, and the perturbations are taken as the true two-particle operators. The intruder state problems of this method are handled using an intruder-state avoidance technique derived by Witek *et al.*[322]. The combination of the effective Hamiltonian used in

XMCQDPT2 with the internal contraction used in CASPT2 has led to the development of an extended multistate (XMS) CASPT2 method.[291]

Other approaches within the MRPT framework — in particular the generalized Van Vleck perturbation theory (GVVPT),[323] state-specific multireference perturbation theory (SS-MRPT) (Ref. [324] and references therein), and multiconfiguration perturbation theory (MCPT) (Ref. [325] and references therein) — have been tested on the calculations of ground and excited states of LiH and BeH_2,[326] discussing their performance with respect to the size-consistency and the intruder state problems.

The problem of the size-consistency of multireference perturbation methods has been discussed in further studies (see Ref. [327]). The size-extensive approaches invariant with respect to rotations among the active orbitals are size-consistent. The methods that are not invariant can be still size-consistent as long as the active orbitals are localized on the asymptotic fragments. Such behavior has been discussed based on the performance of orbitally non-invariant Unitary Group Adapted State Specific Multireference Second-Order Perturbation Theory (UGA-SSMRPT2)[327] to describe the fragmentation of small di- and triatomic in their ground and excited states.

Relevant for the development of MRMP theories is the introduction of the driven similarity renormalization group (DSRG) by Evangelista and collaborators.[328–330] The DSRG provides an alternative approach to treat dynamic correlation effects. It is based on a series of infinitesimal unitary transformations of the Hamiltonian controlled by a flow parameter related to an energy cutoff. Within this formalism, the multireference DSRG (MR-DSRG) and its second-order (DSRG-MRPT2) and third-order perturbation (DSRG-MRPT3) theories have been implemented. This approach shows a promising potential concerning limitations of the computational scaling as observed in the CASPT2 and NEVPT methods, as well as handling intruder states problems.

Recent developments of the DMRG-based algorithms for chemical systems have allowed for implementation of other MRPT methods in which the multireference problem is solved within the DMRG framework. They are reviewed in section 2.7.1.

2.5. MRCI with semiempirical Hamiltonians

Semiempirical methods have a history that parallels that of quantum mechanics.[331] From earlier Hückel-type[332,333] and Pariser-Parr-Pople[334,335] models for small organic systems, they have evolved to account for most of the elements in the periodic table,[336,337] including *spd* basis sets,[338] orthogonalization corrections,[339] parametrizations based on advanced algorithms,[340] and extensions into density functional theory.[341,342] Shared by all these developments, the goal of semiempirical methods has been to enable affordable large-scale simulations.[343]

Semiempirical methods, in general, start from an ab initio formalism and then neglect the selected terms in the Hamiltonian matrix. The errors introduced by the partially strong approximations are corrected by empirical terms, which are calibrated against experimental or ab-initio data.[331] The core approximation for many semiempirical methods is the *neglect of differential overlap* (NDO), which employs an HF SCF-MO treatment for the valence electrons on a minimal bass set and neglects three-center and four-center two-electron Integrals.[344]

Multireference methods have benefitted from semiempirical approaches as well. Some of these implementations are *in-house* programs developed for specific applications, such as, for instance, the MR-CISD based on configuration state functions using the MNDOC (*modified neglect of diatomic overlap for correlation*) parametrization[345] reported in Ref. [346] or the MR-CISD based on determinants built on INDO (*intermediate neglect of differential overlap*) described in Ref. [347].

One of the first general semiempirical MRCI implementations is due to Strodel and Tavan,[348] who developed an algorithm based on the *symmetric group approach* (SGA).[349] In their method, the reference space is defined by an individual selection (IS) procedure and the CI space is split into two sets of configurations: those strongly coupled to the references are treated variationally (MRCI), while the effects of the remaining configurations are accounted for by *second-order perturbation theory* (PERT). The IS/MRCI/PERT scheme is applied within the *orthogonalization model 2* (OM2) semiempirical Hamiltonian.[339]

Semiempirical implementations of GUGA MRCI with analytical gradients have been reported by Koslowski et al.[350] and later by Lei et al.[351] The former is a general program allowing arbitrary spin states and excitation levels. It was developed in the framework of the Hamiltonian models MNDOC[345] and OM2.[339] The implementation by Lei and co-workers is limited to MR-CISD, and it is based on the MNDO Hamiltonian.[352] It profits from doubly-contracted CI calculations for improved performance.

Due to the limited flexibility of the minimal atomic orbital basis used in semiempirical methods, none of the previous implementations take into account orbital relaxation as in an MCSCF procedure; and nondynamical electron correlation is recovered by the CI procedure itself.[350]

A different approach has been adopted by Granucci and Toniolo, who developed the semiempirical CI with floating-occupation molecular orbitals (FOMO-CI), including analytical gradients.[127] In this method, orbital occupations are allowed to assume fractional values between 0 and 2. These occupations are determined in each SCF optimization step for a single determinant, under the global restriction that they should sum up to the total number of electrons. After SCF convergence, the determinant formed from the floating-occupation orbitals is used as the reference

for a CI calculation. The FOMO-CI approach has been implemented for AM1, PM3, and PM6 Hamiltonians. Ab initio versions of this algorithm have also been developed.[128,353] Although the FOMO-CI is not strictly a multireference approach, its single-reference wavefunction emulates a CASSCF wavefunction by populating virtual orbitals. Thus, it correctly describes homolytic dissociation at MO level and provides a balanced treatment of degenerate orbitals.[354]

In all methods surveyed above, the semiempirical approximations are applied to the electronic Hamiltonian. By contrast, in the DFT/MRCI method,[355] the semiempirical approximations are applied to the CI matrix elements themselves. This approach, corresponding to a semiempirical MRCI based on Kohn-Sham DFT, is discussed in detail in Section 2.6.2.

An extensive benchmark of semiempirical full CI, CISDTQ, and MR-CISD results for vertical excitations based on OM*x* Hamiltonians has been published in Ref.[356]. As shown in Table 1, the mean value of the MR-CISD excitation energies calculated for the Mülheim molecular set tends to underestimate the best theoretical values by between -0.36 eV in the simplest model (OM1) to -0.22 eV in the most sophisticated one (OM3). For all models, standard deviations are about ~0.6 eV.

Table 1. Statistical results for a set of vertical excitation energies (in eV) for using MR-CISD/OM*x*, with references weight summing to at least 90% of the CI wavefunction. Theoretical best estimates are taken as reference. OM*x* results from the Supporting Information of Ref. [356] (Table S 22); DFT/MRCI and TD-B3LYP results from Ref. [357].

	OM1	OM2	OM3	DFT/MRCI	TD-B3LYP
Count [a]	166	166	166	104	104
Mean	-0.36	-0.35	-0.22	-0.13	-0.07
Abs. Mean	0.46	0.48	0.44	0.22	0.27
Std. Deviation	0.56	0.58	0.53	0.29	0.33
Max. (+) dev.	0.76	1.45	1.77	0.75	1.02
Min. (-) dev.	1.34	1.39	1.19	0.90	0.75

[a] Number of transitions included.

The use of MRCI with semiempirical Hamiltonians has gone beyond computation of vertical spectrum, and it has been used to explore other regions of the configurational space, including excited state isomerization processes[358] and conical intersections.[359–361]

The multireference semiempirical models have also been fundamental to enable nonadiabatic dynamics simulations based on direct approaches, where potential energies and couplings are determined simultaneously to the trajectory propagation.[362] In fact, the first *on-the-fly* surface hopping simulation[363] was performed based on the semiempirical molecular mechanics / parameterized valence bond (MMVB) method developed by Bernardi, Olivuccci, and Robb,[364] designed to simulate CASSCF potential energy surfaces. Since then, methods like FOMO-CI and MRCI/OM2 have been intensively explored for nonadiabatic dynamics,[365–372] pushing the boundaries regarding statistical ensembles[373] and research domains.[374]

The drawback of multireference semiempirical approaches is the same as in any semiempirical method, the quality and transferability of parameters. This issue is even more critical for dynamics simulations, which explore regions of the configuration space far away from those employed for parameterization. In some cases, there is evidence that semiempirical simulations may even provide qualitatively different results in comparison to those obtained by ab initio calculations.[375] Recent advances in Machine Learning algorithms for parameterization, however, may improve this situation. For instance, their use for reparameterization of OM2 has reduced the absolute errors in atomization enthalpies computed for a benchmark of six thousand $C_7H_{10}O_2$ constitutional isomers from 6.3 kcal/mol to 1.7 kcal/mol.[340]

2.6. Multireference Density Functional Theory

2.6.1. Nondynamical electron correlation in DFT

The treatment of nondynamical electron correlation is one of the most significant challenges faced by density functional theory.[376,377] Although the Hohenberg-Kohn theorem[378] can be generalized to deal with degenerate ground states,[379,380] the spectrum of methods available for routine quantum chemistry calculations is still limited, especially if compared to the immense popularity and success of the conventional Kohn-Sham (KS) DFT.

Several approaches have been pursued to derive strongly-correlated DFT or at least alleviate immediate problems within the KS framework, which, by construction, is based on a single-determinant representation of the ground state. Among these approaches, we may cite the spin-flip time-dependent DFT,[381,382] spin-unrestricted broken symmetry,[383] restricted open shell representations,[384] empirical corrections of nondynamical correlation,[385] semi-empirical configuration interaction with DFT,[355,386,387] hybrid wavefunction and DFT,[388,389] multiconfigurational DFT,[390–393] and ensemble DFT with fractional occupations.[379,394–396] It goes much beyond the scope of this review to cover all these fields. (An excellent introduction to the topic can be found in Ref.[397]). Instead, in the next sections, we will focus on four classes of methods, which adopt a multireference perspective. They are summarized in Table 2.

Table 2. Different approaches for including multireference character in DFT.

Type of method	Typical implementation	Functional type	Number of parameters[a]
Semiempirical MRCI with DFT	DFT/MRCI[387]	Conventional KS functionals	2 to 4
Hybrid wavefunction and DFT	CAS-srDFT[398]	Tailored functional	1
Multiconfigurational DFT	CAS-DFT,[397] MC-PDFT[392]	Tailored functional	0
Ensemble DFT	REKS[395]	Conventional KS functionals	0

[a] Apart from parameters used in the functional description.

2.6.2. Semiempirical MRCI with DFT

In 1999, Grimme and Waletzke introduced a combination of KS DFT and semiempirical MRCI (DFT/MRCI),[355] which was aimed at using DFT to recover dynamical electron correlation and MRCI to treat the nondynamical electron correlation. In their approach, the diagonal elements in the Hamiltonian matrix between two CSFs for a CI expansion are modified to

$$\left\langle \Phi_{\varphi\sigma} \left| \hat{H}^{DFT} - E^{DFT} \right| \Phi_{\varphi\sigma} \right\rangle = \left\langle \Phi_{\varphi\sigma} \left| \hat{H}^{HF} - E^{HF} \right| \Phi_{\varphi\sigma} \right\rangle + \Omega\left[p_J, p\left[N_0\right]\right] \tag{27}$$

while the off-diagonal elements are changed to

$$\left\langle \Phi_{\varphi\sigma} \left| \hat{H}^{DFT} - E^{DFT} \right| \Phi_{\varphi'\sigma'} \right\rangle = p_1 e^{-p_2 \Delta E^4_{\varphi\varphi'}} \left\langle \Phi_{\varphi\sigma} \left| \hat{H}^{HF} - E^{HF} \right| \Phi_{\varphi'\sigma'} \right\rangle \tag{28}$$

In these equations, σ represents the spin-coupling pattern and φ, the spatial occupation. Ω is a function that replaces all HF orbital energies by KS counterparts and also adds scaled two-electron contributions to the single excitation energies. Coulomb integrals are scaled by a parameter p_J and exchange integrals by $p\left[N_0\right]$; p_J is taken as a simple function of the fraction of exact exchange in the KS functional and $p\left[N_0\right]$ is empirically determined for each multiplicity.

For the off-diagonal elements (Eq. (28)), the original HF terms are rescaled by other two parameters, p_1 and p_2. The exponential function of the energy difference between the diagonal elements of the two CSF, $\Delta E_{\varphi\varphi'}$, quickly damps these elements to avoid double counting of dynamical correlation already included via DFT.

Recently, aiming at improving the performance of DFT/MRCI for the treatment of excitations of bi-chromophores, Lyskov et al.[387] have proposed small changes to the basic Grimme-Waletzcke Hamiltonian design, including a new damping function for the off-diagonal

terms. With these changes, the method, named DFT/MRCI-R, is spin independent and able to describe configurations with four open shells (as present in bi-chromophore excitations).

Either with the original DFT/MRCI or with DFT/MRCI-R, the CI expansion is controlled by a CSF-selection procedure based on an energy-gap criterion, which takes into account only the CSFs below a certain energy cut-off. This procedure, which is justified by the fact that the dynamical correlation is not supposed to be recovered by the CI procedure, leads to a dramatic reduction of the CI expansion and high computational efficiency.

Beck and co-workers have also implemented a GUGA-based version of the Grimme-Waletzke method.[386] In their approach, they use a correlation-only functional with 100% HF exchange but retaining the original off-diagonal damping format. Such choice implies in $p_J = p\left[N_0\right] = 0$, reducing the parametrization of the method from four to two parameters, p_1 and p_2. Moreover, the method is also spin independent. For technical reasons, the energy cut-off employed in the original DFT/MRCI cannot be used in a GUGA-based approach. Instead, the reduction of the CI expansion was achieved by freezing the highest virtual orbitals.

The evaluation of vertical excitations calculated for the Mülheim molecular set composed of 27 small organic molecules showed that the original DFT/MRCI method has excellent performance, with a mean absolute deviation of 0.22 eV for singlet excitations as compared to the best theoretical estimates (Table 1).[357] (In contrast, the same work showed that the mean absolute deviation for TD-B3LYP is 0.27 eV.) For a more challenging molecular set, like the Halons-9 composed of 9 Halons molecules, the mean absolute error of DFT/MRCI is 0.53 eV (against 0.85 eV of TD-B3LYP).[399] Spectral simulations for the spectrum of a metal-carbonyl complex ($Cr(CO)_6$), - including also TDDFT, coupled cluster, and CASPT2 calculations - showed that DFT/MRCI had by far the best performance in comparison to the experimental results.[400] Such

robustness of the Grimme-Waletzke DFT/MRCI is certainly impressive, especially considering that the original parameters fitted almost twenty years ago are still in use. Unfortunately, the method does not count on analytical energy gradients and couplings, which precludes many advanced usages.

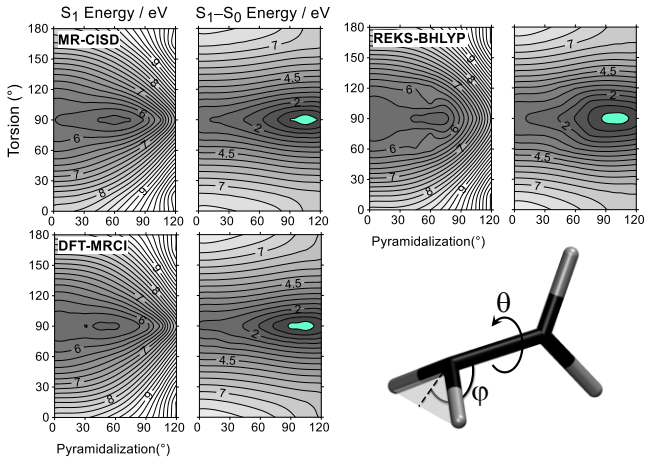

Figure 5. Topography of the S_1 state energy and of the S_1-S_0 energy gap around the conical intersection of ethylene calculated with MR-CISD, DFT/MRCI, and REKS(2,2). The green regions indicate the crossing seam. In the illustration, ethylene has $\theta = 90°$ and $\varphi = 45°$. Reproduced with permission from Ref. [401]. Copyright 2016 Springer Nature.

Going beyond vertical excitations, DFT/MRCI also has a good performance for describing regions of conical intersections. Figure 5, for instance, illustrates the S_1 energy and the S_1-S_0 energy gap around the twisted-pyramidalized conical intersection of ethylene calculated with different methods. The DFT/MRCI results are in quantitative agreement with the MR-CISD results.

2.6.3. Hybrid wavefunction and DFT

In hybrid wavefunction and density functional theories (WFT-DFT), the two-electron interaction is split into two complementary contributions for the short range (sr) and the long range (lr). Then, the exact ground-state energy is obtained variationally by minimizing the wavefunction Ψ in the multiconfigurational (M,N) wavefunction subspace including the long-range electron-electron interaction and adding a Hartree-exchange-correlation energy functional $E_{Hxc}^{sr,\mu}$ restricted to the short-range interaction:[389,398]

$$E_0 = \min_{\Psi \in S^{(M,N)}} \{ \langle \Psi | \underbrace{\hat{T} + \hat{V}_{ne} + \hat{V}_{ee}}_{\text{CAS: nondyn. correl.}} | \Psi \rangle + \underbrace{E_c^{dyn}\left[\rho^{\Psi}\right]}_{\text{DFT: dyn. correl.}} \} \tag{29}$$

where $\hat{T}$ is the kinetic energy operator, $\hat{V}_{ne}$ is the nuclear potential operator, $\hat{V}_{ee}^{lr,\mu}$ is the long-range two-electron repulsion operator, and $E_{Hxc}^{sr,\mu}$ is a functional of the CAS(M,N) density ρ^{Ψ}.[398] A parameter μ controls the transition between the lr and sr domains, such that when $\mu = 0$, KS-DFT is recovered and when $\mu \to \infty$, WFT is recovered. Thus, the problem can be split into a CAS calculation to obtain the nondynamical correlation and a density functional calculation to obtain the dynamical correlation. Such a partition has motivated a class of hybrid methods combining multiconfigurational wavefunctions theory (MC-WFT) and DFT, like the CAS-srDFT method.[398]

The range of applications of hybrid MC-WFT/srDFT has been recently extended into the excited-state domain. New developments, either based on time-dependent approach[389] or based on a combination of hybrid MC-WFT/srDFT with ensemble DFT[402,403] allow the determination of excitation energies and other properties.

The development of functionals for hybrid MC-WFT/srDFT approaches is an active research field (see Ref.[404] and references therein). A significant challenge faced by this approach is that the nondynamical correlation is not a purely range-dependent effect.[398] Despite several

promising results, hybrid MC-WFT/srDFT is still in early development stages, being applicable so far to atoms and small molecules only.

2.6.4. Multiconfigurational DFT

A class of methods, which we may call *multiconfigurational DFT* (MC-DFT), closely follows the conventional KS DFT formalism,[405] but modifies the KS Ansatz from a Slater determinant to a multiconfigurational reference, given as a linear combination of Slater determinants.[397]

Different from the hybrid WFT-DFT methods discussed in the previous section (in which the double counting of electron-correlation is avoided by splitting the electron-electron interaction treatment into short- and long-ranges), in MC-DFT, tailored exchange-correlation functionals are built to provide proper correlation balance.[391,397,406]

The difficulty is that ideally, the MC reference should exclusively account for nondynamical correlation, while the DFT part should exclusively recover dynamical correlation. Nevertheless, the MC wavefunction always includes a fraction of dynamical correlation, while DFT may contain a fraction of nondynamical correlation as well, as there is no clear separation between them.[377]

Depending on the MC reference, the MC-DFT approach gives rise to different approximations, as the GVB-DFT (*generalized valence bond DFT*), CAS-DFT (CAS wavefunction without orbital relaxation), CASSCF-DFT (CAS wavefunction with orbital relaxation),[384,407] and, more recently, DFVB (density-functional-based valence bond)[408] and MC-PDFT (multiconfigurational pair-density functional theory).[392,409] State-specific ground-state analytical gradients for MC-PDFT have recently been reported in Ref.[410]

The MC-DFT approaches work on a partially interacting frame, where the $\hat{V}_{ee}$ operator is present even in the non-interacting system. Kurzweil and co-workers[390] have shown that this partially interacting character is responsible for the MC wavefunction of the interacting system still to map onto an MC wavefunction in the non-interacting system. If a full non-interacting system were assumed, the MC wavefunction of the interacting system would map onto a single determinant in the non-interacting system, exactly like in conventional KS. (In case of degeneracy, the MC wavefunction would map onto a sum of determinants.)

2.6.5. Ensemble DFT

KS-DFT assumes a pure-state *v*-representability (PS-*v*R), which means that the ground state density can be mapped onto a density ρ_s corresponding to a single Slater determinant of a fictitious system of non-interacting particles subject to an external potential. Nevertheless, the PS-*v*R is a particular case, and the existence of the KS external potential for any fermionic ground-state system can be asserted only within an ensemble-state *v*-representability (ES-*v*R) condition, in which the density ρ_s corresponds to that of a weighted average of several KS determinants[411–413]

$$\rho_s(\mathbf{r}) = \sum_L \lambda_L \rho_L(\mathbf{r}), \quad 0 \le \lambda_L \le 1, \quad \sum_L \lambda_L = 1 \tag{30}$$

Such result has been demonstrated in practice for the C_2 molecule, whose ground state has multideterminant character.[414,415]

The ensemble theory has also been formulated for excited states.[379,396,416] For computing the first excited state, for instance, an ensemble with the ground state energy is built leading to

$$E_\omega = (1-\omega)E_0 + \omega E_1$$
$$\rho_\omega = (1-\omega)\rho_0 + \omega\rho_1 \tag{31}$$

Then, by variationally minimizing E_ω with respect to ρ_ω , the excitation energy is given either by

$$\Delta E_{01} = \frac{E_\omega - E_0}{\omega} \tag{32}$$

or by

$$\Delta E_{01} = \frac{dE_\omega}{d\omega} \tag{33}$$

Although the ES-*v*R approach opened the way for a rigorous multireference DFT approach, this field is clearly underdeveloped in comparison to conventional KS DFT. The leading development has been the *spin-restricted ensemble-referenced Kohn-Sham* (REKS) method,[394] which uses *quasi-degenerate perturbation theory* (QDPT) to derive a ground state energy in the form of

$$E_0 = \sum_L C_L E[\rho_L] \tag{34}$$

where C_L are functions of fractional occupation numbers. An optimal set of orthonormal one-electron orbitals (and their fractional occupations) can be then obtained from the minimization of the ground state energy with respect to the density.

The basic implementation of REKS relies on a 2 electron/2 orbitals subspace (REKS(2,2)). Excited states were made available in the state-averaged (SA) REKS and state interaction (SI) SA REKS.[395,417] This latter is an analog of the *generalized valence bond restricted CI* (GVB/RCI) able to treat the excited states on the same footing as the ground state. One of the intrinsic difficulties to extend the method to larger spaces is that the dimension of the QDPT equations is larger than the number of fractional occupations, which implies that additional restrictions must be imposed

to determine C_L. Recently, an implementation of (SA) REKS(4,4) has been reported, based on the GVB Ansatz.[418–420]

REKS has shown an outstanding performance for treatment of bond breaking, excitation energies, avoided crossings, and conical intersections.[421] The good performance of REKS(2,2) near a conical intersection is illustrated in Figure 5. Analytical gradients and nonadiabatic couplings have been made available recently for REKS(2,2).[422]

An alternative approach for calculating excitation energies based on a combination of ensemble DFT and hybrid wavefunction and DFT is discussed in Ref.[402]. The construction of functionals tailored for ensemble DFT is discussed in Ref. [403,423].

2.7. Emerging algorithms: DMRG, FCIQMC

The conventional CASSCF approach to the multireference problem, which uses a full configuration interaction (FCI) scheme, is limited by the size of an active space of approximately 16 electrons and 16 orbitals. This limitation is caused by the exponential scaling of the number of CSFs (or determinants) with the system size and makes the calculations of more extended system prohibitive. Two alternative approaches that avoid this limitation, the density matrix renormalization group (DMRG) algorithm and full configuration interaction quantum Monte Carlo (FCIQMC), are discussed in the following subsections.

2.7.1. DMRG

The DMRG method is a variational approximation to FCI, which scales polynomially with the size of the system.[424,425] It has been originally implemented to solve strongly correlated systems in condensed matter physics and later introduced into the *ab initio* quantum chemistry (QC-DMRG) by White and collaborators.[426,427] In DMRG, molecular orbitals occupy sites forming

superblocks, which are divided into subsystems called *block*s. In the two-site DMRG algorithm, the blocks are defined as the (i) *system* (*left, L*) block, (ii) *the environment* (*right, R*) block, and (iii) two sites in between. Using the spin-orbital occupation number representation, the four possible states of each spatial orbital σ are denoted as $|00\rangle,|10\rangle,|01\rangle,|11\rangle$. The total number of states for *L* and *R* blocks are 4^{n_L} and $4^{n-n_{L-2}}$, where *n* is the total number of correlated sites and n_L is the number of sites in the left block. The middle block contains 4^2 sites. The wavefunction of the superblock is defined as a tensor product space of the block states.

$$|\Psi\rangle = \sum_{a_L\sigma_L\sigma_R a_R} |a_L\rangle \otimes |\sigma_L\rangle \otimes |\sigma_R\rangle \otimes |a_R\rangle = \sum_{i_L i_R} |i_L\rangle \otimes |i_R\rangle \tag{35}$$

The exponential scaling of the number of parameters in equation (1) can be reduced by the number of many-electron states describing the *L* and *R* blocks with the threshold (*M*) for the maximum of states. DMRG wavefunction is optimized using a sweep algorithm. The sequence of steps for a single iteration consists of *blocking*, *diagonalization*, and *decimation*.[428]

The wavefunction is optimized via a series of macroiterations called *sweeps*. They proceed in the *left-to-right* and *right-to-left* directions and are repeated until the convergence is reached, *i.e*. until the energy change (in the middle of the sweep) between the sweeps is smaller than the given threshold. Since the orbitals are not divided into occupied and virtual, they all appear on an equal footing in the DMRG ansatz making it well-balanced for describing nondynamic correlation in multireference problems (see references in Ref [429]).

An important contribution to the development of the DMRG algorithm has been made by Ostlund and Rommer, who showed that the block states in DMRG could be represented as matrix product states (MPSs).[430] The variational matrix product space (MPS) ansatz,[431,432] is expressed, in connection with a Hamiltonian, as a matrix product operator (MPO).[433] The MPO-based

implementation (see Ref. [429] for a review of implementations) of the DMRG algorithm may be referred to as a second-generation DMRG algorithm in quantum chemistry.[434] Properties of the MPS wavefunction ansatz have been discussed by Sharma et al.[435] and Wouters et al.[436] A similar approach has been used in the construction of multifacet generalization of the graphically contracted function (MFGCF) constructed in terms of GUGA.[437,438] In contrast to the DMRG approach, which minimizes sequentially one site at a time keeping the others fixed, in MFGCF *all* arc factors are varied simultaneously during each optimization step. MPS efficiently represents the ground and excited states of one-dimensional quantum systems. Treatments of chemical systems with higher dimensions have led to introducing a generalization of the MPS structure, so-called Tensor Network States (TNS) (see Ref. [433] and references therein).

Since the first applications of DMRG in quantum chemistry, major developments, such as better initial guesses, non-Abelian symmetry, spin-adaption, parallelization, and orbital ordering and optimization have been made to improve the DMRG efficiency (for a review of algorithmic developments and application of DMRG-based methods in the field of quantum chemistry see Refs. [439–442]), including the use of a quantum informational approaches to evaluate the electron correlation and speed up the DMRG convergence.[443–445]

Implementations of DMRG in the CASSCF algorithm (see e.g. Refs. [446–448]) have allowed for multireference treatment using active spaces constructed from several tens of electrons and orbitals. To account for high-order descriptions of the dynamic correlation effects, post-DMRG methods have been implemented. These include DMRG linear response theory (DMRG-LRT),[449] DMRG-CIS, DMRG-TDA,[450] and DMRG random phase approximation (DMRG-RPA)[450,451] found by linearizing the time-dependent variational principle for matrix product states[452] or the canonical transformation theory.[453] Promising approaches to treat excited state problems are

provided by DMRG-MRCI,[69] DMRG-CASPT2,[454] DMRG-NEVPT2,[455] MPS-PT,[456] quasi-degenerate MPS-PT[457], and DMRG-TCCSD[458] methods. These implementations require evaluations of the fourth-order (or even higher-orders) reduced density matrix (4-RDM) of the reference wavefunction, which significantly limit the size of active spaces. This problem is solved via cumulant reconstruction, e.g. cu(4) approximation, as has been done in conjunction with state-specific CASPT2,[459,460] NEVPT2,[455] and MRCI.[70] Extension in a different direction is exampled by developing of a multistate version of the DMRG-CASPT2 method by Yanai et al.[461]

DMRG-based methods have been used to calculate the lowest excited states of small systems LiF,[461,462] CH_2,[463] HNCO,[464] C_2,[465] N_2,[466] Cr_2,[466] ethylene,[457,467] H_2O,[451,466] CsH,[468] CoH,[469] Fe_2S_2 ,[435] NiCO,[470] a prototype of carbonyl metal complex, and moderate-sized molecules, e.g. uracil[471] and indole[466] to demonstrate efficiency of implemented algorithms.

The feasibility of the DMRG approach to handle large active spaces in excited states calculations has been documented mainly on polymeric organic systems and complexes with transition metals. The DMRG-CASSCF method has been used to calculate low-lying excited states of conjugated polyenes, including β-carotene;[446] being able to reproduce previously unidentified low-lying dark states, and the energy gap between the singlet and high-spin states of polycarbenes,[472,473] (using the active space as large as (46, 46)), revealing a strong multireference character of the low-spin states. DMRG-based excited state calculations in combination with quantum information theory have been employed to evaluate the entanglement structure inside of narrow graphene nanoribbons.[474]

The applicability and scalability of post-DMRG methods — particularly DMRG-TDA,[451] perturbative treatments via CASPT2[459,475] or NEVPT2,[310,476] and variational treatment via MRCI[69] — have been demonstrated on excited state calculations of polyenes[69,310,459] polyacenes[475] and

poly(p-phenylenevinylene)[476] (for systems with up to 32 carbon atoms, using full-π-valence active space). It has also been demonstrated in the evaluation of the singlet-triplet gap of free-base porphyrin[69] and investigations of photochromic reactions, such as photoswitching of diarylethenes[461] and spiropyran-merocyanine interconversion.[477] DMRG and DMRG-CASPT2 have been used to study excited states of polymer associates, *e.g.*, optical properties of phenacene dimers[478] and the emitting state of naphthalene excimer.[479] They have also been applied to obtain ground and excited-state wavefunctions and energies for the Hückel-Hubbard-Ohno model of the hydrocarbon polymer dimers (e.g., polydiacetylene, polyenes, polyacetylenes) and to evaluate the excited state physical properties, including exciton energy, exciton binding energies, and optical phonons.[467,480–482] Implementation of DMRG-CI gradients has allowed for excited state optimization of polyenes up to $C_{20}H_{22}$ and discussion of exciton, soliton, and singlet fission phenomena.[483]

The DMRG-CASSCF method with extended active spaces has emerged as a promising approach to solve challenging problems in determining the ground state multiplicity and oxidation state of a transition metal coupled to organic chromophoric systems, as shown by calculations on Fe(II)-porphyrin,[441,447] oxo-Mn(Salen),[484] and iron-oxo porhyrfin[70] complexes. Calculations on [2Fe-2S][451,485,486] and [4Fe-4S][486] clusters, active sites in ferredoxins and other iron-sulfur proteins have identified low-lying excited states not previously described either by theory or experiment. Similarly, they have confirmed the experimentally observed structural and electronic properties of the S_1 state and provided candidates for S_2 state of the Mn_4CaO_5 cluster,[487] located at the center of the oxygen evolving complex in the photosystem II. Based on calculations by Sayfutyarova and Chan, performed on complexes with multi-metal sites, DMRG shows a large potential to evaluate

the magnetochemistry of complex transition metal systems, especially when the spin-orbit coupling is included.[485]

Recently, Hedegard and Reiher[488] have reported the implementation of an approach that couples a polarized embedding with DMRG to study the environmental effects on the first excited state of a water molecule and the blue-shift due to the channel rhodopsin protein on the $S_0 \rightarrow S_1$ excitation of the retinylidene Schiff base.

2.7.2. FCIQMC

The Full Configuration Interactions Quantum Monte Carlo (FCIQMC) method[489,490] combines QMC and FCI methodologies. It provides an alternative approach to the traditional FCI method, scaling with the number of determinants in the FCI space with a smaller prefactor than traditional FCI. In contrast to the (nonstochastic) iterative diagonalization FCI procedure to obtain CI coefficients, FCIQMC is based on the simulation of the imaginary-time Schrödinger equation (TDSE) performing stochastic population dynamics of a set of walkers residing on a basis state. These walkers are projected on the ground state by repeated application of an operator $\hat{P}$ defined as

$$\hat{P} = 1 - \Delta\tau\left(\hat{H} - S\mathbf{1}\right) \tag{36}$$

where S is a shift parameter used to control the walkers population, $\mathbf{1}$ is the identity operator, and $\Delta\tau$ is a time shift. With sufficiently small $\Delta\tau$, the application of $\hat{P}$ projects the initial state to the ground state of Hamiltonian $\hat{H}$. The method carries many similarities with diffusion Monte Carlo[491] and other projector Monte Carlo methods. The crucial difference lies in the sampling in FCIQMC, which is performed in a discrete basis set composed of basis states within the Slater determinant space that satisfy the antisymmetry of the exact fermionic wavefunction.

In FCIQMC, the projection is only performed on an average, leading to a stochastic sampling of the ground state wavefunction, avoiding the prohibitive storage of the full CI vector with coefficient of the CI expansions sampled by a population of signed walkers. The walkers are Kronecker delta functions that reside on a specific determinant D_i. In case the α-th walker resides on $|i_\alpha\rangle$, the corresponding Kronecker delta is δ_{i,i_α}. Each walker is characterized by a sign $s_\alpha = \pm 1$. Thus, with a set of N_w walkers, the signed number of walkers residing on $|i\rangle$ is $N_i = \sum_\alpha s_\alpha \delta_{i,i_\alpha}$. Using a population of walkers, the C_i expansion coefficient is proportional to the signed sum of walkers (N_i) ($C_i \sim N_i$). N_i can be positive or negative, the total number of walkers N_w is, however, defined as the sum of the absolute values of N_i.

The population dynamics consists of a set of stochastic processes:

(i) The spawning step, in which the child particles are created from their parents: For a walker α located on D_{i_α} a coupled determinant D_j is selected with probability $p_{gen}(j|i_\alpha)$. The probability to spawn a child for a time step $\delta\tau$ is given by

$$p_s(j \mid i_\alpha) = \frac{\delta\tau |K_{i_\alpha j}|}{p_{gen}(j|i_\alpha)} \tag{37}$$

where $K_{ij} = \langle D_i | H | D_j \rangle - E_{\mathrm{HF}}\delta_{ij}$. The sign of the child is the same as that of the parent if $K_{i_\alpha j} < 0$. If $p_s > 1$, then multiple copies are spawned on *j*.

(ii) The death/cloning step, in which parent walkers are stochastically removed: The probability the walker on determinant D_i dies at each cycle of the algorithm is given by

$$p_d = \tau\left(\langle D_i | H - E_0 | D_i \rangle - S\right) \tag{38}$$

If $p_d > 0$, the walker dies and it is cloned otherwise. The cloning is successful only if $S > 0$ and $\langle D_i | K | D_i \rangle < S$.

(iii) The annihilation step, in which newly spawned and surviving parent walkers are removed from the simulation in the case they are present on the same determinant but with opposite sign.

The iteration is terminated by merging parents and newly spawned walkers, which enter into the next time cycle. The simulation can be run in the shift S or a constant number of walkers N_w mode. For an extended period of imaginary time, the population of walkers on each determinant is proportional to the expansion coefficient C_i. The ground-state energy is obtained from the long-time average of the projected energy

$$\langle E \rangle = E_0 + \frac{\left\langle \sum_i N_i \left\langle D_0 \middle| \hat{H} \middle| D_i \right\rangle \right\rangle_\tau}{\langle N_0 \rangle_\tau} \tag{39}$$

where D_0 is the reference determinant and $\langle N_0 \rangle_\tau$ is the time-averaged number of walkers on it. The summation is performed over single and double excitations of D_0.

The originally implemented algorithm[489] was later improved to accelerate the convergence of FCIQMC method controlling the growth of walkers, referred in the literature as the initiator FCIQMC (i-FCIQMC).[492] Further improvements have been achieved using a semi-stochastic adaptation,[493,494] which combines deterministic and stochastic application of the projection operator.

Several approaches have been used to calculate excited states in the FCIQMC framework. Booth and Chan[495] have used a projection operator $\hat{P} = e^{-\beta^2 (H-S)^2}$, which for sufficiently large imaginary time β converges to the eigenstate of Hamiltonian H with energy being closest in the

energy to the chosen value *S*. Ten-no[496] has proposed the use of an FCIQMC, which stochastically samples the contribution outside the model space to the effective Hamiltonian in the energy-dependent Löwdin partitioning. The method can solve quasi-degenerate electronic states with bond dissociations and electronic excitations, as shown on small model systems of H_4 and N_2.

Other approaches have used modified probabilities and matrix elements that restrict the population dynamics to the orthogonal complement of lower lying states and projects out the next highest excited state,[497] or orthogonalization of FCIQMC wavefunctions against those for lower states.[498] These methods have been tested on calculations of the ground and excited states of small molecules and dimers, including , LiH, helium dimer, and carbon dimer. Tubman *et al.*[499] have used FCIQMC to generate a deterministic algorithm and calculated the ground and excited states of molecules as exemplified in carbon dimer model. Similarly, Thomas *et al.*[500] have implemented a multiconfigurational SCF treatment in which the optimization of linear determinant coefficients of the MCSCF wavefunction, solved stochastically via FCIQMC, and orbital rotation parameters, solved deterministically, are decoupled. The variational parameters for orbital rotations scale as $O\left(M^2\right)$, where *M* is the total number of orbitals in the full space. The method has been used to investigate a series of two-dimensional polycyclic aromatic hydrocarbons with up to a CAS(24, 24). A potential of this method to calculate excited state is in an implementation of a state-averaged CASSCF.

The so-called FCIQMC-CASSCF method[501] uses a two-step combination of a stochastic solution of the CAS configuration interaction secular equations within the FCIQMC approach and orbital rotations performed with an approximated form of the Super-CI method. It has been used to study the ground-state multiplicity of free and metal-containing porphyrin complexes (Fe(II)- and Mg(II)-porphyrin) with the active space up to CAS(32, 29).

Improvements of the excited state calculations using FCIQMC can be made with explicitly correlated approaches, the $[2]_{R12}$ method[502] and the explicitly correlated canonical transcorrelation approach,[503] denoted as FCIQMC-R12[504,505] and CT-FCIQMC,[505] respectively. These methods provide promising approaches to obtain accurate results of excited states of strongly correlated systems with only small basis sets.[505] It has been shown recently on the calculations of excited states of beryllium dimer that FCIQMC-R12 allows to fully converge to the basis set and correlation limit.[506]

Calculations on larger systems, in particular, singlet-triplet gaps of benzene and *m*-xylylene, have been performed using fully stochastic calculation with multireference linearized coupled cluster theory.[507] The zeroth-order wavefunction is computed with the FCIQMC using one population of signed walkers. A second population of walkers is used in a different set of stochastic processes to sample the first-order wavefunction.[508] This fully stochastic method allows for recovering the static correlation treating large active spaces and the dynamical correlation using perturbation theory. This method has been shown to provide better results of the singlet-triplet gap of the *m*-xylylene diradical than the CASPT2 method.

Recently Blunt et al.[509] have reported on developments on calculations of reduced density matrices in the excited-state FCIQMC approach[510] and performed calculations of excited-state dipole and transition dipole moments for LiH, BH, and MgO molecules.

Other stochastic approaches to the excited state calculations involve the use the projector Monte Carlo based on the Slater determinants[511] in which the imaginary-time propagator is used to obtain the excited states from the lower states, or Monte Carlo Configuration Interaction with state averaging.[512] Recently Holmes et al.[513] have proposed an approach to excited state calculations, which uses a combination of Heat-bath Configuration Interaction (HCI) algorithm[514]

and semi-stochastic perturbation theory.[515] The former belongs to the category of so-called s*elected configuration interaction plus perturbation theory* (SCI+PT) methods. The method has been used to calculate the low-lying potential energy surfaces of carbon dimer[513] and to investigate the challenging problem of the ground-state multiplicity of Mn-salen[515] and Fe-porphyrine[513] complexes employing active spaces CAS(28, 22) and CAS(44, 44), respectively.

2.8. Aspects of analytic gradients and nonadiabatic couplings

In this section, the main facts needed for understanding the theory of analytic gradients of MR methods will be reviewed. The following paragraphs aim to illustrate the main equations occurring rather than to present a rigorous derivation and leave some of the more technical details aside. For a more comprehensive review, we refer the reader to Refs [111,516]. First, it is worth realizing that the wavefunction given in Eq. (1) generally depends on the CI-coefficients **c** as well as the orbital coefficients **K**, i.e. $\Psi^I = \Psi(\mathbf{c}, \mathbf{K})$, while the Hamiltonian given in Eq. (3) depends on the molecular geometry **R**, i.e. $H = \mathrm{H}(\mathbf{R})$. Thus, the energy of state *I* is given in the following form (assuming a normalized wavefunction)

$$E^I = \left\langle \Psi^I \middle| H \middle| \Psi^I \right\rangle = \left\langle \Psi(\mathbf{c},\mathbf{K}) \middle| \mathrm{H}(\mathbf{R}) \middle| \Psi(\mathbf{c},\mathbf{K}) \right\rangle \tag{40}$$

Furthermore, the **c** and **K** coefficients are determined through the CI and MCSCF methods, respectively, and thus also depend implicitly on the geometry. The total derivative of Eq. (40) with respect to a geometric displacement *x* is of the following form.

$$\frac{\mathrm{d}E^I}{\mathrm{d}x} = \left\langle \Psi^I \middle| \frac{\partial H}{\partial x} \middle| \Psi^I \right\rangle + \frac{\partial E^I}{\partial \mathbf{K}} \cdot \frac{\partial \mathbf{K}}{\partial x} + \frac{\partial E^I}{\partial \mathbf{c}} \cdot \frac{\partial \mathbf{c}}{\partial x} \tag{41}$$

The three terms correspond to the Hellmann-Feynman term, the orbital response, and the wavefunction response. If the CI-coefficients are optimized variationally, which is the case for MCSCF and MR-CI, it follows that $\partial E^I / \partial \mathbf{c} = 0$ and, consequently, the wavefunction response vanishes. For state-specific MCSCF, also the orbital coefficients are optimal for the state of

interest, i.e. $\partial E^I / \partial \mathbf{K} = 0$ and only the first term in Eq. (41) has to be evaluated. In practice, evaluating this term requires the computation of 1- and 2-electron density matrices and contraction with the corresponding derivative integrals. In general, it is also necessary to consider orthogonality constraints for the CSFs and to resolve redundancies in the orbital optimization - regarding these more technical details the reader is referred to the literature. [111,516]

In the cases of SA-MCSCF or MR-CI, the orbital coefficients are optimized for the state-averaged energy or the reference state, respectively, by solving an equation of the form

$$\mathbf{f}_{\text{ref}} = \frac{\partial E_{ref}}{\partial \mathbf{K}} = 0 \tag{42}$$

where $\mathbf{f}_{\text{ref}}$ is the orbital gradient of the state-averaged energy or reference state. In this case, the derivative $\partial E^I / \partial \mathbf{K}$ does not vanish when the **c** vector for the individual state of interest is inserted. To compute the effect of this term, one first differentiates Eq. (42) with respect to a geometric displacement yielding in analogy to Eq. (41)

$$\frac{\mathrm{d}\,\mathbf{f}_{\text{ref}}}{\mathrm{d}\,x} = \frac{\partial \mathbf{f}_{\text{ref}}}{\partial \mathbf{K}} \cdot \frac{\partial \mathbf{K}}{\partial x} + \frac{\partial \mathbf{f}_{\text{ref}}}{\partial x} = 0 \tag{43}$$

Writing **B** for the orbital Hessian matrix $\partial \mathbf{f}_{\text{ref}} / \partial \mathbf{K}$, this equation can be recast as

$$\frac{\partial \mathbf{K}}{\partial x} = -\mathbf{B}^{-1} \frac{\partial \mathbf{f}_{\text{ref}}}{\partial x} = 0 \tag{44}$$

Insertion into Eq. (41) yields (under the assumption that the CI coefficients are optimized variationally)

$$\frac{dE^I}{dx} = \left\langle \Psi^I \middle| \frac{\partial H}{\partial x} \middle| \Psi^I \right\rangle - \frac{\partial E^I}{\partial \mathbf{K}} \mathbf{B}^{-1} \frac{\partial \mathbf{f}_{\text{ref}}}{\partial x} \tag{45}$$

The second part of the right-hand side of this equation can be evaluated most efficiently[517] by precomputing the term

$$\lambda_I^{\mathrm{T}} = -\frac{\partial E^I}{\partial \mathbf{K}} \mathbf{B}^{-1} \tag{46}$$

in the form of a linear equation system denoted the Z-vector equation:

$$\lambda_I^{\mathrm{T}} \mathbf{B} = -\frac{\partial E^I}{\partial \mathbf{K}} \tag{47}$$

Note that this equation needs to be solved only once for every state and is independent of the perturbation. Nonetheless, it is typically this step in SA-MCSCF and MR-CI gradient computations that can cause convergence problems. To summarize, there are three important computational procedures involved: (i) evaluation of the density matrices, (ii) solving of the Z-vector equation and updating the density, and (iii) contraction with the derivative integrals.

The initial implementations of MCSCF and MR-CI gradients appeared about 30 years ago[518–520] and a more general implementation for uncontracted MR-CI,[521] including state-averaged orbitals, was reported later.[111] The field is still active and newer developments are concerned with speeding up the computations through density fitting[522] and through optimizing the algorithms for graphical processing units[523] as well as with the replacement of the Z-vector Equation (47) by a numerical differentiation with respect to state-averaging weights.[524] In addition, different implementations for computing gradients at the DMRG level of theory have been reported in recent years.[477,483] Finally, it is worth noting that no implementation for gradients of internally contracted MR-CI has been reported because the evaluation of density matrices is significantly more challenging in this case. In the case of non-variational methods, such as perturbation theory, the $\partial E^I / \partial \mathbf{c}$ term in Eq.(41) no longer vanishes, which means that the formalism is significantly more involved. Nonetheless, gradients have been reported for internally contracted CASPT2[299]

and XMS-CASPT2.[291] A new implementation for fully internally contracted CASPT2 based on automatic code generation has been reported more recently.[525]

The nonadiabatic coupling matrix element between two states *I* and *J* with respect to a geometric displacement *x* is defined as

$$h_{IJ}^{x} = \left\langle \Psi^{I} \left| \tfrac{\partial}{\partial x} \Psi^{J} \right\rangle \right. \tag{48}$$

Combining all such elements computed for the different geometric displacements into a vector leads to the nonadiabatic coupling vector $\mathbf{h}_{IJ}$. Inserting Eq. (1) into Eq. (48) and applying the product rule for differentiation leads to the form

$$h_{IJ}^{x} = \sum_{i} c_i^I \tfrac{\partial c_i^J}{\partial x} + \sum_{ij} c_i^I c_j^J \left\langle \psi_i \left| \tfrac{\partial}{\partial x} \psi_j \right\rangle \right. \tag{49}$$

The first term in this expression, also called $h_{IJ}^{CI,x}$, depends on the changes in the CI-coefficients, whereas the second term, also called $h_{IJ}^{CSF,x}$, depends on the underlying CSFs, which is in turn determined by the MOs. The term $h_{IJ}^{CI,x}$ can be rearranged by differentiating Eq. (4) with respect to *x* and multiplying to the left with $\mathbf{c}^{J}$. Reorganizing the terms leads to the form

$$h_{IJ}^{\mathrm{CI},x} = \frac{1}{E^J - E^I} (\mathbf{c}^I)^{\mathrm{T}} \frac{\partial \mathbf{H}}{\partial x} \mathbf{c}^J \tag{50}$$

It is, thus, closely related to the theory of analytical gradients. Therefore, implementations of nonadiabatic coupling vectors can build on gradient codes already available.[526] Nonadiabatic couplings have been implemented for a variety of multireference methods discussed in the previous paragraph, e.g., MR-CISD,[527] SA-MCSCF,[528] and (X)MS-CASPT2.[529] For comparison, see the derivation of nonadiabatic coupling terms at EOM-CC level.[530]

An alternative way for computing nonadiabatic coupling proceeds by a finite difference scheme by considering that the nonadiabatic coupling is essentially the derivative of the overlap between

wavefunctions computed at different geometries. [531] The projection of the nonadiabatic coupling on a specific coordinate can then be evaluated in a finite difference scheme by computing the overlap between two wavefunctions at displaced geometries. Two general implementations,[531,532] applicable to multireference methods, have been made available and are widely used for trajectory dynamics simulations.

2.9. Diagnostics of multireference character, analysis of excited states

Understanding the results of multireference computations can be a formidable challenge, requiring patience and expert knowledge, since it is often necessary to analyze many interacting configurations and orbitals. Furthermore, the interpretation of the results can strongly depend on the orbital representation chosen. Whereas in the case of single-reference computations there is usually one set of well-defined canonical orbitals, there are different types of orbitals commonly used to discuss multireference computations. On the one hand, one has to differentiate whether state-averaged orbitals are computed that pertain to the whole computation or state-specific orbitals that are relevant to one specific state. On the other hand, one has to distinguish what quantity is used to construct the orbitals, e.g., a Fock matrix, density matrix, or transition density matrix. To exemplify this problem, four different representations are chosen to visualize the dominant pair of orbitals involved in the S_3 state of adenine at a displaced geometry (Figure 6). As a first option, the dominant configuration of the CI-vector, as expressed in terms of state-averaged natural orbitals (NOs), is considered and the two singly occupied orbitals are plotted. This is usually the default way to discuss excited states in multireference computations. The representation reveals that the state is primarily of $n\pi^*$ character. However, because the weight of this configuration amounts to only 47% of the total CI-vector, no more detailed information can be gained. To yield an orbital representation that is tailored to the state of interest, it is possible to

construct state-specific orbitals. As a first option, the natural orbitals are computed. These are obtained by diagonalization of the spin-free density matrix **D** of the state of interest according to

$$\mathbf{U}^{\mathrm{T}}\mathbf{D}\mathbf{U} = \mathrm{diag}(n_1, n_2, \ldots) \tag{51}$$

where the **U** matrix contains the NO coefficients and n_1, n_2, … are their occupation numbers. Figure 6 shows that the state-specific NOs possess the same overall shape as the state-averaged NOs, but clear differences are visible especially concerning the weakly occupied NO (shown on top). This orbital can be identified as a π* orbital, similarly to the state-averaged NO but it possesses different contributions on the three atoms shown on the left. In addition, it does not show the expected nodal structure of a pure π* orbital and partial admixture of an n orbital is seen.

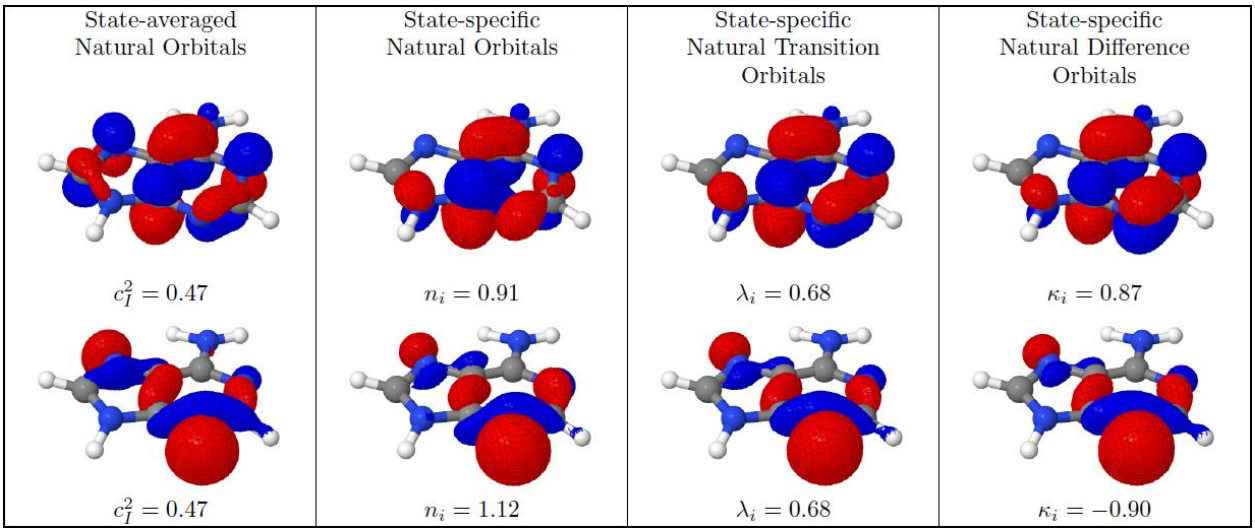

Figure 6. The dominant transition of the S_3 state of adenine visualized using different orbital representations. c_I^2 is the weight of the relevant CI configuration; n_i, λ_i, and κ_i, are the weights of the NOs, NTOs, and NDOs, respectively.

As a third option, the natural transition orbitals (NTOs) are computed through a singular value decomposition of the transition density matrix between the ground state and the excited state of interest.[533,534] The NTOs are displayed in the third panel of Figure 6 showing a clearly distinct

shape of the orbitals as opposed to the previous two representations. As opposed to the state-specific NOs, the NTO shown on top again possesses the expected nodal structure of a π* orbital. Finally, the natural difference orbitals (NDO), obtained through a diagonalization of the difference density matrix between the ground and excited state[192,535] are shown. Also, these possess somewhat altered shapes as opposed to the previous cases.

The above example illustrates that a precise assignment of excited-state character can be quite challenging even in fairly simple cases. More difficulties come into play in the cases of larger molecules or interacting chromophores,[534,536] or if orbital relaxation effects play a dominant role.[537] For this reason, an extended toolbox for the analysis of excited-state wavefunctions has been developed.[534,535,538,539] These tools have been made available for various multireference methods and computer codes.[534,535,540] As an alternative route, it is possible to compare wavefunctions constructed at different levels of theory (e.g., different one-electron basis set, molecular orbitals, or CI expansion) through computing the many-electron overlap integral between the two wavefunctions.[541] This has been achieved by applying a code that was originally developed for nonadiabatic dynamics simulations.[531]

Aside from the question of assigning the excited-state character, also the definition of multireference character itself is an active research topic, and no unique solution exists. One of the simplest ways of quantifying multireference character is by considering the weight of the closed-shell configuration in the ground-state wavefunction of a CASSCF computation. If this weight is significantly below 1, then a state can be considered as multireference. However, this strategy has two major problems. First, it is not size-consistent and the weight will decrease with larger system size. Second, the wavefunction expansion and, thus, the weights of the different configurations depend on the orbitals used. To obtain a more well-defined measure, it is favorable to consider the

NOs of a state of interest. It is now possible to evaluate the multireference character considering the occupations of the highest strongly occupied NO, and the lowest weakly occupied NO. Alternatively, it is possible to compute the total number of unpaired electrons and visualize their distribution using the density matrix as a whole.[542,543] We found the formalism by Head-Gordon[544] quantifying the deviations of the occupation numbers from 0 and 2 particularly intuitive (cf. Figure 18 in Section 3.3.5). Here, two indices can be defined based on the NO occupation numbers (n_i, defined in Eq.(52)) using the linear formula

$$n_U = \sum_i \min\left(n_i, 2 - n_i\right) \tag{52}$$

counting the total number of electrons and the non-linear formula

$$n_{U,nl} = \sum_i n_i^2 \left(2 - n_i\right)^2 \tag{53}$$

which suppresses contributions from dynamic correlation and focuses on strong correlation. In the simple case of two singly occupied NOs both measures, n_U and $n_{U,nl}$, give the value 2, whereas in general the $n_{U,nl}$ value is somewhat lower than n_U. In an alternative approach, the number of unpaired electrons is computed from a fractional orbital density in DFT.[545]

Further measures of multireference character and nondynamic correlation can be obtained by considering the two-electron density matrix.[546,547] Alternatively, the focus can be shifted from reduced electron density matrices to reduced orbital density matrices and measures for orbital entanglement can be computed.[548] In the case of excited states, the multiconfigurational character can be computed based on an entanglement measure computed from the NTO singular values.[549]

As an alternative, diagnostics have been developed that do not require performing a multireference computation at all. These are usually applied to judge the reliability of single-reference computations. As one option, the T_1[550] and D_1 diagnostics,[551] which are based on the

single-substitution vector in a coupled cluster computation, are sometimes applied. However, it has been pointed that out, by construction, these diagnostics measure orbital relaxation in the reference determinant and are not generally suited for characterizing multireference effects.[552] However, the D_2 diagnostic,[553] measuring double substitutions with respect to the reference determinant can be used as a more suitable criterion of multireference character.

3. Applications of multireference methods to molecular excited states

In this section, a series of representative classes of examples and applications is presented. This list has been chosen from the point of view of demonstrating the current progress in MR theory in terms of applications and, at the same time using these examples, to discuss interesting issues of excited states for important classes of chemical compounds. The discussion starts with a section on the excited states of diatomic molecules. They form a basic series of compounds which has been studied traditionally for a long time and can also serve as good examples to test the performance of new methods. Because of its biological interest, singlet oxygen has been given a special section. Polyenes and polycyclic aromatic hydrocarbons are of principal importance in chemistry. Especially the latter class of compounds has gained significant attention as new materials with attractive optoelectronic and magnetic properties. Nucleic acids, DNA strands, amino acids, and proteins are basic constituents in biological systems; the inclusion of their spectroscopic properties in the present MR context is important from both methodological perspective as also form the view of immense practical interest.

3.1. Diatomics and small molecules

Small molecular systems, such as diatomic molecules, are the natural candidates to test the performance of electronic structure methodologies. However, it is well known that their electronic

structures are complex and, therefore, difficult to describe from first principles. Ideally, full CI is the method that should be applied since it provides the exact solution in a given basis. However, even up to today it is computationally still very demanding and applicable only for describing bond-breaking, molecular properties, potential energy curves for ground- and excited states of systems with light elements and few electrons using small or medium-sized basis sets.[554–560] MR methods provide good possibilities to compute ground and excited states of diatomic molecules and their molecular properties, such as dissociation energies, electronic and rovibrational spectroscopy.

For diatomic molecules involving light atoms up to Ar, the characterization of the electronic structure and the spectroscopic parameters of the ground and excited states is well established by the use of multireference methodologies. These approaches have successfully predicted the properties of the ground and excited electronic states for the main group elements investigated lately.[561–580] Most of these studies were carried out using the *internally contracted* MRCI (*ic*-MRCI, see Section 2.1.4). Sivalingam et al.[65] have compared the performance of this method for the ground and excited states of selected diatomic molecules with the *strongly contracted* MRCI (SC-MRCI) method, showing that the two methods are bounded from below by the *uncontracted* MRCI (*uc*-MRCI). Also, Müller at al.[581] compared the performance of MRCI with MR-AQCC methods for the first row homonuclear diatomic molecules. More recently South et al.[582] have used the *multi-reference correlation consistent composite approach* (MR-ccCA) to calculate the potential energy curves for diatomic molecules containing third-row elements. The multireference methodology based on MR second-order Møller–Plesset perturbation theory (MR-MP2) and the semi-empirical MRCI with DFT (DFT/MRCI, see Section 2.6.2) were also used to

test their performance on the electronic excitation energies and spin–orbit matrix elements of diatomic molecules.[583]

Considering the performance of several schemes of *ic*-MRCI approaches in comparison to *uc*-MRCI, Sivalingam et al.[65] analyzed the dissociation of a single-bond in HF and a triple-bond in N_2, showing a good agreement between the *partially contracted* (PC-MRCI) and *fully internally contracted* (FIC-MRCI) with the *uc*-MRCI results. They also investigated the accuracy of the MRCI contracted methods to the vertical excitation energies for several singlet, doublet, and triplet states of a set of small diatomic molecules. Table 3 compares the performance of the PC-MRCI, FIC-MRCI and strongly contracted (SC-MRCI) in relation to *uc*-MRCI (see Ref.[65] for an explanation of the contraction schemes). From this set of data, one can highlight: (a) the reference relaxation computed with uc-MRCI (ΔER) plays a minor role; (b) FIC-MRCI misses 2%-3% of the correlation energy; (c) the error ranges are substantially larger for SC-MRCI with values about 4%-6%; (d) the orbital non-invariance calculated comparing SC-MRCI and SC-MRCI with localized virtual orbitals (SC-MRCI[LExt]) does not affect the excitation energies due to error cancellation; and (e) the excitation energies are in excellent agreement with the *uc*-MRCI results. The vertical excitation energies are more accurately reproduced because the ground- and excited-state errors are of a similar size for all of the three contracted methods. However, the error is fairly large for total energies.

Table 3. Deviations from the uc-MRCI correlation energy (in [mE_h]) for a test set of diatomic molecules. Data from Ref. [65] (Table. IX)

Molecule	State	PC-MRCI	FIC-MRCI	SC-MRCI	SC-MRCI(L.Ext)	ΔER
CH	$^2\Pi$	0.8	1.2	3.9	9.1	0.3
	$^2\Delta$		0.8	4.3	9.0	0.3
	$^2\Sigma^-$		1.6	4.3	9.0	0.6
	$^2\Sigma^+$		1.3	5.0	10.4	0.6
CN	$^2\Sigma^+$		3.7	9.3	23.1	0.6
	$^2\Pi$		4.1	9.5	24.4	0.9

	$2\text{-}^2\Sigma^+$		4.2	11.1	25.2	0.9
CO	$^1\Sigma^+$	3.3	4.5	11.3	27.5	1.5
	$^1\Pi$		6.1	15.9	33.4	1.7
	$^1\Sigma^-$		5.5	12.9	30.5	1.0
	$^1\Delta$		5.0	12.9	30.4	0.9
	$^3\Pi$	4.3	6.3	15.6	32.0	2.7
	$^3\Sigma^+$		5.7	13.7	31.3	1.0
	$^3\Delta$		5.6	13.2	31.0	0.9
	$^3\Sigma^-$		5.0	12.6	30.5	0.9
CO^+	$^2\Sigma^+$	2.4	3.1	9.0	19.3	0.9
	$^2\Pi$		4.4	10.6	22.0	1.8
	$2\text{-}^2\Sigma^+$		4.7	11.9	22.8	2.1
N_2	$^1\Sigma^+$	3.4	4.1	9.5	25.6	0.8
	$^1\Pi$		5.6	13.8	30.8	0.9
	$^1\Sigma^-$		6.1	12.7	30.4	1.0
	$^1\Delta$		5.8	13.1	31.1	1.1
	$^3\Sigma^+$	4.5	5.4	11.7	28.7	0.9
	$^3\Pi$		6.3	14.3	31.8	1.2
	$^3\Delta$		5.8	12.3	30.0	0.9
	$^3\Sigma^-$		5.6	12.5	30.4	1.2
O_2	$^1\Delta$	5.1	6.3	11.8	37.5	1.5
	$^1\Sigma^+$		5.7	11.2	37.5	1.2
	$^3\Sigma^+$	5.7	7.3	13.9	38.0	2.1
	$^3\Delta$		5.4	11.0	35.1	0.8
OH	$^2\Pi$	1.6	2.0	5.6	18.3	0.4
	$^2\Sigma^+$		2.4	5.8	18.6	0.9

More challenging is the accurate description of the diatomic systems involving, at least one transition metal atom. These molecules have several low-lying electronic states with different spin multiplicities closely spaced, which make their electronic structure much more complex and difficult to be treated. In 2000, Harrison[584] delivered an excellent overview concerning the reliability of molecular electronic calculations to describe the electronic properties of transition metal diatomic molecules.

Recently, Tennyson et al.[585] reviewed the latest progress on the performance of the ab initio methodologies to describe the molecular electronic properties of open-shell diatomic molecules containing a transition metal. Among several properties analyzed in their review, the dissociation energy calculated by single and multireference methods using large basis sets for the ground state neutral and charged transition metal oxides were compared with experimental data. They showed

a similar error, around 500 – 2000 cm^{-1} (1.43 – 5.72 kcal mol^{-1}) for a total dissociation energy of 45,000 – 60,000 cm^{-1} (128.66 – 171.54 kcal mol^{-1}). Right afterwards, the dissociation energies of a database of diatomic transition metal molecules based on the performance of the single reference coupled cluster theory were discussed by Fang et al.[586] and Cheng et al.[587] This dataset (called 3dMLBE20), consisting of 20 diatomic molecules containing 3d transition metals, was set up by Xu et al.[588] in a work comparing the performance of CCSD(T) with several DFT methods. Concerning the DFT performance for the bond dissociation energy of bimetallic diatomic molecules that involve metal–metal multiple bonds, one should also consider the recent work of Bao et al.[589] An excellent study of a collection of 60 transition metal diatomic molecules was performed lately by Aoto et al.[590] In this work, the authors used a composite computational approach based on coupled-cluster theory including mutireference effects based on the internally contracted multireference coupled-cluster (ic-MRCC), with basis set extrapolation, inclusion of core-valence correlation, and corrections for relativistic effects. They compared their results for the dissociation energies with experimental data and with those calculated by Fang et al.,[586] Cheng et al.[587] and Xu et al.[588] as well as analyzed the performance of several DFT methods.

The high accuracy of the current *ab initio* calculations is achieved to a lesser degree for the excitation energies of the transition metal diatomics. The density of closely spaced states connected to the complex nature of these excited states makes the accurate description more challenging. Tennyson et al.[585] have collected several electronic excitation energy calculations for diatomic transition metal oxides and compared with available experimental data, showing that the errors often exceed 1000 cm^{-1}, especially for the higher lying states. However, for the highest accuracy calculations, the error is around 100 cm^{-1}.

The accurate description of the electronic structure of polyatomic systems, even with a small number of atoms and electrons, remains a current challenging problem, despite the sophisticated theoretical methods available. The calculation of the vibration-rotation energy levels and transition intensities requires a high-quality description of the potential energy surface (PES) and dipole moment surface (DMS), which should be treated, in principle, by multi-reference methods. Tennyson[591] provided a review of the state-of-art of obtaining high-accuracy rotation-vibration spectra of the simplest triatomic molecule, H_3^+. This review can also be taken as an example of the extent of problems that one has to face for an accurate description of the PES and DMS of small molecules by electronic structure methodology. The theoretical description by means of single and multireference methods of the ground and excited states of triatomic molecules, including PES, DMS, and rotation-vibration spectrum can be found in the following recent calculations and references therein.[75,591–609]

A good example showing the importance of accurately describing the global PES of a triatomic molecule is the case of ozone. In 2013, Dawes et al.[606] determined an accurate PES based on extended *ic*MRCI calculations which were carried out with several reference states starting from an SA-CASSCF wave function using the 13 lowest singlet states and dynamic weighting. These calculations did not show the spurious reef in the entrance channel of the $O + O_2$ reaction which was previously obtained in other computational studies using internally contracted multiconfigurational methods.[610–612] Using this PES, Dawes et al. were able to reproduce the temperature dependence of the exchange rate coefficients as well as the large kinetic isotope effects (KIEs) in wavepacket-based quantum-scattering calculations. They also showed that the reef affects the highest lying vibrational levels and that its absence was important for achieving agreement with experimental level progressions. It was also shown in previous work[75] that the

internal contraction introduced small but kinetically significant errors in the bottleneck region of the PES of the reaction H + O_2.

Recently, Powell et al.[601] revisited the asymptotic region of the ozone surface. They explored some of the factors contributing to the spurious entrance channel energy barrier through systematical calculations performed by uncontracted and internally contracted MRCI and by uncontracted MR-AQCC methods with extrapolation to the complete basis set limit (CBS). Figure 7 summarizes these results together with the reference potential energy curve as recommended by Dawes et al.,[606] which was taken as reference. It was found that the *ic*-MRCI error indeed plays a significant role in producing the reef feature as compared to the *uc*-MRCI results. The *uc*-MRCI and *ic*-MRCI+Q results agree very well and produce only a very small barrier of 15 – 25 cm^{-1}. However, this good coincidence has to be regarded as a fortuitous fact and not due to a systematic agreement. The *uc*-MRCI+Q approach gave a monotonically decreasing curve, which was, however, too attractive in comparison to the reference PES. In short, these results provide a snapshot of the current situation to accurately describe the asymptotic region of the ground-state energy surface of ozone.

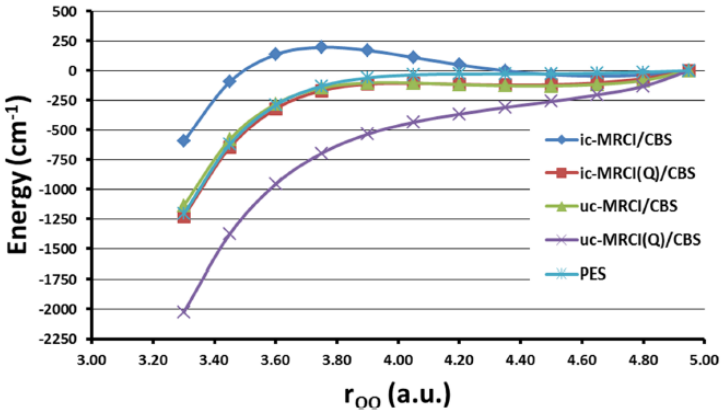

Figure 7. Comparison of *ic*-MRCI, *uc*-MRCI, *ic*-MRCI+Q, and *uc*-MRCI+Q at the CBS limit. The PES is the Dawes et al.[606] used as reference, Zero of energy is set at r_{OO} = 4.95 a.u., roughly 243 cm^{-1} below

the asymptote, as explained in the text of Ref.[601]. Reproduced with permission from Ref. [601]. Copyright 2017 AIP Publishing.

The high-level characterizations of the PESs for polyatomic systems are also of fundamental importance in the dynamical studies of nonadiabatic processes. In these studies, a full-dimensional set of coupled diabatic PESs is built by fitting large numbers of highly accurate ab initio electronic structure data points. As good examples, one can see the studies of the hydroxymethyl (CH_2OH) dissociation[613–616] and the $H_2CC \rightleftharpoons HCCH$ isomerization unimolecular reaction[617–619].

3.2. Singlet oxygen photosensitization

The ground state of oxygen O_2 is a triplet ($X^3\Sigma_g^-$) followed by two singlet states, $a^1\Delta_g$ and $b^1\Sigma_g^+$. The lowest singlet state, $a^1\Delta_g$, is a reactive state playing an important role in atmospheric chemistry, materials science, biology, and medicine (phototherapy as well as immunosuppression).[620,621] For the generation of the oxygen singlet state, photosensitizers (PS) are frequently used.[622] They indirectly populate the lowest singlet states of oxygen through an excitation energy transfer (EET) process, avoiding the spin-forbidden process in the isolated oxygen molecule.

The scheme in Figure 8 shows the different steps leading to the creation of singlet oxygen by EET.[623] The first step is the excitation of the PS within the singlet manifold, with subsequent relaxation to S_1. This process is followed by intersystem crossing to the triplet manifold and relaxation to T_1. The PS in the triplet state may encounter a triplet oxygen molecule in the environment, and, in this case, an excitation energy transfer from ^3PS to $^3O_2$ may create singlet oxygen. Alternatively, ^3PS may return to S_0 before reacting with $^3O_2$, in which case the process is

non-productive. In principle, both singlet states mentioned before can be excited. It has been found, however, that at least in solution the $b^1\Sigma_g^+$ state rapidly decays to $a^1\Delta_g$.[624] Thus, the term singlet oxygen is usually associated with the latter singlet state.

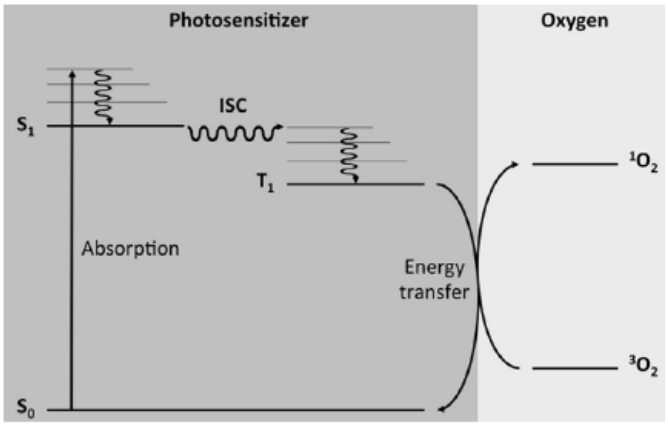

Figure 8. Scheme for generating singlet oxygen through excitation energy transfer from the photosensitizer in the triplet state. Reproduced with permission from Ref. [623]. Copyright 2017 Elsevier.

Since the electronic states have open-shell character, treatment of the whole photosensitization process requires treating open-shell systems, a fact that makes MR methods the appropriate choice. The interactions between the PS or solvent molecules with O_2 are relatively weak.[625] Even though their effects on the spectral shifts on the $X^3\Sigma_g^-/a^1\Delta_g$ and $X^3\Sigma_g^-/b^1\Sigma_g^+$ transitions for O_2 are quite small, the transition moments can be affected significantly because these transitions are forbidden in the isolated molecule. For example, for the isolated O_2 molecule the lifetime of the $a^1\Delta_g$ state is about one hour, whereas there is a dramatic reduction to the microsecond range for typical solvents.[620]

The initial relaxation of the PS and its internal conversion to the T_1 state is a unimolecular process that can be treated by standard quantum chemical methods.[626,627] However, the situation becomes more challenging once the interaction between the PS and oxygen is considered. The

theory of nonadiabatic reactions for weakly coupled systems, needed to describe such a process, has been developed by Harvey and Aschi[628] based on nonadiabatic Rice–Ramsperger–Kassel–Marcus (RRKM) theory. However, its strict application to the present case of singlet oxygen generation poses prohibitive computational cost due to the large geometric dependence of the intermolecular interactions in the PS/O_2 complex and the strong variation of the coupling strength. Therefore, a more cost-effective procedure based on inverted Marcus theory has been developed by Bai and Barbatti[629] for the discussion of the crucial step of the photosensitization. This step is written as an internal conversion process (Eq. (54)) between the singlet-coupled PS and O_2 components in their initial triplet and final singlet states, respectively:

$$^1\left[{}^3\mathrm{PS} + {}^3\mathrm{O_2}\right] \rightarrow {}^1\left[{}^1\mathrm{PS} + {}^1\mathrm{O_2}\right] \tag{54}$$

Figure 9a shows a one-dimensional picture in parabolic potentials in terms of an intramolecular coordinate **R**, and in Figure 9b an extended picture including an intermolecular tuning mode **D**. These situations should be applicable to the intersystem crossing of $^3\mathrm{PS} \rightarrow {}^1\mathrm{PS}$ or the internal conversion of Eq. (54). All necessary data for applying Marcus theory are being calculated in orthogonal segments of the **D**-**R** space in the spirit of the divide-to-conquer approach.

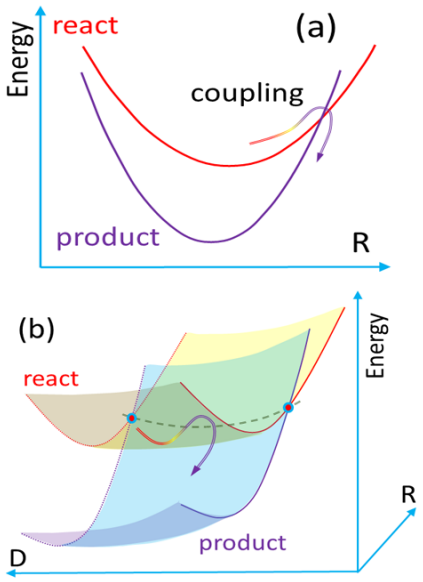

Figure 9. (a) Inverted Marcus model for energy transfer when PS is distorted along R. (b) Extension of the inverted Marcus model along the intermolecular (tuning) coordinate **D** and intramolecular (crossing) coordinate **R**. Reproduced from *J. Chem. Theory Comput.* **2017**, *13*, 5528–5538. Copyright 2017 American Chemical Society.

As a test example, the interaction of O_2 with 6-aza-2-thiothymine (6n-2tThy) had been chosen since it shows a relatively large singlet oxygen yield. The calculation of the excited states of the isolated molecules has been performed at MS-CASPT2 level using a CAS(10,7) for 6n-2tThy and a CAS(6,6) for O_2. The calculations on the PS-O_2 complex including excited states and nonadiabatic couplings have been performed at SA-CASSCF(12,9) level. The results show a strong dependence on the direction of approach of O_2 with rates differing by a factor of 1000. In a follow-up work, expanding the simulations to fifteen different PS-O_2 incidence directions, rates were found to span five orders of magnitude.[625] Singlet oxygen yield in the $b^1\Sigma_g^+$ state is larger than the one in the $a^1\Delta_g$ state by a factor of 10.

Extended CASPT2 calculations have also been performed by Serrano-Pérez et al.[630] on furocoumarins (psoralens) used in PUVA (psoralen+UVA) therapy. In this work, the kinetics of the triplet state generation and the EET has been calculated by using Fermi's Golden Rule. For the required coupling matrix elements, the respective spin-orbit coupling terms have been used in the first case and an energy gap based method for the EET process. An empirical constant value was assumed for the density of states. From reaction rates and lifetimes, the efficiency of the phototherapeutic action for different members of the furocoumarin family could be predicted.

α-Terthiophene (α-T) produced by Asteraceae plants shows an allelopathic effect, which prevents germination of competing seedlings and kills insect larvae. The phototoxicity of α-T is believed to be the ability to generate singlet oxygen. In this context, the singlet oxygen generation process by a single thiophene molecule has been investigated by Sumita and Morihashi.[631] CASSCF calculations augmented by an MRMP2 approach were used to perform geometry optimizations, minimum-energy-path (MEP), and intrinsic reaction coordinate (IRC) investigations. The calculations show that the exciplex of triplet O_2 and triplet thiophene may lead either to singlet O_2 generation (Eq. (54)) or 2+4 cycloaddition with the latter reaction being the favorable one.

The availability of a high concentration of oxygen is crucial for the efficient formation of singlet oxygen. This requirement can pose problems in applications where the singlet oxygen should be created under oxygen-depleted conditions as is the case, for example, of vascular damaged tumors. For such a case, alternative photosensitive oxygen carriers, which can release singlet oxygen upon activation through light irradiation, have been proposed, e.g., in the form of tetraantraporphyrazine.[632] This molecule can eject singlet oxygen due to four anthraceneendoperoxide (APO) moieties by which the phophyrazine core is substituted. A model

endoperoxide, the cyclohexadieneendoperoxide (CHDEPO), has been investigated by Martínez-Fernández et al.[633] by means of CASSCF(14,12) and MS-CASPT2 calculations. This system shows an eight-fold degeneracy containing four singlet and four triplet states. In addition to the static investigation of the energy surfaces at the CASPT2 level, surface hopping dynamics investigations at CASSCF level have been performed using the surface hopping in adiabatic representation including arbitrary couplings (SHARC).[634]

CASSCF and CASPT2 have been the basis for investigation not only of the singlet oxygen formation from CHDEPO carriers but of its dissociation as well.[633] Figure 10 shows the homolytic O-O cleavage mechanism leading ultimately to the formation of benzoquinone and H_2. In Figure 11, the alternative pathway of singlet oxygen formation is shown. The surface hopping dynamics simulations show no reversion to the original CHDEPO. The yield of cycloreversion is found to be 30%, in good agreement with experimental results. The leading photodeactivation process is O-O homolysis with a yield of 65%, which is also in line with experiment.

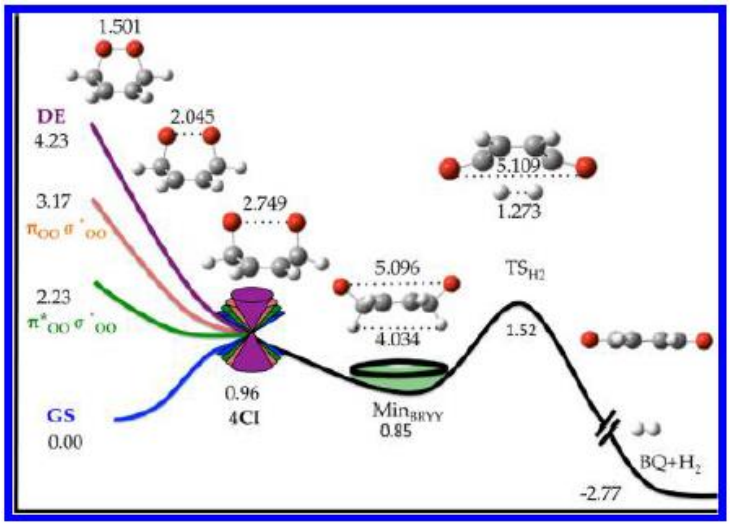

Figure 10. Global static picture of the O−O homolysis mechanism of CHDEPO based on MEP calculations. Final energies relative to the ground state (GS) minimum (in eV) were calculated at MS-CASPT2//SA4-CASSCF(14,12)/ANO-RCC level of theory. Bond distances in angstroms. The state labeling

was inferred from the final products of the MEP. The label 4CI stands for a degeneracy of four singlet states. Reproduced from *J. Chem. Theory Comput*. **2015**, *11*, 406-414. Copyright 2015 American Chemical Society.

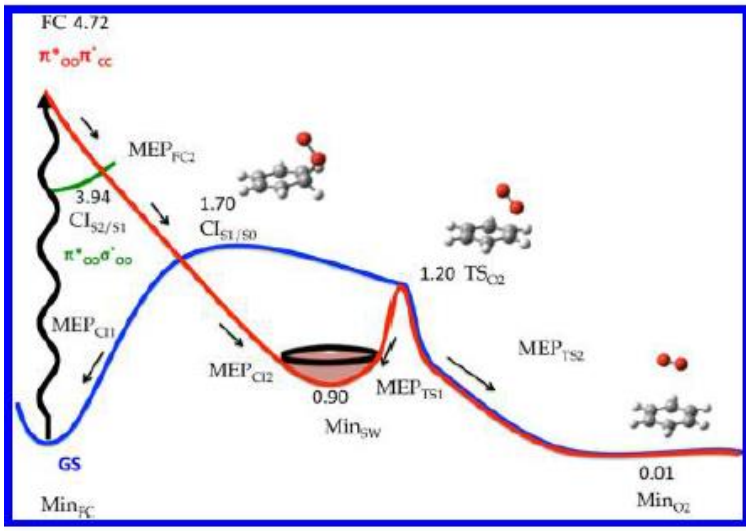

Figure 11. Global static picture of the cyclo-reversion mechanism of CHDEPO based on MEP calculations. Final energies relative to the GS minimum (in eV) were calculated at MS-CASPT2//SA4-CASSCF(14,12)/ANO-RCC level of theory. Reproduced from *J. Chem. Theory Comput*. **2015**, *11*, 406-414. Copyright 2015 American Chemical Society.

The prohibitive cost associated with the calculation of large PS has led to the use of hybrid approaches, combining DFT and multireference methods for different tasks. Boggio-Pasqua et al.[623], for instance, have recently studied the self-sensitized photo-oxygenation and singlet oxygen thermal release in a dimethyldihydropyrene (DHP) derivative (Figure 12), using broken symmetry unrestricted DFT followed by calculations of TDDFT excitation energies and CASSCF spin-orbit couplings. Figure 12 shows the energy transfer process creating singlet oxygen, the formation of a ring-opened structure **2** and of an endoperoxide (EPO) **2-O$_2$**.

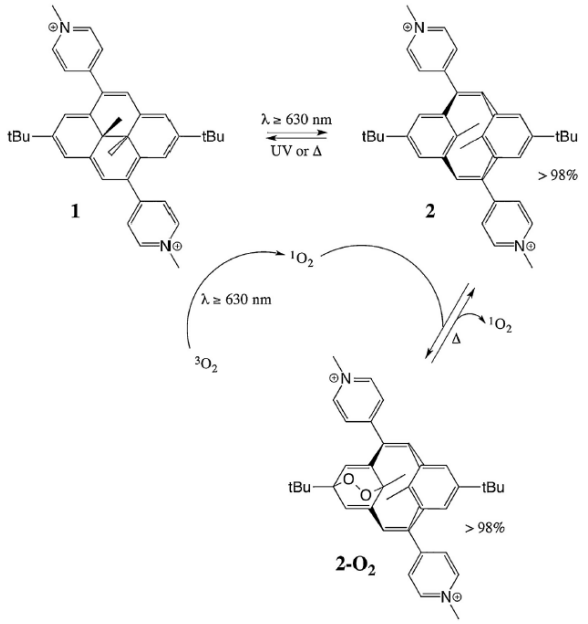

Figure 12. Conversion processes between **1**, **2** and **2-O₂**. Reproduced with permission from Ref. [623]. Copyright 2017 Elsevier.

The following steps are discussed in detail. Electronic excitation and isomerization lead to the open ring cyclophanediene (CPD) isomer **2**:

$$\mathbf{1}(S_0) + h\nu \rightarrow \mathbf{1}(S_1) \rightarrow \mathbf{2} \tag{55}$$

Alternatively, **1**(S_1) can also switch to **1**(T_1) via ISC

$$\mathbf{1}(S_1) \rightarrow \mathbf{1}(T_1) \tag{56}$$

1(T_1) can act as a PS and produce singlet oxygen via the reaction

$$\mathbf{1}(T_1) + O_2(T_0) \rightarrow \mathbf{1}(S_0) + O_2(S_1) \tag{57}$$

which is equivalent to Eq. (54). The singlet oxygen reacts with **2** to form an EPO **2-O₂**

$$O_2(S_1) + \mathbf{2} \underset{\Delta}{\rightleftarrows} \mathbf{2\text{-}O_2} \tag{58}$$

which can release singlet O_2 again on warming.

In the work of Boggio-Pasqua et al.,[623] photophysical and photochemical reaction paths were calculated. The ISC pathway, Eq. (56), was characterized by an easily accessible crossing between S_1 and T_2. The latter state can then decay to T_1 by internal conversion. The EET of Eq. (57) was characterized as a quasi-barrierless process. The thermal pathway for EPO-CPD formation (Eq. (58)) based on a concerted mechanism involves a barrier of 0.61 eV, whereas a reverse energy barrier of 0.93 eV was found, consistent with the experimental findings.

3.3. Conjugated π systems

3.3.1. Excited States of Polyenes:

The study of the electronic spectra of linear all-trans polyenes has a long tradition,[635] which is explained by the general importance of understanding conjugated π systems for the development of molecular orbital (MO) and valence bond (VB) theory, and the fact that polyenes play an important role as model chromophores in biological systems such as carotenoids or retinal.

The electronic states can be characterized by the C_{2h} symmetry of the molecular framework. Additionally, it is customary to label the states by an additional index + or -, which has first been introduced by Pariser based on degenerate transitions ($i \rightarrow j$') and ($j \rightarrow i$'),[334] having its origin in the alternacy symmetry of Hückel or Pariser–Parr–Pople (PPP) theory. Orbitals *i* and *i*' are called conjugate pairs, where *i* represents an occupied orbital and *i*' and unoccupied one. The occupied orbitals are numbered from the highest one down and the unoccupied orbitals from the lowest one up. The *minus* state is antisymmetric, and the *plus* state is symmetric, with respect to the interchange of conjugated pairs of orbitals.[316] The doubly excited states $(i)^2 \rightarrow (j')^2$ behave like *minus* states as does the ground state. The *minus* states are termed covalent states while the *plus* states are ionic states according to VB theory.[316,636] The +/- labeling is strictly valid only in zero

differential overlap (ZDO) methods but is often used also in cases where this classification does not strictly apply.

Many of the general rules governing the spectra of polyenes have been deduced by a comparison of PPP calculations including double excitations and VB calculations,[636] the latter being important for the correct description of the covalent states. It was found that noncovalent (ionic) states, which include the optically allowed transitions such as $^1B_u^+$ were well described in the SCF-MO approach with single-excitation CI. The optically inactive covalent states such as $^1A_g^-$ and $^1B_u^-$ are well described by VB theory. For an accurate description at SCF-MO level, higher excited configurations had to be taken into account.

This picture has been extended by PPP multireference CI (MRD-CI)[637] and also applied to the investigation of infinite polyenes.[638] A VB description of covalent excited stats in polyenes up to a chain length of $C_{28}H_{30}$ with emphasis on the 2^1A_g state can be found in Ref. [639] Full configuration interaction PPP (PPP-FCI) calculations have been performed for the polyene series concentrating on the analysis of the bright, ionic $1^1B_{1u}^+$ and the dark, covalent $1^1B_u^-$ states, using a new reparameterization scheme for the one- and two-electron integrals.[640]

Before discussing the evolution of electronic states for the polyene series up to larger chain lengths, we want to analyze the results for the smaller, first members of the series up to octatetraene, including ethylene, for which more extended calculations can be performed.

In the case of ethylene, one main question for the correct description of the first valence excited state, the ionic $1^1B_{1u}^+$ state, arose concerning the actual valence character of this state since SCF and π-CASSCF calculations showed the π* orbital to have significant Rydberg character. Without going into the details of the history of ethylene calculations (see, e.g., Refs. [641–643]) we

only want to refer to the need of including dynamic σ-π correlation,[644,645] especially for accurate calculations of ionic states. The need for including σ-π polarization has been taken up in extended MR-CISD and MR-AQCC calculations.[646] and analyzed in detail in Refs. [647] and [648]. This polarization is not only of interest for ethylene but needs to be also considered in larger polyenes and polyacenes.[316]

In Table 4, vertical and, where available, also adiabatic excitation energies are collected for the $1^1B_{1u}^+$ and $2\,^1A_g^-$ states using different methods with emphasis on MR approaches. For butadiene, the ionic $1^1B_{1u}^+$ state is about 0.2-0.3 eV lower than the covalent $2\,^1A_g^-$ state for most of the MR calculations. For hexatriene, these two states become isoenergetic in most MR results. For octatetraene, the $2\,^1A_g^-$ is the lowest one in most cases. The semiempirical OM2 results,[649] which are also based on the MR concept, fit quite well into the series of *ab initio* results. In case of the stability of the $2\,^1A_g^-$ state, they support the experimental data shown in Table 5 for butadiene and hexatriene in contrast to the MR *ab initio* data (see the discussion on the comparison with experimental vertical excitation energies below).

In Table 4, there are also results for two SR methods. In the extended algebraic diagrammatic construction (ADC(2)-x) method, the treatment of double excitations is extended to first order as compared to the standard zeroth-order treatment. It shows, however, the stability of the $2\,^1A_g^-$ significantly overestimated, at least in comparison to the other results listed in this table. However, increasing the level of theory to the ADC(3) method raises the $2\,^1A_g^-$ excitation energies by more than 0.5 eV in the cases of hexatriene[650] and octatetraene.[651] The CC3 results for

hexatriene and octatetraene are significantly shifted beyond the higher end of MR results. CCSD excitation energies for the $2\,^1A_g^-$ state[189] (not shown) are much too high by 0.6 to 1.4 eV.

At this point, it is interesting to analyze the performance of TDDFT especially for the calculation of the $2\,^1A_g^-$ state, which requires the inclusion of at least double excitations as discussed above. Linear-response TDDFT has been applied to the calculation of the excitation energies of the $1^1B_{1u}^+$ and $2\,^1A_g^-$ states.[652] It is noted that this method only accounts for single excitations. Therefore, it is surprising that TDDFT describes the $2\,^1A_g^-$ state pretty well, for BLYP in the Tamm-Dancoff approximation (TDA) it is even the lowest state for the larger polyenes. This situation has been analyzed in more detail in Ref. [653], in comparison to the ADC(2)-x method mentioned above. For N = 14, TDA/BLYP values are 3.17 and 2.79 eV for the $1^1B_{1u}^+$ and $2\,^1A_g^-$, respectively, in good agreement with the experimental values given in Table 5. The wavefunction of the $2\,^1A_g^-$ is a linear combination of HOMO-1 $\rightarrow$ LUMO and HOMO $\rightarrow$ LUMO+1 single excitations, and not by double excitations. In a more recent paper, Shu and Truhlar[654] have argued that the $2\,^1A_g^-$ state of butadiene can be accurately described by local functionals because they allow an approximate description of the relevant multireference effects. On the contrary, it has been argued by Mewes at al.[651] that in the case of octatetraene the agreement between TDA/BLYP and experiment is largely spurious considering that TDA/BLYP is neither able to describe the doubly excited character of the $2\,^1A_g^-$ state nor the bound excitonic character of the $1^1B_{1u}^+$ state.

At spin-flip (SF)/TDA level, the wavefunction shows for the $2\,^1A_g^-$ state the same single excitation character as found for TDDFT and thus, does not show any significant qualitative

improvement. The explanation for the relative good numerical performance of TDDFT in spite of a qualitatively wrong character of the excited state is given in Ref. [653] by the observation that the amount of double excitation character increases in the ground state with increasing chain length. In fact, this growth is more important for the ground state than for the $2\,^1A_g^-$ state, a situation which is only insufficiently accounted for by the exchange functional. Thus, it can be expected that at some point the errors due to missing double excitations in the ground state will match those for the $2\,^1A_g^-$ state leading to a favorable error compensation.

Table 4. Comparison of vertical (adiabatic in parentheses) excitation energies (eV) for the all trans structures of butadiene, hexatriene, and octatetraene computed with different theoretical methods.

	$1^1B_{1u}^+$	$2\,^1A_g^-$	Method
Butadiene			
	6.39	6.35 (5.17)	QDVPT[655,656]
	6.23	6.27	SS-CASPT2[657]
	6.47	6.83	MS-CASPT2[189]
	6.21 (5.93)	6.31 (5.49)	MRMP[658]
	6.20	6.59	MR-AQCC[659]
	6.46	6.91	SC-NEVPT2[455]
	5.84	5.73	OM2/MRCI$_s$(σ,π)[649]
	6.69	5.19	ADC(2)-x[653]
	6.58	6.77	CC3[189]
Hexatriene			
	5.01	5.20	SS-CASPT2[657]
	5.31	5.42	MS-CASPT2[189]
	5.10 (4.84)	5.09 (4.17)	MRMP[658]
	5.35	5.60	SC-NEVPT2[455]
	4.94 (4.67)	4.98 (4.08)	DFT/MRCI[660]
	4.96	4.61	OM2/MRCI$_s$(σ,π)[649]
	5.44	3.99	ADC(2)-x[653]
	5.58	5.72	CC3[189]
Octatetraene			
	4.42 (4.35)	4.38 (3.61)	SS-CASPT2[661]
	4.70	4.64	MS-CASPT2[189]
	4.66 (4.34)	4.47 (3.50)	MRMP[658]
	~4.8 (4.76)	~4.8 (3.75)	QD-PC2[662]
	4.47	4.71	SC-NEVPT2[455]
	4.24	4.08	DFT/MRCI[660]
	4.41	3.92	OM2/MRCI$_s$(σ,π)[649]
	4.67	3.24	ADC(2)-x[653]
	4.94	4.97	CC3[189]

In Table 5, experimental estimates of gas phase vertical and 0-0 transitions as presented in Ref. [649] (Table S4) are collected. For the polyenes up to $N = 8$ gas phase data are available. For the bright $1^1B_u^+$ state, the band maximum usually agrees with the 0-0 transition. According to Franck-Condon considerations,[663] the vertical excitation might be higher by no more than about 0.1 eV. For the forbidden transitions, techniques such as resonance Raman excitation profiles are used to determine the vibrational progressions whereas 0-0 transitions are readily available. For the larger polyenes, gas phase transitions have to be extrapolated using dielectric and refractive properties of the solvents. Necessary spectroscopic data are not always available. In such cases, linear extrapolation against 1/(N + 1) have been made. In case of methylated compounds, additive corrections can be made. For more details on these procedures see the discussion in Ref. [649], Supporting Material.

Comparison of the computed vertical excitations of Table 4 with the respective experimental data (Table 5) for the bright $1^1B_u^+$ state shows for the MR methods a reasonable agreement with a certain, expected scattering. The most critical case might be the smallest member in the series, the butadiene. In case of the dark transitions to the $2^1A_g^-$ state, the butadiene and hexatriene cases are problematic. In particular, the MR results for the vertical transition are located unequivocally higher than that for the $1^1B_u^+$ state. For a detailed analysis of computed results see, e.g., Ref. [656]. For the 0-0 transition, however, the computed location of the $2^1A_g^-$ state is found in good agreement with experiment. In case of the $2^1A_g^-$ state for hexatriene, a near degeneracy of the $1^1B_u^+$ and $2^1A_g^-$ states (4.94 – 4.98 eV) is found in DFT/MRCI (Section 2.6.2) calculations,[660] whereas two seemingly conflicting sets of experimental observations ($2^1A_g^-$ state at 5.21 eV[664]

and 4.26 eV (band origin))[665,666] have been reported. It is found, however, in the DFT/MRCI calculations that geometry relaxation has a much more pronounced effect on the $2\,^1A_g^-$ state stabilizing it at 4.08 eV. This situation is brought into coincidence in the computational study by positioning the $2\,^1A_g^-$ state slightly above $1^1B_u^+$ for the vertical excitation (in agreement with the larger experimental excitation energy of 5.21 eV), but assigning the lower experimental excitation value to a relaxed $2\,^1A_g^-$ state. This result is also in agreement with the broad peak in the absorption spectrum,[667] which has been explained by an ultrafast internal conversion to a lower-lying singlet state.

Table 5. Experimental estimates for gas phase excitation energies of polyenes (in eV). Data taken from Ref. [649] (Table S4).

	$2\,^1A_g^-$		$1^1B_u^+$		$1^1B_u^-$	$3\,^1A_g^-$
N	$\Delta E_{0\text{-}0}$	ΔE_v	$\Delta E_{0\text{-}0}$	ΔE_v	$\Delta E_{0\text{-}0}$	$\Delta E_{0\text{-}0}$
4	5.40[668]	5.67[668]	5.75[668]	5.95[668]		
6	4.25[665]	4.57[665]	4.93[669]	4.93[669]		
8	3.57[670]	4.02[671]	4.40[670]	4.40[670]		
10	3.04[671]	3.39[671]	4.02[671]	4.02[671]		
12	2.70[671]	3.04[671]	3.75[671]	3.75[671]		
14	2.42[671]	2.75[671]	3.54[672]	3.54[672]	3.46[672]	
16	2.20[673]	2.59[673]	3.39[a]	3.39[a]	3.11[b]	
18	2.04[673]	2.40[673]	3.26[a]	3.26[a]	2.83[b]	
20	1.90[673]	2.29[673]	3.17[a]	3.17[a]	2.59[b]	2.47[673]
22	1.78[673]	2.16[673]	3.07[a]	3.07[a]	2.42[b]	2.24[673]
24	1.70[673]	2.06[673]	3.01[a]	3.01[a]	2.21[b]	1.99[673]
26	1.58[673]	1.97[673]	2.95[a]	2.95[a]	2.07[b]	1.85[673]

[a] Ref. [673], shifted by $\Delta E_{s,m}(1^1B_u^+) = 0.61$ eV; [b] Ref. [673], shifted by $\Delta E_{s,m}(1^1B_u^-) = 0.41$ eV.

The evolution of the lowest singlet experimental 0-0 excitation energies with the number of π-electrons is shown in Figure 13A for four states of interest, the dark covalent minus states $2\,^1A_g^-$, $3\,^1A_g^-$, and $1\,^1B_u^-$ and the bright $1^1B_u^+$ state. Figure 13B demonstrates the linear behavior of the excitation energies with $1/(N + 1)$ — N being the number of π electrons — and the increasing gap

between the $1^1B_u^+$ and $2^1A_g^-$ states. Figure 13A shows that for the chain lengths calculated, the $2^1A_g^-$ state is always the lowest. For $N \geq 14$ the $1^1B_u^-$ state becomes S_2, but for $N \geq 20$ this role is taken over by the $3^1A_g^-$ state. Figure 14 displays the evolution of the same four states computed at the CASCI-MRMP level for vertical excitations.[674] The shape of the curves shown in this figure is quite similar to the one based on experimental data (Figure 13). In the calculation, the $1^1B_u^-$ also becomes more stable than the $1^1B_u^+$ state for $N \geq 14$ and the $3^1A_g^-$ curve crosses the one for $1^1B_u^+$ at $N = 22$.

In Figure 15, the energetic dependence of the three lowest covalent states and the ionic state vs. polyene chain length is displayed based on DMRG-SCF and matrix product state t-MPS-NEVPT2 calculations. The complete π-valence active DMRG-SCF method gives the correct ordering of the three covalent states but shows the ionic $1^1B_u^+$ state significantly too high, even above the $3^1A_g^-$ state. This result drastically shows the afore-mentioned importance of σ-π electron correlation, which also cannot be replaced by an extensive treatment of the π space alone. The inclusion of dynamic electron correlation via the t-MPS-NEVPT2 method stabilizes preferentially the $1^1B_u^+$ state, which is now the lowest state along the polyene series. Thus, no crossing of this state is observed with the covalent $2^1A_g^-$ and $1^1B_u^-$ states, in contrast to the just-discussed experimental and MRMP results.

In Figure 16, the vertical excitation energies calculated by means of the two-electron reduced density matrix (2-RDM) from the anti-Hermitian contracted Schrödinger equation (ACSE) are shown for the $2^1A_g^-$ and $1^1B_u^+$ states. In this formalism, a CASSCF calculation

provides the static electron correlation energy, and the following ACSE approach adds the dynamic electron correlation. MRPT2 results are given in the figure for comparison. Figure 16 shows that in the ACSE approach the $2\,^1A_g^-$ is always the lowest state, in agreement with experimental findings. The ACSE excitation energies agree well with the MRPT2 results up to five C=C bonds, but are significantly destabilized for longer chains in comparison to the latter values and also in relation to the experimental values (Table 5). The excitation energies of the $1^1B_u^+$ state are always somewhat too large.

Recently, the combination of DMRG with the CASPT2 method in the form of a DMRG-CASSCF/CASPT2 has been reported,[125] which brings significantly enhanced computational efficiency when using extended active spaces. The method has been applied to polyenes up to twenty carbon atoms with a full π valence space. So far, only ground state calculations have been performed.

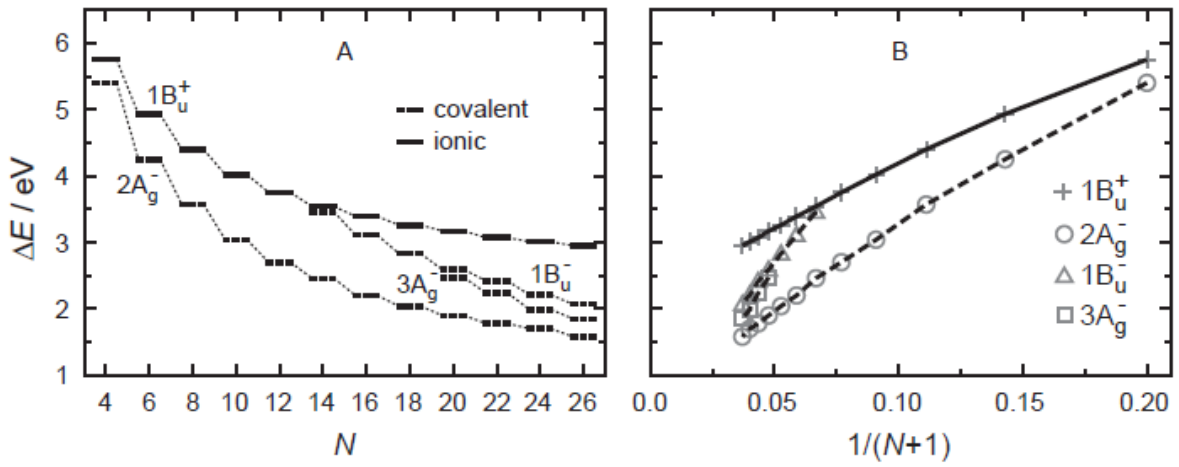

Figure 13. Gas phase values for the experimental 0-0 excitation energies of singlet states in polyenes with 4 ≤ N ≤ 26 π-electrons as functions of *N* (A) and 1/(N + 1) (B) constructed from various sources. Reproduced with permission from Ref. [649], (Fig. S16). Copyright 2012 AIP Publishing.

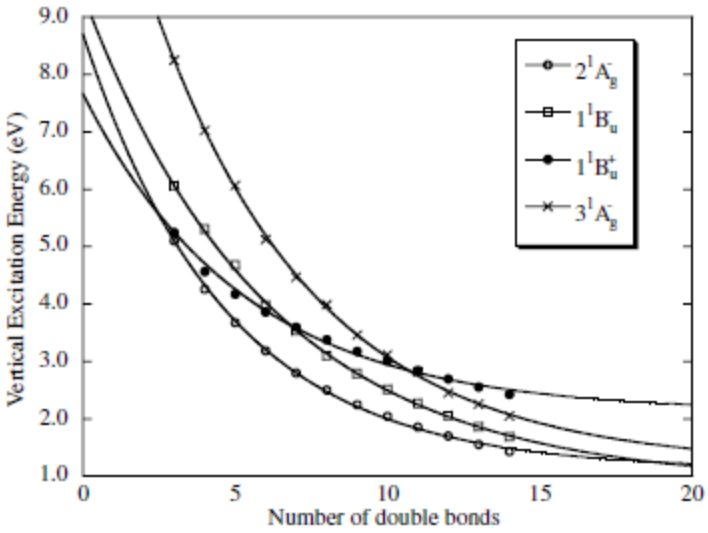

Figure 14. Vertical excitations computed with the CASCI-MRMP method. Reproduced with permission from Ref. [674]. Copyright 2004 Elsevier.

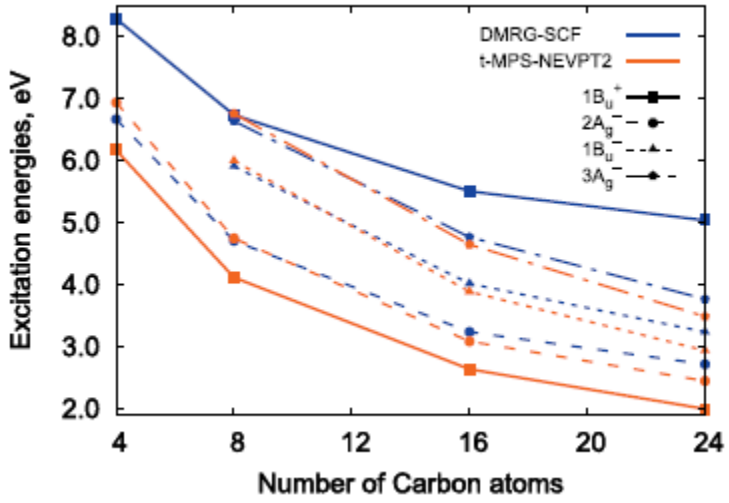

Figure 15. DMRG-SCF and t-MPS-NEVPT2 excitation energies with the cc-pVDZ basis set for polyenes ranging from N= 4 to N = 24. Reproduced with permission from Ref. [310]. Copyright 2017 AIP Publishing.

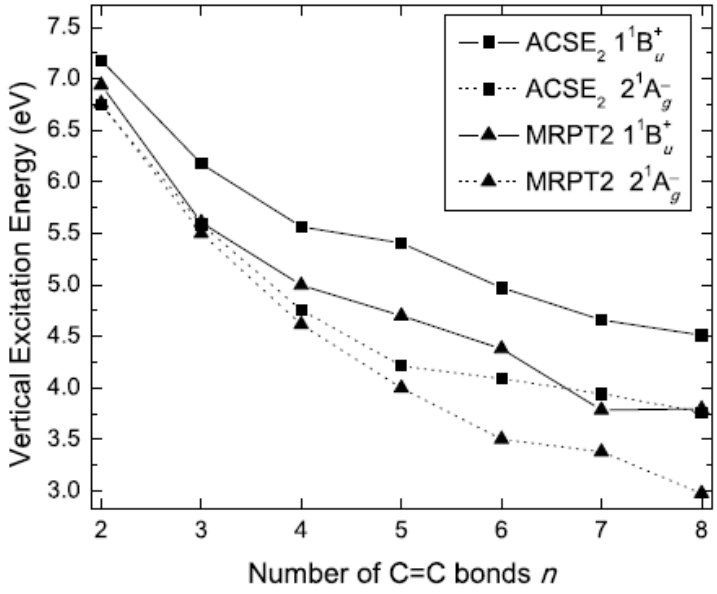

Figure 16. Vertical excitation energies for the polyene series using the MRPT2 and $ACSE_2$ methods. Reproduced with permission from Ref. [675]. Copyright 2015 AIP Publishing.

3.3.2. Protonated Schiff bases:

Protonated Schiff bases (PSB), with the general formula CH_2-$(CH)_{n-2}$-NH_2^+ (PSB*n*), have been under exceptional attention in computational chemistry. Their study was originally motivated by their role in the primary mechanism of vision, in which the photoisomerization of a PSB is the fundamental process. (For the reader interested in these phenomenological aspects, we suggest Ref. [676] for a recent review on the topic.) With time, a large literature corpus of computational studies about PSBs has been accumulated,[358,677–693] turning these molecules into the basic prototype to test new methodologies. Computational benchmarks encompassing the most employed computational chemistry methods are available for the PSB3 species, for instance, delivering comparative information on diverse properties, including its excited-state reaction pathways.[195,289,694,695]

The photophysics of a PSB species starts with an ultrafast (sub-picosecond) isomerization following the photoexcitation.[696] Still on this time scale, the molecule finds a conical intersection where it deactivates to the ground state.[697] The isomerization itself involves the twist of multiple bonds (which depends on the PSB size and environment[698]), and it is coupled to other modes, characteristically, the bond-length-alternation (BLA) stretching and hydrogen-out-of-plane (HOOP) wagging.[699] During isomerization, charge-transfer (ground) and diradical (excited) states cross, and a balanced description of these two different characters is a challenge for many quantum-chemical methods.[289] Moreover, at the crossing point, the multireference character of the ground state poses an additional challenge.

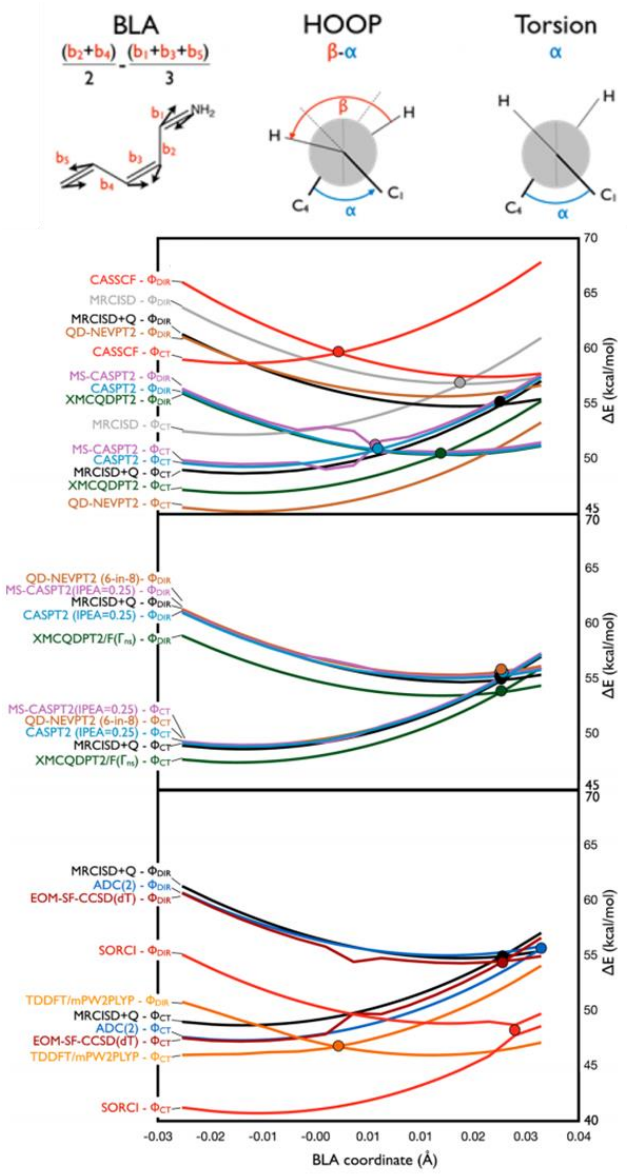

Figure 17. Top: Illustration of torsion, BLA, and HOOP modes in PSB3. Bottom: Potential energy profiles for PSB3 along the BLA coordinate computed with several quantum-chemical methods. Adapted from *J. Chem. Theory Comput*. **2012**, *8*, 4069-4080.Copyright 2012 American Chemical Society.

The multireference character at the conical intersection has motivated to use CASSCF in many investigations, especially in nonadiabatic dynamics simulations,[700–703] in which the computational cost is a significant issue. Nevertheless, as shown in Figure 17, the relative energy between the charge transfer (CT) and the diradical (DIR) states is not well balanced at this level, leading to a

crossing at much shorter BLA than that observed with MR-CISD+Q. The origin of the disbalance in CASSCF is in the missing dynamic correlation, which has a more substantial impact in the CT state than in the DIR state due to the larger charge displacements in relation to the reference in the former.[289,694,695]

Even though the CASSCF curves are almost parallel to MR-CISD+Q, they may lead to a wrong description of the isomerization process. Quantum Monte Carlo simulations,[685] for instance, indicate that the BLA inversion predicted by CASSCF may, in fact, be an artifact. Also diverging from the fast isomerization predicted by CASSCF for PSB3 and PSB4, CASPT2 optimizations stabilize a non-bond-inverting minimum for these short species, indicating that the torsional motion may be delayed or even impeded at the fully correlated level.[704] This point is not, however, completely settled yet, as multiple spawning simulations of PSB3 at CASPT2 level show fast torsional isomerization,[688] which could still be a side-effect of the non-polarized basis set employed in that work.

Concerning the multireference methods in Figure 17, note in the upper graph that the perturbative methods (CASPT2, MS-CASPT2, NEVPT2, XMCQDPT2) may also show results substantially divergent from the variational MR-CISD+Q. The MRPT results, however, can be improved (Figure 17, middle) by small modifications, as, for instance, the inclusion of IPEA shift in CASPT2, increasing the active space in NEVPT2, or modifying the operator in XMCQDPT2.

In addition to methodological studies, the investigations in the field have evolved toward complex systems including the PSB within protein cavities. Such type of study is chiefly performed employing CASPT2/MM for reaction path explorations[705–708] and surface hopping on CASSCF/MM surfaces for dynamics;[709–711] both profiting from hybrid QM/MM methodology.[712] These investigations including the protein are reviewed in Section 3.3.4.2.

In Ref. [687], two variants of Quantum Monte Carlo approaches have been used to explore the minimum energy path of PSB3; and in Ref. [688], a multiple spawning dynamics simulation based on CASPT2 was carried out, also for PSB3. Such investigations based on highly-correlated methods may be indicating a methodological shift to nonadiabatic dynamics methods beyond CASSCF studies in the near future.

3.3.3. Nucleic acids: from nucleobases to double strands

The photophysics and photochemistry of UV-excited nucleic acids have been under intense scrutiny in the last decade. This research has been orbiting some central themes, including the photostability of the genetic code,[713] the development of early biotic species,[714] mutagenic and carcinogenic effects of radiation,[715] and the potential use of nucleic acids for photonic developments.[716]

Computational studies have been essential to aid the interpretation of steady and time-resolved spectroscopic investigations in the field, allowing to characterize excited states and map the deactivation pathways in diverse types of nucleic acid fragments, from isolated nucleobases to solvated double strands. Some of the main theoretical contributions based on multireference methods are surveyed in the next subsections. The reader interested in other accounts of this broad field may profit from previous reviews on photoexcitation of nucleic acids,[713,717–721] modified bases,[722] and nucleobases in solution,[723] as well as reviews on physiologic,[724] prebiotic,[725,726] and technological aspects.[727]

3.3.3.1. Nucleobases and derivatives

The low luminescence yield of the canonical nucleobases adenine (Ade), guanine (Gua), cytosine (Cyt), thymine (Thy), and uracil (Ura) has been a significant indicator for decades that internal conversion is the dominant mechanism for their deactivation after UV excitation.[728,729]

Time-resolved spectroscopy has further revealed that this deactivation takes place on the pico- and subpicosecond timescales.[721,730] Since then, many studies have been dedicated to mapping the deactivation pathways, from the initial excitation in the Franck-Condon region to the intersection seam between the first excited and the ground states. The central role of the internal conversion in these processes has brought multireference methods to the first plane in this research area.

CASPT2 has been the workhorse of the field since the late 1990s, when Fülscher, Serrano-Andrés, and Roos determined the vertical excitation spectra of the nucleobases in the gas phase.[731,732] From then on, the CASPT2//CASSCF protocol has been the most used approach to optimize conical intersections and determine reaction pathways (Ade,[733–738] Gua,[739–741] Cyt,[742–745] Thy,[745–749] Ura[745,748]). In addition to CASPT2, MRCI (Ade,[750,751] Cyt,[752–755] Ura,[751,756]) and DFT/MRCI (Ade,[757,758] Gua,[759] Cyt[760]) have also been often used to map the reaction pathways.

These investigations on reaction pathways have been fundamental to show the existence of different competing internal conversion mechanisms. These mechanisms involve different states and types of nuclear distortions, including among them relaxation through $\pi\pi^*$ states correlated to out-of-plane ring distortions,[757] relaxation through $\pi\sigma^*$ states correlated to NH stretching,[738] and even relaxation through three-state conical intersections.[753] The CASPT2 reaction paths, in particular, have been employed as a basis for the first attempts of rationalizing these different processes under a unified model.[737,739,745]

In addition to reaction path studies, the computational research on nucleobases based on multireference methods has delivered information on different kinds of spectroscopy, including photoelectron spectroscopy (all nucleobases,[761] Ura,[762] Cyt[763]), frequency-resolved (Ade,[758] Ura[764]), and time-resolved (Ade,[765,766] Thy,[767] Ura[767]). Multireference methods coupled to nonadiabatic mixed quantum-classical approaches — specially surface hopping and multiple

spawning — have also allowed numerous dynamics simulations.[719] Nevertheless, the high computational cost of MR-CISD and the lack of energy gradients for CASPT2 have posed significant impediments to the use of these methods in such simulations. This situation opened space for dynamics based on less demanding multireference approaches, including CASSCF (Cyt,[752,768–770] Thy,[767,768] Ura[767,768,771–774]), MRCIS (Ade,[768,775] Gua[768,776]), semiempirical OM2/MRCI (Ade,[777] Gua,[778] pyrimidine bases[779]), and semiempirical FOMO-CI (all nucleobases and several other DNA fragments[780]). In fact, to cope with computational costs, the range of computational methods has been extended to encompass single-reference methods as well (coupled cluster, algebraic diagrammatic construction, time-dependent density functional theory) in investigations of steady properties[781–785] and dynamics[786–791] of excited nucleobases and nucleobase derivatives.

The dynamics studies added another information layer to the reaction path investigations by telling the relative importance of each possible relaxation mechanism. It has been shown, for instance, that while in the purine bases (Ade, Gua) a single mechanism dominates the ultrafast internal conversion, in the pyrimidine bases (Cyt, Thy, Ura), there is a strong competition between few different mechanisms.[768] Dynamics has also revealed exotic mechanisms, not predicted by steady-state studies, as the S_2 trapping of thymine[792] or the solvent-chromophore electron transfer in 7H-adenine.[788] Concerning the three-state conical intersections, according to the dynamics they seem to be limited to a minor process occurring in cytosine.[770,793]

Although downgrading the computational level from multireference methods used for reaction paths to approaches based on partially-correlated methods (like CASSCF or TDDFT) for dynamics has been fundamental to enable the investigation on the relative importance of the different reaction paths, it had as a side effect an expected reduction in the accuracy of the

results.[375] Recently, these low-correlated dynamics started to be reevaluated in the light of new experimental data[794] and other computational methods (Ade,[375,786] Thy[787]), including CASPT2 (Ade[795]), for which analytical energy gradients have been recently implemented.[529] Thus, the aforementioned S_2 trapping of thymine, for instance, has been as attributed to a possible artifact of the CASSCF method.[794] On the other hand, analysis of the reaction paths with the CASPT2//CASSCF and CASPT2//CASPT2 protocols for thymine did not reveal major differences between them.[796] Along the same lines, comparative assessment of the accuracy of CASSCF and ADC(2) surfaces for isocytosine has favored the former one.[797] A recent benchmark on solvation methods has also made clear how the main approaches to include environmental effects in CASPT2 results for cytosine may differently impact the results.[798]

As soon as the picture of the internal conversion processes of isolated nucleobases started to clarify, the investigation of internal conversion in isolated canonical nucleobases based on multireference methods quickly spilled over to internal conversion and intersystem crossing processes in solvated nucleobases, modified nucleobases, tautomers, nucleosides, nucleotides, and larger nucleic acid fragments. Once more, CASPT2 was the leading method driving the reaction path studies (2-aminopurine,[736] vinyl-Gua,[799] GMP,[800] xanthine,[801] pyrimidine nucleosides in water,[802] methyl-Cyt,[803] 5F-Cyt,[742] Cyd in water,[804] ISC in Thy,[805] aza-Ura,[806] ISC in all nucleobases[807]), accompanied by MRCI (oxo-Gua[808]), and DFT/MRCI (7H-Ade,[809] acetyl-Ade,[758] Cyt tautomers,[760] Gua tautomers[759]); and with dynamics carried out with CASSCF (ISC in Cyt[810–812]) and semiempirical methods (Ade in water[371,813]). Among the modified nucleobases, thio-modifications have recently been in the spotlight due to the discovery of sub-picosecond intersystem crossing process in thio-nucleobases[814,815] and the potential use of these substances as singlet-oxygen photosensitizers,[816] leading to many computational investigations on reaction paths

(CASPT2: tThy,[817–821] tUra;[822–825] DFT/MRCI: tThy[819]), dynamics (CASSCF: tCyt[826], CASPT2 and ADC(2): tUra[827,828]), and kinetics (CASPT2: aza-tThy+O_2[629]).

3.3.3.2. Interacting nucleobases and DNA/RNA fragments

Whereas the dynamical processes relevant to isolated nucleobases are largely understood, new phenomena come into play when larger fragments of nucleic acids are investigated. These include steric interactions, electronic phenomena such as exciton formation and charge transfer, and phenomena involving nuclear as well as electronic rearrangements, such as excimer formation and dimerization.[829] Computations studying these phenomena and the challenges present have been reviewed extensively in recent articles.[720,830] For multireference computations not only the general size of the system is demanding, but it is also particularly challenging to maintain a balanced distribution of the active orbitals over the involved nucleobases. Therefore, SR methods such as DFT/TDDFT[720,831–833] and CC/ADC[188,738,834,835] have been the main workhorse in this field, and only a smaller number of MR computations have been performed. These computations can be grouped into three categories considering in the QM region either (i) only one nucleobase, (ii) a hydrogen-bonded base pair, or (iii) stacked bases.

The first option, i.e. including only one nucleobase at the QM level, allows studying the influence of steric and electrostatic interactions as well as hydrogen bonding of neighboring bases and the solvent. A deactivation path of adenine embedded in a double helix was computed at the CASPT2 level showing that the reaction path is flatter in the embedded system, thus suggesting longer decay time.[836] In agreement with this, a surface hopping study using semi-empirical multireference methods concluded that the decay times in the embedded system are about 10 times longer than for isolated bases.[837] A study employing CASSCF (cytosine) and MR-CIS (guanine) concluded that hydrogen bonds have a strong influence by inhibiting puckering of the guanine

base, which would be required for excited-state deactivation.[838] Finally, QM/MM dynamics were performed on 4-aminopyridine to investigate stacking effects finding only minor influences on the decay times but a somewhat altered mechanism.[839]

The interest in hydrogen-bonded base pairs was sparked by a seminal paper by Sobolewski and Domcke[840] that, based on CASPT2 computations, proposed a new deactivation channel in Watson-Crick paired guanine-cytosine through a proton transfer, which is feasible at least in the gas phase. The same process was subsequently studied using CASSCF surface hopping dynamics of a guanine-cytosine base pair embedded in a double helix.[841]

Stacking interactions can give rise to excitonic and charge transfer states as well as forming the basis for excimer formation and dimerization. Electronic couplings between two stacked thymine molecules were investigated by a variety of methods including CASSCF, showing that the excited-state energies are very sensitive to the computational method whereas the couplings are not.[842] Exciton delocalization and charge transfer interactions were studied at the MS-CASPT2 level for the complete set of 16 DNA nucleobase dimers in B-DNA configuration.[843] By applying a systematic exciton analysis formalism,[534] the authors highlighted the important effect of direct orbital interactions on the electronic couplings.[843] Excimer formation was examined at the CASPT2 level in the cases of the cytosine[844] and adenine dimers,[845] emphasizing the neutral (rather than charge-transfer) character of the excimers. Later studies combining ab initio single- and multireference methods highlighted structural deformations, leading to partial charge transfer[846] and transient bonding between the bases.[834] Subsequent CASPT2 reaction path computations on two stacked adenines embedded in a double helix showed that a charge-transfer excimer is energetically accessible and also highlighted the potential importance of slow intramonomer relaxation processes.[847] The same group also performed two recent studies on the formation of the

6-4 thymine dimer photoproduct employing CASSCF.[848,849] The photodynamical formation of the cyclobutane thymine dimer was studied recently by nonadiabatic dynamics at the CASSCF level showing that doubly excited singlet states are important in this process and triplet states are not.[850]

3.3.4. Aminoacids and proteins

Fluorescent properties of proteins provide valuable information on their structure and dynamics. Presence of light absorbing amino acids tyrosine (Tyr), tryptophan (Trp), histidine (His), and phenylalanine (Phe) in fluorescent proteins makes it possible to study the native protein structure, conformational changes, protein-substrate binding, structure dynamics, as well as excitation energy transfer processes.[851–853] Due to a low abundance of tryptophan in protein and a low fluorescence quantum yield of phenylalanine,[854] non-natural amino acids with useful spectroscopic properties are utilized as well.

After the light absorption, the main relaxation channel is fluorescence.[851] Its quantum yield is reduced by alternative processes, such as radiationless relaxation on the one hand, in which the ground-state chromophore is restored, and various photo-induced transformations on the other hand. Light-induced phenomena, such as Stokes shift, photoactivation, photoswitching, and photoconversion observed in fluorescent proteins make them useful for further applications.[851] Many experimental and theoretical studies have been performed to improve our knowledge of the structure-function relationship of fluorescent proteins.[855–860] The exploration of the photophysics and photochemistry of amino acids, short polypeptides and larger protein models at the atomic level has become subject of many theoretical studies, including those that employ multireference methods discussed below.

3.3.4.1. Isolated amino acids and small peptide models

In earlier studies, the gas-phase absorption spectra of Trp and His chromophores indole and imidazole, respectively have been investigated. The calculations of the absorption spectra have been performed using the CASPT2 approach for isolated indole[861,862] and imidazole.[863,864] Additionally, calculations of absorption spectra employing the DFT/MRCI and MRCI methods have been performed for the gas-phase indole[865] and imidazole.[866] For both systems, the two low-lying singlet excited states have been identified as ^1L_b and ^1L_a, both resulting from $\pi \rightarrow \pi^*$ transitions.

The CASPT2 approach has also been used to evaluate the spectroscopic behavior of the modified chromophore 5-hydroxyindole and 7-azaindole,[867–869] which is integrated into proteins as 7-aza-Trp. Arulmozhiraja and Coote[870] have reported studies on the reliability of DFT functionals to model the absorption spectra of indole, in particular, the order of the two lowest excited states labelled ^1L_a and ^1L_b, the energy gap between the states, their oscillator strengths, and dipole moments. All tested functionals, including hybrid, meta-GGA and long-range corrected, have failed to reproduce the discussed properties.

Extension to a more realistic model has been performed in calculations that have considered the full Trp molecule. CASPT2[871] and DFT/MRCI[872] methods have been used to evaluate effects of alanyl side chain conformation on the characters of the spectra, in particular, the oscillator strengths and dipole moments of Trp and effects of the protonation on the relative energies of Trp conformers in their ground and excited states, respectively. Notably, TDDFT does not provide reliable results for these properties. [871]

Computational studies employing the CASPT2 method have been performed on the gas-phase absorption spectra of non-chromophore Glycine (Gly) and N-acetyl-glycine to explore the

effect of the terminal amino and carboxyl groups on the spectral properties of proteins and peptide bond, respectively.[873] The calculations assigned the absorption bands in the 5.5 – 6.5 eV region to $n \rightarrow \pi^*$ transitions, and the bands at 8.1 and 10.2 eV to $\pi \rightarrow \pi^*$ transitions. The bands at 7.0, 8.5, and 9.0 eV have been assigned to Rydberg states. The intense band at 7.5 eV observed in the experimental spectra of proteins and not found in the calculations has been predicted to originate from the electron transfer between neighboring peptides.[873]

A step towards understanding protein emission spectra in solvent has been made using multireference studies, mainly CASPT2, on indole, in which the solvent has been modeled by self-consistent reaction field with continuum polarized model.[861,874,875] Based on the evaluation of the dipole moment of the two lowest excited states and the extent of their stabilization in a polar solvent, the emission from the ^1L_a state, S_2 in the Franck-Condon region, has been predicted. The CASPT2 approach has been also used to evaluate the solvent effect on the spectra of His. In particular, spectral shifts and effects of protonation[863] (see also Ref. [875] and references therein) are expected to occur even at neutral pH. Benchmark studies of Schreiber *et al*. on medium-sized molecules, including imidazole, have reported relatively large deviation of the excitation energies obtained with the CC2 and CCSD methods compared to the CASPT2 method.[189]

Multireference approaches have frequently been used to map the alternative nonradiative relaxation pathways of chromophore amino acids aiming to explain effects of surrounding protein on their emitting properties. The experimental studies performed on Trp and Tyr chromophores indole (Ref. [876] and references therein) and phenol,[877–880] as well as the multireference computational studies employing the CASPT2 protocol,[789,881–889] have concentrated on the characterization of the excited-state detachment and hydrogen transfer, driven by repulsive states, as proposed by Sobolewski and Domcke.[882] Relevant to this mechanism, the effect of the vibronic

coupling of ^1L_a and ^1L_b states has been explored at the CASSCF and DFT/MRCI levels.[865] DFT/MRCI, CC2, and SCS-CC2 methods have also been used to study the character of S_1 and S_2 states of modified 4-, 5-, and 6-Fluoroindole.[890] Notably, the original CC2 method fails to describe the mixed character of states predicted by the DFT/MRCI and SCS-CC2 methods.

A crucial step toward understanding the role of πσ* state has been taken with studies of 4-OH- and 5-OH-indole. H-Rydberg atom fragmentation translational spectroscopy in combination with the EOM-CCSD and CASPT2 studies have shown that while the O-H bond fission is dominant in 4-hydroxyindole, the N-H bond fission dominates the relaxation mechanism in 5-hydroxyindole.[891] As an alternative non-radiative pathway, fluorescence quenching via zwitterionic tryptophan has been studied at the CASSCF level.[892] It has been proposed that at neutral and slightly acidic pH either a complete hydrogen transfer and formation of a different ground state tautomer or decarboxylation and tryptamine product occurred. The optimization using the CASSCF method has been able to identify several conical intersections of imidazole, the His chromophore, characterized by NH or CN bond dissociation and puckering of the five-membered ring at N or N-H sites explaining its non-fluorescent character.[893]

The *ab initio* molecular dynamics simulations based on the full multiple spawning algorithm coupled with the CASSCF method have been performed on isolated neutral[894] and microhydrated zwitterionic Gly.[895] While there has been no conformation dependence observed for the isolated species, the results predict that the photodynamics of solvated species is strongly conformation-dependent. The effect of the solvent environment on the Gly photodynamics has also been investigated with the combined CC2 and CASSCF study[896] explaining the high quantum yield of NH_3 in the UV photolysis of non-aromatic amino acids.

In agreement with the experiment on absorption of circularly polarized UV light, the molecular dynamics simulations based on the gradients obtained from the semi-empirical multireference OM2/MRCI method[897] have shown that photolysis leads to enantiomeric enrichment of either right- or left-handed enantiomer depending on the helicity of the laser field.

Importantly, while only minor changes have been observed in the absorption bands between the bare amino acids and those integrated into proteins, their fluorescence properties significantly differ. This feature indicates the presence of efficient non-radiative mechanisms due to the interaction between the chromophore amino acids and the peptide backbone.[898] Although the CC2 method has been mostly used to reveal the charge transfer as the leading relaxation mechanism in peptides,[898,899] multireference approaches have also appeared in the literature, *e.g.*, to study the photoinduced charge transfer states in glycine dimer (using the CASPT2 method),[900] which models the β-turn in proteins. The CASPT2 approach has also been used to benchmark the following studies: the charge transfer in the peptide model of N-acetyphenylalaninylamide (NAPA) and its derivatives,[901] the CC2 and TDDFT methods in surface hopping nonadiabatic dynamics of NAPA,[898] and TDDFT description of charge transfer in Trp-Phe dipeptide.[902]

3.3.4.2. Proteins

Among the fluorescent proteins, the green fluorescent protein (GFP) is the brightest protein known.[857] The internal cyclization in the Ser-Tyr-Gly amino acids sequence results in the formation of *p*-hydroxybenzylideneimidazolidinone (HBDI), GFP chromophore, a conjugated photoacid from which the proton is transferred via surrounding water molecules and Ser to Glu residues.[903] The chromophore is buried in the beta-barrel protein structure, which allows for highly specific contacts and a hydrogen bond between these two parts (see references in Ref. [904]). The photophysical properties of GFP are useful in imaging techniques, which have opened several

areas for the life sciences. Due to their exciting applications, GFPs have become the subject of many experimental and theoretical studies recently.[858] These studies have helped to design new fluorescent proteins with improved properties.

A unique property of fluorescent proteins is the low electron detachment of their anionic forms resulting in the metastable character with respect to electron detachment making computational studies of GFP challenging. While the absorption spectra of HBDI are only negligibly affected by the protein matrix, significant changes have been observed upon polar solvation. In addition, contrary to HBDI buried in the protein, isolated HBDI is a non-fluorescent species, showing that the protein matrix significantly prevents relaxation mechanisms dominant in the chromophore itself. GFPs have attracted much attention due to their rich photochemistry, which includes processes such as photoisomerization, photoinduced oxidative processes, and excited-state proton transfer. The features mentioned above have been a matter of a large number of computational studies (see Ref [851] and references therein) among which the multireference studies substantially increased the level of understanding.

In particular, the calculations of the spectral properties of the gas-phase HBDI performed with the MCSCF/MCQDPT[905] and the CASPT2 methods,[906,907] have confirmed the results of fluorescence excitation and emission spectra[908] interpreted by the existence of neutral or ionic forms. Also, the semi-empirical multireference NDDO-G approach has been used to study the effect of solvent on the absorption spectra of the anion, cation, and neutral and zwitter-ion with respect to the protonation site[909] and have suggested a strong dependence on the protonation site.

Effects of both, protein matrix and solvent on spectral characteristics and excited state behavior of GFP have been discussed in the literature (see references in Ref. [851]). Among others, an effect of the protein matrix on the optical properties[910] and photoinduced dynamics[911] of HBDI

have been investigated using the semi-empirical multi-reference CAS-CI/DFT approach, as well as using QM/MM calculations employing the CASPT2 method.[912] While these studies reveal only non-significant changes of the optical spectra upon the influence of the protein matrix, the studies on the excitation spectra of the neutral, cationic and anionic HBDI in the polarizable continuum model, performed at the same level theory, show significant changes of the later form upon the solvation.[913]

The *cis-trans* isomerization (Z/E diastereoisomerization) is the fundamental reaction of photoswitchable fluorescent protein. The character of the cis-trans HBDI isomerization pathway requires a multireference description already at the ground state.[914] Indeed, both DFT and SOS-MP2 fail to describe the twisted geometries involved in the isomerization process.

Calculations on the mechanism of the photoinduced *cis-trans* isomerization of the gas-phase HBDI have been performed at the multireference level using semi-empirical NDDO method,[904] CASSCF,[915] CASPT2 methods.[907,916] Dynamics has been investigated with *ab initio* multiple spawning with CASSCF,[917] identifying the photoizomerization path about alternate bonds of the bridge connecting the two chromophore rings. Further extensions, which include aqueous solvent in the QM/MM calculations,[918,370] employing semiempirical FOMO-CI in the QM part, have shown a significant reduction of the excited-state lifetime upon solvation.

Among the unique properties of GFP, its excited-state proton transfer has been the subject of several experimental and computational studies (see references in Ref. [851]). The originally proposed scenario obtained using classical molecular dynamics simulations[903] suggests the proton transfer to hydrogen bonded water followed by transfer to Serine (Ser) residue and Glutamic acid (Glu). More details on the mechanism have been revealed using CASPT2 studies.[919,920] These have been further extended by molecular dynamics simulations performed with the multiconfigurational

time-dependent Hartree method,[921,922] predicting the wire-like path between the phenolic proton, hydrogen bonded water, Ser, and Glu, which proceeds almost synchronously on the femtosecond timescale.

The multireference approach has appeared as an efficient tool to describe excited-state properties of other GFP-like proteins, such as the reversible photoswitching Dronpa[923] and the kindling mechanism of as FP595.[924,925] Rhodopsins are another class of proteins that have attracted substantial attention of both experimental and computational studies, in particular the light-induced double bond isomerization of a polyenal protonated Schiff base (PSB) of retinal, which induces various biological functions. Spectroscopic studies reveal a subpicosecond timescale of the photoisomerization and S_1 decay in less than 100 fs.[926] (PSBs are reviewed in Section 3.3.2)

In an earlier study, the CASPT2 method has been used to reveal the *11-cis* (PSB11, type II rhodopsin) to *all-trans* (PSBAT, type I rhodopsin) isomerization.[926] Lately, protein environment has been included in QM/MM approaches, which rely on the CASPT2 approach.[701,709,854] The same methodology has been used to explain an experimentally observed increase (from a sub-picosend time scale to about 90 ps) of the excited state lifetime [927] of bovine Rhodopsin by blocking of the C11-C12 double bond of the chromophore.[928]

QM/MM molecular dynamics employing the CASSCF approach, combined with the CASPT2 evaluation of critical points of PES, has been employed to explain the time-resolved 2D electronic spectra of photoisomerization pathway of Rhodopsin type II.[929] The CASSCF method has been used in the QM part of the QM/MM protocol to compare the photodynamics of isorhodopsin containing *9-cis* instead of *11-cis* retinal of rhodopsin.[709] Recently Luk et al. have performed molecular dynamics simulation employing the CASSCF method and subsequent CASPT2, as well as extended multiconfigurational quasidegenerate PT2 (XMCQDPT2)

calculations[926] to explain the evolutionary scenario of a common ancestor to retynilidene proteins supported by an experimental study of Devine et al.[930]

As stated above, the character of the emission spectrum of Trp is widely used to monitor changes in proteins reflecting the local structure and dynamics.[931] Among the computational studies on the fluorescent Trp-containing proteins, the CASSCF calculations of indole and 5-hydroxy-indole coupled with the TDDFT treatment of larger protein structure have been used to evaluate variations of fluorescent spectra of Trp and 5-OH-Trp in various proteins matrices in the study of Robinson *et al.*[932] Similarly, the CASPT2 level has provided benchmark data for the TDDFT calculations on the effect of substitution and local environment of different Trp residues on the UV-B absorption spectra in the photoreceptor Arabidopsis thaliana UV RESISTANCE LOCUS8 (UVR8) protein.[933]

The fact that Trp radicals have an important catalytic role in many enzymatic reactions stimulated other experimental and computational studies (Ref. [934] and reference therein). Among these Bernini *et al*.[934] calculated EPR, UV-VIS and resonance Raman spectra of a long-lived Trp radical in Pseudomonas aeruginosa azurin mutants using QM/MM protocol employing the CASPT2 level in the QM part.

Multireference CASSCF and MS-CASPT2 approaches have also been used in studies of spectroscopic properties of Trp residues (Trp 233 and Trp285) to reveal the UV-B induced dissociation mechanism of the UVR8 homodimer.[935] The subsequent ONIOM studies employing both the MS-CASPT2 and SAC-CI levels of theory have identified Trp285 as the major chromophore of UVR8 and Trp233 as the residue responsible for the exciton coupling. Notably, MS-CASPT2, CASSCF, SAC-CI methods together with TDDFT studies employing several functionals have been evaluated to benchmark the results on the absorption and emission energies

of 3-methylindole in the gas phase. Contrary to MS-CASPT2 and SAC-CI methods, none of the twenty tested DFT functionals succeeded to properly describe a correct ordering of ^1L_a and ^1L_b excited states.

3.3.5. Polycyclic aromatic systems: monomers and dimers

Polycyclic aromatic hydrocarbons (PAH), as exemplified by polyacenes, periacenes, and many more intricate molecular structures of Kekulé and non-Kekulé type, play a significant role in astrochemistry,[936] and in materials science due to their potential as versatile organic semiconductors,[937] for singlet fission,[938] spintronics,[939] and energy storage.[940] The property that serves as a basis for all these applications, is that by changing the size and shapes of the PAHs, their frontier orbital energies can be fine-tuned to induce the formation of polyradical character and spin polarization.[835,941] On the one hand, it is precisely this property that makes multireference methods indispensable for their description. On the other hand, the size of these systems is challenging for multireference methods. Including all π-orbitals in the computation requires a CAS(*n*,*n*) for a system of *n* unsaturated carbon atoms, which is feasible only for the smaller systems. But in many cases, systems of interest feature *n* above 100 and several different multireference methods have been tested.

Polyacenes have been studied intensely with the objective of unraveling their specific properties as well as being a testing ground for evaluating different methods. A topic that has been discussed in detail by computational studies using multireference methods is to what extent the lowest singlet state of polyacenes of different sizes has biradicaloid or polyradicaloid character and whether the lowest triplet state is lower in energy than the singlet. Initially, a combination of DFT and CASSCF methods was applied up to decacene, finding that the larger systems have a singlet diradical ground state.[942] This view was corroborated in a study using DMRG, which

allowed inclusion of the complete π-space into the active space, and, based on NO occupations, it was shown that larger acenes do not only possess diradical character but even polyradical character but that, nonetheless, a finite singlet-triplet gap remains.[943] These findings were contested by a later study arguing, based on a combination of CASSCF, CASPT2, and high order single-reference coupled cluster computations for up to heptacene, that these systems retain largely closed-shell character.[944] A subsequent study using two-electron reduced-density-matrix (2RDM) theory with an active space encompassing the complete π-space again revealed the onset of bi- and polyradical formation in acenes.[945]

The formation of an open-shell singlet ground state with no singlet-triplet crossover was also found in a study using MR-CISD on top of a Pariser-Parr-Pople (PPP) Hamiltonian.[946] As an alternative strategy, the MR-AQCC approach was applied to polyacenes finding pronounced polyradical formation as well,[835] and that the singlet-triplet gap stays positive but rapidly goes to zero.[947] The data was subsequently used to benchmark a highly efficient model for computing unpaired electrons based on Hückel theory, and good agreement was found.[948] Formation of open-shell character was also found in a study applying the particle-particle random phase approximation (ppRPA), and the authors used a valence-bond-like description to illustrate the diradical formation on the two edges of the molecule.[949] A recent study applying the coupled-cluster valence-bond singles and doubles method also found significant formation of polyradical character but pointed out that this character is reduced when all the electrons are correlated.[950]

Aside from the topic of the character of the ground state, also electronic excitations in polyacenes have been studied. The ground and excited state absorption spectra of octacene and nonacene were computed at the MR-CISD/PPP level of theory.[946] Using DFT/MRCI, a number of electronic states were characterized, and the importance of new doubly excited states that come

into play for larger acenes was emphasized.[951] In the context of ppRPA computations, a detailed valence-bond-like interpretation of various polyacene excited states was given.[949] A recent CASPT2 study investigated the different computational requirements for describing the L_a and L_b states of polyacenes.[952] As opposed to the MR studies, which showed rather uniform trends for the excitation energies, a DFT study presented some evidence suggesting that the optical gaps oscillate with increasing size of the oligoacene.[953] Finally, a recent CASPT2 study[540] illustrated the importance of dynamic correlation for the ^1L_a state of tetracene. It, furthermore, showed that the computational description of this state was significantly improved when moving from the 6-31G** basis set to a more sophisticated atomic natural orbital basis set even though both basis sets have the same computational cost in the CASSCF and CASPT2 steps. The ionization potentials and characters of the ionized states of various acenes have been studied by MR-AQCC and MR-CI computations.[954]

In addition to polyacenes, a wide range of other PAHs have been studied by multireference methods. The main result of these studies was that slight modifications in the molecular structure can have considerable influence on the electronic properties. A variety of PAHs of up to eight fused rings were studied by 2RDM theory, displaying important changes between different molecular structures.[955] Polyacenes, phenacenes, periacenes, and circumacenes were studied using MR-AQCC, highlighting that slight structural changes can have a dramatic impact on the observed radical character.[835] In this study, it was of particular importance to have a well-defined method for quantifying unpaired electrons. For this purpose the total number of unpaired electrons,[544] specifically its non-linear version $n_{U,nl}$ defined in Eq. (53), was employed. This analysis allowed for a visualization of the distribution of unpaired electrons in space, as exemplified in Figure 18 (a) as well as for a comparison of the total number of unpaired electrons in a variety of different

PAHs Figure 18 (b). Subsequently, the formation of unpaired electrons was studied using the MR-AQCC method in a variety of systems with a non-standard bonding pattern, such as triangular non-Kekulé structures and zethrenes.[956] Different systems containing six fused benzene rings were studied using CASSCF and other methods, suggesting a new molecule called uthrene possessing a triplet ground state.[957] Unpaired electron in PAHs were also examined using a fractional occupation number weighted electron density[545] and NO occupation numbers in a wide range of different PAHs were studied using thermally-assisted-occupation DFT.[958]

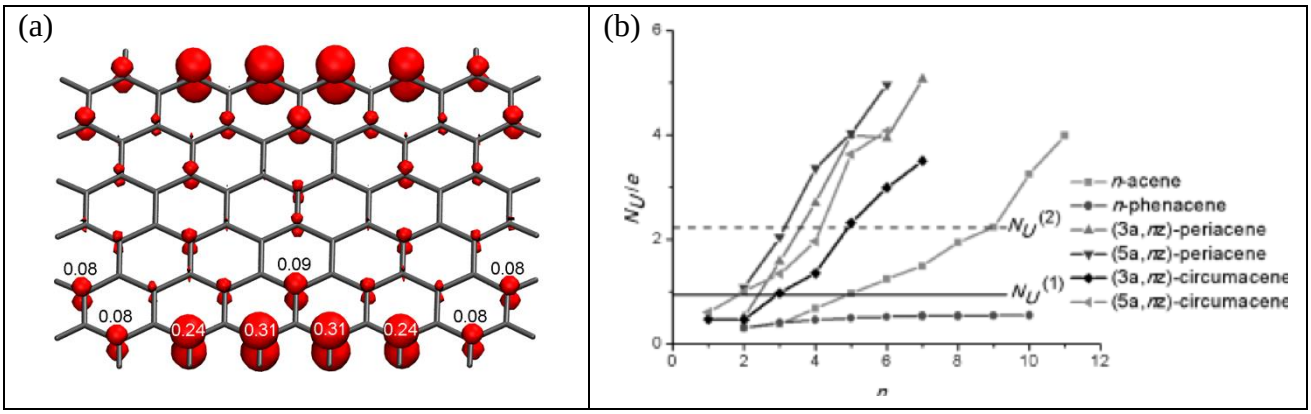

Figure 18. Analysis of unpaired electrons in PAHs: (a) density of unpaired electrons of the (5a,6z) periacene molecule and (b) total number of unpaired electrons in a variety of PAHs of different sizes and shapes. Reproduced with permission from Ref. [835]. Copyright 2013 John Wiley and Sons.

Also, substitution patterns were investigated. A wide range of different substituents placed on a graphene nanoflake with a high-spin ground state were studied by DFT and CASSCF, showing that especially cyano groups favor a singlet ground state.[959] Using similar methodology, nitrogen doping in grapheme nanoribbons was also investigated.[960] *Locally-correlated* MRCI and MR-AQCC computations showed that simultaneous insertion of two push-substituents or two pull-substituents can increase the polyradical character of zethrenes.[91] Using MRCI and MR-AQCC, the effects of a vacancy defect[961] as well as of boron and nitrogen doping were investigated.[962]

Molecular associates of aromatic species open a new field of applications, in which excited-state dimers play a significant role. These species are named aromatic excimers and exciplexes (AE's) in the case of identical and non-identical chromophores, respectively. The use of AEs as chemosensors[963], molecular beacons, [964] and light-harvesting materials[965] have made them subjects of detailed investigations. A large variety of aromatic associates have been studied discussing their electronic properties such as charge separation, energy transfer, and photochemical reactions[966].

The pyrene excimer, the first AE observed experimentally,[967] has become probably the most representative species among all AEs (see *e.g.*, Ref [968] and references therein for the application of the pyrene-based excited state associates). The most important property of pyrene AE is the concentration dependence of its fluorescence spectrum, characterized by a singly red-shifted, broad and structureless band. It has been predicted that the splitting of the first L_b and second L_a excited states of monomer causes reordering of the states in the dimer, with the emission originating from the L_a state.[969,967]

An important property of the excimers/exciplexes is their larger stability with respect to the ground state.[970] The theory underlying the excimer stability, molecular exciton interactions, and electronic excitation transfer has been presented by Scholes and Ghiggino[971] for the naphthalene dimer. Within the framework of the multireference wavefunction, the interaction in the excited-state dimer results from the excitonic resonance (ER) and charge resonance (CR). In terms of monomers *A* and *B*, the ER terms are

$$\Phi_1 = \frac{1}{\sqrt{2}}\left(\left|A^* B\right\rangle - \left|AB^*\right\rangle\right) \tag{59}$$

$$\Phi_2 = \frac{1}{\sqrt{2}}\left(\left|A^* B\right\rangle + \left|AB^*\right\rangle\right) \tag{60}$$

while the CR terms are

$$\Phi_3 = \frac{1}{\sqrt{2}}\left(\left|A^- B^+\right\rangle + \left|A^+ B^-\right\rangle\right) \tag{61}$$

$$\Phi_4 = \frac{1}{\sqrt{2}}\left(\left|A^- B^+\right\rangle - \left|A^+ B^-\right\rangle\right) \tag{62}$$

where excitations are indicated by an asterisk. The ER and CR contributions originate from the interaction between the transition dipole moments of monomers and charge-transfer interactions, respectively. In terms of the generalized valence bond theory, the ER terms correspond to covalent contributions and the CR to ionic contributions. Both interaction terms and mixing between them are responsible for the formation of AEs. From a practical viewpoint, it is worth noting that a quantification of ER and CR contributions in *ab initio* computations can be highly challenging and requires either a detailed consideration of the phases of the orbitals and wavefunction coefficients[972] or the application of specialized analysis tools.[534]

The earlier computational studies of AEs have been performed with semi-empirical and configuration interaction singles (CIS) methods. [972] The semiempirical CNDOL method has been used to evaluate the Coulomb and Exchange contributions to the interactions of the excited states benzene dimers depending on their mutual orientation in benzene aggregates.[973] Lately, the TDDFT method has been used to investigate the benzene,[974–976] and larger polycyclic aromatic dimers.[974,977–983] Alternatively to the TDDFT method, the properties of the benzene dimer have been calculated using the linear response coupled cluster[46,984,985] and EOM-CCSD methods.[986]

Multireference methods have been used not only to account for the character of the wavefunction but also to benchmark the methods utilizing the single-reference approach. A

moderate size of the benzene dimer, with the full π-valence active space of twelve electrons in twelve orbitals has allowed to calculate the CASPT2 potential energy surface.[987] Calculations have revealed the existence of two minima, bound excimer with eclipsed stacked conformation and additional tilted T-shape local minimum separated by distorted T-shape saddle point.

Properties of eclipsed stacked benzene excimer have been investigated using the CASPT2[987,988] and MCQDPT methods.[989] In particular, emission wavelength, intermolecular distance, and binding energies have been discussed. The reported CASPT2 emission energies of 3.92[988] and 4.16 eV[987] agree with experimental values of 3.91 eV.[990,991] Also in agreement with the single-reference methods listed above, the multireference methods give the benzene excimer intermolecular distances shorter and binding energies larger compared to the those computed for the ground state benzene dimer.

Suitability of the single-reference approaches to estimate the benzene excimer binding energy has been discussed based on the comparison with the CASPT2 calculations.[984,981] The counterpoise-corrected CASPT2 binding energy of 0.43 eV is in good agreement with the experimental values of 0.34 – 0.36 eV.[990,991] This accuracy is reached using the single-reference linear-response coupled cluster method with triple excitations (CCSDR(3)) included.[984] Concerning suitability of the TDDFT approach,[992,981] the TD-B3LYP binding energy is slightly overestimated,[975] still close to the results of the CASPT2 method. Such agreement has been suggested to result from an error cancelation due to a poor description of the dispersion energy.[993] The dispersion corrections lower the energy at the equilibrium structure with respect to the dissociation limit, causing even larger overestimation of the binding energy.[974]

The effect of the multireference description has been shown by MCQDPT calculations of the excited states of methylene-bridged [2.2]paracyclophane ([2.2]PCP), [3.3]paracyclophane

([3.3]PCP), and siloxane-bridged paracyclophane (SiPCP)[993] (see Figure 19). The analyses of the CASSCF wavefunctions indicate mixing of the ER and CR states, similarly as found for the wavefunction of the benzene dimer. The MCQDPT method has also been used to calculate excited state interactions between phenyl rings[989] to fit the analytic potential, which has been further used to explain the observation of fully and partially overlapped excimers in fluorescent emission spectra of poly(vinylcarazole).

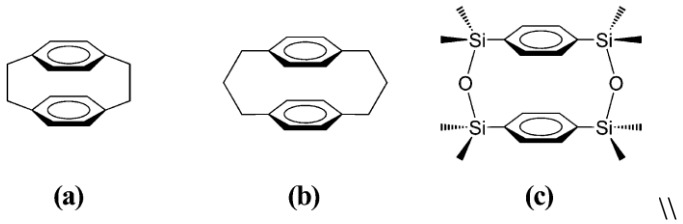

Figure 19. Structures of (a) [2,2]paracyclophane ([2,2]PCP), (b) [3,3]paracyclophane ([3,3]PCP), and (c) siloxane-bridged paracyclophane (SiPCP). Reproduced from J. Phys. Chem. A **2012**, *116*, 10194–10202. Copyright 2012 American Chemical Society.

Extension to larger polycyclic aromatic systems raises a serious problem when using conventional multi-reference methods since the π-valence active space grows exponentially with increasing size of the system. An important step towards computational studies based on the multireference treatment of the polycyclic aromatic excimers has been taken by Shirai *et al.*[966] The MCQDPT method employing a minimum size of active space (4,4) has been used to investigate the naphthalene, anthracene, pyrene, and perylene excimers. The analyses of the CASSCF wavefunctions have shown that the excimer formation is driven by a strong attraction intermolecular forces resulting from the mixing of CR and ER states with their almost equal contribution to the total wavefunction of the L_a states. Calculations performed with full π-valence (20,20) active space[479] have confirmed this finding. The L_b state, on the other hand, has been found to be of almost purely of ER character.[479] Since the transition dipole moments, responsible for the

ER interactions, are larger for the L_a state, the attractive interactions are much stronger in this state even in the absence of the CR state. These analyses explain the inversion of the L_a and L_b states of naphthalene, hypothetized by Förster.[969] Strong multireference character of the latter state makes its description using single-reference methods[479,545,981] and even the CASPT2 approach employing a truncated active space[479] questionable. Additionally, description of CR states at the TDDFT method should be critically examined. Excimer wavefunctions have also been investigated based on an analysis of the transition density matrix showing that excimer formation is accompanied by about a 50/50 mixture of ER and CR character in the cases of the naphthalene,[534] adenine,[846] and pyridine[538] dimers. It was also highlighted, that the change in wavefunction character could be monitored in terms of the NTO singular values: Whereas two NTO pairs are needed to describe the excitonic states at a larger separations, only one NTO pair is required for the excimer.[534,549]

The character of the stabilizing interactions in AEs has also been discussed based on the topological analyses of electron density $\rho(\mathbf{r})$ by means of the quantum theory of atoms in molecules.[994] CASPT2//CASSCF(12,12) has been used to provide the information on the natural orbitals.[988] The authors have not found any indication that intermolecular charge transfer contributes to excimer formation and have claimed that a net increase of electrons delocalized between the monomers observed upon the excitation very likely contributes to the excimer stability.

Concerning larger polyacenes, an attempt to better understand the singlet fission mechanism observed in the crystalline pentacene[995] has motivated studies on pentacene dimers. The linear-response TDDFT approach is not adequate since it is incapable to describe the states with multi-exciton character involved in the singlet-fission mechanism. The multireference perturbation calculations on the pentacene dimers[995] have revealed splitting of the photoexcited

state into two triplet states via an intermediate dark state of multi-exciton character. Calculations based on the restricted active space spin-flip method (RAS-2SF) method,[996,997] in combination with TDDFT calculations performed on the tetracene and pentacene dimers in the crystal-structure orientation (see Figure 20 for pentacene dimer), have suggested a nonadiabatic coupling between the optically allowed exciton and dark multi-exciton states. [998] Based on the dipole moment, it was argued that no interference of the charge-transfer states was present.[998] However, this interpretation was subsequently challenged,[999] considering that in the case of CR states there is a cancellation between two CT processes occurring in opposite directions leading to no change in the dipole moment despite the presence of CT. Different experimental observations of the singlet fission process of tetracene and pentacene have been explained by changes in energy ordering of states, which causes the triplet-triplet annihilation to compete in the former system. Alternatively, based on the studies performed using the extended multi-configuration quasi-degenerate perturbation theory (XMCQDPT) and a diabatization scheme, the charge-transfer state has been proposed to induce mixing of the multi- and single-exciton states.[1000] This observation confirms the previously proposed mechanism[938,1001] according to which the singlet fission proceeds via a coherent mechanism.[1002]

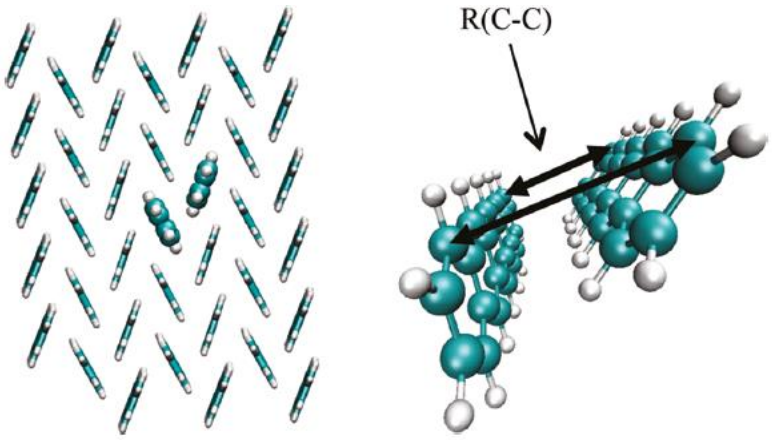

Figure 20. The pentacene dimer (right side) within the herringbone structure (left side), which represents one layer of the organic crystal. Reproduced from J. Am. Chem. Soc. **2011**, *133*, 19944–19952. Copyright 2011 American Chemical Society.

3.3.6. Transition metal complexes: metalloporphyrins

Metal-porphyrin complexes serve as active sites of metalloproteins and are involved in a large number of enzymatic processes.[1003] The large size of these systems, their high density of states, and their multiple spin states pose significant challenges for theoreticians.[1004]

Given the scale of metal-porphyrin complexes, the natural methodological choice is to use DFT and TDDFT, as recently reviewed by Visser and Stillman.[1005] Nevertheless, even the description of the ground state of the several multiplets at the DFT level is extremely dependent on the functional, which may deliver wrong state orders and divergences in the energy gaps up to 2 eV, as shown in a recent benchmark of Fe-porphyrins.[1006] Similar deviations have been found when comparing DFT and CASPT2 for Mn-porphyrins[1007] and Cu-corroles (a species closely related to porphyrin).[1008] DFT has also been shown to have a performance inferior to that of CASPT2 for calculations of relative spin-state energies of diverse heme models in Ref.[1009]. In the same paper, CASPT2 accuracy is gauged against CCSD(T) for small heme models, showing systematic errors of about 5 kcal/mol. A recent study comparing TDDFT to correlated SR methods

found that the local BLYP functional provided good excitation energies of Mg-porphyrin while giving a poor description of the wavefunctions in terms of several density-matrix-based wavefunction descriptors (exciton size and electron-hole correlation) whereas the opposite (i.e. good wavefunctions and poor energies) was true for the range-separated CAM-B3LYP functional.[651]

The superiority of CASPT2 over DFT on the studies of transition metal complexes goes beyond accuracy. Roos and co-authors,[1010] for instance, have unambiguously shown by means of CASPT2 calculations that chloroiron corrole is a noninnocent ligand, with an S = 3/2 Fe(III) antiferromagnetically coupled to a corrole radical, ending a debate on whether it would be an S = 1 Fe(IV) coupling.

Shaik and Chen[1004] have focused on a conceptual interpretation of heme systems, expanding their multiconfigurational wavefunction into valence-bond configurations based on localized orbitals. Their goal was to unify the descriptions of DFT and multiconfigurational methods. Among their findings, they have shown that multiconfigurational and multireference calculations are more sensitive to the environment than DFT calculations. They also found out that hybrid functionals tend to mimic multireference and multiconfigurational results by assuming symmetry-broken solutions with partially occupied natural Kohn-Sham orbitals.

Metal-porphyrin complexes feature a high density of excited states, with different origins, including d→d, π→π*, d→π*, and double excitations. The energetic proximity between these states makes it difficult to properly determine their order. Moreover, when computed with MS-CASPT2, these states show different dependencies on the IPEA parameter, with d→d state not being sensitive to IPEA choice and π→π* states changing by 1 eV between IPEA 0 and 1 a.u.[1011]

In fact, Kerridge has recommended not to use IPEA shifts in the simulations of the free base, Mn-, and Zn-porphyrins.[1012]

With the focus on the computational efficiency, it has been shown that RASSCF may be an efficient approach to calculate excited states of the free base and metalloporphyrins.[1012] If considered for the conjugated π-system, the full space should correlate 26 electrons in 24 orbitals, well beyond the capability of conventional CASSCF. However, using restricted spaces (RAS1 and RAS3), it is possible to simulate highly correlated spaces at a fraction of the CASSCF cost,[1012] allowing the calculation not only of vertical excitations but also reaction pathways and minimum energy intersystem crossing points.[1013] Naturally, dynamic correlation plays a significant role in these systems and must be accounted for, usually via RASPT2 calculations.[295] The performance of RASPT2 for calculations of first-row transition-metal systems has been systematically investigated in Ref.[1014]. Recently, Vlaisavljevich and Shiozaki have reported the XMS-CASPT2 optimization of Cu-corrole,[1015] paving the way for investigations beyond the conventional CASPT2//CASSCF protocol.

Accurate multireference simulations of this class of systems start to be possible thanks to DMRG methodology, which allows the treatment of unprecedently large active spaces (Section 2.7). In Ref. [1016], for instance, the reactivity of a non-heme iron active site was investigated with active spaces as large as 35 electrons in 26 orbitals. In Ref. [1017], Phung and coauthors have tested the accuracy of DMRG-cu(4)-CASPT2 (in which the 4-cumulant is discarded) against that of DMRG-CASPT2 (with exact 4-particle reduced matrix) for the calculation of the excited states of Fe-porphyrin, Mn-porphyrin, and other transition metal complexes up to cu(4)-CASPT2(28,30). They found out that the cu(4) approximation works well as long as the active space is smaller than

24 orbitals. DMRG-MRCI+Q calculations for the free base and Fe-porphyrin, including active spaces in the CASSCF section as large as (29,29), has been described in Refs.[69,70].

4. Conclusions

In this review, the different types of MR methods for calculations on excited states have been discussed in detail. Due to the pronounced manifestations of quasi-degeneracies in orbital energies and electronic states, MR theory and efficient computational techniques are strongly needed for successful simulations. The MRCI method is certainly one of the oldest methods in this field. In the form of the uncontracted version, it is also the conceptually simplest one, derived by a straightforward application of the Ritz variational principle. Due to efficient parallelization, the large expansion spaces encountered in *uc*-MRCI can be handled quite well and interesting chemical applications can be treated. However, the discussion of methods also showed that significant specialization and formal development has to be invested for enhancing the computational efficiency, which then allows the treatment of molecular systems similar in size than of ground state calculations, while simultaneously coping with the complexities of the excited state problems. Internal contraction is one major tool to achieve this efficiency. It has been used in MRCI and MRPT methods. The CASPT2 method is probably the most popular and successful outcome and is expected to keep this position even though other perturbation approaches such MRMP2 and NEVPT2 should be considered as well. In combination with methods such as DMRG, new horizons of applications will be made available.

From experience with the high accuracy of SR coupled cluster theory, the extension to the MR domain is strongly needed but still limited in its generality by many formal problems, which still have to be solved. In the search for enhanced computational efficiency, the MR aspects have

been introduced and combined with DFT, a development that has led to great benefit for the calculation of excited states. Even more progress has to be expected from these approaches. Interestingly, semiempirical methods contribute a non-negligible share to the success of MR calculations on excited states.

MR methods will probably never be as popular as, for instance, Kohn-Sham DFT. Their intrinsic complexity requires an advanced knowledge of quantum chemistry to be used and the computational and resource requirements are inevitably very large. Moreover, another challenge (which is absolutely not restricted to MR methods) is the availability of a large number of methods with no clear hierarchy between them. Nevertheless, we may expect that a series of developments will positively impact the field, bringing the MR methods near to black-box approaches (requiring minimal intervention from the users) and turning them doable for medium-sized molecules composed of few tens of atoms. Among these developments, DMRG (Section 2.7.1) is the leading promise to allow to increase the active spaces beyond the current limits. The implementation of MR methods on GPUs[126] should reduce wall-time resources. The development of algorithms for automatic construction of active and reference spaces[1018] may also be the seed for the popularization of MR methods beyond specialized circles.

The applications discussed cover a deep analysis of the electronic states of diatomics to larger molecular systems, mostly characterized by conjugated π systems as chromophores. The evolution of excited states in polyenes represents not only a critical testbed for methods but also reflects the paradigmatic importance of this class of compounds for chemistry. Extension to polycyclic aromatic compounds leads into the field of Materials Science by creating model systems for finite graphitic systems. The knowledge of the photophysics and photochemistry of nucleic acids, DNA, aminoacids, and proteins is of immense relevance for understanding of biological

processes. All achieved progress is unthinkable without the dominating contributions of MR theories. We hope that the present review of methods and applications will encourage increased activities in this field and will also result in the creation of an increasing number of new success stories.

Acknowledgements

FBCM, AJAA, and HL thank the Fundação de Amparo à Pesquisa do Estado de São Paulo (FAPESP)/Tianjin University SPRINT program (Project No. 2017/50157-4) for travel support. AJAA and HL acknowledge financial support from the School of Pharmaceutical Science and Technology, Tianjin University, China. DN acknowledges the supports from research project RVO (61388963) of the IOCB of the CAS and of the Czech Science Foundation (GA16-16959S). Financial support for PGS has been provided by the National Research, Innovation and Development Office (NKFIH) of Hungary, Grant No KH124293. FBCM thanks Fundação de Amparo à Pesquisa do Estado de São Paulo (FAPESP) under grant 2017/07707-3, and Conselho Nacional de Desenvolvimento Científico e Tecnológico (CNPq) under grants 307052/2016-8, 404337/2016-3. MB work was supported by Excellence Initiative of Aix-Marseille University (A*MIDEX) and the project Equip@Meso (ANR-10-EQPX-29-01), both funded by the French Government “Investissements d’Avenir” program. MB also acknowledges funding from and of the WSPLIT project (ANR-17-CE05-0005-01). The authors thank for discussions with M. Filatov, E. Fromager, and R. Lindh.

References

(1) Middleton, C. T.; de La Harpe, K.; Su, C.; Law, Y. K.; Crespo-Hernández, C. E.; Kohler, B. DNA Excited-State Dynamics: From Single Bases to the Double Helix. *Annu. Rev. Phys. Chem.* **2009**, *60*, 217–239.

(2) Cheng, Y.-C.; Fleming, G. R. Dynamics of Light Harvesting in Photosynthesis. *Annu. Rev. Phys. Chem.* **2009**, *60*, 241–262.

(3) Wenderich, K.; Mul, G. Methods, Mechanism, and Applications of Photodeposition in Photocatalysis: A Review. *Chem. Rev.* **2016**, *116*, 14587–14619.

(4) Mazzio, K. A.; Luscombe, C. K. The Future of Organic Photovoltaics. *Chem. Soc. Rev.* **2015**, *44*, 78–90.

(5) Petrenko, T.; Neese, F. Analysis and Prediction of Absorption Band Shapes, Fluorescence Band Shapes, Resonance Raman Intensities, and Excitation Profiles Using the Time-Dependent Theory of Electronic Spectroscopy. *J. Chem. Phys.* **2007**, *127*, 164319.

(6) Stolow, A.; Bragg, A. E.; Neumark, D. M. Femtosecond Time-Resolved Photoelectron Spectroscopy. *Chem. Rev.* **2004**, *104*, 1719–1758.

(7) Born, M.; Oppenheimer, R. Zur Quantentheorie der Molekeln. *Ann. Phys.* **1927**, *389*, 457–484.

(8) Born, M.; Huang, K. *Dynamical Theory of Crystal Lattices*; Oxford University Press; Oxford, UK, 1954.

(9) Negri, F.; Zgierski, M. Z. On the Vibronic Structure of the $S_0 \leftrightarrow S_1$ Transitions in Azulene. *J. Chem. Phys.* **1993**, *99*, 4318–4326.

(10) Dierksen, M.; Grimme, S. Density Functional Calculations of the Vibronic Structure of Electronic Absorption Spectra. *J. Chem. Phys.* **2004**, *120*, 3544–3554.

(11) Mebel, A. M.; Hayashi, M.; Liang, K. K.; Lin, S. H. Ab Initio Calculations of Vibronic Spectra and Dynamics for Small Polyatomic Molecules: Role of Duschinsky Effect. *J. Phys. Chem. A* **1999**, *103*, 10674–10690.

(12) Foresman, J. B.; Head-Gordon, M.; Pople, J. A.; Frisch, M. J. Toward a Systematic Molecular Orbital Theory for Excited States. *J. Phys. Chem.* **1992**, *96*, 135–149.

(13) Stanton, J. F.; Bartlett, R. J. The Equation of Motion Coupled-cluster Method. A Systematic Biorthogonal Approach to Molecular Excitation Energies, Transition Probabilities, and Excited State Properties. *J. Chem. Phys.* **1993**, *98*, 7029–7039.

(14) Bartlett, R. J. Coupled-Cluster Theory and Its Equation-of-Motion Extensions. *Wiley Interdiscip. Rev. Comput. Mol. Sci.* **2012**, *2*, 126–138.

(15) Krylov, A. I. Equation-of-Motion Coupled-Cluster Methods for Open-Shell and Electronically Excited Species: The Hitchhiker's Guide to Fock Space. *Annu. Rev. Phys. Chem.* **2008**, *59*, 433–462.

(16) Casida, M. E. Time-Dependent Density Functional Response Theory for Molecules. In *Recent Advances in Density Functional Methods (Part I)*; Chong, D. P., Ed.; World Scientific: Singapore, 1995; pp 155–192.

(17) Furche, F.; Ahlrichs, R. Adiabatic Time-Dependent Density Functional Methods for Excited State Properties. *J. Chem. Phys.* **2002**, *117*, 7433–7447.

(18) Shavitt, I. The Method of Configuration Interaction. In *Methods of Electronic Structure Theory*; Schaefer, H. F., Ed.; Plenum: New York, 1977; pp 189–275.

(19) Shavitt, I. The History and Evolution of Configuration Interaction. *Mol. Phys.* **1998**, *94*, 3–17.

(20) Buenker, R. J.; Peyerimhoff, S. D. Individualized Configuration Selection in CI Calculations with Subsequent Energy Extrapolation. *Theor. Chim. Acta* **1974**, *35*, 33–58.

(21) Buenker, R. J.; Peyerimhoff, S. D.; Butscher, W. Applicability of the Multi-Reference Double-Excitation CI (MRD-CI) Method to the Calculation of Electronic Wavefunctions and Comparison with Related Techniques. *Mol. Phys.* **1978**, *35*, 771–791.

(22) Szalay, P. G.; Müller, T.; Gidofalvi, G.; Lischka, H.; Shepard, R. Multiconfiguration Self-Consistent Field and Multireference Configuration Interaction Methods and Applications. *Chem. Rev.* **2012**, *112*, 108–181.

(23) Shavitt, I. The History and Evolution of Configuration Interaction. *Mol. Phys.* **1998**, *94*, 3–17.

(24) Meyer, W. Configuration Expansion by Means of Pseudonatural Orbitals. In *Methods of Electronic Structure Theory*; Schaefer, H. F., Ed.; Modern Theoretical Chemistry; Plenum: New York, 1977; pp 413–446.

(25) Siegbahn, P. E. M. Direct Configuration Interaction with a Reference State Composed of Many Reference Configurations. *Int. J. Quantum Chem.* **1980**, *18*, 1229–1242.

(26) Werner, H.-J.; Reinsch, E.-A. The Self-consistent Electron Pairs Method for Multiconfiguration Reference State Functions. *J. Chem. Phys.* **1982**, *76*, 3144–3156.

(27) Buenker, R. J.; Peyerimhoff, S. D. Ab Initio Calculations Close to the Full CI Level of Accuracy and Their Use for the Interpretation of Molecular Spectra. In *New Horizons of Quantum Chemistry*; Löwdin, P.-O., Pullmann, B., Eds.; Springer Netherlands: Dordrecht,

1983; pp 183–219.

(28) Bartlett, R. J. Many-Body Perturbation Theory and Coupled Cluster Theory for Electron Correlation in Molecules. *Annu. Rev. Phys. Chem.* **1981**, *32*, 359–401.

(29) Pople, J. A.; Binkley, J. S.; Seeger, R. Theoretical Models Incorporating Electron Correlation. *Int. J. Quantum Chem.* **1976**, *10*, 1–19.

(30) Davidson, E. R. Configuration Interaction Description of Electron Correlation. In *The World of Quantum Chemistry*; Daudel, R., Pullman, B., Eds.; Springer Netherlands: Dordrecht, 1974; pp 17–30.

(31) Langhoff, S. R.; Davidson, E. R. Configuration Interaction Calculations on the Nitrogen Molecule. *Int. J. Quantum Chem.* **1974**, *8*, 61–72.

(32) Gdanitz, R. J.; Ahlrichs, R. The Averaged Coupled-Pair Functional (ACPF): A Size-Extensive Modification of MR CI(SD). *Chem. Phys. Lett.* **1988**, *143*, 413–420.

(33) Szalay, P. G.; Nooijen, M.; Bartlett, R. J. Alternative Ansätze in Single Reference Coupled-cluster Theory. III. A Critical Analysis of Different Methods. *J. Chem. Phys.* **1995**, *103*, 281–298.

(34) Szalay, P. G.; Bartlett, R. J. Multi-Reference Averaged Quadratic Coupled-Cluster Method: A Size-Extensive Modification of Multi-Reference CI. *Chem. Phys. Lett.* **1993**, *214*, 481–488.

(35) Andersson, K.; Malmqvist, P. A.; Roos, B. O.; Sadlej, A. J.; Wolinski, K. Second-Order Perturbation Theory with a CASSCF Reference Function. *J. Phys. Chem.* **1990**, *94*, 5483–5488.

(36) Andersson, K.; Malmqvist, P. A.; Roos, B. O. Second-order Perturbation Theory with a

Complete Active Space Self-consistent Field Reference Function. *J. Chem. Phys.* **1992**, *96*, 1218–1226.

(37) Finley, J.; Malmqvist, P. A.; Roos, B. O.; Serrano-Andrés, L. The Multi-State CASPT2 Method. *Chem. Phys. Lett.* **1998**, *288*, 299–306.

(38) Roos, B. O.; Andersson, K.; Fülscher, M. P.; Malmqvist, P. A.; Serrano-Andrés, L.; Pierloot, K.; Merchán, M. Multiconfigurational Perturbation Theory: Applications in Electronic Spectroscopy. In *New Methods in Computational Quantum Mechanics*; Prigogine, I., Rice, S. A., Eds.; Advances in Chemical Physics, Vol. XCIII; John Wiley & Sons, Inc.: Hoboken, 1996; pp 219–331.

(39) Hirao, K. Multireference Møller-Plesset Perturbation Theory for High-Spin Open-Shell Systems. *Chem. Phys. Lett.* **1992**, *196*, 397–403.

(40) Angeli, C.; Cimiraglia, R.; Evangelisti, S.; Leininger, T.; Malrieu, J.-P. Introduction of N-Electron Valence States for Multireference Perturbation Theory. *J. Chem. Phys.* **2001**, *114*, 10252–10264.

(41) *Photoinduced Processes in Nucleic Acids*; Barbatti, M., Borin, A. C., Ullrich, S., Eds.; Topics in Current Chemistry, Vols. 355 and 356; Springer: Cham, 2014.

(42) Barbatti, M.; Shepard, R.; Lischka, H. Computational and Methodological Elements for Nonadiabatic Trajectory Dynamics Simulations of Molecules. In *Conical Intersections: Theory, Computation and Experiment*; Domcke, W., Yarkony, D. R., Köppel, H., Eds.; Advanced Series in Physical Chemistry, Vol. 17; World Scientific: Singapore, 2011; pp 415–462.

(43) *Conical Intersections: Electronic Structure, Dynamics and Spectroscopy*; Domcke, W.,

Yarkony, D. R., Köppel, H., Eds.; Advanced Series in Physical Chemistry, Vol. 15; World Scientific: Singapore, 2004.

(44) *Conical Intersections: Theory, Computation and Experiment*; Domcke, W., Yarkony, D. R., Köppel, H., Eds.; Advanced Series in Physical Chemistry, Vol. 17; World Scientific: Singapore, 2011.

(45) Serrano-Andrés, L.; Merchán, M. Quantum Chemistry of the Excited State: 2005 Overview. *J. Mol. Struct. THEOCHEM* **2005**, *729*, 99–108.

(46) Dreuw, A.; Head-Gordon, M. Single-Reference Ab Initio Methods for the Calculation of Excited States of Large Molecules. *Chem. Rev.* **2005**, *105*, 4009–4037.

(47) Krylov, A. I. Spin-Flip Equation-of-Motion Coupled-Cluster Electronic Structure Method for a Description of Excited States, Bond Breaking, Diradicals, and Triradicals. *Acc. Chem. Res.* **2006**, *39*, 83–91.

(48) David Sherrill, C.; Schaefer, H. F. The Configuration Interaction Method: Advances in Highly Correlated Approaches. In *Advances in Quantum Chemistry*; Löwdin, P.-O., Sabin, J. R., Zerner, M. C., Brändas, E., Eds.; Academic Press: San Diego, 1999; Vol. 34, pp 143–269.

(49) Bartlett, R. J.; Musiał, M. Coupled-Cluster Theory in Quantum Chemistry. *Rev. Mod. Phys.* **2007**, *79*, 291–352.

(50) Helgaker, T.; Jørgensen, P.; Olsen, J. Configuration-Interaction Theory. In *Molecular Electronic-Structure Theory*; John Wiley & Sons, Ltd: Chichester, UK, 2014; pp 523–597.

(51) Roos, B. O.; Taylor, P. R.; Siegbahn, P. E. M. A Complete Active Space SCF Method (CASSCF) Using a Density Matrix Formulated Super-CI Approach. *Chem. Phys.* **1980**, *48*,

157–173.

(52) Shamasundar, K. R.; Knizia, G.; Werner, H.-J. A New Internally Contracted Multi-Reference Configuration Interaction Method. *J. Chem. Phys.* **2011**, *135*, 54101.

(53) Shavitt, I. The Graphical Unitary Group Approach and Its Application to Direct Configuration Interaction Calculations. In *The Unitary Group for the Evaluation of Electronic Energy Matrix Elements*; Hinze, J., Ed.; Lecture Notes in Chemistry, Vol. 22; Springer-Verlag: Berlin, 1981; pp 51–99.

(54) Duch, W.; Karwowski, J. Symmetric Group Approach to Configuration Interaction Methods. *Comput. Phys. Reports* **1985**, *2*, 93–170.

(55) Lischka, H.; Müller, T.; Szalay, P. G.; Shavitt, I.; Pitzer, R. M.; Shepard, R. Columbus-a Program System for Advanced Multireference Theory Calculations. *Wiley Interdiscip. Rev. Comput. Mol. Sci.* **2011**, *1*, 191–199.

(56) Davidson, E. R. The Iterative Calculation of a Few of the Lowest Eigenvalues and Corresponding Eigenvectors of Large Real-Symmetric Matrices. *J. Comput. Phys.* **1975**, *17*, 87–94.

(57) Olsen, J.; Jørgensen, P.; Simons, J. Passing the One-Billion Limit in Full Configuration-Interaction (FCI) Calculations. *Chem. Phys. Lett.* **1990**, *169*, 463–472.

(58) Roos, B.; Siegbahn, P. E. M. The Direct Configuration Interaction Method from Molecular Integrals. In *Methods of Electronic Structure Theory*; Schaefer, H. F., Ed.; Modern Theoretical Chemistry; Plenum: New York, 1977; pp 277–318.

(59) de Jong, W. A.; Bylaska, E.; Govind, N.; Janssen, C. L.; Kowalski, K.; Muller, T.; Nielsen, I. M. B.; van Dam, H. J. J.; Veryazov, V.; Lindh, R. Utilizing High Performance Computing

for Chemistry: Parallel Computational Chemistry. *Phys. Chem. Chem. Phys.* **2010**, *12*, 6896–6920.

(60) Dachsel, H.; Lischka, H.; Shepard, R.; Nieplocha, J.; Harrison, R. J. A Massively Parallel Multireference Configuration Interaction Program: The Parallel COLUMBUS Program. *J. Comput. Chem.* **1997**, *18*, 430–448.

(61) Bartlett, R. J. Many-Body Perturbation Theory and Coupled Cluster Theory for Electron Correlation in Molecules. *Annu. Rev. Phys. Chem.* **1981**, *32*, 359–401.

(62) Langhoff, S. R.; Davidson, E. R. Configuration Interaction Calculations on the Nitrogen Molecule. *Int. J. Quantum Chem.* **1974**, *8*, 61–72.

(63) Szalay, P. G.; Bartlett, R. J. Approximately Extensive Modifications of the Multireference Configuration Interaction Method: A Theoretical and Practical Analysis. *J. Chem. Phys.* **1995**, *103*, 3600–3612.

(64) Szalay, P. G.; Müller, T.; Lischka, H. Excitation Energies and Transition Moments by the Multireference Averaged Quadratic Coupled Cluster (MR-AQCC) Method. *Phys. Chem. Chem. Phys.* **2000**, *2*, 2067–2073.

(65) Sivalingam, K.; Krupicka, M.; Auer, A. A.; Neese, F. Comparison of Fully Internally and Strongly Contracted Multireference Configuration Interaction Procedures. *J. Chem. Phys.* **2016**, *145*, 054104.

(66) Werner, H.-J.; Knowles, P. J. An Efficient Internally Contracted Multiconfiguration–reference Configuration Interaction Method. *J. Chem. Phys.* **1988**, *89*, 5803–5814.

(67) Knowles, P. J.; Werner, H.-J. An Efficient Method for the Evaluation of Coupling Coefficients in Configuration Interaction Calculations. *Chem. Phys. Lett.* **1988**, *145*, 514–

522.

(68) Werner, H.-J.; Knowles, P. J.; Knizia, G.; Manby, F. R.; Schütz, M. Molpro: A General-Purpose Quantum Chemistry Program Package. *Wiley Interdiscip. Rev. Comput. Mol. Sci.* **2012**, *2*, 242–253.

(69) Saitow, M.; Kurashige, Y.; Yanai, T. Multireference Configuration Interaction Theory Using Cumulant Reconstruction with Internal Contraction of Density Matrix Renormalization Group Wave Function. *J. Chem. Phys.* **2013**, *139*, 044118.

(70) Saitow, M.; Kurashige, Y.; Yanai, T. Fully Internally Contracted Multireference Configuration Interaction Theory Using Density Matrix Renormalization Group: A Reduced-Scaling Implementation Derived by Computer-Aided Tensor Factorization. *J. Chem. Theory Comput.* **2015**, *11*, 5120–5131.

(71) Angeli, C.; Cimiraglia, R.; Malrieu, J.-P. N-Electron Valence State Perturbation Theory: A Fast Implementation of the Strongly Contracted Variant. *Chem. Phys. Lett.* **2001**, *350*, 297–305.

(72) Neese, F. The ORCA Program System. *Wiley Interdiscip. Rev. Comput. Mol. Sci.* **2012**, *2*, 73–78.

(73) Bauschlicher, C. W.; Langhoff, S. R. Full Configuration-interaction Study of the Ionic–neutral Curve Crossing in LiF. *J. Chem. Phys.* **1988**, *89*, 4246–4254.

(74) Knowles, P. J.; Werner, H.-J. Internally Contracted Multiconfiguration-Reference Configuration Interaction Calculations for Excited States. *Theor. Chim. Acta* **1992**, *84*, 95–103.

(75) Harding, L. B.; Klippenstein, S. J.; Lischka, H.; Shepard, R. Comparison of Multireference

Configuration Interaction Potential Energy Surfaces for H + O_2 → HO_2: The Effect of Internal Contraction. *Theor. Chem. Acc.* **2014**, *133*, 1–7.

(76) Buenker, R. J.; Peyerimhoff, S. D.; Butscher, W. Applicability of the Multi-Reference Double-Excitation CI (MRD-CI) Method to the Calculation of Electronic Wavefunctions and Comparison with Related Techniques. *Mol. Phys.* **1978**, *35*, 771–791.

(77) Hanrath, M.; Engels, B. New Algorithms for an Individually Selecting MR-CI Program. *Chem. Phys.* **1997**, *225*, 197–202.

(78) Stampfuss, P.; Wenzel, W.; Keiter, H. The Parallel Implementation of Configuration-selecting Multireference Configuration Interaction Method. *J. Comput. Chem.* **1999**, *20*, 1559–1570.

(79) Stampfuß, P.; Hamacher, K.; Wenzel, W. Massively Parallel Individually Selecting Configuration Interaction. *J. Mol. Struct. THEOCHEM* **2000**, *506*, 99–106.

(80) Engels, B.; Hanrath, M.; Lennartz, C. Individually Selecting Multi-Reference CI and Its Application to Biradicalic Cyclizations. *Comput. Chem.* **2001**, *25*, 15–38.

(81) Evangelista, F. A. Adaptive Multiconfigurational Wave Functions. *J. Chem. Phys.* **2014**, *140*, 124114.

(82) Schriber, J. B.; Evangelista, F. A. Adaptive Configuration Interaction for Computing Challenging Electronic Excited States with Tunable Accuracy. *J. Chem. Theory Comput.* **2017**, *13*, 5354–5366.

(83) Ahlrichs, R.; Lischka, H.; Zurawski, B.; Kutzelnigg, W. PNO-CI (Pair-Natural-Orbital Configuration Interaction) and CEPA-PNO (Coupled Electron Pair Approximation with Pair Natural Orbitals) Calculations of Molecular Systems. IV. The Molecules N_2, F_2, C_2H_2,

C_2H_4, and C_2H_6. *J. Chem. Phys.* **1975**, *63*, 4685–4694.

(84) Pulay, P. Localizability of Dynamic Electron Correlation. *Chem. Phys. Lett.* **1983**, *100*, 151–154.

(85) Saebo, S.; Pulay, P. Local Treatment of Electron Correlation. *Annu. Rev. Phys. Chem.* **1993**, *44*, 213–236.

(86) Walter, D.; Carter, E. A. Multi-Reference Weak Pairs Local Configuration Interaction: Efficient Calculations of Bond Breaking. *Chem. Phys. Lett.* **2001**, *346*, 177–185.

(87) Walter, D.; Venkatnathan, A.; Carter, E. A. Local Correlation in the Virtual Space in Multireference Singles and Doubles Configuration Interaction. *J. Chem. Phys.* **2003**, *118*, 8127–8139.

(88) Krisiloff, D. B.; Carter, E. A. Approximately Size Extensive Local Multireference Singles and Doubles Configuration Interaction. *Phys. Chem. Chem. Phys.* **2012**, *14*, 7710–7717.

(89) Venkatnathan, A.; Szilva, A. B.; Walter, D.; Gdanitz, R. J.; Carter, E. A. Size Extensive Modification of Local Multireference Configuration Interaction. *J. Chem. Phys.* **2004**, *120*, 1693–1704.

(90) Krisiloff, D. B.; Dieterich, J. M.; Libisch, F.; Carter, E. A. Numerical Challenges in a Cholesky-Decomposed Local Correlation Quantum Chemistry Framework. In *Mathematical and Computational Modeling: With Applications in Natural and Social Sciences, Engineering, and the Arts*; Melnik, R., Ed.; John Wiley & Sons, Inc: Hoboken, 2015; pp 59–91.

(91) Das, A.; Müller, T.; Plasser, F.; Krisiloff, D. B.; Carter, E. A.; Lischka, H. Local Electron Correlation Treatment in Extended Multireference Calculations: Effect of Acceptor–Donor

Substituents on the Biradical Character of the Polycyclic Aromatic Hydrocarbon Heptazethrene. *J. Chem. Theory Comput.* **2017**, *13*, 2612–2622.

(92) Escorihuela, J.; Das, A.; Looijen, W. J. E.; van Delft, F. L.; Aquino, A. J. A.; Lischka, H.; Zuilhof, H. Kinetics of the Strain-Promoted Oxidation-Controlled Cycloalkyne-1,2-Quinone Cycloaddition: Experimental and Theoretical Studies. *J. Org. Chem.* **2018**, *83*, 244–252.

(93) Chwee, T. S.; Szilva, A. B.; Lindh, R.; Carter, E. A. Linear Scaling Multireference Singles and Doubles Configuration Interaction. *J. Chem. Phys.* **2008**, *128*, 224106.

(94) Chwee, T. S.; Carter, E. A. Cholesky Decomposition within Local Multireference Singles and Doubles Configuration Interaction. *J. Chem. Phys.* **2010**, *132*, 74104.

(95) Chwee, T. S.; Carter, E. A. Density Fitting of Two-Electron Integrals in Local Multireference Single and Double Excitation Configuration Interaction Calculations. *Mol. Phys.* **2010**, *108*, 2519–2526.

(96) Chwee, T. S.; Carter, E. A. Valence Excited States in Large Molecules via Local Multireference Singles and Doubles Configuration Interaction. *J. Chem. Theory Comput.* **2011**, *7*, 103–111.

(97) Löwdin, P.-O. Quantum Theory of Many-Particle Systems. I. Physical Interpretations by Means of Density Matrices, Natural Spin-Orbitals, and Convergence Problems in the Method of Configurational Interaction. *Phys. Rev.* **1955**, *97*, 1474–1489.

(98) Lu, Z.; Matsika, S. High-Multiplicity Natural Orbitals in Multireference Configuration Interaction for Excited States. *J. Chem. Theory Comput.* **2012**, *8*, 509–517.

(99) Barr, T. L.; Davidson, E. R. Nature of the Configuration-Interaction Method In. *Phys. Rev.*

A **1970**, *1*, 644–658.

(100) Landau, A.; Khistyaev, K.; Dolgikh, S.; Krylov, A. I. Frozen Natural Orbitals for Ionized States within Equation-of-Motion Coupled-Cluster Formalism. *J. Chem. Phys.* **2010**, *132*, 14109.

(101) Bofill, J. M.; Pulay, P. The Unrestricted Natural Orbital–complete Active Space (UNO–CAS) Method: An Inexpensive Alternative to the Complete Active Space–self-consistent-field (CAS–SCF) Method. *J. Chem. Phys.* **1989**, *90*, 3637–3646.

(102) Abrams, M. L.; Sherrill, C. D. Natural Orbitals as Substitutes for Optimized Orbitals in Complete Active Space Wavefunctions. *Chem. Phys. Lett.* **2004**, *395*, 227–232.

(103) Neese, F. A Spectroscopy Oriented Configuration Interaction Procedure. *J. Chem. Phys.* **2003**, *119*, 9428–9443.

(104) Aquilante, F.; Todorova, T. K.; Gagliardi, L.; Pedersen, T. B.; Roos, B. O. Systematic Truncation of the Virtual Space in Multiconfigurational Perturbation Theory. *J. Chem. Phys.* **2009**, *131*, 34113.

(105) Potts, D. M.; Taylor, C. M.; Chaudhuri, R. K.; Freed, K. F. The Improved Virtual Orbital-Complete Active Space Configuration Interaction Method, a "Packageable" Efficient Ab Initio Many-Body Method for Describing Electronically Excited States. *J. Chem. Phys.* **2001**, *114*, 2592–2600.

(106) Lu, Z.; Matsika, S. High-Multiplicity Natural Orbitals in Multireference Configuration Interaction for Excited State Potential Energy Surfaces. *J. Phys. Chem. A* **2013**, *117*, 7421–7430.

(107) Shepard, R. The Multiconfiguration Self-Consistent Field Method. In *Ab Initio Methods in*

Quantum Chemistry, Part 2; Lawley, K. P., Ed.; Advances in Chemical Physics, Vol. LXIX; John Wiley & Sons, Ltd.: Hoboken, 1987; Vol. 69, pp 63–200.

(108) Werner, H.-J. Matrix-Formulated Direct Multiconfiguration Self-Consistent Field and Multiconfiguration Reference Configuration-Interaction Methods. In *Ab Initio Methods in Quantum Chemistry Part 2*; Lawley, K. P., Ed.; Advances in Chemical Physics, Vol. LXIX; John Wiley & Sons, Ltd.: Hoboken, 1987; pp 1–62.

(109) Roos, B. O. The Complete Active Space Self-Consistent Field Method and Its Applications in Electronic Structure Calculations. In *Ab Initio Methods in Quantum Chemistry Part 2*; Lawley, K. P., Ed.; Advances in Chemical Physics, Vol. LXIX; John Wiley & Sons, Ltd.: Hoboken, 1987; pp 399–445.

(110) Werner, H.-J.; Meyer, W. A Quadratically Convergent MCSCF Method for the Simultaneous Optimization of Several States. *J. Chem. Phys.* **1981**, *74*, 5794–5801.

(111) Lischka, H.; Dallos, M.; Shepard, R. Analytic MRCI Gradient for Excited States: Formalism and Application to the n-π* Valence- and n-(3s,3p) Rydberg States of Formaldehyde. *Mol. Phys.* **2002**, *100*, 1647–1658.

(112) Weyl, H. *The Classical Groups: Their Invariants and Representations*, 2nd ed.; Mathematics Series; Princeton University Press, 1946.

(113) Malmqvist, P. A.; Rendell, A.; Roos, B. O. The Restricted Active Space Self-Consistent-Field Method, Implemented with a Split Graph Unitary Group Approach. *J. Phys. Chem.* **1990**, *94*, 5477–5482.

(114) Ivanic, J. Direct Configuration Interaction and Multiconfigurational Self-Consistent-Field Method for Multiple Active Spaces with Variable Occupations. I. Method. *J. Chem. Phys.*

2003, *119*, 9364–9376.

(115) Ma, D.; Li Manni, G.; Gagliardi, L. The Generalized Active Space Concept in Multiconfigurational Self-Consistent Field Methods. *J. Chem. Phys.* **2011**, *135*, 044128.

(116) Veryazov, V.; Malmqvist, P. A.; Roos, B. O. How to Select Active Space for Multiconfigurational Quantum Chemistry? *Int. J. Quantum Chem.* **2011**, *111*, 3329–3338.

(117) Pulay, P.; Hamilton, T. P. UHF Natural Orbitals for Defining and Starting MC-SCF Calculations. *J. Chem. Phys.* **1988**, *88*, 4926–4933.

(118) Keller, S.; Boguslawski, K.; Janowski, T.; Reiher, M.; Pulay, P. Selection of Active Spaces for Multiconfigurational Wavefunctions. *J. Chem. Phys.* **2015**, *142*, 244104.

(119) Jensen, H. J. A.; Jørgensen, P.; Ågren, H.; Olsen, J. Second-order Møller–Plesset Perturbation Theory as a Configuration and Orbital Generator in Multiconfiguration Self-consistent Field Calculations. *J. Chem. Phys.* **1988**, *88*, 3834–3839.

(120) Boggio-Pasqua, M.; Groenhof, G. On the Use of Reduced Active Space in CASSCF Calculations. *Comput. Theor. Chem.* **2014**, *1040–1041*, 6–13.

(121) Krausbeck, F.; Mendive-Tapia, D.; Thom, A. J. W.; Bearpark, M. J. Choosing RASSCF Orbital Active Spaces for Multiple Electronic States. *Comput. Theor. Chem.* **2014**, *1040–1041*, 14–19.

(122) Das, G.; Wahl, A. C. Extended Hartree-Fock Wavefunctions: Optimized Valence Configurations for H_2 and Li_2 , Optimized Double Configurations for F_2. *J. Chem. Phys.* **1966**, *44*, 87–96.

(123) Lee, T. J.; Allen, W. D.; Schaefer, H. F. The Analytic Evaluation of Energy First Derivatives for Two-configuration Self-consistent-field Configuration Interaction (TCSCF-CI) Wave

Functions. Application to Ozone and Ethylene. *J. Chem. Phys.* **1987**, *87*, 7062–7075.

(124) Sun, Q.; Yang, J.; Chan, G. K.-L. A General Second Order Complete Active Space Self-Consistent-Field Solver for Large-Scale Systems. *Chem. Phys. Lett.* **2017**, *683*, 291–299.

(125) Nakatani, N.; Guo, S. Density Matrix Renormalization Group (DMRG) Method as a Common Tool for Large Active-Space CASSCF/CASPT2 Calculations. *J. Chem. Phys.* **2017**, *146*, 94102.

(126) Snyder, J. W.; Curchod, B. F. E.; Martínez, T. J. GPU-Accelerated State-Averaged Complete Active Space Self-Consistent Field Interfaced with Ab Initio Multiple Spawning Unravels the Photodynamics of Provitamin D3. *J. Phys. Chem. Lett.* **2016**, *7*, 2444–2449.

(127) Granucci, G.; Toniolo, A. Molecular Gradients for Semiempirical CI Wavefunctions with Floating Occupation Molecular Orbitals. *Chem. Phys. Lett.* **2000**, *325*, 79–85.

(128) Slavicek, P.; Martinez, T. J. Ab Initio Floating Occupation Molecular Orbital-Complete Active Space Configuration Interaction: An Efficient Approximation to CASSCF. *J. Chem. Phys.* **2010**, *132*, 234102.

(129) Shepard, R. A Discussion of Some Aspects of the MCSCF Method. In *Relativistic and Electron Correlation Effects in Molecules and Solids, NATO ASI Series vol. 318*; Malli, G. L., Ed.; Plenum: New York, 1992; p 161.

(130) McLean, A. D.; Lengsfield, B. H.; Pacansky, J.; Ellinger, Y. Symmetry Breaking in Molecular Calculations and the Reliable Prediction of Equilibrium Geometries. The Formyloxyl Radical as an Example. *J. Chem. Phys.* **1985**, *83*, 3567–3576.

(131) Ayala, P. Y.; Schlegel, H. B. A Nonorthogonal CI Treatment of Symmetry Breaking in Sigma Formyloxyl Radical. *J. Chem. Phys.* **1998**, *108*, 7560–7567.

(132) Rauk, A.; Yu, D.; Borowski, P.; Roos, B. CASSCF, CASPT2, and MRCI Investigations of Formyloxyl Radical (HCOO·). *Chem. Phys.* **1995**, *197*, 73–80.

(133) Stanton, J. F.; Kadagathur, N. S. Pseudorotational Interconversion of the $^2A_1$ and $^2B_2$ States of HCOO. *J. Mol. Struct.* **1996**, *376*, 469–474.

(134) Blahous, C. P.; Yates, B. F.; Xie, Y.; Schaefer, H. F. Symmetry Breaking in the NO_2 σ Radical: Construction of the $^2A_1$ and $^2B_2$ States with Cs Symmetry Complete Active Space Self-consistent-field Wave Functions. *J. Chem. Phys.* **1990**, *93*, 8105–8109.

(135) Saeh, J. C.; Stanton, J. F. Application of an Equation-of-Motion Coupled Cluster Method Including Higher-Order Corrections to Potential Energy Surfaces of Radicals. *J. Chem. Phys.* **1999**, *111*, 8275–8285.

(136) Martin, J. M. L.; El-Yazal, J.; François, J.-P.; Gijbels, R. The Structure and Energetics of B_3N_2, B_2N_3, and BN_4. *Mol. Phys.* **1995**, *85*, 527–537.

(137) Asmis, K. R.; Taylor, T. R.; Neumark, D. M. Anion Photoelectron Spectroscopy of B_2N^-. *J. Chem. Phys.* **1999**, *111*, 8838–8851.

(138) Gwaltney, S. R.; Head-Gordon, M. Calculating the Equilibrium Structure of the BNB Molecule: Real vs. Artifactual Symmetry Breaking. *Phys. Chem. Chem. Phys.* **2001**, *3*, 4495–4500.

(139) Kalemos, A.; Dunning, T. H.; Mavridis, A. On Symmetry Breaking in BNB: Real or Artifactual? *J. Chem. Phys.* **2004**, *120*, 1813–1819.

(140) Russ, N. J.; Crawford, T. D.; Tschumper, G. S. Real versus Artifactual Symmetry-Breaking Effects in Hartree–Fock, Density-Functional, and Coupled-Cluster Methods. *J. Chem. Phys.* **2004**, *120*, 7298–7306.

(141) Stanton, J. F. An Unusually Large Nonadiabatic Error in the BNB Molecule. *J. Chem. Phys.* **2010**, *133*, 174309.

(142) Li, X.; Paldus, J. Analysis and Classification of Symmetry Breaking in Linear ABA-Type Triatomics. *J. Chem. Phys.* **2009**, *130*, 164116.

(143) Kalemos, A. Symmetry Breaking in a Nutshell: The Odyssey of a Pseudo Problem in Molecular Physics. The $\tilde{X}^2\Sigma_u^+$ BNB Case Revisited. *J. Chem. Phys.* **2013**, *138*, 224302.

(144) Stanton, J. F. Note: Is It Symmetric or Not? *J. Chem. Phys.* **2013**, *139*, 46102.

(145) Stanton, J. F.; Gauss, J.; Bartlett, R. J. On the Choice of Orbitals for Symmetry Breaking Problems with Application to NO_3. *J. Chem. Phys.* **1992**, *97*, 5554–5559.

(146) Eisfeld, W.; Morokuma, K. A Detailed Study on the Symmetry Breaking and Its Effect on the Potential Surface of NO_3. *J. Chem. Phys.* **2000**, *113*, 5587–5597.

(147) Szalay, P. G.; Császár, A. G.; Fogarasi, G.; Karpfen, A.; Lischka, H. An Ab Initio Study of the Structure and Vibrational Spectra of Allyl and 1,4-Pentadienyl Radicals. *J. Chem. Phys.* **1990**, *93*, 1246–1256.

(148) Löwdin, P.-O. Discussion on The Hartree-Fock Approximation. *Rev. Mod. Phys.* **1963**, *35*, 496–501.

(149) Davidson, E. R.; Borden, W. T. Symmetry Breaking in Polyatomic Molecules: Real and Artifactual. *J. Phys. Chem.* **1983**, *87*, 4783–4790.

(150) Shu, Y.; Levine, B. G. Reducing the Propensity for Unphysical Wavefunction Symmetry Breaking in Multireference Calculations of the Excited States of Semiconductor Clusters. *J. Chem. Phys.* **2013**, *139*, 74102.

(151) Kalemos, A. Revisiting the Symmetry Breaking in the $\tilde{X}^2\Sigma_u^+$ State of BNB. *J. Chem. Phys.* **2016**, *144*, 234315.

(152) Bartlett, R. J. Coupled-Cluster Approach to Molecular Structure and Spectra: A Step toward Predictive Quantum Chemistry. *J. Phys. Chem.* **1989**, *93*, 1697–1708.

(153) Bartlett, R. J.; Stanton, J. F. Applications of Post-Hartree-Fock Methods: A Tutorial. In *Reviews in Computational Chemistry*; John Wiley & Sons, Inc., 2007; pp 65–169.

(154) Gauss, J. Coupled-Cluster Theory. In *Encyclopedia of Computational Chemistry*; John Wiley & Sons, Ltd, 2002.

(155) Bartlett, R. J. The Coupled-Cluster Revolution. *Mol. Phys.* **2010**, *108*, 2905–2920.

(156) Lyakh, D. I.; Musiał, M.; Lotrich, V. F.; Bartlett, R. J. Multireference Nature of Chemistry: The Coupled-Cluster View. *Chem. Rev.* **2012**, *112*, 182–243.

(157) Bartlett, R. J. To Multireference or Not to Multireference: That Is the Question? *Int. J. Mol. Sci.* **2002**, *3*, 579–603.

(158) Bartlett, R. J.; Purvis, G. D. Molecular Applications of Coupled Cluster and Many-Body Perturbation Methods. *Phys. Scr.* **1980**, *21*, 255–265.

(159) Purvis, G. D.; Bartlett, R. J. A Full Coupled-cluster Singles and Doubles Model: The Inclusion of Disconnected Triples. *J. Chem. Phys.* **1982**, *76*, 1910–1918.

(160) Noga, J.; Bartlett, R. J. The Full CCSDT Model for Molecular Electronic Structure. *J. Chem. Phys.* **1987**, *86*, 7041–7050.

(161) Christiansen, O.; Koch, H.; Jørgensen, P. The Second-Order Approximate Coupled Cluster Singles and Doubles Model CC2. *Chem. Phys. Lett.* **1995**, *243*, 409–418.

(162) Stanton, J. F.; Gauss, J. Perturbative Treatment of the Similarity Transformed Hamiltonian in Equation-of-motion Coupled-cluster Approximations. *J. Chem. Phys.* **1995**, *103*, 1064–1076.

(163) Raghavachari, K.; Trucks, G. W.; Pople, J. A.; Head-Gordon, M. A Fifth-Order Perturbation Comparison of Electron Correlation Theories. *Chem. Phys. Lett.* **1989**, *157*, 479–483.

(164) Lee, Y. S.; Bartlett, R. J. A Study of Be_2 with Many-body Perturbation Theory and a Coupled-cluster Method Including Triple Excitations. *J. Chem. Phys.* **1984**, *80*, 4371–4377.

(165) Urban, M.; Noga, J.; Cole, S. J.; Bartlett, R. J. Towards a Full CCSDT Model for Electron Correlation. *J. Chem. Phys.* **1985**, *83*, 4041–4046.

(166) Noga, J.; Bartlett, R. J.; Urban, M. Towards a Full CCSDT Model for Electron Correlation. CCSDT-n Models. *Chem. Phys. Lett.* **1987**, *134*, 126–132.

(167) Koch, H.; Christiansen, O.; Jørgensen, P.; Sanchez de Merás, A. M.; Helgaker, T. The CC3 Model: An Iterative Coupled Cluster Approach Including Connected Triples. *J. Chem. Phys.* **1997**, *106*, 1808–1818.

(168) Monkhorst, H. J. Calculation of Properties with the Coupled-Cluster Method. *Int. J. Quantum Chem.* **1977**, *12*, 421–432.

(169) Sekino, H.; Bartlett, R. J. A Linear Response, Coupled-Cluster Theory for Excitation Energy. *Int. J. Quantum Chem.* **1984**, *26*, 255–265.

(170) Koch, H.; Jørgensen, P. Coupled Cluster Response Functions. *J. Chem. Phys.* **1990**, *93*, 3333–3344.

(171) Koch, H.; Kobayashi, R.; Sanchez de Merás, A.; Jørgensen, P. Calculation of Size-intensive Transition Moments from the Coupled Cluster Singles and Doubles Linear Response

Function. *J. Chem. Phys.* **1994**, *100*, 4393–4400.

(172) Kánnár, D.; Szalay, P. G. Benchmarking Coupled Cluster Methods on Valence Singlet Excited States. *J. Chem. Theory Comput.* **2014**, *10*, 3757–3765.

(173) Comeau, D. C.; Bartlett, R. J. The Equation-of-Motion Coupled-Cluster Method. Applications to Open- and Closed-Shell Reference States. *Chem. Phys. Lett.* **1993**, *207*, 414–423.

(174) Koch, H.; Jensen, H. J. A.; Jørgensen, P.; Helgaker, T. Excitation Energies from the Coupled Cluster Singles and Doubles Linear Response Function (CCSDLR). Applications to Be, CH^+, CO, and H_2O. *J. Chem. Phys.* **1990**, *93*, 3345–3350.

(175) Kucharski, S. A.; Włoch, M.; Musiał, M.; Bartlett, R. J. Coupled-Cluster Theory for Excited Electronic States: The Full Equation-of-Motion Coupled-Cluster Single, Double, and Triple Excitation Method. *J. Chem. Phys.* **2001**, *115*, 8263–8266.

(176) Hald, K.; Jørgensen, P.; Olsen, J.; Jaszuński, M. An Analysis and Implementation of a General Coupled Cluster Approach to Excitation Energies with Application to the B_2 Molecule. *J. Chem. Phys.* **2001**, *115*, 671–679.

(177) Gwaltney, S. R.; Nooijen, M.; Bartlett, R. J. Simplified Methods for Equation-of-Motion Coupled-Cluster Excited State Calculations. *Chem. Phys. Lett.* **1996**, *248*, 189–198.

(178) Trofimov, A. B.; Schirmer, J. An Efficient Polarization Propagator Approach to Valence Electron Excitation Spectra. *J. Phys. B At. Mol. Opt. Phys.* **1995**, *28*, 2299–2324.

(179) Trofimov, A. B.; Stelter, G.; Schirmer, J. A Consistent Third-Order Propagator Method for Electronic Excitation. *J. Chem. Phys.* **1999**, *111*, 9982–9999.

(180) Harbach, P. H. P.; Wormit, M.; Dreuw, A. The Third-Order Algebraic Diagrammatic

Construction Method (ADC(3)) for the Polarization Propagator for Closed-Shell Molecules: Efficient Implementation and Benchmarking. *J. Chem. Phys.* **2014**, *141*, 064113.

(181) Head-Gordon, M.; Rico, R. J.; Oumi, M.; Lee, T. J. A Doubles Correction to Electronic Excited States from Configuration Interaction in the Space of Single Substitutions. *Chem. Phys. Lett.* **1994**, *219*, 21–29.

(182) Christiansen, O.; Koch, H.; Jørgensen, P. Response Functions in the CC3 Iterative Triple Excitation Model. *J. Chem. Phys.* **1995**, *103*, 7429–7441.

(183) Watts, J. D.; Bartlett, R. J. Iterative and Non-Iterative Triple Excitation Corrections in Coupled-Cluster Methods for Excited Electronic States: The EOM-CCSDT-3 and EOM-CCSD(T̃) Methods. *Chem. Phys. Lett.* **1996**, *258*, 581–588.

(184) Christiansen, O.; Koch, H.; Jørgensen, P. Perturbative Triple Excitation Corrections to Coupled Cluster Singles and Doubles Excitation Energies. *J. Chem. Phys.* **1996**, *105*, 1451–1459.

(185) Matthews, D. A.; Stanton, J. F. A New Approach to Approximate Equation-of-Motion Coupled Cluster with Triple Excitations. *J. Chem. Phys.* **2016**, *145*, 124102.

(186) Watts, J. D.; Bartlett, R. J. Economical Triple Excitation Equation-of-Motion Coupled-Cluster Methods for Excitation Energies. *Chem. Phys. Lett.* **1995**, *233*, 81–87.

(187) Kánnár, D.; Tajti, A.; Szalay, P. G. Accuracy of Coupled Cluster Excitation Energies in Diffuse Basis Sets. *J. Chem. Theory Comput.* **2017**, *13*, 202–209.

(188) Szalay, P. G.; Watson, T.; Perera, A.; Lotrich, V.; Bartlett, R. J. Benchmark Studies on the Building Blocks of DNA. 3. Watson–Crick and Stacked Base Pairs. *J. Phys. Chem. A* **2013**, *117*, 3149–3157.

(189) Schreiber, M.; Silva-Junior, M. R.; Sauer, S. P. A.; Thiel, W. Benchmarks for Electronically Excited States: CASPT2, CC2, CCSD, and CC3. *J. Chem. Phys.* **2008**, *128*, 134110.

(190) Sauer, S. P. A.; Schreiber, M.; Silva-Junior, M. R.; Thiel, W. Benchmarks for Electronically Excited States: A Comparison of Noniterative and Iterative Triples Corrections in Linear Response Coupled Cluster Methods: CCSDR(3) versus CC3. *J. Chem. Theory Comput.* **2009**, *5*, 555–564.

(191) Silva-Junior, M. R.; Sauer, S. P. A.; Schreiber, M.; Thiel, W. Basis Set Effects on Coupled Cluster Benchmarks of Electronically Excited States: CC3, CCSDR(3) and CC2. *Mol. Phys.* **2010**, *108*, 453–465.

(192) Kánnár, D.; Szalay, P. G. Benchmarking Coupled Cluster Methods on Singlet Excited States of Nucleobases. *J. Mol. Model.* **2014**, *20*, 2503.

(193) Köhn, A.; Tajti, A. Can Coupled-Cluster Theory Treat Conical Intersections? *J. Chem. Phys.* **2007**, *127*, 44105.

(194) Kjønstad, E. F.; Myhre, R. H.; Martínez, T. J.; Koch, H. Crossing Conditions in Coupled Cluster Theory. *J. Chem. Phys.* **2017**, *147*, 164105.

(195) Tuna, D.; Lefrancois, D.; Wolański, Ł.; Gozem, S.; Schapiro, I.; Andruniów, T.; Dreuw, A.; Olivucci, M. Assessment of Approximate Coupled-Cluster and Algebraic-Diagrammatic-Construction Methods for Ground- and Excited-State Reaction Paths and the Conical-Intersection Seam of a Retinal-Chromophore Model. *J. Chem. Theory Comput.* **2015**, *11*, 5758–5781.

(196) Jeziorski, B.; Monkhorst, H. J. Coupled-Cluster Method for Multideterminantal Reference States. *Phys. Rev. A* **1981**, *24*, 1668–1681.

(197) Mukherjee, D.; Moitra, R. K.; Mukhopadhyay, A. Correlation Problem in Open-Shell Atoms and Molecules. *Mol. Phys.* **1975**, *30*, 1861–1888.

(198) Banerjee, A.; Simons, J. The Coupled-Cluster Method with a Multiconfiguration Reference State. *Int. J. Quantum Chem.* **1981**, *19*, 207–216.

(199) Banerjee, A.; Simons, J. Applications of Multiconfigurational Coupled-cluster Theory. *J. Chem. Phys.* **1982**, *76*, 4548–4559.

(200) Mukherjee, D. Normal Ordering and a Wick-like Reduction Theorem for Fermions with Respect to a Multi-Determinantal Reference State. *Chem. Phys. Lett.* **1997**, *274*, 561–566.

(201) Kutzelnigg, W.; Mukherjee, D. Normal Order and Extended Wick Theorem for a Multiconfiguration Reference Wave Function. *J. Chem. Phys.* **1997**, *107*, 432–449.

(202) Oliphant, N.; Adamowicz, L. Multireference Coupled-cluster Method Using a Single-reference Formalism. *J. Chem. Phys.* **1991**, *94*, 1229–1235.

(203) Krylov, A. I. Spin-Flip Configuration Interaction: An Electronic Structure Model That Is Both Variational and Size-Consistent. *Chem. Phys. Lett.* **2001**, *350*, 522–530.

(204) Levchenko, S. V; Krylov, A. I. Equation-of-Motion Spin-Flip Coupled-Cluster Model with Single and Double Substitutions: Theory and Application to Cyclobutadiene. *J. Chem. Phys.* **2003**, *120*, 175–185.

(205) Köhn, A.; Hanauer, M.; Mück, L. A.; Jagau, T.-C.; Gauss, J. State-Specific Multireference Coupled-Cluster Theory. *Wiley Interdiscip. Rev. Comput. Mol. Sci.* **2013**, *3*, 176–197.

(206) Jeziorski, B. Multireference Coupled-Cluster Ansatz. *Mol. Phys.* **2010**, *108*, 3043–3054.

(207) Szalay, P. G. On Our Efforts Constructing a Proper Multireference Coupled-Cluster

Method. *Mol. Phys.* **2010**, *108*, 3055–3065.

(208) Bartlett, R. J.; Trickey, S. B. Foreword. *Mol. Phys.* **2010**, *108*, 2815–2822.

(209) Kucharski, S. A.; Bartlett, R. J. Hilbert Space Multireference Coupled-cluster Methods. I. The Single and Double Excitation Model. *J. Chem. Phys.* **1991**, *95*, 8227–8238.

(210) Li, X.; Paldus, J. General-Model-Space State-Universal Coupled-Cluster Theory: Connectivity Conditions and Explicit Equations. *J. Chem. Phys.* **2003**, *119*, 5320–5333.

(211) Balková, A.; Kucharski, S. A.; Meissner, L.; Bartlett, R. J. The Multireference Coupled-cluster Method in Hilbert Space: An Incomplete Model Space Application to the LiH Molecule. *J. Chem. Phys.* **1991**, *95*, 4311–4316.

(212) Kucharski, S. A.; Balková, A.; Szalay, P. G.; Bartlett, R. J. Hilbert Space Multireference Coupled-cluster Methods. II. A Model Study on H_8. *J. Chem. Phys.* **1992**, *97*, 4289–4300.

(213) Piecuch, P.; Paldus, J. Orthogonally Spin-Adapted Multi-Reference Hilbert Space Coupled-Cluster Formalism: Diagrammatic Formulation. *Theor. Chim. Acta* **1992**, *83*, 69–103.

(214) Li, X.; Paldus, J. Automation of the Implementation of Spin-adapted Open-shell Coupled-cluster Theories Relying on the Unitary Group Formalism. *J. Chem. Phys.* **1994**, *101*, 8812–8826.

(215) Li, X.; Paldus, J. Performance of the General-Model-Space State-Universal Coupled-Cluster Method. *J. Chem. Phys.* **2004**, *120*, 5890–5902.

(216) Evangelista, F. A.; Allen, W. D.; Schaefer, H. F. High-Order Excitations in State-Universal and State-Specific Multireference Coupled Cluster Theories: Model Systems. *J. Chem. Phys.* **2006**, *125*, 154113.

(217) Balková, A.; Bartlett, R. J. The Two-determinant Coupled-cluster Method for Electric Properties of Excited Electronic States: The Lowest $^1B_1$ and $^3B_1$ States of the Water Molecule. *J. Chem. Phys.* **1993**, *99*, 7907–7915.

(218) Balková, A.; Bartlett, R. J. On the Singlet–triplet Separation in Methylene: A Critical Comparison of Single- versus Two-determinant (Generalized Valence Bond) Coupled Cluster Theory. *J. Chem. Phys.* **1995**, *102*, 7116–7123.

(219) Balková, A.; Bartlett, R. J. A Multireference Coupled-cluster Study of the Ground State and Lowest Excited States of Cyclobutadiene. *J. Chem. Phys.* **1994**, *101*, 8972–8987.

(220) Neogrády, P.; Szalay, P. G.; Kraemer, W. P.; Urban, M. Coupled-Cluster Study of Spectroscopic Constants of the Alkali Metal Diatomics: Ground and the Singlet Excited States of Na_2, NaLi, NaK, and NaRb. *Collect. Czech. Chem. Commun.* **2005**, *70*, 951–978.

(221) Li, X.; Paldus, J. Multireference General-Model-Space State-Universal and State-Specific Coupled-Cluster Approaches to Excited States. *J. Chem. Phys.* **2010**, *133*, 184106.

(222) Li, X.; Paldus, J. A Multireference Coupled-Cluster Study of Electronic Excitations in Furan and Pyrrole. *J. Phys. Chem. A* **2010**, *114*, 8591–8600.

(223) Li, X.; Paldus, J. Multi-Reference State-Universal Coupled-Cluster Approaches to Electronically Excited States. *J. Chem. Phys.* **2011**, *134*, 214118.

(224) Hubač, I.; Neogrády, P. Size-Consistent Brillouin-Wigner Perturbation Theory with an Exponentially Parametrized Wave Function: Brillouin-Wigner Coupled-Cluster Theory. *Phys. Rev. A* **1994**, *50*, 4558–4564.

(225) Mášik, J.; Hubač, I.; Mach, P. Single-Root Multireference Brillouin-Wigner Coupled-Cluster Theory: Applicability to the F_2 Molecule. *J. Chem. Phys.* **1998**, *108*, 6571–6579.

(226) Mahapatra, U. S.; Datta, B.; Mukherjee, D. A State-Specific Multi-Reference Coupled Cluster Formalism with Molecular Applications. *Mol. Phys.* **1998**, *94*, 157–171.

(227) Mahapatra, U. S.; Datta, B.; Mukherjee, D. A Size-Consistent State-Specific Multireference Coupled Cluster Theory: Formal Developments and Molecular Applications. *J. Chem. Phys.* **1999**, *110*, 6171–6188.

(228) Mahapatra, U. S.; Chattopadhyay, S. Potential Energy Surface Studies via a Single Root Multireference Coupled Cluster Theory. *J. Chem. Phys.* **2010**, *133*, 74102.

(229) Mahapatra, U. S.; Chattopadhyay, S. Evaluation of the Performance of Single Root Multireference Coupled Cluster Method for Ground and Excited States, and Its Application to Geometry Optimization. *J. Chem. Phys.* **2011**, *134*, 44113.

(230) Pittner, J. Continuous Transition between Brillouin–Wigner and Rayleigh–Schrödinger Perturbation Theory, Generalized Bloch Equation, and Hilbert Space Multireference Coupled Cluster. *J. Chem. Phys.* **2003**, *118*, 10876–10889.

(231) Kong, L. Connection between a Few Jeziorski-Monkhorst Ansatz-Based Methods. *Int. J. Quantum Chem.* **2009**, *109*, 441–447.

(232) Datta, D.; Mukherjee, D. The Spin-Free Analogue of Mukherjee's State-Specific Multireference Coupled Cluster Theory. *J. Chem. Phys.* **2011**, *134*, 54122.

(233) Das, S.; Mukherjee, D.; Kállay, M. Full Implementation and Benchmark Studies of Mukherjee's State-Specific Multireference Coupled-Cluster Ansatz. *J. Chem. Phys.* **2010**, *132*, 74103.

(234) Hanrath, M. An Exponential Multireference Wave-Function Ansatz. *J. Chem. Phys.* **2005**, *123*, 84102.

(235) Hanrath, M. Initial Applications of an Exponential Multi-Reference Wavefunction Ansatz. *Chem. Phys. Lett.* **2006**, *420*, 426–431.

(236) Engels-Putzka, A.; Hanrath, M. Multi-Reference Coupled-Cluster Study of the Potential Energy Surface of the Hydrogen Fluoride Dissociation Including Excited States. *J. Mol. Struct. THEOCHEM* **2009**, *902*, 59–65.

(237) Šimsa, D.; Demel, O.; Bhaskaran-Nair, K.; Hubač, I.; Mach, P.; Pittner, J. Multireference Coupled Cluster Study of the Oxyallyl Diradical. *Chem. Phys.* **2012**, *401*, 203–207.

(238) Jagau, T.-C.; Gauss, J. Linear-Response Theory for Mukherjee's Multireference Coupled-Cluster Method: Excitation Energies. *J. Chem. Phys.* **2012**, *137*, 44116.

(239) Samanta, P. K.; Mukherjee, D.; Hanauer, M.; Köhn, A. Excited States with Internally Contracted Multireference Coupled-Cluster Linear Response Theory. *J. Chem. Phys.* **2014**, *140*, 134108.

(240) Chattopadhyay, S.; Mahapatra, U. S.; Mukherjee, D. Development of a Linear Response Theory Based on a State-Specific Multireference Coupled Cluster Formalism. *J. Chem. Phys.* **2000**, *112*, 7939–7952.

(241) Stanton, F. J.; Gauss, J.; Harding, M. E.; Szalay, P. G.; From, with contributions; Auer, A. A.; Bartlett, R. J.; Benedikt, U.; Berger, C.; Bernholdt, D. E.; et al. CFOUR, Coupled-Cluster Techniques for Computational Chemistry, a Quantum Chemical Program Package.

(242) Evangelista, F. A.; Gauss, J. Insights into the Orbital Invariance Problem in State-Specific Multireference Coupled Cluster Theory. *J. Chem. Phys.* **2010**, *133*, 44101.

(243) Mukherjee, D.; Moitra, R. K.; Mukhopadhyay, A. Applications of a Non-Perturbative Many-Body Formalism to General Open-Shell Atomic and Molecular Problems:

Calculation of the Ground and the Lowest π-π* Singlet and Triplet Energies and the First Ionization Potential of Trans-Butadiene. *Mol. Phys.* **1977**, *33*, 955–969.

(244) Evangelista, F. A.; Gauss, J. An Orbital-Invariant Internally Contracted Multireference Coupled Cluster Approach. *J. Chem. Phys.* **2011**, *134*, 114102.

(245) Hanauer, M.; Köhn, A. Pilot Applications of Internally Contracted Multireference Coupled Cluster Theory, and How to Choose the Cluster Operator Properly. *J. Chem. Phys.* **2011**, *134*, 204111.

(246) Datta, D.; Kong, L.; Nooijen, M. A State-Specific Partially Internally Contracted Multireference Coupled Cluster Approach. *J. Chem. Phys.* **2011**, *134*, 214116.

(247) Hanauer, M.; Köhn, A. Communication: Restoring Full Size Extensivity in Internally Contracted Multireference Coupled Cluster Theory. *J. Chem. Phys.* **2012**, *137*, 131103.

(248) Yanai, T.; Chan, G. K.-L. Canonical Transformation Theory for Multireference Problems. *J. Chem. Phys.* **2006**, *124*, 194106.

(249) Yanai, T.; Chan, G. K.-L. Canonical Transformation Theory from Extended Normal Ordering. *J. Chem. Phys.* **2007**, *127*, 104107.

(250) Chen, Z.; Hoffmann, M. R. Orbitally Invariant Internally Contracted Multireference Unitary Coupled Cluster Theory and Its Perturbative Approximation: Theory and Test Calculations of Second Order Approximation. *J. Chem. Phys.* **2012**, *137*, 14108.

(251) Aoto, Y. A.; Köhn, A. Internally Contracted Multireference Coupled-Cluster Theory in a Multistate Framework. *J. Chem. Phys.* **2016**, *144*, 074103.

(252) Datta, D.; Nooijen, M. Multireference Equation-of-Motion Coupled Cluster Theory. *J. Chem. Phys.* **2012**, *137*, 204107.

(253) Demel, O.; Datta, D.; Nooijen, M. Additional Global Internal Contraction in Variations of Multireference Equation of Motion Coupled Cluster Theory. *J. Chem. Phys.* **2013**, *138*, 134108.

(254) Nooijen, M.; Demel, O.; Datta, D.; Kong, L.; Shamasundar, K. R.; Lotrich, V.; Huntington, L. M.; Neese, F. Communication: Multireference Equation of Motion Coupled Cluster: A Transform and Diagonalize Approach to Electronic Structure. *J. Chem. Phys.* **2014**, *140*, 81102.

(255) Huntington, L. M. J.; Nooijen, M. Application of Multireference Equation of Motion Coupled-Cluster Theory to Transition Metal Complexes and an Orbital Selection Scheme for the Efficient Calculation of Excitation Energies. *J. Chem. Phys.* **2015**, *142*, 194111.

(256) Liu, Z.; Huntington, L. M. J.; Nooijen, M. Application of the Multireference Equation of Motion Coupled Cluster Method, Including Spin–orbit Coupling, to the Atomic Spectra of Cr, Mn, Fe and Co. *Mol. Phys.* **2015**, *113*, 2999–3013.

(257) Huntington, L. M. J.; Demel, O.; Nooijen, M. Benchmark Applications of Variations of Multireference Equation of Motion Coupled-Cluster Theory. *J. Chem. Theory Comput.* **2016**, *12*, 114–132.

(258) Stanton, J. F.; Gauss, J.; Perera, S. A.; Watts, J. D.; Yau, A. D.; Nooijen, M.; Oliphant, N.; Szalay, P. G.; Lauderdale, W. J.; Gwaltney, S. R.; et al. ACES II Is a Program Product of the Quantum Theory Project, University of Florida.

(259) Kállay, M.; Szalay, P. G.; Surján, P. R. A General State-Selective Multireference Coupled-Cluster Algorithm. *J. Chem. Phys.* **2002**, *117*, 980–990.

(260) Kowalski, K.; Piecuch, P. The Active-Space Equation-of-Motion Coupled-Cluster Methods

for Excited Electronic States: The EOMCCSDt Approach. *J. Chem. Phys.* **2000**, *113*, 8490–8502.

(261) Piecuch, P. Active-Space Coupled-Cluster Methods. *Mol. Phys.* **2010**, *108*, 2987–3015.

(262) Kinoshita, T.; Hino, O.; Bartlett, R. J. Coupled-Cluster Method Tailored by Configuration Interaction. *J. Chem. Phys.* **2005**, *123*, 74106.

(263) Ivanov, V. V; Adamowicz, L.; Lyakh, D. I. Excited States in the Multireference State-Specific Coupled-Cluster Theory with the Complete Active Space Reference. *J. Chem. Phys.* **2006**, *124*, 184302.

(264) Lyakh, D. I.; Ivanov, V. V; Adamowicz, L. A Generalization of the State-Specific Complete-Active-Space Coupled-Cluster Method for Calculating Electronic Excited States. *J. Chem. Phys.* **2008**, *128*, 74101.

(265) Kállay, M.; Gauss, J. Calculation of Excited-State Properties Using General Coupled-Cluster and Configuration-Interaction Models. *J. Chem. Phys.* **2004**, *121*, 9257–9269.

(266) Köhn, A.; Olsen, J. Coupled-Cluster with Active Space Selected Higher Amplitudes: Performance of Seminatural Orbitals for Ground and Excited State Calculations. *J. Chem. Phys.* **2006**, *125*, 174110.

(267) Musiał, M.; Kucharski, S. A.; Bartlett, R. J. Multireference Double Electron Attached Coupled Cluster Method with Full Inclusion of the Connected Triple Excitations: MR-DA-CCSDT. *J. Chem. Theory Comput.* **2011**, *7*, 3088–3096.

(268) Musiał, M.; Kowalska-Szojda, K.; Lyakh, D. I.; Bartlett, R. J. Potential Energy Curves via Double Electron-Attachment Calculations: Dissociation of Alkali Metal Dimers. *J. Chem. Phys.* **2013**, *138*, 194103.

(269) Demel, O.; Pittner, J. Multireference Brillouin–Wigner Coupled Cluster Method with Singles, Doubles, and Triples: Efficient Implementation and Comparison with Approximate Approaches. *J. Chem. Phys.* **2008**, *128*, 104108.

(270) Hanrath, M. Higher Excitations for an Exponential Multireference Wavefunction Ansatz and Single-Reference Based Multireference Coupled Cluster Ansatz: Application to Model Systems H_4, P_4, and BeH_2. *J. Chem. Phys.* **2008**, *128*, 154118.

(271) Evangelista, F. A.; Simmonett, A. C.; Allen, W. D.; Schaefer, H. F.; Gauss, J. Triple Excitations in State-Specific Multireference Coupled Cluster Theory: Application of Mk-MRCCSDT and Mk-MRCCSDT-n Methods to Model Systems. *J. Chem. Phys.* **2008**, *128*, 124104.

(272) Das, S.; Kállay, M.; Mukherjee, D. Inclusion of Selected Higher Excitations Involving Active Orbitals in the State-Specific Multireference Coupled-Cluster Theory. *J. Chem. Phys.* **2010**, *133*, 234110.

(273) Hanauer, M.; Köhn, A. Perturbative Treatment of Triple Excitations in Internally Contracted Multireference Coupled Cluster Theory. *J. Chem. Phys.* **2012**, *136*, 204107.

(274) Pulay, P. A Perspective on the CASPT2 Method. *Int. J. Quantum Chem.* **2011**, *111*, 3273–3279.

(275) Sinha Ray, S.; Ghosh, P.; Chaudhuri, R. K.; Chattopadhyay, S. Improved Virtual Orbitals in State Specific Multireference Perturbation Theory for Prototypes of Quasidegenerate Electronic Structure. *J. Chem. Phys.* **2017**, *146*, 64111.

(276) Hirao, K. Multireference Møller-Plesset Method. *Chem. Phys. Lett.* **1992**, *190*, 374–380.

(277) Hirao, K. Multireference Møller-Plesset Perturbation Treatment of Potential Energy Curve

of N_2. *Int. J. Quantum Chem.* **1992**, *44*, 517–526.

(278) Angeli, C.; Cimiraglia, R.; Malrieu, J.-P. N-Electron Valence State Perturbation Theory: A Spinless Formulation and an Efficient Implementation of the Strongly Contracted and of the Partially Contracted Variants. *J. Chem. Phys.* **2002**, *117*, 9138–9153.

(279) Angeli, C.; Pastore, M.; Cimiraglia, R. New Perspectives in Multireference Perturbation Theory: The n-Electron Valence State Approach. *Theor. Chem. Acc.* **2007**, *117*, 743–754.

(280) Roca-Sanjuán, D.; Aquilante, F.; Lindh, R. Multiconfiguration Second-Order Perturbation Theory Approach to Strong Electron Correlation in Chemistry and Photochemistry. *Wiley Interdiscip. Rev. Comput. Mol. Sci.* **2012**, *2*, 585–603.

(281) Roos, B. O.; Lindh, R.; Malmqvist, P. A.; Veryazov, V.; Widmark, P.-O. CASPT2/CASSCF Applications. In *Multiconfigurational Quantum Chemistry*; John Wiley & Sons, Inc.: Hoboken, NJ, USA, 2016; pp 157–219.

(282) Zobel, J. P.; Nogueira, J. J.; González, L. The IPEA Dilemma in CASPT2. *Chem. Sci.* **2017**, *8*, 1482–1499.

(283) Pulay, P. A Perspective on the CASPT2 Method. *Int. J. Quantum Chem.* **2011**, *111*, 3273–3279.

(284) Ghigo, G.; Roos, B. O.; Malmqvist, P. A. A Modified Definition of the Zeroth-Order Hamiltonian in Multiconfigurational Perturbation Theory (CASPT2). *Chem. Phys. Lett.* **2004**, *396*, 142–149.

(285) Roos, B. O.; Andersson, K. Multiconfigurational Perturbation Theory with Level Shift - the Cr_2 Potential Revisited. *Chem. Phys. Lett.* **1995**, *245*, 215–223.

(286) Roos, B. O.; Andersson, K.; Fülscher, M. P.; Serrano-Andrés, L.; Pierloot, K.; Merchán,

M.; Molina, V. Applications of Level Shift Corrected Perturbation Theory in Electronic Spectroscopy. *J. Mol. Struct. THEOCHEM* **1996**, *388*, 257–276.

(287) Forsberg, N.; Malmqvist, P. A. Multiconfiguration Perturbation Theory with Imaginary Level Shift. *Chem. Phys. Lett.* **1997**, *274*, 196–204.

(288) Levine, B. G.; Ko, C.; Quenneville, J.; MartÍnez, T. J. Conical Intersections and Double Excitations in Time-Dependent Density Functional Theory. *Mol. Phys.* **2006**, *104*, 1039–1051.

(289) Gozem, S.; Melaccio, F.; Valentini, A.; Filatov, M.; Huix-Rotllant, M.; Ferré, N.; Frutos, L. M.; Angeli, C.; Krylov, A. I.; Granovsky, A. A.; et al. Shape of Multireference, Equation-of-Motion Coupled-Cluster, and Density Functional Theory Potential Energy Surfaces at a Conical Intersection. *J. Chem. Theory Comput.* **2014**, *10*, 3074–3084.

(290) Granovsky, A. A. Extended Multi-Configuration Quasi-Degenerate Perturbation Theory: The New Approach to Multi-State Multi-Reference Perturbation Theory. *J. Chem. Phys.* **2011**, *134*, 214113.

(291) Shiozaki, T.; Győrffy, W.; Celani, P.; Werner, H.-J. Communication: Extended Multi-State Complete Active Space Second-Order Perturbation Theory: Energy and Nuclear Gradients. *J. Chem. Phys.* **2011**, *135*, 081106.

(292) Shavitt, I. Multi-State Multireference Rayleigh–Schrödinger Perturbation Theory for Mixed Electronic States: Second and Third Order. *Int. J. Mol. Sci.* **2002**, *3*, 639–655.

(293) Yost, S. R.; Kowalczyk, T.; Van Voorhis, T. A Multireference Perturbation Method Using Non-Orthogonal Hartree-Fock Determinants for Ground and Excited States. *J. Chem. Phys.* **2013**, *139*, 174104.

(294) Malmqvist, P. A.; Pierloot, K.; Shahi, A. R. M.; Cramer, C. J.; Gagliardi, L. The Restricted Active Space Followed by Second-Order Perturbation Theory Method: Theory and Application to the Study of CuO_2 and Cu_2O_2 Systems. *J. Chem. Phys.* **2008**, *128*, 204109.

(295) Sauri, V.; Serrano-Andrés, L.; Shahi, A. R. M.; Gagliardi, L.; Vancoillie, S.; Pierloot, K. Multiconfigurational Second-Order Perturbation Theory Restricted Active Space (RASPT2) Method for Electronic Excited States: A Benchmark Study. *J. Chem. Theory Comput.* **2011**, *7*, 153–168.

(296) Werner, H.-J. Third-Order Multireference Perturbation Theory The CASPT3 Method. *Mol. Phys.* **1996**, *89*, 645–661.

(297) Grabarek, D.; Walczak, E.; Andruniów, T. Assessing the Accuracy of Various Ab Initio Methods for Geometries and Excitation Energies of Retinal Chromophore Minimal Model by Comparison with CASPT3 Results. *J. Chem. Theory Comput.* **2016**, *12*, 2346–2356.

(298) Celani, P.; Stoll, H.; Werner, H.-J.; Knowles, P. J. The CIPT2 Method: Coupling of Multi-Reference Configuration Interaction and Multi-Reference Perturbation Theory. Application to the Chromium Dimer. *Mol. Phys.* **2004**, *102*, 2369–2379.

(299) Celani, P.; Werner, H.-J. Analytical Energy Gradients for Internally Contracted Second-Order Multireference Perturbation Theory. *J. Chem. Phys.* **2003**, *119*, 5044–5057.

(300) Shiozaki, T.; Werner, H.-J. Communication: Second-Order Multireference Perturbation Theory with Explicit Correlation: CASPT2-F12. *J. Chem. Phys.* **2010**, *133*, 141103.

(301) Rintelman, J. M.; Adamovic, I.; Varganov, S.; Gordon, M. S. Multireference Second-Order Perturbation Theory: How Size Consistent Is “Almost Size Consistent.” *J. Chem. Phys.* **2005**, *122*, 44105.

(302) Chen, F.; Fan, Z. A New Size Extensive Multireference Perturbation Theory. *J. Comput. Chem.* **2014**, *35*, 121–129.

(303) Dyall, K. G. The Choice of a Zeroth-order Hamiltonian for Second-order Perturbation Theory with a Complete Active Space Self-consistent-field Reference Function. *J. Chem. Phys.* **1995**, *102*, 4909–4918.

(304) Angeli, C.; Borini, S.; Cimiraglia, R. An Application of Second-Order n-Electron Valence State Perturbation Theory to the Calculation of Excited States. *Theor. Chem. Acc.* **2004**, *111*, 352–357.

(305) Angeli, C.; Borini, S.; Ferrighi, L.; Cimiraglia, R. Ab Initio N-Electron Valence State Perturbation Theory Study of the Adiabatic Transitions in Carbonyl Molecules: Formaldehyde, Acetaldehyde, and Acetone. *J. Chem. Phys.* **2005**, *122*, 114304.

(306) Pastore, M.; Angeli, C.; Cimiraglia, R. The Vertical Electronic Spectrum of Pyrrole: A Second and Third Order n-Electron Valence State Perturbation Theory Study. *Chem. Phys. Lett.* **2006**, *422*, 522–528.

(307) Guo, Y.; Sivalingam, K.; Valeev, E. F.; Neese, F. Explicitly Correlated N-Electron Valence State Perturbation Theory (NEVPT2-F12). *J. Chem. Phys.* **2017**, *147*, 64110.

(308) Angeli, C.; Borini, S.; Cestari, M.; Cimiraglia, R. A Quasidegenerate Formulation of the Second Order N-Electron Valence State Perturbation Theory Approach. *J. Chem. Phys.* **2004**, *121*, 4043–4049.

(309) Sokolov, A. Y.; Chan, G. K.-L. A Time-Dependent Formulation of Multi-Reference Perturbation Theory. *J. Chem. Phys.* **2016**, *144*, 64102.

(310) Sokolov, A. Y.; Guo, S.; Ronca, E.; Chan, G. K.-L. Time-Dependent N-Electron Valence

Perturbation Theory with Matrix Product State Reference Wavefunctions for Large Active Spaces and Basis Sets: Applications to the Chromium Dimer and All-Trans Polyenes. *J. Chem. Phys.* **2017**, *146*, 244102.

(311) Grimme, S.; Waletzke, M. Multi-Reference Moller-Plesset Theory: Computational Strategies for Large Molecules. *Phys. Chem. Chem. Phys.* **2000**, *2*, 2075–2081.

(312) Celani, P.; Werner, H.-J. Multireference Perturbation Theory for Large Restricted and Selected Active Space Reference Wave Functions. *J. Chem. Phys.* **2000**, *112*, 5546–5557.

(313) Nakano, H.; Hirao, K. A Quasi-Complete Active Space Self-Consistent Field Method. *Chem. Phys. Lett.* **2000**, *317*, 90–96.

(314) Nakano, H.; Nakatani, J.; Hirao, K. Second-Order Quasi-Degenerate Perturbation Theory with Quasi-Complete Active Space Self-Consistent Field Reference Functions. *J. Chem. Phys.* **2001**, *114*, 1133–1141.

(315) Choe, Y.-K.; Nakao, Y.; Hirao, K. Multireference Møller–Plesset Method with a Complete Active Space Configuration Interaction Reference Function. *J. Chem. Phys.* **2001**, *115*, 621–629.

(316) Hashimoto, T.; Nakano, H.; Hirao, K. Theoretical Study of the Valence π→π* Excited States of Polyacenes: Benzene and Naphthalene. *J. Chem. Phys.* **1996**, *104*, 6244–6258.

(317) Nakano, H. Quasidegenerate Perturbation Theory with Multiconfigurational Self-consistent-field Reference Functions. *J. Chem. Phys.* **1993**, *99*, 7983–7992.

(318) Nakano, H. MCSCF Reference Quasidegenerate Perturbation Theory with Epstein-Nesbet Partitioning. *Chem. Phys. Lett.* **1993**, *207*, 372–378.

(319) Nakano, H.; Uchiyama, R.; Hirao, K. Quasi-Degenerate Perturbation Theory with General

Multiconfiguration Self-Consistent Field Reference Functions. *J. Comput. Chem.* **2002**, *23*, 1166–1175.

(320) Miyajima, M.; Watanabe, Y.; Nakano, H. Relativistic Quasidegenerate Perturbation Theory with Four-Component General Multiconfiguration Reference Functions. *J. Chem. Phys.* **2006**, *124*, 44101.

(321) Ebisuzaki, R.; Watanabe, Y.; Nakano, H. Efficient Implementation of Relativistic and Non-Relativistic Quasidegenerate Perturbation Theory with General Multiconfigurational Reference Functions. *Chem. Phys. Lett.* **2007**, *442*, 164–169.

(322) Witek, H. A.; Choe, Y.-K.; Finley, J. P.; Hirao, K. Intruder State Avoidance Multireference Møller–Plesset Perturbation Theory. *J. Comput. Chem.* **2002**, *23*, 957–965.

(323) Khait, Y. G.; Song, J.; Hoffmann, M. R. Explication and Revision of Generalized Van Vleck Perturbation Theory for Molecular Electronic Structure. *J. Chem. Phys.* **2002**, *117*, 4133–4145.

(324) Ghosh, P.; Chattopadhyay, S.; Jana, D.; Mukherjee, D. State-Specific Multi-Reference Perturbation Theories with Relaxed Coefficients: Molecular Applications. *Int. J. Mol. Sci.* **2002**, *3*, 733–754.

(325) Szabados, Á.; Rolik, Z.; Tóth, G.; Surján, P. R. Multiconfiguration Perturbation Theory: Size Consistency at Second Order. *J. Chem. Phys.* **2005**, *122*, 114104.

(326) Hoffmann, M. R.; Datta, D.; Das, S.; Mukherjee, D.; Szabados, Á.; Rolik, Z.; Surján, P. R. Comparative Study of Multireference Perturbative Theories for Ground and Excited States. *J. Chem. Phys.* **2009**, *131*, 204104.

(327) Sen, A.; Sen, S.; Mukherjee, D. Aspects of Size-Consistency of Orbitally Noninvariant

Size-Extensive Multireference Perturbation Theories: A Case Study Using UGA-SSMRPT2 as a Prototype. *J. Chem. Theory Comput.* **2015**, *11*, 4129–4145.

(328) Li, C.; Evangelista, F. A. Multireference Driven Similarity Renormalization Group: A Second-Order Perturbative Analysis. *J. Chem. Theory Comput.* **2015**, *11*, 2097–2108.

(329) Hannon, K. P.; Li, C.; Evangelista, F. A. An Integral-Factorized Implementation of the Driven Similarity Renormalization Group Second-Order Multireference Perturbation Theory. *J. Chem. Phys.* **2016**, *144*, 204111.

(330) Evangelista, F. A. A Driven Similarity Renormalization Group Approach to Quantum Many-Body Problems. *J. Chem. Phys.* **2014**, *141*, 054109.

(331) Thiel, W. Semiempirical Quantum-Chemical Methods. *Wiley Interdiscip. Rev. Comput. Mol. Sci.* **2014**, *4*, 145–157.

(332) Hückel, E. Quantentheoretische Beiträge zum Benzolproblem. *Z. Phys.* **1931**, *72*, 310–337.

(333) Hoffmann, R. An Extended Hückel Theory. I. Hydrocarbons. *J. Chem. Phys.* **1963**, *39*, 1397–1412.

(334) Pariser, R.; Parr, R. G. A Semi-Empirical Theory of the Electronic Spectra and Electronic Structure of Complex Unsaturated Molecules. I. *J. Chem. Phys.* **1953**, *21*, 466–471.

(335) Pople, J. A. Electron Interaction in Unsaturated Hydrocarbons. *Trans. Faraday Soc.* **1953**, *49*, 1375.

(336) Stewart, J. J. P. Optimization of Parameters for Semiempirical Methods V: Modification of NDDO Approximations and Application to 70 Elements. *J. Mol. Model.* **2007**, *13*, 1173–1213.

(337) Stewart, J. J. P. Optimization of Parameters for Semiempirical Methods VI: More Modifications to the NDDO Approximations and Re-Optimization of Parameters. *J. Mol. Model.* **2013**, *19*, 1–32.

(338) Thiel, W.; Voityuk, A. A. Extension of the MNDO Formalism Tod Orbitals: Integral Approximations and Preliminary Numerical Results. *Theor. Chim. Acta* **1992**, *81*, 391–404.

(339) Weber, W.; Thiel, W. Orthogonalization Corrections for Semiempirical Methods. *Theor. Chem. Acc.* **2000**, *103*, 495–506.

(340) Dral, P. O.; von Lilienfeld, O. A.; Thiel, W. Machine Learning of Parameters for Accurate Semiempirical Quantum Chemical Calculations. *J. Chem. Theory Comput.* **2015**, *11*, 2120–2125.

(341) Elstner, M.; Porezag, D.; Jungnickel, G.; Elsner, J.; Haugk, M.; Frauenheim, T.; Suhai, S.; Seifert, G. Self-Consistent-Charge Density-Functional Tight-Binding Method for Simulations of Complex Materials Properties. *Phys. Rev. B* **1998**, *58*, 7260–7268.

(342) Elstner, M.; Seifert, G. Density Functional Tight Binding. *Philos. Trans. R. Soc. London, Ser. A Phys. Sci. Eng.* **2014**, *372*, 20120483.

(343) Ratcliff, L. E.; Mohr, S.; Huhs, G.; Deutsch, T.; Masella, M.; Genovese, L. Challenges in Large Scale Quantum Mechanical Calculations. *Wiley Interdiscip. Rev. Comput. Mol. Sci.* **2017**, *7*, e1290.

(344) Pople, J. A.; Santry, D. P.; Segal, G. A. Approximate Self-Consistent Molecular Orbital Theory. I. Invariant Procedures. *J. Chem. Phys.* **1965**, *43*, S129–S135.

(345) Thiel, W. The MNDOC Method, a Correlated Version of the MNDO Model. *J. Am. Chem. Soc.* **1981**, *103*, 1413–1420.

(346) Steuhl, H.-M.; Klessinger, M.; Mathies, R. A. Excited States of Cyclic-Conjugated Anions: A Theoretical Study of the Photodecarboxylation of Cycloheptatriene and Cyclopentadiene Carboxylate Anions. *J. Chem. Soc. Perkin Trans. 2* **1998**, *84*, 2035–2038.

(347) Yi, Y.; Zhu, L.; Shuai, Z. The Correction Vector Method for Three-Photon Absorption: The Effects of π Conjugation in Extended Rylenebis(Dicarboximide)S. *J. Chem. Phys.* **2006**, *125*, 164505.

(348) Strodel, P.; Tavan, P. A Revised MRCI-Algorithm. I. Efficient Combination of Spin Adaptation with Individual Configuration Selection Coupled to an Effective Valence-Shell Hamiltonian. *J. Chem. Phys.* **2002**, *117*, 4667–4676.

(349) Tavan, P.; Schulten, K. An Efficient Approach to CI: General Matrix Element Formulas for Spin-coupled Particle–hole Excitations. *J. Chem. Phys.* **1980**, *72*, 3547–3576.

(350) Koslowski, A.; Beck, M. E.; Thiel, W. Implementation of a General Multireference Configuration Interaction Procedure with Analytic Gradients in a Semiempirical Context Using the Graphical Unitary Group Approach. *J. Comput. Chem.* **2003**, *24*, 714–726.

(351) Lei, Y.; Suo, B.; Dou, Y.; Wang, Y.; Wen, Z. New Implementations of MRCI in Semiempirical Frameworks. *J. Comput. Chem.* **2010**, *31*, 1752–1758.

(352) Dewar, M. J. S.; Thiel, W. Ground States of Molecules. 38. The MNDO Method. Approximations and Parameters. *J. Am. Chem. Soc.* **1977**, *99*, 4899–4907.

(353) Toniolo, A.; Persico, M.; Pitea, D. An Ab Initio Study of Spectroscopy and Predissociation of ClO. *J. Chem. Phys.* **2000**, *112*, 2790.

(354) Persico, M.; Granucci, G. An Overview of Nonadiabatic Dynamics Simulations Methods, with Focus on the Direct Approach versus the Fitting of Potential Energy Surfaces. *Theor.*

Chem. Acc. **2014**, *133*, 1526.

(355) Grimme, S.; Waletzke, M. A Combination of Kohn-Sham Density Functional Theory and Multi-Reference Configuration Interaction Methods. *J. Chem. Phys.* **1999**, *111*, 5645–5655.

(356) Silva-Junior, M. R.; Thiel, W. Benchmark of Electronically Excited States for Semiempirical Methods: MNDO, AM1, PM3, OM1, OM2, OM3, INDO/S, and INDO/S2. *J. Chem. Theory Comput.* **2010**, *6*, 1546–1564.

(357) Silva-Junior, M. R.; Schreiber, M.; Sauer, S. P. A.; Thiel, W. Benchmarks for Electronically Excited States: Time-Dependent Density Functional Theory and Density Functional Theory Based Multireference Configuration Interaction. *J. Chem. Phys.* **2008**, *129*, 104103.

(358) Keal, T.; Wanko, M.; Thiel, W. Assessment of Semiempirical Methods for the Photoisomerisation of a Protonated Schiff Base. *Theor. Chem. Acc.* **2009**, *123*, 145–156.

(359) Spezia, R.; Burghardt, I.; Hynes, J. T. Conical Intersections in Solution: Non-Equilibrium versus Equilibrium Solvation. *Mol. Phys.* **2006**, *104*, 903–914.

(360) Izzo, R.; Klessinger, M. Optimization of Conical Intersections Using the Semiempirical MNDOC–CI Method with Analytic Gradients. *J. Comput. Chem.* **2000**, *21*, 52–62.

(361) Keal, T. W.; Koslowski, A.; Thiel, W. Comparison of Algorithms for Conical Intersection Optimisation Using Semiempirical Methods. *Theor. Chem. Acc.* **2007**, *118*, 837–844.

(362) de Carvalho, F.; Bouduban, M.; Curchod, B.; Tavernelli, I. Nonadiabatic Molecular Dynamics Based on Trajectories. *Entropy* **2014**, *16*, 62–85.

(363) Smith, B. R.; Bearpark, M. J.; Robb, M. A.; Bernardi, F.; Olivucci, M. Classical Wavepacket Dynamics through a Conical Intersection - Application to the S_1/S_0 Photochemistry of Benzene. *Chem. Phys. Lett.* **1995**, *242*, 27–32.

(364) Bernardi, F.; Olivucci, M.; Robb, M. A. Simulation of MC-SCF Results on Covalent Organic Multi-Bond Reactions: Molecular Mechanics with Valence Bond (MM-VB). *J. Am. Chem. Soc.* **1992**, *114*, 1606–1616.

(365) Granucci, G.; Persico, M.; Toniolo, A. Direct Semiclassical Simulation of Photochemical Processes with Semiempirical Wave Functions. *J. Chem. Phys.* **2001**, *114*, 10608–10615.

(366) Barbatti, M.; Granucci, G.; Persico, M.; Lischka, H. Semiempirical Molecular Dynamics Investigation of the Excited State Lifetime of Ethylene. *Chem. Phys. Lett.* **2005**, *401*.

(367) Fabiano, E.; Keal, T. W.; Thiel, W. Implementation of Surface Hopping Molecular Dynamics Using Semiempirical Methods. *Chem. Phys.* **2008**, *349*, 334–347.

(368) Morelli, J.; Hammes-Schiffer, S. Surface Hopping and Fully Quantum Dynamical Wavepacket Propagation on Multiple Coupled Adiabatic Potential Surfaces for Proton Transfer Reactions. *Chem. Phys. Lett.* **1997**, *269*, 161–170.

(369) Goyal, P.; Schwerdtfeger, C. A.; Soudackov, A. V; Hammes-Schiffer, S. Nonadiabatic Dynamics of Photoinduced Proton-Coupled Electron Transfer in a Solvated Phenol–Amine Complex. *J. Phys. Chem. B* **2015**, *119*, 2758–2768.

(370) Toniolo, A.; Olsen, S.; Manohar, L.; Martínez, T. J. Conical Intersection Dynamics in Solution: The Chromophore of Green Fluorescent Protein. *Faraday Discuss.* **2004**, *127*, 149–163.

(371) Lan, Z.; Lu, Y.; Fabiano, E.; Thiel, W. QM/MM Nonadiabatic Decay Dynamics of 9H-Adenine in Aqueous Solution. *Chemphyschem* **2011**, *12*, 1989–1998.

(372) Hollas, D.; Šištík, L.; Hohenstein, E. G.; Martínez, T. J.; Slavíček, P. Nonadiabatic Ab Initio Molecular Dynamics with the Floating Occupation Molecular Orbital-Complete Active

Space Configuration Interaction Method. *J. Chem. Theory Comput.* **2018**, *14*, 339–350.

(373) Weingart, O.; Lan, Z.; Koslowski, A.; Thiel, W. Chiral Pathways and Periodic Decay in Cis-Azobenzene Photodynamics. *J. Phys. Chem. Lett.* **2011**, *2*, 1506–1509.

(374) Granucci, G.; Persico, M.; Spighi, G. Surface Hopping Trajectory Simulations with Spin-Orbit and Dynamical Couplings. *J. Chem. Phys.* **2012**, *137*, 22A501.

(375) Barbatti, M.; Lan, Z.; Crespo-Otero, R.; Szymczak, J. J.; Lischka, H.; Thiel, W. Critical Appraisal of Excited State Nonadiabatic Dynamics Simulations of 9H-Adenine. *J. Chem. Phys.* **2012**, *137*, 22A503-14.

(376) Becke, A. D. Perspective: Fifty Years of Density-Functional Theory in Chemical Physics. *J. Chem. Phys.* **2014**, *140*, 18A301.

(377) Cremer, D. Density Functional Theory: Coverage of Dynamic and Non-Dynamic Electron Correlation Effects. *Mol. Phys.* **2001**, *99*, 1899–1940.

(378) Hohenberg, P.; Kohn, W. Inhomogeneous Electron Gas. *Phys. Rev.* **1964**, *136*, B864–B871.

(379) Gross, E. K. U.; Oliveira, L. N.; Kohn, W. Density-Functional Theory for Ensembles of Fractionally Occupied States. I. Basic Formalism. *Phys. Rev. A* **1988**, *37*, 2809–2820.

(380) Katriel, J.; Zahariev, F.; Burke, K. Symmetry and Degeneracy in Density Functional Theory. *Int. J. Quantum Chem.* **2001**, *85*, 432–435.

(381) Shao, Y.; Head-Gordon, M.; Krylov, A. I. The Spin–flip Approach within Time-Dependent Density Functional Theory: Theory and Applications to Diradicals. *J. Chem. Phys.* **2003**, *118*, 4807–4818.

(382) Wang, F.; Ziegler, T. The Performance of Time-Dependent Density Functional Theory

Based on a Noncollinear Exchange-Correlation Potential in the Calculations of Excitation Energies. *J. Chem. Phys.* **2005**, *122*, 74109.

(383) Gräfenstein, J.; Kraka, E.; Filatov, M.; Cremer, D. Can Unrestricted Density-Functional Theory Describe Open Shell Singlet Biradicals? *Int. J. Mol. Sci.* **2002**, *3*, 360–394.

(384) Gräfenstein, J.; Cremer, D.; Nichols, J.; Nachtigall, P.; Whangbo, M.-H.; Wolfe, S. Can Density Functional Theory Describe Multi-Reference Systems? Investigation of Carbenes and Organic Biradicals. *Phys. Chem. Chem. Phys.* **2000**, *2*, 2091–2103.

(385) Jiang, W.; Jeffrey, C. C.; Wilson, A. K. Empirical Correction of Nondynamical Correlation Energy for Density Functionals. *J. Phys. Chem. A* **2012**, *116*, 9969–9978.

(386) Beck, E. V; Stahlberg, E. A.; Burggraf, L. W.; Blaudeau, J.-P. A Graphical Unitary Group Approach-Based Hybrid Density Functional Theory Multireference Configuration Interaction Method. *Chem. Phys.* **2008**, *349*, 158–169.

(387) Lyskov, I.; Kleinschmidt, M.; Marian, C. M. Redesign of the DFT/MRCI Hamiltonian. *J. Chem. Phys.* **2016**, *144*, 34104.

(388) Sharkas, K.; Savin, A.; Jensen, H. J. A.; Toulouse, J. A Multiconfigurational Hybrid Density-Functional Theory. *J. Chem. Phys.* **2012**, *137*, 44104.

(389) Fromager, E.; Knecht, S.; Jensen, H. J. A. Multi-Configuration Time-Dependent Density-Functional Theory Based on Range Separation. *J. Chem. Phys.* **2013**, *138*, 84101.

(390) Kurzweil, Y.; Lawler, K. V; Head-Gordon, M. Analysis of Multi-Configuration Density Functional Theory Methods: Theory and Model Application to Bond-Breaking. *Mol. Phys.* **2009**, *107*, 2103–2110.

(391) Nakata, K.; Ukai, T.; Yamanaka, S.; Takada, T.; Yamaguchi, K. CASSCF Version of

Density Functional Theory. *Int. J. Quantum Chem.* **2006**, *106*, 3325–3333.

(392) Li Manni, G.; Carlson, R. K.; Luo, S.; Ma, D.; Olsen, J.; Truhlar, D. G.; Gagliardi, L. Multiconfiguration Pair-Density Functional Theory. *J. Chem. Theory Comput.* **2014**, *10*, 3669–3680.

(393) Fromager, E.; Toulouse, J.; Jensen, H. J. A. On the Universality of the Long-/Short-Range Separation in Multiconfigurational Density-Functional Theory. *J. Chem. Phys.* **2007**, *126*, 074111.

(394) Filatov, M.; Shaik, S. A Spin-Restricted Ensemble-Referenced Kohn-Sham Method and Its Application to Diradicaloid Situations. *Chem. Phys. Lett.* **1999**, *304*, 429–437.

(395) Filatov, M. Spin-Restricted Ensemble-Referenced Kohn–Sham Method: Basic Principles and Application to Strongly Correlated Ground and Excited States of Molecules. *Willey Interdiscip. Rev. Comput. Mol. Sci.* **2014**, *5*, 146–167.

(396) Pastorczak, E.; Gidopoulos, N. I.; Pernal, K. Calculation of Electronic Excited States of Molecules Using the Helmholtz Free-Energy Minimum Principle. *Phys. Rev. A* **2013**, *87*, 062501.

(397) Gräfenstein, J.; Cremer, D. Development of a CAS-DFT Method Covering Non-Dynamical and Dynamical Electron Correlation in a Balanced Way. *Mol. Phys.* **2005**, *103*, 279–308.

(398) Fromager, E. On the Exact Formulation of Multi-Configuration Density-Functional Theory: Electron Density versus Orbitals Occupation. *Mol. Phys.* **2015**, *113*, 419–434.

(399) Stojanović, L.; Alyoubi, A. O.; Aziz, S. G.; Hilal, R. H.; Barbatti, M. UV Excitations of Halons. *J. Chem. Phys.* **2016**, *145*, 184306.

(400) Crespo-Otero, R.; Barbatti, M. $Cr(CO)_6$ Photochemistry: Semi-Classical Study of UV

Absorption Spectral Intensities and Dynamics of Photodissociation. *J. Chem. Phys.* **2011**, *134*, 164305.

(401) Barbatti, M.; Crespo-Otero, R. Surface Hopping Dynamics with DFT Excited States. In *Density-Functional Methods for Excited States*; Ferré, N., Filatov, M., Huix-Rotllant, M., Eds.; Topics in Current Chemistry, Vol. 368; Springer International Publishing: Cham, 2016; pp 415–444.

(402) Senjean, B.; Knecht, S.; Jensen, H. J. A.; Fromager, E. Linear Interpolation Method in Ensemble Kohn-Sham and Range-Separated Density-Functional Approximations for Excited States. *Phys. Rev. A* **2015**, *92*, 012518.

(403) Alam, M. M.; Knecht, S.; Fromager, E. Ghost-Interaction Correction in Ensemble Density-Functional Theory for Excited States with and without Range Separation. *Phys. Rev. A* **2016**, *94*, 012511.

(404) Stoyanova, A.; Teale, A. M.; Toulouse, J.; Helgaker, T.; Fromager, E. Alternative Separation of Exchange and Correlation Energies in Multi-Configuration Range-Separated Density-Functional Theory. *J. Chem. Phys.* **2013**, *139*, 134113.

(405) Kohn, W.; Sham, L. J. Self-Consistent Equations Including Exchange and Correlation Effects. *Phys. Rev.* **1965**, *140*, A1133–A1138.

(406) Aquilante, F.; Autschbach, J.; Carlson, R. K.; Chibotaru, L. F.; Delcey, M. G.; De Vico, L.; Fdez. Galván, I.; Ferré, N.; Frutos, L. M.; Gagliardi, L.; et al. Molcas 8: New Capabilities for Multiconfigurational Quantum Chemical Calculations across the Periodic Table. *J. Comput. Chem.* **2016**, *37*.

(407) Gusarov, S.; Malmqvist, P. A.; Lindh, R.; Roos, B. O. Correlation Potentials for a

Multiconfigurational-Based Density Functional Theory with Exact Exchange. *Theor. Chem. Accounts Theory, Comput. Model. (Theoretica Chim. Acta)* **2004**, *112*, 84–94.

(408) Ying, F.; Su, P.; Chen, Z.; Shaik, S.; Wu, W. DFVB: A Density-Functional-Based Valence Bond Method. *J. Chem. Theory Comput.* **2012**, *8*, 1608–1615.

(409) Gagliardi, L.; Truhlar, D. G.; Li Manni, G.; Carlson, R. K.; Hoyer, C. E.; Bao, J. L. Multiconfiguration Pair-Density Functional Theory: A New Way To Treat Strongly Correlated Systems. *Acc. Chem. Res.* **2017**, *50*, 66–73.

(410) Sand, A. M.; Hoyer, C. E.; Sharkas, K.; Kidder, K. M.; Lindh, R.; Truhlar, D. G.; Gagliardi, L. Analytic Gradients for Complete Active Space Pair-Density Functional Theory. *J. Chem. Theory Comput.* **2018**, *14*, 126–138.

(411) Levy, M. Electron Densities in Search of Hamiltonians. *Phys. Rev. A* **1982**, *26*, 1200–1208.

(412) Ullrich, C. A.; Kohn, W. Kohn-Sham Theory for Ground-State Ensembles. *Phys. Rev. Lett.* **2001**, *87*, 093001.

(413) Englisch, H.; Englisch, R. Exact Density Functionals for Ground-State Energies II. Details and Remarks. *Phys. status solidi* **1984**, *124*, 373–379.

(414) Schipper, P. R. T.; Gritsenko, O. V.; Baerends, E. J. One-Determinantal Pure State versus Ensemble Kohn-Sham Solutions in the Case of Strong Electron Correlation: CH_2 and C_2. *Theor. Chem. Accounts Theory, Comput. Model. (Theoretica Chim. Acta)* **1998**, *99*, 329–343.

(415) Morrison, R. C. Electron Correlation and Noninteracting V-Representability in Density Functional Theory: The Be Isoelectronic Series. *J. Chem. Phys.* **2002**, *117*, 10506–10511.

(416) Theophilou, A. K. The Energy Density Functional Formalism for Excited States. *J. Phys. C*

Solid State Phys. **1979**, *12*, 5419–5430.

(417) Kazaryan, A.; Heuver, J.; Filatov, M. Excitation Energies from Spin-Restricted Ensemble-Referenced Kohn−Sham Method: A State-Average Approach. *J. Phys. Chem. A* **2008**, *112*, 12980–12988.

(418) Filatov, M.; Martínez, T. J.; Kim, K. S.; Matito, E.; Olivucci, M.; Ferré, N.; Frutos, L. M.; Angeli, C.; Krylov, A. I.; Granovsky, A. A.; et al. Using the GVB Ansatz to Develop Ensemble DFT Method for Describing Multiple Strongly Correlated Electron Pairs. *Phys. Chem. Chem. Phys.* **2016**, *18*, 21040–21050.

(419) Filatov, M.; Martínez, T. J.; Kim, K. S. Description of Ground and Excited Electronic States by Ensemble Density Functional Method with Extended Active Space. *J. Chem. Phys.* **2017**, *147*, 064104.

(420) Filatov, M.; Liu, F.; Kim, K. S.; Martínez, T. J. Self-Consistent Implementation of Ensemble Density Functional Theory Method for Multiple Strongly Correlated Electron Pairs. *J. Chem. Phys.* **2016**, *145*, 244104.

(421) Huix-Rotllant, M.; Nikiforov, A.; Thiel, W.; Filatov, M. Description of Conical Intersections with Density Functional Methods. In *Density-Functional Methods for Excited States*; Ferré, N., Filatov, M., Huix-Rotllant, M., Eds.; Topics in Current Chemistry, Vol. 368; Springer International Publishing: Cham, 2016; pp 445–476.

(422) Filatov, M.; Liu, F.; Martínez, T. J. Analytical Derivatives of the Individual State Energies in Ensemble Density Functional Theory Method. I. General Formalism. *J. Chem. Phys.* **2017**, *147*, 034113.

(423) Deur, K.; Mazouin, L.; Fromager, E. Exact Ensemble Density Functional Theory for

Excited States in a Model System: Investigating the Weight Dependence of the Correlation Energy. *Phys. Rev. B* **2017**, *95*, 035120.

(424) White, S. R. Density-Matrix Algorithms for Quantum Renormalization Groups. *Phys. Rev. B* **1993**, *48*, 10345–10356.

(425) White, S. R. Density Matrix Formulation for Quantum Renormalization Groups. *Phys. Rev. Lett.* **1992**, *69*, 2863–2866.

(426) Daul, S.; Ciofini, I.; Daul, C.; White, S. R. Full-CI Quantum Chemistry Using the Density Matrix Renormalization Group. *Int. J. Quantum Chem.* **2000**, *79*, 331–342.

(427) White, S. R.; Martin, R. L. Ab Initio Quantum Chemistry Using the Density Matrix Renormalization Group. *J. Chem. Phys.* **1999**, *110*, 4127–4130.

(428) Chan, G. K.-L.; Head-Gordon, M. Highly Correlated Calculations with a Polynomial Cost Algorithm: A Study of the Density Matrix Renormalization Group. *J. Chem. Phys.* **2002**, *116*, 4462–4476.

(429) Chan, G. K.-L.; Keselman, A.; Nakatani, N.; Li, Z.; White, S. R. Matrix Product Operators, Matrix Product States, and Ab Initio Density Matrix Renormalization Group Algorithms. *J. Chem. Phys.* **2016**, *145*, 14102.

(430) Östlund, S.; Rommer, S. Thermodynamic Limit of Density Matrix Renormalization. *Phys. Rev. Lett.* **1995**, *75*, 3537–3540.

(431) Keller, S.; Reiher, M. Spin-Adapted Matrix Product States and Operators. *J. Chem. Phys.* **2016**, *144*, 134101.

(432) Li, Z.; Chan, G. K.-L. Spin-Projected Matrix Product States: Versatile Tool for Strongly Correlated Systems. *J. Chem. Theory Comput.* **2017**, *13*, 2681–2695.

(433) Pirvu, B.; Murg, V.; Cirac, J. I.; Verstraete, F. Matrix Product Operator Representations. *New J. Phys.* **2010**, *12*, 025012.

(434) Keller, S.; Dolfi, M.; Troyer, M.; Reiher, M. An Efficient Matrix Product Operator Representation of the Quantum Chemical Hamiltonian. *J. Chem. Phys.* **2015**, *143*, 244118.

(435) Sharma, S.; Chan, G. K.-L. Spin-Adapted Density Matrix Renormalization Group Algorithms for Quantum Chemistry. *J. Chem. Phys.* **2012**, *136*, 124121.

(436) Wouters, S.; Limacher, P. A.; Van Neck, D.; Ayers, P. W. Longitudinal Static Optical Properties of Hydrogen Chains: Finite Field Extrapolations of Matrix Product State Calculations. *J. Chem. Phys.* **2012**, *136*, 134110.

(437) Shepard, R.; Gidofalvi, G.; Brozell, S. R. The Multifacet Graphically Contracted Function Method. I. Formulation and Implementation. *J. Chem. Phys.* **2014**, *141*, 064105.

(438) Shepard, R.; Gidofalvi, G.; Brozell, S. R. The Multifacet Graphically Contracted Function Method. II. A General Procedure for the Parameterization of Orthogonal Matrices and Its Application to Arc Factors. *J. Chem. Phys.* **2014**, *141*, 064106.

(439) Szalay, S.; Pfeffer, M.; Murg, V.; Barcza, G.; Verstraete, F.; Schneider, R.; Legeza, Ö. Tensor Product Methods and Entanglement Optimization for Ab Initio Quantum Chemistry. *Int. J. Quantum Chem.* **2015**, *115*, 1342–1391.

(440) Yanai, T.; Kurashige, Y.; Mizukami, W.; Chalupský, J.; Lan, T. N.; Saitow, M. Density Matrix Renormalization Group for Ab Initio Calculations and Associated Dynamic Correlation Methods: A Review of Theory and Applications. *Int. J. Quantum Chem.* **2015**, *115*, 283–299.

(441) Olivares-Amaya, R.; Hu, W.; Nakatani, N.; Sharma, S.; Yang, J.; Chan, G. K.-L. The Ab-

Initio Density Matrix Renormalization Group in Practice. *J. Chem. Phys.* **2015**, *142*, 34102.

(442) Knecht, S.; Hedegård, E. D.; Keller, S.; Kovyrshin, A.; Ma, Y.; Muolo, A.; Stein, C. J. .; Reiher, M. New Approaches for Ab Initio Calculations of Molecules with Strong Electron Correlation. *Chim. Int. J. Chem.* **2016**, *70*, 244–251.

(443) Legeza, Ö.; Noack, R. M.; Sólyom, J.; Tincani, L. Applications of Quantum Information in the Density-Matrix Renormalization Group. In *Computational Many-Particle Physics*; Fehske, H., Schneider, R., Weiße, A., Eds.; Lecture Notes in Physics, Vol. 739; Springer Berlin Heidelberg: Berlin, Heidelberg, 2008; pp 653–664.

(444) Rissler, J.; Noack, R. M.; White, S. R. Measuring Orbital Interaction Using Quantum Information Theory. *Chem. Phys.* **2006**, *323*, 519–531.

(445) Boguslawski, K.; Tecmer, P.; Legeza, Ö.; Reiher, M. Entanglement Measures for Single- and Multireference Correlation Effects. *J. Phys. Chem. Lett.* **2012**, *3*, 3129–3135.

(446) Ghosh, D.; Hachmann, J.; Yanai, T.; Chan, G. K.-L. Orbital Optimization in the Density Matrix Renormalization Group, with Applications to Polyenes and β-Carotene. *J. Chem. Phys.* **2008**, *128*, 144117.

(447) Sun, Q.; Yang, J.; Chan, G. K.-L. A General Second Order Complete Active Space Self-Consistent-Field Solver for Large-Scale Systems. *Chem. Phys. Lett.* **2017**, *683*, 291–299.

(448) Ma, Y.; Knecht, S.; Keller, S.; Reiher, M. Second-Order Self-Consistent-Field Density-Matrix Renormalization Group. *J. Chem. Theory Comput.* **2017**, *13*, 2533–2549.

(449) Dorando, J. J.; Hachmann, J.; Chan, G. K.-L. Analytic Response Theory for the Density Matrix Renormalization Group. *J. Chem. Phys.* **2009**, *130*, 184111.

(450) Wouters, S.; Nakatani, N.; Van Neck, D.; Chan, G. K.-L. Thouless Theorem for Matrix

Product States and Subsequent Post Density Matrix Renormalization Group Methods. *Phys. Rev. B* **2013**, *88*, 75122.

(451) Nakatani, N.; Wouters, S.; Van Neck, D.; Chan, G. K.-L. Linear Response Theory for the Density Matrix Renormalization Group: Efficient Algorithms for Strongly Correlated Excited States. *J. Chem. Phys.* **2014**, *140*, 24108.

(452) Haegeman, J.; Cirac, J. I.; Osborne, T. J.; Pižorn, I.; Verschelde, H.; Verstraete, F. Time-Dependent Variational Principle for Quantum Lattices. *Phys. Rev. Lett.* **2011**, *107*, 70601.

(453) Yanai, T.; Kurashige, Y.; Neuscamman, E.; Chan, G. K.-L. Extended Implementation of Canonical Transformation Theory: Parallelization and a New Level-Shifted Condition. *Phys. Chem. Chem. Phys.* **2012**, *14*, 7809–7820.

(454) Kurashige, Y.; Yanai, T. Second-Order Perturbation Theory with a Density Matrix Renormalization Group Self-Consistent Field Reference Function: Theory and Application to the Study of Chromium Dimer. *J. Chem. Phys.* **2011**, *135*, 94104.

(455) Zgid, D.; Ghosh, D.; Neuscamman, E.; Chan, G. K.-L. A Study of Cumulant Approximations to N-Electron Valence Multireference Perturbation Theory. *J. Chem. Phys.* **2009**, *130*, 194107.

(456) Sharma, S.; Chan, G. K.-L. Communication: A Flexible Multi-Reference Perturbation Theory by Minimizing the Hylleraas Functional with Matrix Product States. *J. Chem. Phys.* **2014**, *141*, 111101.

(457) Sharma, S.; Jeanmairet, G.; Alavi, A. Quasi-Degenerate Perturbation Theory Using Matrix Product States. *J. Chem. Phys.* **2016**, *144*, 34103.

(458) Veis, L.; Antalík, A.; Brabec, J.; Neese, F.; Legeza, Ö.; Pittner, J. Coupled Cluster Method

with Single and Double Excitations Tailored by Matrix Product State Wave Functions. *J. Phys. Chem. Lett.* **2016**, *7*, 4072–4078.

(459) Kurashige, Y.; Chalupský, J.; Lan, T. N.; Yanai, T. Complete Active Space Second-Order Perturbation Theory with Cumulant Approximation for Extended Active-Space Wavefunction from Density Matrix Renormalization Group. *J. Chem. Phys.* **2014**, *141*, 174111.

(460) Kurashige, Y. Multireference Electron Correlation Methods with Density Matrix Renormalisation Group Reference Functions. *Mol. Phys.* **2014**, *112*, 1485–1494.

(461) Yanai, T.; Saitow, M.; Xiong, X.-G.; Chalupský, J.; Kurashige, Y.; Guo, S.; Sharma, S. Multistate Complete-Active-Space Second-Order Perturbation Theory Based on Density Matrix Renormalization Group Reference States. *J. Chem. Theory Comput.* **2017**, *13*, 4829–4840.

(462) Legeza, O.; Roder, J.; Hess, B. A. QC-DMRG Study of the Ionic-Neutral Curve Crossing of LiF. *Mol. Phys.* **2003**, *101*, 2019–2028.

(463) Legeza, Ö.; Röder, J.; Hess, B. A. Controlling the Accuracy of the Density-Matrix Renormalization-Group Method: The Dynamical Block State Selection Approach. *Phys. Rev. B* **2003**, *67*, 125114.

(464) Zgid, D.; Nooijen, M. On the Spin and Symmetry Adaptation of the Density Matrix Renormalization Group Method. *J. Chem. Phys.* **2008**, *128*, 14107.

(465) Wouters, S.; Poelmans, W.; Ayers, P. W.; Van Neck, D. CheMPS2: A Free Open-Source Spin-Adapted Implementation of the Density Matrix Renormalization Group for Ab Initio Quantum Chemistry. *Comput. Phys. Commun.* **2014**, *185*, 1501–1514.

(466) Ma, Y.; Wen, J.; Ma, H. Density-Matrix Renormalization Group Algorithm with Multi-Level Active Space. *J. Chem. Phys.* **2015**, *143*, 34105.

(467) Timár, M.; Barcza, G.; Gebhard, F.; Veis, L.; Legeza, Ö. Hückel–Hubbard–Ohno Modeling of π-Bonds in Ethene and Ethyne with Application to Trans-Polyacetylene. *Phys. Chem. Chem. Phys.* **2016**, *18*, 18835–18845.

(468) Moritz, G.; Wolf, A.; Reiher, M. Relativistic DMRG Calculations on the Curve Crossing of Cesium Hydride. *J. Chem. Phys.* **2005**, *123*, 184105.

(469) Marti, K. H.; Reiher, M. DMRG Control Using an Automated Richardson-Type Error Protocol. *Mol. Phys.* **2010**, *108*, 501–512.

(470) Marti, K. H.; Ondík, I. M.; Moritz, G.; Reiher, M. Density Matrix Renormalization Group Calculations on Relative Energies of Transition Metal Complexes and Clusters. *J. Chem. Phys.* **2008**, *128*, 14104.

(471) Ma, Y.; Knecht, S.; Reiher, M. Multiconfigurational Effects in Theoretical Resonance Raman Spectra. *ChemPhysChem* **2017**, *18*, 384–393.

(472) Yanai, T.; Kurashige, Y.; Ghosh, D.; Chan, G. K.-L. Accelerating Convergence in Iterative Solution for Large-Scale Complete Active Space Self-Consistent-Field Calculations. *Int. J. Quantum Chem.* **2009**, *109*, 2178–2190.

(473) Mizukami, W.; Kurashige, Y.; Yanai, T. Communication: Novel Quantum States of Electron Spins in Polycarbenes from Ab Initio Density Matrix Renormalization Group Calculations. *J. Chem. Phys.* **2010**, *133*, 91101.

(474) Hagymási, I.; Legeza, Ö. Entanglement, Excitations, and Correlation Effects in Narrow Zigzag Graphene Nanoribbons. *Phys. Rev. B* **2016**, *94*, 165147.

(475) Kurashige, Y.; Yanai, T. Theoretical Study of the π →π* Excited States of Oligoacenes: A Full π-Valence DMRG-CASPT2 Study. *Bull. Chem. Soc. Jpn.* **2014**, *87*, 1071–1073.

(476) Guo, S.; Watson, M. A.; Hu, W.; Sun, Q.; Chan, G. K.-L. N-Electron Valence State Perturbation Theory Based on a Density Matrix Renormalization Group Reference Function, with Applications to the Chromium Dimer and a Trimer Model of Poly(p-Phenylenevinylene). *J. Chem. Theory Comput.* **2016**, *12*, 1583–1591.

(477) Liu, F.; Kurashige, Y.; Yanai, T.; Morokuma, K. Multireference Ab Initio Density Matrix Renormalization Group (DMRG)-CASSCF and DMRG-CASPT2 Study on the Photochromic Ring Opening of Spiropyran. *J. Chem. Theory Comput.* **2013**, *9*, 4462–4469.

(478) Das, M. Computational Investigation on Tunable Optical Band Gap in Armchair Polyacenes. *J. Chem. Phys.* **2015**, *143*, 64704.

(479) Shirai, S.; Kurashige, Y.; Yanai, T. Computational Evidence of Inversion of ^1L_a and ^1L_b-Derived Excited States in Naphthalene Excimer Formation from Ab Initio Multireference Theory with Large Active Space: DMRG-CASPT2 Study. *J. Chem. Theory Comput.* **2016**, *12*, 2366–2372.

(480) Barcza, G.; Gebhard, F.; Legeza, Ö. Rigorous Treatment of Strong Electronic Correlations in Polydiacetylene Chains. *Mol. Phys.* **2013**, *111*, 2506–2515.

(481) Barcza, G.; Legeza, Ö.; Gebhard, F.; Noack, R. M. Density Matrix Renormalization Group Study of Excitons in Polydiacetylene Chains. *Phys. Rev. B* **2010**, *81*, 45103.

(482) Legeza, Ö.; Buchta, K.; Sólyom, J. Unified Phase Diagram of Models Exhibiting a Neutral-Ionic Transition. *Phys. Rev. B* **2006**, *73*, 165124.

(483) Hu, W.; Chan, G. K.-L. Excited-State Geometry Optimization with the Density Matrix

Renormalization Group, as Applied to Polyenes. *J. Chem. Theory Comput.* **2015**, *11*, 3000–3009.

(484) Wouters, S.; Bogaerts, T.; Van Der Voort, P.; Van Speybroeck, V.; Van Neck, D. Communication: DMRG-SCF Study of the Singlet, Triplet, and Quintet States of Oxo-Mn(Salen). *J. Chem. Phys.* **2014**, *140*, 241103.

(485) Sayfutyarova, E. R.; Chan, G. K.-L. A State Interaction Spin-Orbit Coupling Density Matrix Renormalization Group Method. *J. Chem. Phys.* **2016**, *144*, 234301.

(486) Sharma, S.; Sivalingam, K.; Neese, F.; Chan, G. K.-L. Low-Energy Spectrum of Iron–sulfur Clusters Directly from Many-Particle Quantum Mechanics. *Nat. Chem.* **2014**, *6*, 927–933.

(487) Kurashige, Y.; Chan, G. K.-L.; Yanai, T. Entangled Quantum Electronic Wavefunctions of the Mn_4CaO_5 Cluster in Photosystem II. *Nat. Chem.* **2013**, *5*, 660–666.

(488) Hedegård, E. D.; Reiher, M. Polarizable Embedding Density Matrix Renormalization Group. *J. Chem. Theory Comput.* **2016**, *12*, 4242–4253.

(489) Booth, G. H.; Thom, A. J. W.; Alavi, A. Fermion Monte Carlo without Fixed Nodes: A Game of Life, Death, and Annihilation in Slater Determinant Space. *J. Chem. Phys.* **2009**, *131*, 054106.

(490) Booth, G. H.; Grüneis, A.; Kresse, G.; Alavi, A. Towards an Exact Description of Electronic Wavefunctions in Real Solids. *Nature* **2012**, *493*, 365–370.

(491) Foulkes, W. M. C.; Mitas, L.; Needs, R. J.; Rajagopal, G. Quantum Monte Carlo Simulations of Solids. *Rev. Mod. Phys.* **2001**, *73*, 33–83.

(492) Cleland, D.; Booth, G. H.; Alavi, A. Communications: Survival of the Fittest: Accelerating Convergence in Full Configuration-Interaction Quantum Monte Carlo. *J. Chem. Phys.*

2010, *132*, 041103.

(493) Petruzielo, F. R.; Holmes, A. A.; Changlani, H. J.; Nightingale, M. P.; Umrigar, C. J. Semistochastic Projector Monte Carlo Method. *Phys. Rev. Lett.* **2012**, *109*, 230201.

(494) Blunt, N. S.; Smart, S. D.; Kersten, J. A. F.; Spencer, J. S.; Booth, G. H.; Alavi, A. Semi-Stochastic Full Configuration Interaction Quantum Monte Carlo: Developments and Application. *J. Chem. Phys.* **2015**, *142*, 184107.

(495) Booth, G. H.; Chan, G. K.-L. Communication: Excited States, Dynamic Correlation Functions and Spectral Properties from Full Configuration Interaction Quantum Monte Carlo. *J. Chem. Phys.* **2012**, *137*, 191102.

(496) Ten-no, S. Stochastic Determination of Effective Hamiltonian for the Full Configuration Interaction Solution of Quasi-Degenerate Electronic States. *J. Chem. Phys.* **2013**, *138*, 164126.

(497) Humeniuk, A.; Mitrić, R. Excited States from Quantum Monte Carlo in the Basis of Slater Determinants. *J. Chem. Phys.* **2014**, *141*, 194104.

(498) Blunt, N. S.; Smart, S. D.; Booth, G. H.; Alavi, A. An Excited-State Approach within Full Configuration Interaction Quantum Monte Carlo. *J. Chem. Phys.* **2015**, *143*, 134117.

(499) Tubman, N. M.; Lee, J.; Takeshita, T. Y.; Head-Gordon, M.; Whaley, K. B. A Deterministic Alternative to the Full Configuration Interaction Quantum Monte Carlo Method. *J. Chem. Phys.* **2016**, *145*, 044112.

(500) Thomas, R. E.; Sun, Q.; Alavi, A.; Booth, G. H. Stochastic Multiconfigurational Self-Consistent Field Theory. *J. Chem. Theory Comput.* **2015**, *11*, 5316–5325.

(501) Li Manni, G.; Smart, S. D.; Alavi, A. Combining the Complete Active Space Self-

Consistent Field Method and the Full Configuration Interaction Quantum Monte Carlo within a Super-CI Framework, with Application to Challenging Metal-Porphyrins. *J. Chem. Theory Comput.* **2016**, *12*, 1245–1258.

(502) Kong, L.; Valeev, E. F. SF-$[2]_{R12}$: A Spin-Adapted Explicitly Correlated Method Applicable to Arbitrary Electronic States. *J. Chem. Phys.* **2011**, *135*, 214105.

(503) Yanai, T.; Shiozaki, T. Canonical Transcorrelated Theory with Projected Slater-Type Geminals. *J. Chem. Phys.* **2012**, *136*, 084107.

(504) Booth, G. H.; Cleland, D.; Alavi, A.; Tew, D. P. An Explicitly Correlated Approach to Basis Set Incompleteness in Full Configuration Interaction Quantum Monte Carlo. *J. Chem. Phys.* **2012**, *137*, 164112.

(505) Kersten, J. A. F.; Booth, G. H.; Alavi, A. Assessment of Multireference Approaches to Explicitly Correlated Full Configuration Interaction Quantum Monte Carlo. *J. Chem. Phys.* **2016**, *145*, 054117.

(506) Sharma, S.; Yanai, T.; Booth, G. H.; Umrigar, C. J.; Chan, G. K.-L. Spectroscopic Accuracy Directly from Quantum Chemistry: Application to Ground and Excited States of Beryllium Dimer. *J. Chem. Phys.* **2014**, *140*, 104112.

(507) Sharma, S.; Alavi, A. Multireference Linearized Coupled Cluster Theory for Strongly Correlated Systems Using Matrix Product States. *J. Chem. Phys.* **2015**, *143*, 102815.

(508) Jeanmairet, G.; Sharma, S.; Alavi, A. Stochastic Multi-Reference Perturbation Theory with Application to the Linearized Coupled Cluster Method. *J. Chem. Phys.* **2017**, *146*, 044107.

(509) Blunt, N. S.; Booth, G. H.; Alavi, A. Density Matrices in Full Configuration Interaction Quantum Monte Carlo: Excited States, Transition Dipole Moments, and Parallel

Distribution. *J. Chem. Phys.* **2017**, *146*, 244105.

(510) Overy, C.; Booth, G. H.; Blunt, N. S.; Shepherd, J. J.; Cleland, D.; Alavi, A. Unbiased Reduced Density Matrices and Electronic Properties from Full Configuration Interaction Quantum Monte Carlo. *J. Chem. Phys.* **2014**, *141*, 244117.

(511) Ohtsuka, Y.; Nagase, S. Projector Monte Carlo Method Based on Slater Determinants: Test Application to Singlet Excited States of H_2O and LiF. *Chem. Phys. Lett.* **2010**, *485*, 367–370.

(512) Coe, J. P.; Paterson, M. J. State-Averaged Monte Carlo Configuration Interaction Applied to Electronically Excited States. *J. Chem. Phys.* **2013**, *139*, 154103.

(513) Holmes, A. A.; Umrigar, C. J.; Sharma, S. Excited States Using Semistochastic Heat-Bath Configuration Interaction. *J. Chem. Phys.* **2017**, *147*, 164111.

(514) Holmes, A. A.; Tubman, N. M.; Umrigar, C. J. Heat-Bath Configuration Interaction: An Efficient Selected Configuration Interaction Algorithm Inspired by Heat-Bath Sampling. *J. Chem. Theory Comput.* **2016**, *12*, 3674–3680.

(515) Sharma, S.; Holmes, A. A.; Jeanmairet, G.; Alavi, A.; Umrigar, C. J. Semistochastic Heat-Bath Configuration Interaction Method: Selected Configuration Interaction with Semistochastic Perturbation Theory. *J. Chem. Theory Comput.* **2017**, *13*, 1595–1604.

(516) Shepard, R. The Analytic Gradient Method for Configuration Interaction Wave Functions. In *Modern Electronic Structure Theory*; Yarkony, D. R., Ed.; Advanced Series in Physical Chemistry, Vol. 2, Part I; World Scientific: Singapore, 1995; pp 345–458.

(517) Handy, N. C.; Schaefer, H. F. On the Evaluation of Analytic Energy Derivatives for Correlated Wave Functions. *J. Chem. Phys.* **1984**, *81*, 5031.

(518) Page, M.; Saxe, P.; Adams, G. F.; Lengsfield, B. H. Multireference CI Gradients and MCSCF Second Derivatives. *J. Chem. Phys.* **1984**, *81*, 434–439.

(519) Shepard, R. Geometrical Energy Derivative Evaluation With MRCI Wave Functions. *Int. J. Quantum Chem.* **1987**, *31*, 33–44.

(520) Busch, T.; Esposti, A. D.; Werner, H.-J. Analytical Energy Gradients for Multiconfiguration Self-consistent Field Wave Functions with Frozen Core Orbitals. *J. Chem. Phys.* **1991**, *94*, 6708–6715.

(521) Shepard, R.; Lischka, H.; Szalay, P. G.; Kovar, T.; Ernzerhof, M. A General Multireference Configuration Interaction Gradient Program. *J. Chem. Phys.* **1992**, *96*, 2085–2098.

(522) Delcey, M. G.; Pedersen, T. B.; Aquilante, F.; Lindh, R. Analytical Gradients of the State-Average Complete Active Space Self-Consistent Field Method with Density Fitting. *J. Chem. Phys.* **2015**, *143*, 044110.

(523) Snyder, J. W.; Hohenstein, E. G.; Luehr, N.; Martínez, T. J. An Atomic Orbital-Based Formulation of Analytical Gradients and Nonadiabatic Coupling Vector Elements for the State-Averaged Complete Active Space Self-Consistent Field Method on Graphical Processing Units. *J. Chem. Phys.* **2015**, *143*, 154107.

(524) Granovsky, A. A. Communication: An Efficient Approach to Compute State-Specific Nuclear Gradients for a Generic State-Averaged Multi-Configuration Self Consistent Field Wavefunction. *J. Chem. Phys.* **2015**, *143*, 231101.

(525) MacLeod, M. K.; Shiozaki, T. Communication: Automatic Code Generation Enables Nuclear Gradient Computations for Fully Internally Contracted Multireference Theory. *J. Chem. Phys.* **2015**, *142*, 051103.

(526) Lengsfield, B. H.; Saxe, P.; Yarkony, D. R. On the Evaluation of Nonadiabatic Coupling Matrix Elements Using SA-MCSCF/CI Wave Functions and Analytic Gradient Methods. I. *J. Chem. Phys.* **1984**, *81*, 4549.

(527) Lischka, H.; Dallos, M.; Szalay, P. G.; Yarkony, D. R.; Shepard, R. Analytic Evaluation of Nonadiabatic Coupling Terms at the MR-CI Level. I. Formalism. *J. Chem. Phys.* **2004**, *120*, 7322–7329.

(528) Galván, I. F.; Delcey, M. G.; Pedersen, T. B.; Aquilante, F.; Lindh, R. Analytical State-Average Complete-Active-Space Self-Consistent Field Nonadiabatic Coupling Vectors: Implementation with Density-Fitted Two-Electron Integrals and Application to Conical Intersections. *J. Chem. Theory Comput.* **2016**, *12*, 3636–3653.

(529) Park, J. W.; Shiozaki, T. Analytical Derivative Coupling for Multistate CASPT2 Theory. *J. Chem. Theory Comput.* **2017**, *13*, 2561–2570.

(530) Tajti, A.; Szalay, P. G. Analytic Evaluation of the Nonadiabatic Coupling Vector between Excited States Using Equation-of-Motion Coupled-Cluster Theory. *J. Chem. Phys.* **2009**, *131*, 124104.

(531) Plasser, F.; Ruckenbauer, M.; Mai, S.; Oppel, M.; Marquetand, P.; González, L. Efficient and Flexible Computation of Many-Electron Wave Function Overlaps. *J. Chem. Theory Comput.* **2016**, *12*, 1207–1219.

(532) Pittner, J.; Lischka, H.; Barbatti, M. Optimization of Mixed Quantum-Classical Dynamics: Time-Derivative Coupling Terms and Selected Couplings. *Chem. Phys.* **2009**, *356*, 147–152.

(533) Martin, R. L. Natural Transition Orbitals. *J. Chem. Phys.* **2003**, *118*, 4775–4777.

(534) Plasser, F.; Lischka, H. Analysis of Excitonic and Charge Transfer Interactions from Quantum Chemical Calculations. *J. Chem. Theory Comput.* **2012**, *8*, 2777–2789.

(535) Plasser, F.; Wormit, M.; Dreuw, A. New Tools for the Systematic Analysis and Visualization of Electronic Excitations. I. Formalism. *J. Chem. Phys.* **2014**, *141*, 024106.

(536) Mewes, S. A.; Mewes, J.-M.; Dreuw, A.; Plasser, F. Excitons in Poly(para Phenylene Vinylene): A Quantum-Chemical Perspective Based on High-Level Ab Initio Calculations. *Phys. Chem. Chem. Phys.* **2016**, *18*, 2548–2563.

(537) Plasser, F.; Dreuw, A. High-Level Ab Initio Computations of the Absorption Spectra of Organic Iridium Complexes. *J. Phys. Chem. A* **2015**, *119*, 1023–1036.

(538) Bäppler, S. A.; Plasser, F.; Wormit, M.; Dreuw, A. Exciton Analysis of Many-Body Wave Functions: Bridging the Gap between the Quasiparticle and Molecular Orbital Pictures. *Phys. Rev. A* **2014**, *90*, 052521.

(539) Plasser, F.; Thomitzni, B.; Bäppler, S. A.; Wenzel, J.; Rehn, D. R.; Wormit, M.; Dreuw, A. Statistical Analysis of Electronic Excitation Processes: Spatial Location, Compactness, Charge Transfer, and Electron-Hole Correlation. *J. Comput. Chem.* **2015**, *36*, 1609–1620.

(540) Plasser, F.; Mewes, S. A.; Dreuw, A.; González, L. Detailed Wave Function Analysis for Multireference Methods: Implementation in the Molcas Program Package and Applications to Tetracene. *J. Chem. Theory Comput.* **2017**, *13*, 5343–5353.

(541) Plasser, F.; González, L. Communication: Unambiguous Comparison of Many-Electron Wavefunctions through Their Overlaps. *J. Chem. Phys.* **2016**, *145*, 021103.

(542) Takatsuka, K.; Fueno, T.; Yamaguchi, K. Distribution of Odd Electrons in Ground-State Molecules. *Theor. Chim. Acta* **1978**, *183*, 175–183.

(543) Staroverov, V. N.; Davidson, E. R. Distribution of Effectively Unpaired Electrons. *Chem. Phys. Lett.* **2000**, *330*, 161–168.

(544) Head-Gordon, M. Characterizing Unpaired Electrons from the One-Particle Density Matrix. *Chem. Phys. Lett.* **2003**, *372*, 508–511.

(545) Grimme, S.; Hansen, A. A Practicable Real-Space Measure and Visualization of Static Electron-Correlation Effects. *Angew. Chem., Int. Ed.* **2015**, *54*, 12308–12313.

(546) Juhász, T.; Mazziotti, D. A. The Cumulant Two-Particle Reduced Density Matrix as a Measure of Electron Correlation and Entanglement. *J. Chem. Phys.* **2006**, *125*, 174105.

(547) Ramos-Cordoba, E.; Salvador, P.; Matito, E. Separation of Dynamic and Nondynamic Correlation. *Phys. Chem. Chem. Phys.* **2016**, *18*, 24015–24023.

(548) Stein, C. J.; Reiher, M. Measuring Multi-Configurational Character by Orbital Entanglement. *Mol. Phys.* **2017**, *115*, 2110–2119.

(549) Plasser, F. Entanglement Entropy of Electronic Excitations. *J. Chem. Phys.* **2016**, *144*, 194107.

(550) Lee, T. J.; Taylor, P. R. A Diagnostic for Determining the Quality of Single-reference Electron Correlation Methods. *Int. J. Quantum Chem.* **1989**, *36*, 199–207.

(551) Janssen, C. L.; Nielsen, I. M. B. New Diagnostics for Coupled-Cluster and Møller-Plesset Perturbation Theory. *Chem. Phys. Lett.* **1998**, *290*, 423–430.

(552) Watts, J. D.; Urban, M.; Bartlett, R. J. Accurate Electrical and Spectroscopic Properties of $X^1\Sigma^+$ BeO from Coupled-Cluster Methods. *Theor. Chim. Acta* **1995**, *90*, 341–355.

(553) Nielsen, I. M. B.; Janssen, C. L. Double-Substitution-Based Diagnostics for Coupled-

Cluster and Møller–Plesset Perturbation Theory. *Chem. Phys. Lett.* **1999**, *310*, 568–576.

(554) Bauschlicher, C. W.; Langhoff, S. R. The Study of Molecular Spectroscopy by Ab Initio Methods. *Chem. Rev.* **1991**, *91*, 701–718.

(555) Abrams, M. L.; Sherrill, C. D. A Comparison of Polarized Double-Zeta Basis Sets and Natural Orbitals for Full Configuration Interaction Benchmarks. *J. Chem. Phys.* **2003**, *118*, 1604–1609.

(556) Gan, Z.; Grant, D. J.; Harrison, R. J.; Dixon, D. A. The Lowest Energy States of the Group-IIIA–group-VA Heteronuclear Diatomics: BN, BP, AlN, and AlP from Full Configuration Interaction Calculations. *J. Chem. Phys.* **2006**, *125*, 124311.

(557) Bytautas, L.; Nagata, T.; Gordon, M. S.; Ruedenberg, K. Accurate Ab Initio Potential Energy Curve of F_2. I. Nonrelativistic Full Valence Configuration Interaction Energies Using the Correlation Energy Extrapolation by Intrinsic Scaling Method. *J. Chem. Phys.* **2007**, *127*, 164317.

(558) Bytautas, L.; Ruedenberg, K. Accurate Ab Initio Potential Energy Curve of O_2. I. Nonrelativistic Full Configuration Interaction Valence Correlation by the Correlation Energy Extrapolation by Intrinsic Scaling Method. *J. Chem. Phys.* **2010**, *132*, 074109.

(559) Cleland, D.; Booth, G. H.; Overy, C.; Alavi, A. Taming the First-Row Diatomics: A Full Configuration Interaction Quantum Monte Carlo Study. *J. Chem. Theory Comput.* **2012**, *8*, 4138–4152.

(560) Ghanmi, C.; Farjallah, M.; Berriche, H. Theoretical Study of the Alkaline-Earth $(LiBe)^+$ Ion: Structure, Spectroscopy and Dipole Moments. *J. Phys. B At. Mol. Opt. Phys.* **2017**, *50*, 055101.

(561) de Lima Batista, A. P.; de Lima, J. C. B.; Franzreb, K.; Ornellas, F. R. A Theoretical Study of SnF^{2+}, $SnCl^{2+}$, and SnO^{2+} and Their Experimental Search. *J. Chem. Phys.* **2012**, *137*, 154302.

(562) de Lima Batista, A. P.; Ornellas, F. R. Ab Initio Study of the Lowest-Lying Electronic States of the LiAs Molecule. *Comput. Theor. Chem.* **2013**, *1009*, 17–23.

(563) Wang, X.; Shi, D.; Sun, J. Accurate Calculations on 20 Λ–S States of the BP Radical: Potential Energy Curves, Spectroscopic Parameters, and Electronic Transition Properties. *Can. J. Chem.* **2015**, *93*, 1088–1095.

(564) Bauschlicher, C. W. The Low-Lying Electronic States of SiO. *Chem. Phys. Lett.* **2016**, *658*, 76–79.

(565) Liu, H.; Shi, D.; Sun, J.; Zhu, Z. Accurate Multireference Configuration Interaction Calculations of the 24 Λ-S States and 60 Ω States of the BO^+ Cation. *Spectrochim. Acta Part A Mol. Biomol. Spectrosc.* **2016**, *168*, 148–158.

(566) Belinassi, A. R.; Alves, T. V.; Ornellas, F. R. Electronic States and Spectroscopic Parameters of Selenium Monoiodide, SeI: A Theoretical Contribution. *Chem. Phys. Lett.* **2017**, *671*, 78–83.

(567) Fernandes, G. F. S.; Pontes, M. A. P.; de Oliveira, M. H.; Ferrão, L. F. A.; Machado, F. B. C. The Low-Lying States of AlC and GaC: Molecular Constants, Transition Probabilities and Radiative Lifetime. *Chem. Phys. Lett.* **2017**, *687*, 171–177.

(568) Bauschlicher, C. W.; Schwenke, D. W. The Low-Lying Electronic States of MgO. *Chem. Phys. Lett.* **2017**, *683*, 62–67.

(569) Song, Z.; Shi, D.; Sun, J.; Zhu, Z. Accurate MRCI Calculations of the Low-Lying Electronic

States of the NCl Molecule. *Eur. Phys. J. D* **2017**, *71*, 55.

(570) Prajapat, L.; Jagoda, P.; Lodi, L.; Gorman, M. N.; Yurchenko, S. N.; Tennyson, J. ExoMol Molecular Line Lists – XXIII. Spectra of PO and PS. *Mon. Not. R. Astron. Soc.* **2017**, *472*, 3648–3658.

(571) Chakrabarti, K.; Dora, A.; Ghosh, R.; Choudhury, B. S.; Tennyson, J. R -Matrix Study of Electron Impact Excitation and Dissociation of CH^+ Ions. *J. Phys. B At. Mol. Opt. Phys.* **2017**, *50*, 175202.

(572) Mourad, K. A.; Abdulal, S. N.; Korek, M. Electronic Structure with Rovibrational and Dipole Moment Calculation of the Diatomic Molecules AsBr and AsI. *Comput. Theor. Chem.* **2017**, *1103*, 63–70.

(573) Kalemos, A.; Mavridis, A. All Electron Ab Initio Calculations on the ScTi Molecule: A Really Hard Nut to Crack. *Theor. Chem. Acc.* **2013**, *132*, 1408.

(574) Srivastava, S.; Sathyamurthy, N. Ab Initio Potential Energy Curves for the Ground and Low Lying Excited States of NH^- and the Effect of $^2\Sigma^\pm$ States on Λ-Doubling of the Ground State $X^2\Pi$. *J. Phys. Chem. A* **2013**, *117*, 8623–8631.

(575) Alves, T. V.; Ornellas, F. R. Exploring the Electronic States of Iodocarbyne: A Theoretical Contribution. *Phys. Chem. Chem. Phys.* **2014**, *16*, 9530–9537.

(576) Vassilakis, A. A.; Kalemos, A.; Mavridis, A. Accurate First Principles Calculations on Chlorine Fluoride ClF and Its Ions $ClF^\pm$. *Theor. Chem. Acc.* **2014**, *133*, 1436.

(577) Srivastava, S.; Sathyamurthy, N. Ab Initio Potential Energy Curves for the Ground and Low-Lying Excited States of OH and OH^- and a Study of Rotational Fine Structure in Photodetachment. *J. Phys. Chem. A* **2014**, *118*, 6343–6350.

(578) Liu, H.; Shi, D.; Sun, J.; Zhu, Z.; Shulin, Z. Accurate Calculations on the 22 Electronic States and 54 Spin-Orbit States of the O_2 Molecule: Potential Energy Curves, Spectroscopic Parameters and Spin-Orbit Coupling. *Spectrochim. Acta Part A Mol. Biomol. Spectrosc.* **2014**, *124*, 216–229.

(579) de Lima Batista, A. P.; de Oliveira-Filho, A. G. S.; Ornellas, F. R. Ab Initio Characterization of the Lowest-Lying Electronic States of the NaAs Molecule. *Comput. Theor. Chem.* **2015**, *1064*, 56–61.

(580) Magoulas, I.; Papakondylis, A.; Mavridis, A. Structural Parameters of the Ground States of the Quasi-Stable Diatomic Anions CO^- , BF^-, and BCl^- as Obtained by Conventional Ab Initio Methods. *Int. J. Quantum Chem.* **2015**, *115*, 771–778.

(581) Müller, T.; Dallos, M.; Lischka, H.; Dubrovay, Z.; Szalay, P. G. A Systematic Theoretical Investigation of the Valence Excited States of the Diatomic Molecules B_2, C_2, N_2 and O_2. *Theor. Chem. Accounts Theory, Comput. Model. (Theoretica Chim. Acta)* **2001**, *105*, 227–243.

(582) South, C.; Schoendorff, G.; Wilson, A. K. MR-CcCA: A Route for Accurate Ground and Excited State Potential Energy Curves and Spectroscopic Properties for Third-Row Diatomic Molecules. *Comput. Theor. Chem.* **2014**, *1040–1041*, 72–83.

(583) Jovanović, V.; Lyskov, I.; Kleinschmidt, M.; Marian, C. M. On the Performance of DFT/MRCI-R and MR-MP2 in Spin–orbit Coupling Calculations on Diatomics and Polyatomic Organic Molecules. *Mol. Phys.* **2017**, *115*, 109–137.

(584) Harrison, J. F. Electronic Structure of Diatomic Molecules Composed of a First-Row Transition Metal and Main-Group Element (H−F). *Chem. Rev.* **2000**, *100*, 679–716.

(585) Tennyson, J.; Lodi, L.; McKemmish, L. K.; Yurchenko, S. N. The Ab Initio Calculation of Spectra of Open Shell Diatomic Molecules. *J. Phys. B At. Mol. Opt. Phys.* **2016**, *49*, 102001.

(586) Fang, Z.; Vasiliu, M.; Peterson, K. A.; Dixon, D. A. Prediction of Bond Dissociation Energies/Heats of Formation for Diatomic Transition Metal Compounds: CCSD(T) Works. *J. Chem. Theory Comput.* **2017**, *13*, 1057–1066.

(587) Cheng, L.; Gauss, J.; Ruscic, B.; Armentrout, P. B.; Stanton, J. F. Bond Dissociation Energies for Diatomic Molecules Containing 3d Transition Metals: Benchmark Scalar-Relativistic Coupled-Cluster Calculations for 20 Molecules. *J. Chem. Theory Comput.* **2017**, *13*, 1044–1056.

(588) Xu, X.; Zhang, W.; Tang, M.; Truhlar, D. G. Do Practical Standard Coupled Cluster Calculations Agree Better than Kohn-Sham Calculations with Currently Available Functionals When Compared to the Best Available Experimental Data for Dissociation Energies of Bonds to 3d Transition Metals? *J. Chem. Theory Comput.* **2015**, *11*, 2036–2052.

(589) Bao, J. L.; Zhang, X.; Xu, X.; Truhlar, D. G. Predicting Bond Dissociation Energy and Bond Length for Bimetallic Diatomic Molecules: A Challenge for Electronic Structure Theory. *Phys. Chem. Chem. Phys.* **2017**, *19*, 5839–5854.

(590) Aoto, Y. A.; de Lima Batista, A. P.; Köhn, A.; de Oliveira-Filho, A. G. S. How To Arrive at Accurate Benchmark Values for Transition Metal Compounds: Computation or Experiment? *J. Chem. Theory Comput.* **2017**, *13*, 5291–5316.

(591) Tennyson, J. Perspective: Accurate Ro-Vibrational Calculations on Small Molecules. *J. Chem. Phys.* **2016**, *145*, 120901.

(592) Azzam, A. A. A.; Lodi, L.; Yurchenko, S. N.; Tennyson, J. The Dipole Moment Surface for

Hydrogen Sulfide H_2S. *J. Quant. Spectrosc. Radiat. Transf.* **2015**, *161*, 41–49.

(593) Gharaibeh, M. A.; Nagarajan, R.; Clouthier, D. J.; Tarroni, R. An Experimental and Theoretical Study of the Electronic Spectrum of the HBCl Free Radical. *J. Chem. Phys.* **2015**, *142*, 014305.

(594) Hirano, T.; Nagashima, U. Ro-Vibrational Properties of FeCO in the $X^3\Sigma^-$ and $a^5\Sigma^-$ Electronic States: A Computational Molecular Spectroscopy Study. *J. Mol. Spectrosc.* **2015**, *314*, 35–47.

(595) Khiri, D.; Hochlaf, M.; Chambaud, G. Energetic Diagrams and Structural Properties of Monohaloacetylenes HC≡CX (X = F, Cl, Br). *J. Phys. Chem. A* **2016**, *120*, 5985–5992.

(596) Teplukhin, A.; Babikov, D. Efficient Method for Calculations of Ro-Vibrational States in Triatomic Molecules near Dissociation Threshold: Application to Ozone. *J. Chem. Phys.* **2016**, *145*, 114106.

(597) Kłos, J.; Alexander, M. H.; Kumar, P.; Poirier, B.; Jiang, B.; Guo, H. New Ab Initio Adiabatic Potential Energy Surfaces and Bound State Calculations for the Singlet Ground $\tilde{X}^1A_1$ and Excited $\tilde{C}^1B_2(2^1A')$ States of SO_2. *J. Chem. Phys.* **2016**, *144*, 174301.

(598) Koput, J. Ab Initio Potential Energy Surface and Vibration-Rotation Energy Levels of Sulfur Dioxide. *J. Comput. Chem.* **2017**, *38*, 892–900.

(599) Hou, G.-L.; Chen, B.; Transue, W. J.; Yang, Z.; Grützmacher, H.; Driess, M.; Cummins, C. C.; Borden, W. T.; Wang, X.-B. Spectroscopic Characterization, Computational Investigation, and Comparisons of ECX^- (E = As, P, and N; X = S and O) Anions. *J. Am. Chem. Soc.* **2017**, *139*, 8922–8930.

(600) Tchatchouang, M.; Nsangou, M.; Motapon, O. Stability, Metastability and Spectroscopic

Properties of Some Low-Lying Electronic States of C_2H^- and N_2H^-. *Comput. Theor. Chem.* **2017**, *1117*, 241–250.

(601) Powell, A. D.; Dattani, N. S.; Spada, R. F. K.; Machado, F. B. C.; Lischka, H.; Dawes, R. Investigation of the Ozone Formation Reaction Pathway: Comparisons of Full Configuration Interaction Quantum Monte Carlo and Fixed-Node Diffusion Monte Carlo with Contracted and Uncontracted MRCI. *J. Chem. Phys.* **2017**, *147*, 094306.

(602) Leiding, J.; Woon, D. E.; Dunning, T. H. Theoretical Studies of the Excited Doublet States of SF and SCl and Singlet States of SF_2, SFCl, and SCl_2. *J. Phys. Chem. A* **2012**, *116*, 1655–1662.

(603) de Oliveira-Filho, A. G. S.; Ornellas, F. R.; Peterson, K. A. Accurate Ab Initio Potential Energy Surfaces for the $^3A''$ and $^3A'$ Electronic States of the O(^{3}P)+HBr System. *J. Chem. Phys.* **2012**, *136*, 174316.

(604) Huang, X.; Schwenke, D. W.; Tashkun, S. A.; Lee, T. J. An Isotopic-Independent Highly Accurate Potential Energy Surface for CO_2 Isotopologues and an Initial $^{12}C^{16}O_2$ Infrared Line List. *J. Chem. Phys.* **2012**, *136*, 124311.

(605) Miliordos, E.; Ruedenberg, K.; Xantheas, S. S. Unusual Inorganic Biradicals: A Theoretical Analysis. *Angew. Chemie - Int. Ed.* **2013**, *52*, 5736–5739.

(606) Dawes, R.; Lolur, P.; Li, A.; Jiang, B.; Guo, H. Communication: An Accurate Global Potential Energy Surface for the Ground Electronic State of Ozone. *J. Chem. Phys.* **2013**, *139*, 201103.

(607) Gannouni, M. A.; Jaidane, N. E.; Halvick, P.; Stoecklin, T.; Hochlaf, M. Accurate Global Potential Energy Surface for the H + OH^+ Collision. *J. Chem. Phys.* **2014**, *140*, 184306.

(608) Miliordos, E.; Xantheas, S. S. On the Bonding Nature of Ozone (O_3) and Its Sulfur-Substituted Analogues SO_2, OS_2, and S_3: Correlation between Their Biradical Character and Molecular Properties. *J. Am. Chem. Soc.* **2014**, *136*, 2808–2817.

(609) Rocha, C. M. R.; Varandas, A. J. C. Accurate Ab Initio-Based Double Many-Body Expansion Potential Energy Surface for the Adiabatic Ground-State of the C_3 Radical Including Combined Jahn-Teller plus Pseudo-Jahn-Teller Interactions. *J. Chem. Phys.* **2015**, *143*, 074302.

(610) Hernández-Lamoneda, R.; Salazar, M. R.; Pack, R. T. Does Ozone Have a Barrier to Dissociation and Recombination? *Chem. Phys. Lett.* **2002**, *355*, 478–482.

(611) Schinke, R.; Fleurat-Lessard, P. The Transition-State Region of the $O(^3P)+O_2(^3\Sigma_g^-)$ Potential Energy Surface. *J. Chem. Phys.* **2004**, *121*, 5789–5793.

(612) Holka, F.; Szalay, P. G.; Müller, T.; Tyuterev, V. G. Toward an Improved Ground State Potential Energy Surface of Ozone. *J. Phys. Chem. A* **2010**, *114*, 9927–9935.

(613) Xie, C.; Malbon, C. L.; Yarkony, D. R.; Xie, D.; Guo, H. Signatures of a Conical Intersection in Adiabatic Dissociation on the Ground Electronic State. *J. Am. Chem. Soc.* **2018**, *140*, 1986–1989.

(614) Xie, C.; Malbon, C.; Yarkony, D. R.; Guo, H. Nonadiabatic Photodissociation Dynamics of the Hydroxymethyl Radical via the $2^2A(3s)$ Rydberg State: A Four-Dimensional Quantum Study. *J. Chem. Phys.* **2017**, *146*, 224306.

(615) Malbon, C. L.; Yarkony, D. R. Multistate, Multichannel Coupled Diabatic State Representations of Adiabatic States Coupled by Conical Intersections. CH_2OH Photodissociation. *J. Chem. Phys.* **2017**, *146*, 134302.

(616) Malbon, C. L.; Yarkony, D. R. Nonadiabatic Photodissociation of the Hydroxymethyl Radical from the 2^2A State. Surface Hopping Simulations Based on a Full Nine-Dimensional Representation of the 1,2,3^2A Potential Energy Surfaces Coupled by Conical Intersections. *J. Phys. Chem. A* **2015**, *119*, 7498–7509.

(617) DeVine, J. A.; Weichman, M. L.; Laws, B.; Chang, J.; Babin, M. C.; Balerdi, G.; Xie, C.; Malbon, C. L.; Lineberger, W. C.; Yarkony, D. R.; et al. Encoding of Vinylidene Isomerization in Its Anion Photoelectron Spectrum. *Science* **2017**, *358*, 336–339.

(618) Guo, L.; Han, H.; Ma, J.; Guo, H. Quantum Dynamics of Vinylidene Photodetachment on an Accurate Global Acetylene-Vinylidene Potential Energy Surface. *J. Phys. Chem. A* **2015**, *119*, 8488–8496.

(619) Li, J.; Guo, H. Permutationally Invariant Fitting of Intermolecular Potential Energy Surfaces: A Case Study of the Ne-C_2H_2 System. *J. Chem. Phys.* **2015**, *143*, 214304.

(620) Ogilby, P. R. Singlet Oxygen: There Is Indeed Something New under the Sun. *Chem. Soc. Rev.* **2010**, *39*, 3181–3209.

(621) Schweitzer, C.; Schmidt, R. Physical Mechanisms of Generation and Deactivation of Singlet Oxygen. *Chem. Rev.* **2003**, *103*, 1685–1758.

(622) Schweitzer, C.; Mehrdad, Z.; Noll, A.; Grabner, E. W.; Schmidt, R. Mechanism of Photosensitized Generation of Singlet Oxygen during Oxygen Quenching of Triplet States and the General Dependence of the Rate Constants and Efficiencies. *J. Phys. Chem. A* **2003**, *107*, 2192–2198.

(623) Boggio-Pasqua, M.; López Vidal, M.; Garavelli, M. Theoretical Mechanistic Study of Self-Sensitized Photo-Oxygenation and Singlet Oxygen Thermal Release in a

Dimethyldihydropyrene Derivative. *J. Photochem. Photobiol. A Chem.* **2017**, *333*, 156–164.

(624) Shafii, F.; Schmidt, R. Determination of Rate Constants of Formation of O_2 ($^1\Sigma_g^+$), O_2 ($^1\Delta_g$), and O_2 ($^3\Sigma_g^-$) in the Quenching of Triplet States by O_2 for Compounds with Incomplete Intersystem Crossing. *J. Phys. Chem. A* **2001**, *105*, 1805–1810.

(625) Bai, S.; Barbatti, M. Spatial Factors for Triplet Fusion Reaction of Singlet Oxygen Photosensitization. *J. Phys. Chem. Lett.* **2017**, *8*, 5456–5460.

(626) Cakmak, Y.; Kolemen, S.; Duman, S.; Dede, Y.; Dolen, Y.; Kilic, B.; Kostereli, Z.; Yildirim, L. T.; Dogan, A. L.; Guc, D.; et al. Designing Excited States: Theory-Guided Access to Efficient Photosensitizers for Photodynamic Action. *Angew. Chemie Int. Ed.* **2011**, *50*, 11937–11941.

(627) Nogueira, J. J.; Oppel, M.; González, L. Enhancing Intersystem Crossing in Phenotiazinium Dyes by Intercalation into DNA. *Angew. Chemie Int. Ed.* **2015**, *54*, 4375–4378.

(628) N. Harvey, J.; Aschi, M. Spin-Forbidden Dehydrogenation of Methoxy Cation: A Statistical View. *Phys. Chem. Chem. Phys.* **1999**, *1*, 5555–5563.

(629) Bai, S.; Barbatti, M. Divide-to-Conquer: A Kinetic Model for Singlet Oxygen Photosensitization. *J. Chem. Theory Comput.* **2017**, *13*, 5528–5538.

(630) Serrano-Pérez, J. J.; Olaso-González, G.; Merchán, M.; Serrano-Andrés, L. Singlet Oxygen Generation in PUVA Therapy Studied Using Electronic Structure Calculations. *Chem. Phys.* **2009**, *360*, 85–96.

(631) Sumita, M.; Morihashi, K. Theoretical Study of Singlet Oxygen Molecule Generation via an Exciplex with Valence-Excited Thiophene. *J. Phys. Chem. A* **2015**, *119*, 876–883.

(632) Freyer, W.; Stiel, H.; Teuchner, K.; Leupold, D. Photophysics and Photochemistry of Tetraanthraporphyrazines; Attempts to Obtain a New Generation of Photosensitizers. *J. Photochem. Photobiol. A Chem.* **1994**, *80*, 161–167.

(633) Martínez-Fernández, L.; González-Vázquez, J.; González, L.; Corral, I. Time-Resolved Insight into the Photosensitized Generation of Singlet Oxygen in Endoperoxides. *J. Chem. Theory Comput.* **2015**, *11*, 406–414.

(634) Richter, M.; Marquetand, P.; González-Vázquez, J.; Sola, I.; González, L. SHARC: Ab Initio Molecular Dynamics with Surface Hopping in the Adiabatic Representation Including Arbitrary Couplings. *J. Chem. Theory Comput.* **2011**, *7*, 1253–1258.

(635) Hudson, B. S.; Kohler, B. E.; Schulten, K. Excited States, Vol. 6; Academic Press: New York, 1982; p 1.

(636) Schulten, K.; Ohmine, I.; Karplus, M. Correlation Effects in the Spectra of Polyenes. *J. Chem. Phys.* **1976**, *64*, 4422–4441.

(637) Tavan, P.; Schulten, K. The Low-lying Electronic Excitations in Long Polyenes: A PPP-MRD-CI Study. *J. Chem. Phys.* **1986**, *85*, 6602–6609.

(638) Tavan, P.; Schulten, K. Electronic Excitations in Finite and Infinite Polyenes. *Phys. Rev. B* **1987**, *36*, 4337–4358.

(639) Wu, W.; Danovich, D.; Shurki, A.; Shaik, S. Using Valence Bond Theory to Understand Electronic Excited States: Application to the Hidden Excited State (2^1A_g) of $C_{2n}H_{2n+2}$ (n = 2−14) Polyenes. *J. Phys. Chem. A* **2000**, *104*, 8744–8758.

(640) Zhang, D.; Liu, C. Electronic Structures of Low-Lying B_u Excited States in Trans-Oligoenes: Pariser-Parr-Pople and Ab Initio Calculations. *J. Chem. Phys.* **2011**, *135*,

134117.

(641) McMurchie, L. E.; Davidson, E. R. Configuration Interaction Calculations on the Planar $^1(\pi,\pi^*)$ State of Ethylene. *J. Chem. Phys.* **1977**, *66*, 2959–2971.

(642) Buenker, R. J.; Peyerimhoff, S. D.; Shih, S.-K. AB Initio Study of the Spatial Extension of the Ethylene v State. *Chem. Phys. Lett.* **1980**, *69*, 7–13.

(643) Lindh, R.; Roos, B. O. A Theoretical Study of the Diffuseness of the V($^1B_{1u}$) State of Planar Ethylene. *Int. J. Quantum Chem.* **1989**, *35*, 813–825.

(644) Davidson, E. R. The Spatial Extent of the V State of Ethylene and Its Relation to Dynamic Correlation in the Cope Rearrangement. *J. Phys. Chem.* **1996**, *100*, 6161–6166.

(645) Borden, W. T.; Davidson, E. R. The Importance of Including Dynamic Electron Correlation in Ab Initio Calculations. *Acc. Chem. Res.* **1996**, *29*, 67–75.

(646) Müller, T.; Dallos, M.; Lischka, H. The Ethylene 1^1B_{1u} V State Revisited. *J. Chem. Phys.* **1999**, *110*, 7176–7184.

(647) Angeli, C. On the Nature of the $\pi \rightarrow \pi^*$ Ionic Excited States: The V State of Ethene as a Prototype. *J. Comput. Chem.* **2009**, *30*, 1319–1333.

(648) Wu, W.; Zhang, H.; Braïda, B.; Shaik, S.; Hiberty, P. C. The V State of Ethylene: Valence Bond Theory Takes up the Challenge. *Theor. Chem. Acc.* **2014**, *133*, 1441.

(649) Schmidt, M.; Tavan, P. Electronic Excitations in Long Polyenes Revisited. *J. Chem. Phys.* **2012**, *136*, 124309.

(650) Plasser, F.; Bäppler, S. A.; Wormit, M.; Dreuw, A. New Tools for the Systematic Analysis and Visualization of Electronic Excitations. II. Applications. *J. Chem. Phys.* **2014**, *141*,

024107.

(651) Mewes, S. A.; Plasser, F.; Krylov, A.; Dreuw, A. Benchmarking Excited-State Calculations Using Exciton Properties. *J. Chem. Theory Comput.* **2018**, *14*, 710–725.

(652) Hsu, C.-P.; Hirata, S.; Head-Gordon, M. Excitation Energies from Time-Dependent Density Functional Theory for Linear Polyene Oligomers: Butadiene to Decapentaene. *J. Phys. Chem. A* **2001**, *105*, 451–458.

(653) Starcke, J. H.; Wormit, M.; Schirmer, J.; Dreuw, A. How Much Double Excitation Character Do the Lowest Excited States of Linear Polyenes Have? *Chem. Phys.* **2006**, *329*, 39–49.

(654) Shu, Y.; Truhlar, D. G. Doubly Excited Character or Static Correlation of the Reference State in the Controversial 2^1A_g State of Trans-Butadiene? *J. Am. Chem. Soc.* **2017**, *139*, 13770–13778.

(655) Cave, R. J. Size-inconsistency Effects in Molecular Properties for States with Valence-Rydberg Mixing: The Low-lying $\pi \rightarrow \pi^*$ States of Ethylene and Butadiene. *J. Chem. Phys.* **1990**, *92*, 2450–2456.

(656) Lappe, J.; Cave, R. J. On the Vertical and Adiabatic Excitation Energies of the 2^1A_g State of Trans -1,3-Butadiene. *J. Phys. Chem. A* **2000**, *104*, 2294–2300.

(657) Serrano-Andrés, L.; Merchán, M.; Nebot-Gil, I.; Lindh, R.; Roos, B. O. Towards an Accurate Molecular Orbital Theory for Excited States: Ethene, Butadiene, and Hexatriene. *J. Chem. Phys.* **1993**, *98*, 3151–3162.

(658) Nakayama, K.; Nakano, H.; Hirao, K. Theoretical Study of the $\pi \rightarrow \pi^*$ Excited States of Linear Polyenes: The Energy Gap between $1^1B_u^+$ and $2^1A_g^-$ States and Their Character. *Int.*

J. Quantum Chem. **1998**, *66*, 157–175.

(659) Dallos, M.; Lischka, H. A Systematic Theoretical Investigation of the Lowest Valence- and Rydberg-Excited Singlet States of Trans-Butadiene. The Character of the 1^1B_u (V) State Revisited. *Theor. Chem. Accounts Theory, Comput. Model. (Theoretica Chim. Acta)* **2004**, *112*, 16–26.

(660) Marian, C. M.; Gilka, N. Performance of the Density Functional Theory/Multireference Configuration Interaction Method on Electronic Excitation of Extended π-Systems. *J. Chem. Theory Comput.* **2008**, *4*, 1501–1515.

(661) Serrano-Andres, L.; Lindh, R.; Roos, B. O.; Merchan, M. Theoretical Study of the Electronic Spectrum of All-Trans-1,3,5,7-Octatetraene. *J. Phys. Chem.* **1993**, *97*, 9360–9368.

(662) Angeli, C.; Pastore, M. The Lowest Singlet States of Octatetraene Revisited. *J. Chem. Phys.* **2011**, *134*, 184302.

(663) Davidson, E. R.; Jarzęcki, A. A. Zero Point Corrections to Vertical Excitation Energies. *Chem. Phys. Lett.* **1998**, *285*, 155–159.

(664) Fujii, T.; Kamata, A.; Shimizu, M.; Adachi, Y.; Maeda, S. Two-Photon Absorption Study of 1,3,5-Hexatriene by Cars and CSRS. *Chem. Phys. Lett.* **1985**, *115*, 369–372.

(665) Buma, W. J.; Kohler, B. E.; Song, K. Lowest Energy Excited Singlet State of Isolated Cis-hexatriene. *J. Chem. Phys.* **1991**, *94*, 6367–6376.

(666) Petek, H.; Bell, A. J.; Christensen, R. L.; Yoshihara, K. Fluorescence Excitation Spectra of the S1 States of Isolated Trienes. *J. Chem. Phys.* **1992**, *96*, 2412–2415.

(667) Leopold, D. G.; Pendley, R. D.; Roebber, J. L.; Hemley, R. J.; Vaida, V. Direct Absorption

Spectroscopy of Jet-cooled Polyenes. II. The $1^1B^+_u \leftarrow 1^1A^-_g$ Transitions of Butadienes and Hexatrienes. *J. Chem. Phys.* **1984**, *81*, 4218–4229.

(668) Chadwick, R. R.; Zgierski, M. Z.; Hudson, B. S. Resonance Raman Scattering of Butadiene: Vibronic Activity of a b_u Mode Demonstrates the Presence of a ^1A_g Symmetry Excited Electronic State at Low Energy. *J. Chem. Phys.* **1991**, *95*, 7204–7211.

(669) Gavin, R. M.; Risemberg, S.; Rice, S. A. Spectroscopic Properties of Polyenes. I. The Lowest Energy Allowed Singlet-singlet Transition for Cis- and Trans- 1,3,5-hexatriene. *J. Chem. Phys.* **1973**, *58*, 3160–3165.

(670) Gavin, R. M.; Weisman, C.; McVey, J. K.; Rice, S. A. Spectroscopic Properties of Polyenes. III. 1,3,5,7-Octatetraene. *J. Chem. Phys.* **1978**, *68*, 522–529.

(671) Christensen, R. L.; Galinato, M. G. I.; Chu, E. F.; Howard, J. N.; Broene, R. D.; Frank, H. A. Energies of Low-Lying Excited States of Linear Polyenes. *J. Phys. Chem. A* **2008**, *112*, 12629–12636.

(672) Snyder, R.; Arvidson, E.; Foote, C.; Harrigan, L.; Christensen, R. L. Electronic Energy Levels in Long Polyenes: $S_2 \rightarrow S_0$ Emission in All-Trans-1,3,5,7,9,11,13-Tetradecaheptaene. *J. Am. Chem. Soc.* **1985**, *107*, 4117–4122.

(673) Wang, P.; Nakamura, R.; Kanematsu, Y.; Koyama, Y.; Nagae, H.; Nishio, T.; Hashimoto, H.; Zhang, J.-P. Low-Lying Singlet States of Carotenoids Having 8–13 Conjugated Double Bonds as Determined by Electronic Absorption Spectroscopy. *Chem. Phys. Lett.* **2005**, *410*, 108–114.

(674) Kurashige, Y.; Nakano, H.; Nakao, Y.; Hirao, K. The $\pi \rightarrow \pi^*$ Excited States of Long Linear Polyenes Studied by the CASCI-MRMP Method. *Chem. Phys. Lett.* **2004**, *400*, 425–429.

(675) Sand, A. M.; Mazziotti, D. A. Enhanced Computational Efficiency in the Direct Determination of the Two-Electron Reduced Density Matrix from the Anti-Hermitian Contracted Schrödinger Equation with Application to Ground and Excited States of Conjugated π-Systems. *J. Chem. Phys.* **2015**, *143*, 134110.

(676) Gozem, S.; Luk, H. L.; Schapiro, I.; Olivucci, M. Theory and Simulation of the Ultrafast Double-Bond Isomerization of Biological Chromophores. *Chem. Rev.* **2017**, *117*, 13502–13565.

(677) Bonačić-Koutecký, V.; Schöffel, K.; Michl, J. Critically Heterosymmetric Biradicaloid Geometries of of Protonated Schiff Bases. *Theor. Chim. Acta* **1987**, *72*, 459–474.

(678) Weingart, O.; Schapiro, I.; Buss, V. Photochemistry of Visual Pigment Chromophore Models by Ab Initio Molecular Dynamics. *J. Phys. Chem. B* **2007**, *111*, 3782–3788.

(679) Walczak, E.; Szefczyk, B.; Andruniów, T. Geometries and Vertical Excitation Energies in Retinal Analogues Resolved at the CASPT2 Level of Theory: Critical Assessment of the Performance of CASSCF, CC2, and DFT Methods. *J. Chem. Theory Comput.* **2013**, *9*, 4915–4927.

(680) Martin, C. H.; Birge, R. R. Reparametrizing MNDO for Excited-State Calculations by Using Ab Initio Effective Hamiltonian Theory: Application to the 2,4-Pentadien-1-Iminium Cation. *J. Phys. Chem. A* **1998**, *102*, 852–860.

(681) Zaari, R. R.; Wong, S. Y. Y. Photoexcitation of 11-Z-Cis-7,8-Dihydro Retinal and 11-Z-Cis Retinal: A Comparative Computational Study. *Chem. Phys. Lett.* **2009**, *469*, 224–228.

(682) van Keulen, S. C.; Solano, A.; Rothlisberger, U. How Rhodopsin Tunes the Equilibrium between Protonated and Deprotonated Forms of the Retinal Chromophore. *J. Chem. Theory*

Comput. **2017**, *13*, 4524–4534.

(683) Malis, M.; Novak, J.; Zgrablic, G.; Parmigiani, F.; Doslic, N. Mechanism of Ultrafast Non-Reactive Deactivation of the Retinal Chromophore in Non-Polar Solvents. *Phys. Chem. Chem. Phys.* **2017**, *19*, 25970–25978.

(684) Aquino, A. J. A.; Barbatti, M.; Lischka, H. Excited-State Properties and Environmental Effects for Protonated Schiff Bases: A Theoretical Study. *ChemPhysChem* **2006**, *7*, 2089–2096.

(685) Valsson, O.; Filippi, C. Photoisomerization of Model Retinal Chromophores: Insight from Quantum Monte Carlo and Multiconfigurational Perturbation Theory. *J. Chem. Theory Comput.* **2010**, *6*, 1275–1292.

(686) Warshel, A. Bicycle-Pedal Model for the First Step in the Vision Process. *Nature* **1976**, *260*, 679–683.

(687) Zen, A.; Coccia, E.; Gozem, S.; Olivucci, M.; Guidoni, L. Quantum Monte Carlo Treatment of the Charge Transfer and Diradical Electronic Character in a Retinal Chromophore Minimal Model. *J. Chem. Theory Comput.* **2015**, *11*, 992–1005.

(688) Liu, L.; Liu, J.; Martinez, T. J. Dynamical Correlation Effects on Photoisomerization: Ab Initio Multiple Spawning Dynamics with MS-CASPT2 for a Model *Trans* -Protonated Schiff Base. *J. Phys. Chem. B* **2016**, *120*, 1940–1949.

(689) Valsson, O.; Filippi, C.; Casida, M. E. Regarding the Use and Misuse of Retinal Protonated Schiff Base Photochemistry as a Test Case for Time-Dependent Density-Functional Theory. *J. Chem. Phys.* **2015**, *142*, 144104.

(690) Garavelli, M.; Celani, P.; Bernardi, F.; Robb, M. A.; Olivucci, M. The $C_5H_6NH_2^+$

Protonated Shiff Base: An Ab Initio Minimal Model for Retinal Photoisomerization. *J. Am. Chem. Soc.* **1997**, *119*, 6891–6901.

(691) Szymczak, J. J.; Barbatti, M.; Lischka, H. Mechanism of Ultrafast Photodecay in Restricted Motions in Protonated Schiff Bases: The Pentadieniminium Cation. *J. Chem. Theory Comput.* **2008**, *4*, 1189–1199.

(692) Send, R.; Sundholm, D. Stairway to the Conical Intersection: A Computational Study of the Retinal Isomerization. *J. Phys. Chem. A* **2007**, *111*, 8766–8773.

(693) Sekharan, S.; Weingart, O.; Buss, V. Ground and Excited States of Retinal Schiff Base Chromophores by Multiconfigurational Perturbation Theory. *Biophys. J.* **2006**, *91*, L07–L09.

(694) Gozem, S.; Krylov, A. I.; Olivucci, M. Conical Intersection and Potential Energy Surface Features of a Model Retinal Chromophore: Comparison of EOM-CC and Multireference Methods. *J. Chem. Theory Comput.* **2013**, *9*, 284–292.

(695) Huix-Rotllant, M.; Filatov, M.; Gozem, S.; Schapiro, I.; Olivucci, M.; Ferré, N. Assessment of Density Functional Theory for Describing the Correlation Effects on the Ground and Excited State Potential Energy Surfaces of a Retinal Chromophore Model. *J. Chem. Theory Comput.* **2013**, *9*, 3917–3932.

(696) Schoenlein, R. W.; Peteanu, L. A.; Mathies, R. A.; Shank, C. V. The First Step in Vision: Femtosecond Isomerization of Rhodopsin. *Science* **1991**, *254*, 412–415.

(697) Mathies, R. A. Photochemistry: A Coherent Picture of Vision. *Nat. Chem.* **2015**, *7*, 945–947.

(698) Szymczak, J. J.; Barbatti, M.; Lischka, H. Is the Photoinduced Isomerization in Retinal

Protonated Schiff Bases a Single- or Double-Torsional Process. *J. Phys. Chem. A* **2009**, *113*, 11907–11918.

(699) Klaffki, N.; Weingart, O.; Garavelli, M.; Spohr, E. Sampling Excited State Dynamics: Influence of HOOP Mode Excitations in a Retinal Model. *Phys. Chem. Chem. Phys.* **2012**, *14*, 14299.

(700) Weingart, O.; Migani, A.; Olivucci, M.; Robb, M. A.; Buss, V.; Hunt, P. Probing the Photochemical Funnel of a Retinal Chromophore Model via Zero-Point Energy Sampling Semiclassical Dynamics. *J. Phys. Chem. A* **2004**, *108*, 4685–4693.

(701) Frutos, L. M.; Andruniów, T.; Santoro, F.; Ferré, N.; Olivucci, M. Tracking the Excited-State Time Evolution of the Visual Pigment with Multiconfigurational Quantum Chemistry. *Proc. Natl. Acad. Sci.* **2007**, *104*, 7764–7769.

(702) Ruckenbauer, M.; Barbatti, M.; Müller, T.; Lischka, H. Nonadiabatic Photodynamics of a Retinal Model in Polar and Nonpolar Environment. *J. Phys. Chem. A* **2013**, *117*, 2790–2799.

(703) Dokukina, I.; Weingart, O. Spectral Properties and Isomerisation Path of Retinal in C1C2 Channelrhodopsin. *Phys. Chem. Chem. Phys.* **2015**, *17*, 25142–25150.

(704) Dokukina, I.; Marian, C. M.; Weingart, O. New Perspectives on an Old Issue: A Comparative MS-CASPT2 and OM2-MRCI Study of Polyenes and Protonated Schiff Bases. *Photochem. Photobiol.* **2017**, *93*, 1345–1355.

(705) Huntress, M. M.; Gozem, S.; Malley, K. R.; Jailaubekov, A. E.; Vasileiou, C.; Vengris, M.; Geiger, J. H.; Borhan, B.; Schapiro, I.; Larsen, D. S.; et al. Toward an Understanding of the Retinal Chromophore in Rhodopsin Mimics. *J. Phys. Chem. B* **2013**, *117*, 10053–10070.

(706) Coto, P. B.; Strambi, A.; Ferré, N.; Olivucci, M. The Color of Rhodopsins at the Ab Initio Multiconfigurational Perturbation Theory Resolution. *Proc. Natl. Acad. Sci.* **2006**, *103*, 17154–17159.

(707) Cembran, A.; Bernardi, F.; Olivucci, M.; Garavelli, M. Counterion Controlled Photoisomerization of Retinal Chromophore Models: A Computational Investigation. *J. Am. Chem. Soc.* **2004**, *126*, 16018–16037.

(708) Manathunga, M.; Yang, X.; Luk, H. L.; Gozem, S.; Frutos, L. M.; Valentini, A.; Ferrè, N.; Olivucci, M. Probing the Photodynamics of Rhodopsins with Reduced Retinal Chromophores. *J. Chem. Theory Comput.* **2016**, *12*, 839–850.

(709) Polli, D.; Altoe, P.; Weingart, O.; Spillane, K. M.; Manzoni, C.; Brida, D.; Tomasello, G.; Orlandi, G.; Kukura, P.; Mathies, R. A.; et al. Conical Intersection Dynamics of the Primary Photoisomerization Event in Vision. *Nature* **2010**, *467*, 440–443.

(710) Polli, D.; Weingart, O.; Brida, D.; Poli, E.; Maiuri, M.; Spillane, K. M.; Bottoni, A.; Kukura, P.; Mathies, R. A.; Cerullo, G.; et al. Wavepacket Splitting and Two-Pathway Deactivation in the Photoexcited Visual Pigment Isorhodopsin. *Angew. Chemie Int. Ed.* **2014**, *53*, 2504–2507.

(711) Hayashi, S.; Tajkhorshid, E.; Schulten, K. Photochemical Reaction Dynamics of the Primary Event of Vision Studied by Means of a Hybrid Molecular Simulation. *Biophys. J.* **2009**, *96*, 403–416.

(712) Weingart, O. Combined Quantum and Molecular Mechanics (QM/MM) Approaches to Simulate Ultrafast Photodynamics in Biological Systems. *Curr. Org. Chem.* **2017**, *21*, 586–601.

(713) Serrano-Andrés, L.; Merchán, M. Are the Five Natural DNA/RNA Base Monomers a Good Choice from Natural Selection? A Photochemical Perspective. *J. Photochem. Photobiol. C-Photochemistry Rev.* **2009**, *10*, 21–32.

(714) Sagan, C. Ultraviolet Selection Pressure on the Earliest Organisms. *J. Theor. Biol.* **1973**, *39*, 195–200.

(715) Mouret, S.; Baudouin, C.; Charveron, M.; Favier, A.; Cadet, J.; Douki, T. Cyclobutane Pyrimidine Dimers Are Predominant DNA Lesions in Whole Human Skin Exposed to UVA Radiation. *Proc. Natl. Acad. Sci. U. S. A.* **2006**, *103*, 13765–13770.

(716) Steckl, A. J.; Spaeth, H.; You, H.; Gomez, E.; Grote, J. DNA as an Optical Material. *Opt. Photon. News* **2011**, *22*, 34–39.

(717) Giussani, A.; Segarra-Martí, J.; Roca-Sanjuán, D.; Merchán, M. Excitation of Nucleobases from a Computational Perspective I: Reaction Paths. In *Photoinduced Phenomena in Nucleic Acids I*; Barbatti, M., Borin, A. C., Ullrich, S., Eds.; Topics in Current Chemistry, Vol. 355; Springer: Cham, 2013; pp 57–97.

(718) Mai, S.; Richter, M.; Marquetand, P.; González, L. Excitation of Nucleobases from a Computational Perspective II: Dynamics. In *Photoinduced Phenomena in Nucleic Acids I*; Barbatti, M., Borin, A. C., Ullrich, S., Eds.; Topics in Current Chemistry, Vol. 355; Springer: Cham, 2014; pp 99–153.

(719) Barbatti, M.; Borin, A. C.; Ullrich, S. Photoinduced Processes in Nucleic Acids. In *Photoinduced Phenomena in Nucleic Acids I*; Barbatti, M., Borin, A. C., Ullrich, S., Eds.; Topics in Current Chemistry, Vol. 355; Springer: Cham, 2014; pp 1–32.

(720) Improta, R.; Santoro, F.; Blancafort, L. Quantum Mechanical Studies on the Photophysics

and the Photochemistry of Nucleic Acids and Nucleobases. *Chem. Rev.* **2016**, *116*, 3540–3593.

(721) Stavros, V. G.; Verlet, J. R. R. Gas-Phase Femtosecond Particle Spectroscopy: A Bottom-Up Approach to Nucleotide Dynamics. *Annu. Rev. Phys. Chem.* **2016**, *67*, 211–232.

(722) Matsika, S. Modified Nucleobases. In *Photoinduced Phenomena in Nucleic Acids I*; Barbatti, M., Borin, A. C., Ullrich, S., Eds.; Topics in Current Chemistry, Vol 355; Springer: Cham, 2014; pp 209–243.

(723) Improta, R.; Barone, V. Excited States Behavior of Nucleobases in Solution: Insights from Computational Studies. In *Photoinduced Phenomena in Nucleic Acids I*; Barbatti, M., Borin, C. A., Ullrich, S., Eds.; Topics in Current Chemistry, Vol. 355; Springer: Cham, 2014; pp 329–357.

(724) Cadet, J.; Grand, A.; Douki, T. Solar UV Radiation-Induced DNA Bipyrimidine Photoproducts: Formation and Mechanistic Insights. In *Photoinduced Phenomena in Nucleic Acids II*; Barbatti, M., Borin, C. A., Ullrich, S., Eds.; Topics in Current Chemistry, Vol. 356; Springer: Cham, 2015; pp 249–275.

(725) Rios, A. C.; Tor, Y. On the Origin of the Canonical Nucleobases: An Assessment of Selection Pressures across Chemical and Early Biological Evolution. *Isr. J. Chem.* **2013**, *53*, 469–483.

(726) Carota, E.; Botta, G.; Rotelli, L.; Di Mauro, E.; Saladino, R. Current Advances in Prebiotic Chemistry Under Space Conditions. *Curr. Org. Chem.* **2015**, *19*, 1963–1979.

(727) Kawai, K.; Majima, T. Photoinduced Charge-Separation in DNA. In *Photoinduced Phenomena in Nucleic Acids II*; Barbatti, M., Borin, C. A., Ullrich, S., Eds.; Topics in

Current Chemistry, Vol. 356; Springer: Cham, 2015; pp 165–182.

(728) Daniels, M.; Hauswirth, W. Fluorescence of the Purine and Pyrimidine Bases of the Nucleic Acids in Neutral Aqueous Solution at 300 K. *Science* **1971**, *171*, 675–677.

(729) Callis, P. R. Electronic States and Luminescence of Nucleic Acid Systems. *Annu. Rev. Phys. Chem.* **1983**, *34*, 329–357.

(730) Crespo-Hernández, C. E.; Cohen, B.; Hare, P. M.; Kohler, B. Ultrafast Excited-State Dynamics in Nucleic Acids. *Chem. Rev.* **2004**, *104*, 1977–2019.

(731) Fülscher, M. P.; Roos, B. O. Theoretical-Study of the Electronic-Spectrum of Cytosine. *J. Am. Chem. Soc.* **1995**, *117*, 2089–2095.

(732) Fülscher, M. P.; Serrano-Andrés, L.; Roos, B. O. A Theoretical Study of the Electronic Spectra of Adenine and Guanine. *J. Am. Chem. Soc.* **1997**, *119*, 6168–6176.

(733) Blancafort, L. Excited-State Potential Energy Surface for the Photophysics of Adenine. *J. Am. Chem. Soc.* **2006**, *128*, 210–219.

(734) Chen, H.; Li, S. H. Theoretical Study toward Understanding Ultrafast Internal Conversion of Excited 9H-Adenine. *J. Phys. Chem. A* **2005**, *109*, 8443–8446.

(735) Perun, S.; Sobolewski, A. L.; Domcke, W. Ab Initio Studies on the Radiationless Decay Mechanisms of the Lowest Excited Singlet States of 9H-Adenine. *J. Am. Chem. Soc.* **2005**, *127*, 6257–6265.

(736) Serrano-Andrés, L.; Merchán, M.; Borin, A. C. Adenine and 2-Aminopurine: Paradigms of Modern Theoretical Photochemistry. *Proc. Natl. Acad. Sci. U. S. A.* **2006**, *103*, 8691–8696.

(737) Serrano-Andrés, L.; Merchán, M.; Borin, A. C. A Three-State Model for the Photophysics

of Adenine. *Chem. Eur. J.* **2006**, *12*, 6559–6571.

(738) Perun, S.; Sobolewski, A. L.; Domcke, W. Photostability of 9H-Adenine: Mechanisms of the Radiationless Deactivation of the Lowest Excited Singlet States. *Chem. Phys.* **2005**, *313*, 107–112.

(739) Serrano-Andrés, L.; Merchán, M.; Borin, A. C. A Three-State Model for the Photophysics of Guanine. *J. Am. Chem. Soc.* **2008**, *130*, 2473–2484.

(740) Yamazaki, S.; Domcke, W.; Sobolewski, A. L. Nonradiative Decay Mechanisms of the Biologically Relevant Tautomer of Guanine. *J. Phys. Chem. A* **2008**, *112*, 11965–11968.

(741) Chen, H.; Li, S. H. Ab Initio Study on Deactivation Pathways of Excited 9H-Guanine. *J. Chem. Phys.* **2006**, *124*, 154315.

(742) Blancafort, L.; Cohen, B.; Hare, P. M.; Kohler, B.; Robb, M. A. Singlet Excited-State Dynamics of 5-Fluorocytosine and Cytosine: An Experimental and Computational Study. *J. Phys. Chem. A* **2005**, *109*, 4431–4436.

(743) Merchán, M.; Serrano-Andrés, L. Ultrafast Internal Conversion of Excited Cytosine via the Lowest ππ* Electronic Singlet State. *J. Am. Chem. Soc.* **2003**, *125*, 8108–8109.

(744) Blancafort, L. Energetics of Cytosine Singlet Excited-State Decay Paths - A Difficult Case for CASSCF and CASPT2. *Photochem. Photobiol.* **2007**, *83*, 603–610.

(745) Merchán, M.; González-Luque, R.; Climent, T.; Serrano-Andrés, L.; Rodriuguez, E.; Reguero, M.; Pelaez, D. Unified Model for the Ultrafast Decay of Pyrimidine Nucleobases. *J. Phys. Chem. B* **2006**, *110*, 26471–26476.

(746) Perun, S.; Sobolewski, A. L.; Domcke, W. Conical Intersections in Thymine. *J. Phys. Chem. A* **2006**, *110*, 13238–13244.

(747) Asturiol, D.; Lasorne, B.; Robb, M. A.; Blancafort, L. Photophysics of the π,π* and n,π* States of Thymine: MS-CASPT2 Minimum-Energy Paths and CASSCF on-the-Fly Dynamics. *J. Phys. Chem. A* **2009**, *113*, 10211–10218.

(748) Yamazaki, S.; Taketsugu, T. Nonradiative Deactivation Mechanisms of Uracil, Thymine, and 5-Fluorouracil: A Comparative Ab Initio Study. *J. Phys. Chem. A* **2012**, *116*, 491–503.

(749) Zechmann, G.; Barbatti, M. Photophysics and Deactivation Pathways of Thymine. *J. Phys. Chem. A* **2008**, *112*, 8273–8279.

(750) Hassan, W. M. I.; Chung, W. C.; Shimakura, N.; Koseki, S.; Kono, H.; Fujimura, Y. Ultrafast Radiationless Transition Pathways through Conical Intersections in Photo-Excited 9H-Adenine. *Phys. Chem. Chem. Phys.* **2010**, *12*, 5317–5328.

(751) Matsika, S. Three-State Conical Intersections in Nucleic Acid Bases. *J. Phys. Chem. A* **2005**, *109*, 7538–7545.

(752) Barbatti, M.; Aquino, A. J. A.; Szymczak, J. J.; Nachtigallová, D.; Lischka, H. Photodynamical Simulations of Cytosine: Characterization of the Ultrafast Bi-Exponential UV Deactivation. *Phys. Chem. Chem. Phys.* **2011**, *13*, 6145–6155.

(753) Kistler, K. A.; Matsika, S. Three-State Conical Intersections in Cytosine and Pyrimidinone Bases. *J. Chem. Phys.* **2008**, *128*, 215102.

(754) Kistler, K. A.; Matsika, S. Radiationless Decay Mechanism of Cytosine: An Ab Initio Study with Comparisons to the Fluorescent Analogue 5-Methyl-2-Pyrimidinone. *J. Phys. Chem. A* **2007**, *111*, 2650–2661.

(755) Szabla, R.; Kruse, H.; Šponer, J.; Góra, R. W. Water–chromophore Electron Transfer Determines the Photochemistry of Cytosine and Cytidine. *Phys. Chem. Chem. Phys.* **2017**,

19, 17531–17537.

(756) Matsika, S. Radiationless Decay of Excited States of Uracil through Conical Intersections. *J. Phys. Chem. A* **2004**, *108*, 7584–7590.

(757) Marian, C. M. A New Pathway for the Rapid Decay of Electronically Excited Adenine. *J. Chem. Phys.* **2005**, *122*, 104314.

(758) Engler, G.; Seefeld, K.; Schmitt, M.; Tatchen, J.; Grotkopp, O.; Muller, T. J. J.; Kleinermanns, K. Acetylation Makes the Difference: A Joint Experimental and Theoretical Study on Low-Lying Electronically Excited States of 9H-Adenine and 9-Acetyladenine. *Phys. Chem. Chem. Phys.* **2013**, *15*, 1025–1031.

(759) Marian, C. M. The Guanine Tautomer Puzzle: Quantum Chemical Investigation of Ground and Excited States. *J. Phys. Chem. A* **2007**, *111*, 1545–1553.

(760) Tomic, K.; Tatchen, J.; Marian, C. M. Quantum Chemical Investigation of the Electronic Spectra of the Keto, Enol, and Keto-Imine Tautomers of Cytosine. *J. Phys. Chem. A* **2005**, *109*, 8410–8418.

(761) Roca-Sanjuan, D.; Rubio, M.; Merchán, M.; Serrano-Andrés, L. Ab Initio Determination of the Ionization Potentials of DNA and RNA Nucleobases. *J. Chem. Phys.* **2006**, *125*, 84302.

(762) Ruckenbauer, M.; Mai, S.; Marquetand, P.; González, L. Photoelectron Spectra of 2-Thiouracil, 4-Thiouracil, and 2,4-Dithiouracil. *J. Chem. Phys.* **2016**, *144*, 74303.

(763) Ruckenbauer, M.; Mai, S.; Marquetand, P.; González, L. Revealing Deactivation Pathways Hidden in Time-Resolved Photoelectron Spectra. *Sci. Rep.* **2016**, *6*, 35522.

(764) Nachtigallova, D.; Lischka, H.; Szymczak, J. J.; Barbatti, M.; Hobza, P.; Gengeliczki, Z.; Pino, G.; Callahan, M. P.; de Vries, M. S. The Effect of C5 Substitution on the

Photochemistry of Uracil. *Phys. Chem. Chem. Phys.* **2010**, *12*, 4924–4933.

(765) Barbatti, M.; Ullrich, S. Ionization Potentials of Adenine along the Internal Conversion Pathways. *Phys. Chem. Chem. Phys.* **2011**, *13*, 15492–15500.

(766) Nenov, A.; Giussani, A.; Segarra-Martí, J.; Jaiswal, V. K.; Rivalta, I.; Cerullo, G.; Mukamel, S.; Garavelli, M. Modeling the High-Energy Electronic State Manifold of Adenine: Calibration for Nonlinear Electronic Spectroscopy. *J. Chem. Phys.* **2015**, *142*, 212443.

(767) Hudock, H. R.; Levine, B. G.; Thompson, A. L.; Satzger, H.; Townsend, D.; Gador, N.; Ullrich, S.; Stolow, A.; Martínez, T. J. Ab Initio Molecular Dynamics and Time-Resolved Photoelectron Spectroscopy of Electronically Excited Uracil and Thymine. *J. Phys. Chem. A* **2007**, *111*, 8500–8508.

(768) Barbatti, M.; A Aquino, A. J.; Szymczak, J. J.; Nachtigallová, D.; Hobza, P.; Lischka, H. Relaxation Mechanisms of UV-Photoexcited DNA and RNA Nucleobases. *Proc. Natl. Acad. Sci. U. S. A.* **2010**, *107*, 21453–21458.

(769) González-Vázquez, J.; González, L. A Time-Dependent Picture of the Ultrafast Deactivation of Keto-Cytosine Including Three-State Conical Intersections. *Chemphyschem* **2010**, *11*, 3617–3624.

(770) Hudock, H. R.; Martínez, T. J. Excited-State Dynamics of Cytosine Reveal Multiple Intrinsic Subpicosecond Pathways. *ChemPhysChem* **2008**, *9*, 2486–2490.

(771) Szymczak, J. J.; Barbatti, M.; Soo Hoo, J. T.; Adkins, J. A.; Windus, T. L.; Nachtigallova, D.; Lischka, H. Photodynamics Simulations of Thymine: Relaxation into the First Excited Singlet State. *J. Phys. Chem. A* **2009**, *113*, 12686–12693.

(772) Fingerhut, B. P.; Dorfman, K. E.; Mukamel, S. Monitoring Nonadiabatic Dynamics of the RNA Base Uracil by UV Pump–IR Probe Spectroscopy. *J. Phys. Chem. Lett.* **2013**, *4*, 1933–1942.

(773) Richter, M.; Mai, S.; Marquetand, P.; Gonzalez, L. Ultrafast Intersystem Crossing Dynamics in Uracil Unravelled by Ab Initio Molecular Dynamics. *Phys. Chem. Chem. Phys.* **2014**, *16*, 24423–24436.

(774) Nachtigallová, D.; Aquino, A. J. A.; Szymczak, J. J.; Barbatti, M.; Hobza, P.; Lischka, H. Nonadiabatic Dynamics of Uracil: Population Split among Different Decay Mechanisms. *J. Phys. Chem. A* **2011**, *115*, 5247–5255.

(775) Barbatti, M.; Lischka, H. Nonadiabatic Deactivation of 9H-Adenine: A Comprehensive Picture Based on Mixed Quantum-Classical Dynamics. *J. Am. Chem. Soc.* **2008**, *130*, 6831–6839.

(776) Barbatti, M.; Szymczak, J. J.; Aquino, A. J. A.; Nachtigallová, D.; Lischka, H. The Decay Mechanism of Photoexcited Guanine − A Nonadiabatic Dynamics Study. *J. Chem. Phys.* **2011**, *134*, 014304.

(777) Fabiano, E.; Thiel, W. Nonradiative Deexcitation Dynamics of 9H-Adenine: An OM2 Surface Hopping Study. *J. Phys. Chem. A* **2008**, *112*, 6859–6863.

(778) Lan, Z.; Fabiano, E.; Thiel, W. Photoinduced Nonadiabatic Dynamics of 9 H -Guanine. *ChemPhysChem* **2009**, *10*, 1225–1229.

(779) Lan, Z.; Fabiano, E.; Thiel, W. Photoinduced Nonadiabatic Dynamics of Pyrimidine Nucleobases: On-the-Fly Surface-Hopping Study with Semiempirical Methods. *J. Phys. Chem. B* **2009**, *113*, 3548–3555.

(780) Alexandrova, A. N.; Tully, J. C.; Granucci, G. Photochemistry of DNA Fragments via Semiclassical Nonadiabatic Dynamics. *J. Phys. Chem. B* **2010**, *114*, 12116–12128.

(781) Marchetti, B.; Karsili, T. N. V.; Ashfold, M. N. R.; Domcke, W. A 'Bottom up', *Ab Initio* Computational Approach to Understanding Fundamental Photophysical Processes in Nitrogen Containing Heterocycles, DNA Bases and Base Pairs. *Phys. Chem. Chem. Phys.* **2016**, *18*, 20007–20027.

(782) Tuna, D.; Sobolewski, A. L.; Domcke, W. Mechanisms of Ultrafast Excited-State Deactivation in Adenosine. *J. Phys. Chem. A* **2013**, *118*, 122–127.

(783) Improta, R.; Barone, V. The Excited States of Adenine and Thymine Nucleoside and Nucleotide in Aqueous Solution: A Comparative Study by Time-Dependent DFT Calculations. *Theor. Chem. Acc.* **2008**, *120*, 491–497.

(784) Tajti, A.; Fogarasi, G.; Szalay, P. G. Reinterpretation of the UV Spectrum of Cytosine: Only Two Electronic Transitions? *ChemPhysChem* **2009**, *10*, 1603–1606.

(785) Barbatti, M.; Aquino, A. J. A.; Lischka, H. The UV Absorption of Nucleobases: Semi-Classical Ab Initio Spectra Simulations. *Phys. Chem. Chem. Phys.* **2010**, *12*, 4959–4967.

(786) Plasser, F.; Crespo-Otero, R.; Pederzoli, M.; Pittner, J.; Lischka, H.; Barbatti, M. Surface Hopping Dynamics with Correlated Single-Reference Methods: 9H-Adenine as a Case Study. *J. Chem. Theory Comput.* **2014**, *10*, 1395–1405.

(787) Stojanović, L.; Bai, S.; Nagesh, J.; Izmaylov, A.; Crespo-Otero, R.; Lischka, H.; Barbatti, M. New Insights into the State Trapping of UV-Excited Thymine. *Molecules* **2016**, *21*, 1603.

(788) Barbatti, M. Photorelaxation Induced by Water-Chromophore Electron Transfer. *J. Am.*

Chem. Soc. **2014**, *136*, 10246–10249.

(789) Doltsinis, N. L.; Markwick, P. R. L.; Nieber, H.; Langer, H. Ultrafast Radiationless Decay in Nucleic Acids: Insights from Nonadiabatic Ab Initio Molecular Dynamics. In *Radiation Induced Molecular Phenomena in Nucleic Acids*; Shukla, M. K., Leszczynski, J., Eds.; Springer Netherlands, 2008; Vol. 5, pp 265–299.

(790) Mitrić, R.; Werner, U.; Wohlgemuth, M.; Seifert, G.; Bonačić-Koutecký, V. Nonadiabatic Dynamics within Time-Dependent Density Functional Tight Binding Method. *J. Phys. Chem. A* **2009**, *113*, 12700–12705.

(791) Szabla, R. R.; Góra, R. W.; Šponer, J. Ultrafast Excited-State Dynamics of Isocytosine. *Phys. Chem. Chem. Phys.* **2016**, *18*, 20208–20218.

(792) Hudock, H. R.; Levine, H. G.; Thompson, A. L.; Martinez, T. J. First Principles Dynamics of Photoexcited DNA and RNA Bases. *Comput. Mod. Sci. Eng. Vol 2, Pts a B* **2007**, *2*, 219–222.

(793) Roca-Sanjuán, D.; Olaso-González, G.; González-Ramírez, I.; Serrano-Andrés, L.; Merchán, M. Molecular Basis of DNA Photodimerization: Intrinsic Production of Cyclobutane Cytosine Dimers. *J. Am. Chem. Soc.* **2008**, *130*, 10768–10779.

(794) McFarland, B. K.; Farrell, J. P.; Miyabe, S.; Tarantelli, F.; Aguilar, A.; Berrah, N.; Bostedt, C.; Bozek, J. D.; Bucksbaum, P. H.; Castagna, J. C.; et al. Ultrafast X-Ray Auger Probing of Photoexcited Molecular Dynamics. *Nat Commun* **2014**, *5*, 4235.

(795) Park, J. W.; Shiozaki, T. On-the-Fly CASPT2 Surface-Hopping Dynamics. *J. Chem. Theory Comput.* **2017**, *13*, 3676–3683.

(796) Segarra-Martí, J.; Francés-Monerris, A.; Roca-Sanjuán, D.; Merchán, M. Assessment of the

Potential Energy Hypersurfaces in Thymine within Multiconfigurational Theory: CASSCF vs. CASPT2. *Molecules* **2016**, *21*, 1666.

(797) Hu, D.; Liu, Y. F.; Sobolewski, A. L.; Lan, Z. Nonadiabatic Dynamics Simulation of Keto Isocytosine: A Comparison of Dynamical Performance of Different Electronic-Structure Methods. *Phys. Chem. Chem. Phys.* **2017**, *19*, 19168–19177.

(798) Li, Q.; Mennucci, B.; Robb, M. A.; Blancafort, L.; Curutchet, C. Polarizable QM/MM Multiconfiguration Self-Consistent Field Approach with State-Specific Corrections: Environment Effects on Cytosine Absorption Spectrum. *J. Chem. Theory Comput.* **2015**, *11*, 1674–1682.

(799) Kochman, M. A.; Pola, M.; Dwayne Miller, R. J. Theoretical Study of the Photophysics of 8-Vinylguanine, an Isomorphic Fluorescent Analogue of Guanine. *J. Phys. Chem. A* **2016**, *120*, 6200–6215.

(800) Altavilla, S. F.; Segarra-MartÃ-, J.; Nenov, A.; Conti, I.; Rivalta, I.; Garavelli, M. Deciphering the Photochemical Mechanisms Describing the UV-Induced Processes Occurring in Solvated Guanine Monophosphate. *Front. Chem.* **2015**, *3*, 29.

(801) Yamazaki, S.; Sobolewski, A. L.; Domcke, W. Photophysics of Xanthine: Computational Study of the Radiationless Decay Mechanisms. *Phys. Chem. Chem. Phys.* **2009**, *11*, 10165.

(802) Pepino, A. J.; Segarra-Martí, J.; Nenov, A.; Improta, R.; Garavelli, M. Resolving Ultrafast Photoinduced Deactivations in Water-Solvated Pyrimidine Nucleosides. *J. Phys. Chem. Lett.* **2017**, *8*, 1777–1783.

(803) Trachsel, M. A.; Wiedmer, T.; Blaser, S.; Frey, H.-M.; Li, Q.; Ruiz-Barragan, S.; Blancafort, L.; Leutwyler, S. The Excited-State Structure, Vibrations, Lifetimes, and

Nonradiative Dynamics of Jet-Cooled 1-Methylcytosine. *J. Chem. Phys.* **2016**, *145*, 134307.

(804) Martínez-Fernández, L.; Pepino, A. J.; Segarra-Martí, J.; Jovaišaitė, J.; Vaya, I.; Nenov, A.; Markovitsi, D.; Gustavsson, T.; Banyasz, A.; Garavelli, M.; et al. Photophysics of Deoxycytidine and 5-Methyldeoxycytidine in Solution: A Comprehensive Picture by Quantum Mechanical Calculations and Femtosecond Fluorescence Spectroscopy. *J. Am. Chem. Soc.* **2017**, *139*, 7780–7791.

(805) Serrano-Pérez, J. J.; González-Luque, R.; Merchán, M.; Serrano-Andrés, L. On the Intrinsic Population of the Lowest Triplet State of Thymine. *J. Phys. Chem. B* **2007**, *111*, 11880–11883.

(806) Gobbo, J. P.; Borin, A. C.; Serrano-Andrés, L. On the Relaxation Mechanisms of 6-Azauracil. *J. Phys. Chem. B* **2011**, *115*, 6243–6251.

(807) González-Luque, R.; Climent, T.; González-Ramírez, I.; Merchán, M.; Serrano-Andrés, L. Singlet−Triplet States Interaction Regions in DNA/RNA Nucleobase Hypersurfaces. *J. Chem. Theory Comput.* **2010**, *6*, 2103–2114.

(808) Lu, Z.; Beckstead, A. A.; Kohler, B.; Matsika, S. Excited State Relaxation of Neutral and Basic 8-Oxoguanine. *J. Phys. Chem. B* **2015**, *119*, 8293–8301.

(809) Marian, C. M.; Kleinschmidt, M.; Tatchen, J. The Photophysics of 7H-Adenine: A Quantum Chemical Investigation Including Spin–orbit Effects. *Chem. Phys.* **2008**, *347*, 346–359.

(810) Richter, M.; Marquetand, P.; González-Vázquez, J.; Sola, I.; González, L. Femtosecond Intersystem Crossing in the DNA Nucleobase Cytosine. *J. Phys. Chem. Lett.* **2012**, *3*, 3090–3095.

(811) Mai, S.; Marquetand, P.; Richter, M.; González-Vázquez, J.; González, L. Singlet and Triplet Excited-State Dynamics Study of the Keto and Enol Tautomers of Cytosine. *ChemPhysChem* **2013**, *14*, 2920–2931.

(812) Carlos Borin, A.; Mai, S.; Marquetand, P.; Gonzalez, L. Ab Initio Molecular Dynamics Relaxation and Intersystem Crossing Mechanisms of 5-Azacytosine. *Phys. Chem. Chem. Phys.* **2017**, *19*, 5888–5894.

(813) Petersen, J.; Wohlgemuth, M.; Sellner, B.; Bonacic-Koutecky, V.; Lischka, H.; Mitric, R. Laser Pulse Trains for Controlling Excited State Dynamics of Adenine in Water. *Phys. Chem. Chem. Phys.* **2012**, *14*, 4687–4694.

(814) Harada, Y.; Okabe, C.; Kobayashi, T.; Suzuki, T.; Ichimura, T.; Nishi, N.; Xu, Y.-Z. Ultrafast Intersystem Crossing of 4-Thiothymidine in Aqueous Solution. *J. Phys. Chem. Lett.* **2010**, *1*, 480–484.

(815) Pollum, M.; Jockusch, S.; Crespo-Hernández, C. E. 2,4-Dithiothymine as a Potent UVA Chemotherapeutic Agent. *J. Am. Chem. Soc.* **2014**, *136*, 17930–17933.

(816) Kuramochi, H.; Kobayashi, T.; Suzuki, T.; Ichimura, T. Excited-State Dynamics of 6-Aza-2-Thiothymine and 2-Thiothymine: Highly Efficient Intersystem Crossing and Singlet Oxygen Photosensitization. *J. Phys. Chem. B* **2010**, *114*, 8782–8789.

(817) Cui, G. L.; Fang, W. State-Specific Heavy-Atom Effect on Intersystem Crossing Processes in 2-Thiothymine: A Potential Photodynamic Therapy Photosensitizer. *J. Chem. Phys.* **2013**, *138*, 44315.

(818) Cui, G.; Thiel, W. Intersystem Crossing Enables 4-Thiothymidine to Act as a Photosensitizer in Photodynamic Therapy: An Ab Initio QM/MM Study. *J. Phys. Chem.*

Lett. **2014**, *5*, 2682–2687.

(819) Bai, S.; Barbatti, M. Why Replacing Different Oxygens of Thymine with Sulfur Causes Distinct Absorption and Intersystem Crossing. *J. Phys. Chem. A* **2016**, *120*, 6342–6350.

(820) Bai, S.; Barbatti, M. On the Decay of the Triplet State of Thionucleobases. *Phys. Chem. Chem. Phys.* **2017**, *19*, 12674–12682.

(821) Gobbo, J. P.; Borin, A. C. On The Population of Triplet Excited States of 6-Aza-2-Thiothymine. *J. Phys. Chem. A* **2013**, *117*, 5589–5596.

(822) Sánchez-Rodríguez, J. A.; Mohamadzade, A.; Mai, S.; Ashwood, B.; Pollum, M.; Marquetand, P.; González, L.; Crespo-Hernández, C. E.; Ullrich, S. 2-Thiouracil Intersystem Crossing Photodynamics Studied by Wavelength-Dependent Photoelectron and Transient Absorption Spectroscopies. *Phys. Chem. Chem. Phys.* **2017**, *19*, 19756–19766.

(823) Mai, S.; Marquetand, P.; González, L. A Static Picture of the Relaxation and Intersystem Crossing Mechanisms of Photoexcited 2-Thiouracil. *J. Phys. Chem. A* **2015**, *119*, 9524–9533.

(824) Yu, H.; Sanchez-Rodriguez, J. A.; Pollum, M.; Crespo-Hernandez, C. E.; Mai, S.; Marquetand, P.; Gonzalez, L.; Ullrich, S. Internal Conversion and Intersystem Crossing Pathways in UV Excited, Isolated Uracils and Their Implications in Prebiotic Chemistry. *Phys. Chem. Chem. Phys.* **2016**, *18*, 20168–20176.

(825) Gobbo, J. P.; Borin, A. C. 2-Thiouracil Deactivation Pathways and Triplet States Population. *Comput. Theor. Chem.* **2014**, *1040–1041*, 195–201.

(826) Mai, S.; Pollum, M.; Martinez-Fernandez, L.; Dunn, N.; Marquetand, P.; Corral, I.; Crespo-Hernandez, C. E.; Gonzalez, L. The Origin of Efficient Triplet State Population in Sulfur-

Substituted Nucleobases. *Nat. Commun.* **2016**, *7*, 13077.

(827) Mai, S.; Marquetand, P.; González, L. Intersystem Crossing Pathways in the Noncanonical Nucleobase 2-Thiouracil: A Time-Dependent Picture. *J. Phys. Chem. Lett.* **2016**, *7*, 1978–1983.

(828) Mai, S.; Plasser, F.; Pabst, M.; Neese, F.; Köhn, A.; González, L. Surface Hopping Dynamics Including Intersystem Crossing Using the Algebraic Diagrammatic Construction Method. *J. Chem. Phys.* **2017**, *147*, 184109.

(829) Plasser, F.; Aquino, A. J. A.; Lischka, H.; Nachtigallová, D. Electronic Excitation Processes in Single-Strand and Double-Strand DNA: A Computational Approach. *Top. Curr. Chem.* **2015**, *356*, 1–38.

(830) Marquetand, P.; Nogueira, J.; Mai, S.; Plasser, F.; González, L. Challenges in Simulating Light-Induced Processes in DNA. *Molecules* **2017**, *22*, 49.

(831) Tonzani, S.; Schatz, G. C. Electronic Excitations and Spectra in Single-Stranded DNA. *J. Am. Chem. Soc.* **2008**, *130*, 7607–7612.

(832) Lange, A. W.; Herbert, J. M. Both Intra- and Interstrand Charge-Transfer Excited States in Aqueous B-DNA Are Present at Energies Comparable To, or Just Above, the $^{1}\pi\pi^{*}$ Excitonic Bright States. *J. Am. Chem. Soc.* **2009**, *131*, 3913–3922.

(833) Nogueira, J. J.; Plasser, F.; González, L. Electronic Delocalization, Charge Transfer and Hypochromism in the UV Absorption Spectrum of Polyadenine Unravelled by Multiscale Computations and Quantitative Wavefunction Analysis. *Chem. Sci.* **2017**, *8*, 5682–5691.

(834) Spata, V. A.; Matsika, S. Bonded Excimer Formation in π-Stacked 9-Methyladenine Dimers. *J. Phys. Chem. A* **2013**, *117*, 8718–8728.

(835) Plasser, F.; Pašalić, H.; Gerzabek, M. H.; Libisch, F.; Reiter, R.; Burgdörfer, J.; Müller, T.; Shepard, R.; Lischka, H. The Multiradical Character of One- and Two-Dimensional Graphene Nanoribbons. *Angew. Chemie Int. Ed.* **2013**, *52*, 2581–2584.

(836) Conti, I.; Altoe, P.; Stenta, M.; Garavelli, M.; Orlandi, G. Adenine Deactivation in DNA Resolved at the CASPT2//CASSCF/AMBER Level. *Phys. Chem. Chem. Phys.* **2010**, *12*, 5016–5023.

(837) Lu, Y.; Lan, Z. G.; Thiel, W. Hydrogen Bonding Regulates the Monomeric Nonradiative Decay of Adenine in DNA Strands. *Angew. Chemie-International Ed.* **2011**, *50*, 6864–6867.

(838) Zeleny, T.; Ruckenbauer, M.; Aquino, A. J. A.; Muller, T.; Lankas, F.; Drsata, T.; Hase, W. L.; Nachtigallova, D.; Lischka, H. Strikingly Different Effects of Hydrogen Bonding on the Photodynamics of Individual Nucleobases in DNA: Comparison of Guanine and Cytosine. *J. Am. Chem. Soc.* **2012**, *134*, 13662–13669.

(839) Nachtigallova, D.; Zeleny, T.; Ruckenbauer, M.; Muller, T.; Barbatti, M.; Hobza, P.; Lischka, H. Does Stacking Restrain the Photodynamics of Individual Nucleobases? *J. Am. Chem. Soc.* **2010**, *132*, 8261–8263.

(840) Sobolewski, A. L.; Domcke, W. Ab Initio Studies on the Photophysics of the Guanine–cytosine Base Pair. *Phys. Chem. Chem. Phys.* **2004**, *6*, 2763–2771.

(841) Groenhof, G.; Schafer, L. V; Boggio-Pasqua, M.; Goette, M.; Grubmuller, H.; Robb, M. A. Ultrafast Deactivation of an Excited Cytosine-Guanine Base Pair in DNA. *J. Am. Chem. Soc.* **2007**, *129*, 6812–6819.

(842) Kozak, C. R.; Kistler, K. A.; Lu, Z.; Matsika, S. Excited-State Energies and Electronic Couplings of DNA Base Dimers. *J. Phys. Chem. B* **2010**, *114*, 1674–1683.

(843) Blancafort, L.; Voityuk, A. a. Exciton Delocalization, Charge Transfer, and Electronic Coupling for Singlet Excitation Energy Transfer between Stacked Nucleobases in DNA: An MS-CASPT2 Study. *J. Chem. Phys.* **2014**, *140*, 095102.

(844) Olaso-González, G.; Roca-Sanjuán, D.; Serrano-Andrés, L.; Merchán, M. Toward the Understanding of DNA Fluorescence: The Singlet Excimer of Cytosine. *J. Chem. Phys.* **2006**, *125*, 231102.

(845) Olaso-González, G.; Merchán, M.; Serrano-Andrés, L. The Role of Adenine Excimers in the Photophysics of Oligonucleotides. *J. Am. Chem. Soc.* **2009**, *131*, 4368–4377.

(846) Plasser, F.; Lischka, H. Electronic Excitation and Structural Relaxation of the Adenine Dinucleotide in Gas Phase and Solution. *Photochem. Photobiol. Sci.* **2013**, *12*, 1440.

(847) Conti, I.; Nenov, A.; Höfinger, S.; Flavio Altavilla, S.; Rivalta, I.; Dumont, E.; Orlandi, G.; Garavelli, M. Excited State Evolution of DNA Stacked Adenines Resolved at the CASPT2//CASSCF/Amber Level: From the Bright to the Excimer State and Back. *Phys. Chem. Chem. Phys.* **2015**, *17*, 7291–7302.

(848) Conti, I.; Martínez-Fernández, L.; Esposito, L.; Hofinger, S.; Nenov, A.; Garavelli, M.; Improta, R. Multiple Electronic and Structural Factors Control Cyclobutane Pyrimidine Dimer and 6-4 Thymine-Thymine Photodimerization in a DNA Duplex. *Chem. - A Eur. J.* **2017**, *23*, 15177–15188.

(849) Giussani, A.; Conti, I.; Nenov, A.; Garavelli, M. Photoinduced Formation Mechanism of the Thymine–thymine (6–4) Adduct in DNA; a QM(CASPT2//CASSCF):MM(AMBER) Study. *Faraday Discuss.* **2018**.

(850) Rauer, C.; Nogueira, J. J.; Marquetand, P.; González, L. Cyclobutane Thymine

Photodimerization Mechanism Revealed by Nonadiabatic Molecular Dynamics. *J. Am. Chem. Soc.* **2016**, *138*, 15911–15916.

(851) Acharya, A.; Bogdanov, A. M.; Grigorenko, B. L.; Bravaya, K. B.; Nemukhin, A. V; Lukyanov, K. A.; Krylov, A. I. Photoinduced Chemistry in Fluorescent Proteins: Curse or Blessing? *Chem. Rev.* **2017**, *117*, 758–795.

(852) Royer, C. A. Probing Protein Folding and Conformational Transitions with Fluorescence. *Chem. Rev.* **2006**, *106*, 1769–1784.

(853) Mishin, A. S.; Belousov, V. V; Solntsev, K. M.; Lukyanov, K. A. Novel Uses of Fluorescent Proteins. *Curr. Opin. Chem. Biol.* **2015**, *27*, 1–9.

(854) Andruniów, T.; Ferré, N.; Olivucci, M. Structure, Initial Excited-State Relaxation, and Energy Storage of Rhodopsin Resolved at the Multiconfigurational Perturbation Theory Level. *Proc. Natl. Acad. Sci.* **2004**, *101*, 17908–17913.

(855) Meech, S. R. Excited State Reactions in Fluorescent Proteins. *Chem. Soc. Rev.* **2009**, *38*, 2922–2934.

(856) Sample, V.; Newman, R. H.; Zhang, J. The Structure and Function of Fluorescent Proteins. *Chem. Soc. Rev.* **2009**, *38*, 2852–2864.

(857) van Thor, J. J. Photoreactions and Dynamics of the Green Fluorescent Protein. *Chem. Soc. Rev.* **2009**, *38*, 2935–2950.

(858) Bravaya, K. B.; Grigorenko, B. L.; Nemukhin, A. V; Krylov, A. I. Quantum Chemistry Behind Bioimaging: Insights from Ab Initio Studies of Fluorescent Proteins and Their Chromophores. *Acc. Chem. Res.* **2012**, *45*, 265–275.

(859) Lukyanov, K. A.; Serebrovskaya, E. O.; Lukyanov, S.; Chudakov, D. M. Fluorescent

Proteins as Light-Inducible Photochemical Partners. *Photochem. Photobiol. Sci.* **2010**, *9*, 1301–1306.

(860) Subach, F. V; Verkhusha, V. V. Chromophore Transformations in Red Fluorescent Proteins. *Chem. Rev.* **2012**, *112*, 4308–4327.

(861) Rogers, D. M.; Hirst, J. D. Ab Initio Study of Aromatic Side Chains of Amino Acids in Gas Phase and Solution. *J. Phys. Chem. A* **2003**, *107*, 11191–11200.

(862) Borin, A. C.; Serrano-Andrés, L. A Theoretical Study of the Absorption Spectra of Indole and Its Analogs: Indene, Benzimidazole, and 7-Azaindole. *Chem. Phys.* **2000**, *262*, 253–265.

(863) Serrano-Andrés, L.; Fülscher, M. P.; Roos, B. O.; Merchán, M. Theoretical Study of the Electronic Spectrum of Imidazole. *J. Phys. Chem.* **1996**, *100*, 6484–6491.

(864) Barbatti, M.; Lischka, H.; Salzmann, S.; Marian, C. M. UV Excitation and Radiationless Deactivation of Imidazole. *J. Chem. Phys.* **2009**, *130*, 34305.

(865) Brand, C.; Küpper, J.; Pratt, D. W.; Leo Meerts, W.; Krügler, D.; Tatchen, J.; Schmitt, M. Vibronic Coupling in Indole: I. Theoretical Description of the ^1L_a–^1L_b Interaction and the Electronic Spectrum. *Phys. Chem. Chem. Phys.* **2010**, *12*, 4968.

(866) Machado, F. B. C.; Davidson, E. R. A Theoretical Investigation of Some Low-lying Electronic States of Imidazole. *J. Chem. Phys.* **1992**, *97*, 1881–1891.

(867) Borin, A. C.; Serrano-Andrés, L. A Theoretical Study of the Absorption Spectra of Indole and Its Analogs: Indene, Benzimidazole, and 7-Azaindole. *Chem. Phys.* **2000**, *262*, 253–265.

(868) Serrano-andrés, L.; Merchán, M.; Borin, A. C.; Stålring, J.; Paulo, S. Theoretical Studies on

the Spectroscopy of the 7-Azaindole Monomer and Dimer. **2001**, *84*, 181–191.

(869) Serrano-Andrés, L.; Borin, A. C. A Theoretical Study of the Emission Spectra of Indole and Its Analogs: Indene, Benzimidazole, and 7-Azaindole. *Chem. Phys.* **2000**, *262*, 267–283.

(870) Arulmozhiraja, S.; Coote, M. L. ^1L_a and ^1L_b States of Indole and Azaindole: Is Density Functional Theory Inadequate? *J. Chem. Theory Comput.* **2012**, *8*, 575–584.

(871) Gindensperger, E.; Haegy, A.; Daniel, C.; Marquardt, R. Ab Initio Study of the Electronic Singlet Excited-State Properties of Tryptophan in the Gas Phase: The Role of Alanyl Side-Chain Conformations. *Chem. Phys.* **2010**, *374*, 104–110.

(872) Nolting, D.; Marian, C.; Weinkauf, R. Protonation Effect on the Electronic Spectrum of Tryptophan in the Gas Phase. *Phys. Chem. Chem. Phys.* **2004**, *6*, 2633–2640.

(873) Serrano-Andrés, L.; Fülscher, M. P. Theoretical Study of the Electronic Spectroscopy of Peptides. 2. Glycine and N-Acetylglycine. *J. Am. Chem. Soc.* **1996**, *118*, 12200–12206.

(874) Serrano-Andrés, L.; Roos, B. O. Theoretical Study of the Absorption and Emission Spectra of Indole in the Gas Phase and in a Solvent. *J. Am. Chem. Soc.* **1996**, *118*, 185–195.

(875) Serrano-Andrés, L.; Fülscher, M. P.; Karlström, G. Solvent Effects on Electronic Spectra Studied by Multiconfigurational Perturbation Theory. *Int. J. Quantum Chem.* **1997**, *65*, 167–181.

(876) Livingstone, R.; Schalk, O.; Boguslavskiy, A. E.; Wu, G.; Therese Bergendahl, L.; Stolow, A.; Paterson, M. J.; Townsend, D. Following the Excited State Relaxation Dynamics of Indole and 5-Hydroxyindole Using Time-Resolved Photoelectron Spectroscopy. *J. Chem. Phys.* **2011**, *135*, 194307.

(877) Ashfold, M. N. R.; Devine, A. L.; Dixon, R. N.; King, G. A.; Nix, M. G. D.; Oliver, T. A.

A. Exploring Nuclear Motion through Conical Intersections in the UV Photodissociation of Phenols and Thiophenol. *Proc. Natl. Acad. Sci.* **2008**, *105*, 12701–12706.

(878) Hause, M. L.; Heidi Yoon, Y.; Case, A. S.; Crim, F. F. Dynamics at Conical Intersections: The Influence of O–H Stretching Vibrations on the Photodissociation of Phenol. *J. Chem. Phys.* **2008**, *128*, 104307.

(879) Iqbal, A.; Cheung, M. S. Y.; Nix, M. G. D.; Stavros, V. G. Exploring the Time-Scales of H-Atom Detachment from Photoexcited Phenol-H6 and Phenol-D5: Statistical vs Nonstatistical Decay. *J. Phys. Chem. A* **2009**, *113*, 8157–8163.

(880) Nix, M. G. D.; Devine, A. L.; Dixon, R. N.; Ashfold, M. N. R. Observation of Geometric Phase Effect Induced Photodissociation Dynamics in Phenol. *Chem. Phys. Lett.* **2008**, *463*, 305–308.

(881) Sobolewski, A. L.; Domcke, W. Photoinduced Electron and Proton Transfer in Phenol and Its Clusters with Water and Ammonia. *J. Phys. Chem. A* **2001**, *105*, 9275–9283.

(882) Sobolewski, A. L.; Domcke, W.; Dedonder-Lardeux, C.; Jouvet, C. Excited-State Hydrogen Detachment and Hydrogen Transfer Driven by Repulsive $^1\pi\sigma^*$ States: A New Paradigm for Nonradiative Decay in Aromatic Biomolecules. *Phys. Chem. Chem. Phys.* **2002**, *4*, 1093–1100.

(883) Xie, C.; Guo, H. Photodissociation of Phenol via Nonadiabatic Tunneling: Comparison of Two Ab Initio Based Potential Energy Surfaces. *Chem. Phys. Lett.* **2017**, *683*, 222–227.

(884) An, H.; Baeck, K. K. Quantum Wave Packet Propagation Study of the Photochemistry of Phenol: Isotope Effects (Ph-OD) and the Direct Excitation to the $^1\pi\sigma^*$ State. *J. Phys. Chem. A* **2011**, *115*, 13309–13315.

(885) Ramesh, S. G.; Domcke, W. A Multi-Sheeted Three-Dimensional Potential-Energy Surface for the H-Atom Photodissociation of Phenol. *Faraday Discuss.* **2013**, *163*, 73–94.

(886) Lan, Z.; Domcke, W.; Vallet, V.; Sobolewski, A. L.; Mahapatra, S. Time-Dependent Quantum Wave-Packet Description of the $^1\pi\sigma^*$ Photochemistry of Phenol. *J. Chem. Phys.* **2005**, *122*, 224315.

(887) Dixon, R. N.; Oliver, T. A. A.; Ashfold, M. N. R. Tunnelling under a Conical Intersection: Application to the Product Vibrational State Distributions in the UV Photodissociation of Phenols. *J. Chem. Phys.* **2011**, *134*, 194303.

(888) Vieuxmaire, O. P. J.; Lan, Z.; Sobolewski, A. L.; Domcke, W. Ab Initio Characterization of the Conical Intersections Involved in the Photochemistry of Phenol. *J. Chem. Phys.* **2008**, *129*, 224307.

(889) Sobolewski, A. L.; Domcke, W. Ab Initio Investigations on the Photophysics of Indole. *Chem. Phys. Lett.* **1999**, *315*, 293–298.

(890) Wilke, J.; Wilke, M.; Brand, C.; Spiegel, J. D.; Marian, C. M.; Schmitt, M. Modulation of the L_a/L_b Mixing in an Indole Derivative: A Position-Dependent Study Using 4-, 5-, and 6-Fluoroindole. *J. Phys. Chem. A* **2017**, *121*, 1597–1606.

(891) Oliver, T. A. A.; King, G. A.; Ashfold, M. N. R. Position Matters: Competing O-H and N-H Photodissociation Pathways in Hydroxy- and Methoxy-Substituted Indoles. *Phys. Chem. Chem. Phys.* **2011**, *13*, 14646–14662.

(892) Blancafort, L.; González, D.; Olivucci, M.; Robb, M. A. Quenching of Tryptophan $^1(\pi,\pi^*)$ Fluorescence Induced by Intramolecular Hydrogen Abstraction via an Aborted Decarboxylation Mechanism. *J. Am. Chem. Soc.* **2002**, *124*, 6398–6406.

(893) Hadden, D. J.; Wells, K. L.; Roberts, G. M.; Bergendahl, L. T.; Paterson, M. J.; Stavros, V. G. Time Resolved Velocity Map Imaging of H-Atom Elimination from Photoexcited Imidazole and Its Methyl Substituted Derivatives. *Phys. Chem. Chem. Phys.* **2011**, *13*, 10342–10349.

(894) Muchová, E.; Slavíček, P.; Sobolewski, A. L.; Hobza, P. Glycine in an Electronically Excited State: Ab Initio Electronic Structure and Dynamical Calculations. *J. Phys. Chem. A* **2007**, *111*, 5259–5269.

(895) Oncak, M.; Lischka, H.; Slavicek, P. Photostability and Solvation: Photodynamics of Microsolvated Zwitterionic Glycine. *Phys. Chem. Chem. Phys.* **2010**, *12*, 4906–4914.

(896) Sobolewski, A. L.; Domcke, W. Computational Studies of the Photophysics of Neutral and Zwitterionic Glycine in an Aqueous Environment: The Glycine-$(H_2O)_2$ Cluster. *Chem. Phys. Lett.* **2008**, *457*, 404–407.

(897) Wohlgemuth, M.; Mitrić, R. Photochemical Chiral Symmetry Breaking in Alanine. *J. Phys. Chem. A* **2016**, *120*, 8976–8982.

(898) Mališ, M.; Došlić, N. Nonradiative Relaxation Mechanisms of UV Excited Phenylalanine Residues: A Comparative Computational Study. *Molecules* **2017**, *22*, 493.

(899) Shemesh, D.; Sobolewski, A. L.; Domcke, W. Role of Excited-State Hydrogen Detachment and Hydrogen-Transfer Processes for the Excited-State Deactivation of an Aromatic Dipeptide: N-Acetyl Tryptophan Methyl Amide. *Phys. Chem. Chem. Phys.* **2010**, *12*, 4899–4905.

(900) Marazzi, M.; Sancho, U.; Castaño, O.; Domcke, W.; Frutos, L. M. Photoinduced Proton Transfer as a Possible Mechanism for Highly Efficient Excited-State Deactivation in

Proteins. *J. Phys. Chem. Lett.* **2010**, *1*, 425–428.

(901) Došlić, N.; Kovačević, G.; Ljubić, I. Signature of the Conformational Preferences of Small Peptides: A Theoretical Investigation. *J. Phys. Chem. A* **2007**, *111*, 8650–8658.

(902) Clavaguéra, C.; Piuzzi, F.; Dognon, J.-P. Electronic Spectrum of Tryptophan-Phenylalanine. A Correlated Ab Initio and Time-Dependent Density Functional Theory Study. *J. Phys. Chem. B* **2009**, *113*, 16443–16448.

(903) Lill, M. A.; Helms, V. Proton Shuttle in Green Fluorescent Protein Studied by Dynamic Simulations. *Proc. Natl. Acad. Sci.* **2002**, *99*, 2778–2781.

(904) Weber, W.; Helms, V.; McCammon, J. A.; Langhoff, P. W. Shedding Light on the Dark and Weakly Fluorescent States of Green Fluorescent Proteins. *Proc. Natl. Acad. Sci.* **1999**, *96*, 6177–6182.

(905) Helms, V.; Winstead, C.; Langhoff, P. W. Low-Lying Electronic Excitations of the Green Fluorescent Protein Chromophore. *J. Mol. Struct. THEOCHEM* **2000**, *506*, 179–189.

(906) Andersen, L. H.; Lapierre, A.; Nielsen, S. B.; Nielsen, I. B.; Pedersen, S. U.; Pedersen, U. V; Tomita, S. Chromophores of the Green Fluorescent Protein Studied in the Gas Phase. *Eur. Phys. J. D - At. Mol. Opt. Plasma Phys.* **2002**, *20*, 597–600.

(907) Martin, M. E.; Negri, F.; Olivucci, M. Origin, Nature, and Fate of the Fluorescent State of the Green Fluorescent Protein Chromophore at the CASPT2//CASSCF Resolution. *J. Am. Chem. Soc.* **2004**, *126*, 5452–5464.

(908) Chattoraj, M.; King, B. A.; Bublitz, G. U.; Boxer, S. G. Ultra-Fast Excited State Dynamics in Green Fluorescent Protein: Multiple States and Proton Transfer. *Proc. Natl. Acad. Sci.* **1996**, *93*, 8362–8367.

(909) Voityuk, A. A.; Kummer, A. D.; Michel-Beyerle, M.-E.; Rösch, N. Absorption Spectra of the GFP Chromophore in Solution: Comparison of Theoretical and Experimental Results. *Chem. Phys.* **2001**, *269*, 83–91.

(910) Laino, T.; Nifosì, R.; Tozzini, V. Relationship between Structure and Optical Properties in Green Fluorescent Proteins: A Quantum Mechanical Study of the Chromophore Environment. *Chem. Phys.* **2004**, *298*, 17–28.

(911) Tozzini, V.; Nifosì, R. Ab Initio Molecular Dynamics of the Green Fluorescent Protein (GFP) Chromophore: An Insight into the Photoinduced Dynamics of Green Fluorescent Proteins. *J. Phys. Chem. B* **2001**, *105*, 5797–5803.

(912) Sinicropi, A.; Andruniow, T.; Ferré, N.; Basosi, R.; Olivucci, M. Properties of the Emitting State of the Green Fluorescent Protein Resolved at the CASPT2//CASSCF/CHARMM Level. *J. Am. Chem. Soc.* **2005**, *127*, 11534–11535.

(913) Altoe', P.; Bernardi, F.; Garavelli, M.; Orlandi, G.; Negri, F. Solvent Effects on the Vibrational Activity and Photodynamics of the Green Fluorescent Protein Chromophore: A Quantum-Chemical Study. *J. Am. Chem. Soc.* **2005**, *127*, 3952–3963.

(914) Epifanovsky, E.; Polyakov, I.; Grigorenko, B.; Nemukhin, A.; Krylov, A. I. Quantum Chemical Benchmark Studies of the Electronic Properties of the Green Fluorescent Protein Chromophore. 1. Electronically Excited and Ionized States of the Anionic Chromophore in the Gas Phase. *J. Chem. Theory Comput.* **2009**, *5*, 1895–1906.

(915) Toniolo, A.; Ben-Nun, M.; Martínez, T. J. Optimization of Conical Intersections with Floating Occupation Semiempirical Configuration Interaction Wave Functions. *J. Phys. Chem. A* **2002**, *106*, 4679–4689.

(916) Polyakov, I. V; Grigorenko, B. L.; Epifanovsky, E. M.; Krylov, A. I.; Nemukhin, A. V. Potential Energy Landscape of the Electronic States of the GFP Chromophore in Different Protonation Forms: Electronic Transition Energies and Conical Intersections. *J. Chem. Theory Comput.* **2010**, *6*, 2377–2387.

(917) Olsen, S.; Lamothe, K.; Martínez, T. J. Protonic Gating of Excited-State Twisting and Charge Localization in GFP Chromophores: A Mechanistic Hypothesis for Reversible Photoswitching. *J. Am. Chem. Soc.* **2010**, *132*, 1192–1193.

(918) Toniolo, A.; Granucci, G.; Martínez, T. J. Conical Intersections in Solution: A QM/MM Study Using Floating Occupation Semiempirical Configuration Interaction Wave Functions. *J. Phys. Chem. A* **2003**, *107*, 3822–3830.

(919) Vendrell, O.; Gelabert, R.; Moreno, M.; Lluch, J. M. Potential Energy Landscape of the Photoinduced Multiple Proton-Transfer Process in the Green Fluorescent Protein: Classical Molecular Dynamics and Multiconfigurational Electronic Structure Calculations. *J. Am. Chem. Soc.* **2006**, *128*, 3564–3574.

(920) Vendrell, O.; Gelabert, R.; Moreno, M.; Lluch, J. M. Photoinduced Proton Transfer from the Green Fluorescent Protein Chromophore to a Water Molecule: Analysis of the Transfer Coordinate. *Chem. Phys. Lett.* **2004**, *396*, 202–207.

(921) Vendrell, O.; Gelabert, R.; Moreno, M.; Lluch, J. M. Operation of the Proton Wire in Green Fluorescent Protein. A Quantum Dynamics Simulation. *J. Phys. Chem. B* **2008**, *112*, 5500–5511.

(922) Vendrell, O.; Gelabert, R.; Moreno, M.; Lluch, J. M. Exploring the Effects of Intramolecular Vibrational Energy Redistribution on the Operation of the Proton Wire in Green Fluorescent

Protein. *J. Phys. Chem. B* **2008**, *112*, 13443–13452.

(923) Li, X.; Chung, L. W.; Mizuno, H.; Miyawaki, A.; Morokuma, K. A Theoretical Study on the Nature of On- and Off-States of Reversibly Photoswitching Fluorescent Protein Dronpa: Absorption, Emission, Protonation, and Raman. *J. Phys. Chem. B* **2010**, *114*, 1114–1126.

(924) Grigorenko, B.; Savitsky, A.; Topol, I.; Burt, S.; Nemukhin, A. Ground-State Structures and Vertical Excitations for the Kindling Fluorescent Protein AsFP595. *J. Phys. Chem. B* **2006**, *110*, 18635–18640.

(925) Bravaya, K. B.; Bochenkova, A. V; Granovsky, A. A.; Savitsky, A. P.; Nemukhin, A. V. Modeling Photoabsorption of the AsFP595 Chromophore. *J. Phys. Chem. A* **2008**, *112*, 8804–8810.

(926) Luk, H. L.; Melaccio, F.; Rinaldi, S.; Gozem, S.; Olivucci, M. Molecular Bases for the Selection of the Chromophore of Animal Rhodopsins. *Proc. Natl. Acad. Sci.* **2015**, *112*, 15297–15302.

(927) Kandori, H.; Furutani, Y.; Nishimura, S.; Shichida, Y.; Chosrowjan, H.; Shibata, Y.; Mataga, N. Excited-State Dynamics of Rhodopsin Probed by Femtosecond Fluorescence Spectroscopy. *Chem. Phys. Lett.* **2001**, *334*, 271–276.

(928) Laricheva, E. N.; Gozem, S.; Rinaldi, S.; Melaccio, F.; Valentini, A.; Olivucci, M. Origin of Fluorescence in 11-Cis Locked Bovine Rhodopsin. *J. Chem. Theory Comput.* **2012**, *8*, 2559–2563.

(929) Polli, D.; Altoe, P.; Weingart, O.; Spillane, K. M.; Manzoni, C.; Brida, D.; Tomasello, G.; Orlandi, G.; Kukura, P.; Mathies, R. A.; et al. Conical Intersection Dynamics of the Primary Photoisomerization Event in Vision. *Nature* **2010**, *467*, 440–443.

(930) Devine, E. L.; Oprian, D. D.; Theobald, D. L. Relocating the Active-Site Lysine in Rhodopsin and Implications for Evolution of Retinylidene Proteins. *Proc. Natl. Acad. Sci.* **2013**, *110*, 13351–13355.

(931) Vivian, J. T.; Callis, P. R. Mechanisms of Tryptophan Fluorescence Shifts in Proteins. *Biophys. J.* **2001**, *80*, 2093–2109.

(932) Robinson, D.; Besley, N. A.; O'Shea, P.; Hirst, J. D. Calculating the Fluorescence of 5-Hydroxytryptophan in Proteins. *J. Phys. Chem. B* **2009**, *113*, 14521–14528.

(933) Wu, Q.; Huang, B.; Niehaus, T. A.; Yang, X.; Fan, J.; Zhang, R.-Q. The Role of Tryptophans in the UV-B Absorption of a UVR8 Photoreceptor - a Computational Study. *Phys. Chem. Chem. Phys.* **2015**, *17*, 10786–10794.

(934) Bernini, C.; Andruniów, T.; Olivucci, M.; Pogni, R.; Basosi, R.; Sinicropi, A. Effects of the Protein Environment on the Spectral Properties of Tryptophan Radicals in Pseudomonas Aeruginosa Azurin. *J. Am. Chem. Soc.* **2013**, *135*, 4822–4833.

(935) Li, X.; Chung, L. W.; Morokuma, K.; Li, G. Theoretical Study on the UVR8 Photoreceptor: Sensing Ultraviolet-B by Tryptophan and Dissociation of Homodimer. *J. Chem. Theory Comput.* **2014**, *10*, 3319–3330.

(936) Candian, A.; Mackie, C. J. Anharmonic Interstellar PAH Molecules. *Int. J. Quantum Chem.* **2017**, *117*, 146–150.

(937) Anthony, J. E. The Larger Acenes: Versatile Organic Semiconductors. *Angew. Chem., Int. Ed.* **2008**, *47*, 452–483.

(938) Smith, M. B.; Michl, J. Singlet Fission. *Chem. Rev.* **2010**, *110*, 6891–6936.

(939) Son, Y.-W.; Cohen, M. L.; Louie, S. G. Half-Metallic Graphene Nanoribbons. *Nature* **2006**,

444, 347–349.

(940) Morita, Y.; Nishida, S.; Murata, T.; Moriguchi, M.; Ueda, A.; Satoh, M.; Arifuku, K.; Sato, K.; Takui, T. Organic Tailored Batteries Materials Using Stable Open-Shell Molecules with Degenerate Frontier Orbitals. *Nat. Mater.* **2011**, *10*, 947–951.

(941) Hinkel, F.; Freudenberg, J.; Bunz, U. H. F. A Stable π-Conjugated Singlet Biradical. *Angew. Chemie Int. Ed.* **2016**, *55*, 9830–9832.

(942) Bendikov, M.; Duong, H. M.; Starkey, K.; Houk, K. N.; Carter, E. A.; Wudl, F. Oligoacenes: Theoretical Prediction of Open-Shell Singlet Diradical Ground States. *J. Am. Chem. Soc.* **2004**, *126*, 7416–7417.

(943) Hachmann, J.; Dorando, J. J.; Avilés, M.; Chan, G. K.-L. The Radical Character of the Acenes: A Density Matrix Renormalization Group Study. *J. Chem. Phys.* **2007**, *127*, 134309.

(944) Hajgató, B.; Szieberth, D.; Geerlings, P.; De Proft, F.; Deleuze, M. S. A Benchmark Theoretical Study of the Electronic Ground State and of the Singlet-Triplet Split of Benzene and Linear Acenes. *J. Chem. Phys.* **2009**, *131*, 224321.

(945) Gidofalvi, G.; Mazziotti, D. A. Active-Space Two-Electron Reduced-Density-Matrix Method: Complete Active-Space Calculations without Diagonalization of the N-Electron Hamiltonian. *J. Chem. Phys.* **2008**, *129*, 134108.

(946) Chakraborty, H.; Shukla, A. Pariser-Parr-Pople Model Based Investigation of Ground and Low-Lying Excited States of Long Acenes. *J. Phys. Chem. A* **2013**, *117*, 14220–14229.

(947) Horn, S.; Plasser, F.; Müller, T.; Libisch, F.; Burgdörfer, J.; Lischka, H. A Comparison of Singlet and Triplet States for One- and Two-Dimensional Graphene Nanoribbons Using

Multireference Theory. *Theor. Chem. Acc.* **2014**, *133*, 1511.

(948) Luzanov, A. V; Plasser, F.; Das, A.; Lischka, H. Evaluation of the Quasi Correlated Tight-Binding (QCTB) Model for Describing Polyradical Character in Polycyclic Hydrocarbons. *J. Chem. Phys.* **2017**, *146*, 064106.

(949) Yang, Y.; Davidson, E. R.; Yang, W. Nature of Ground and Electronic Excited States of Higher Acenes. *PNAS* **2016**, *113*, E5098–E5107.

(950) Lee, J.; Small, D. W.; Epifanovsky, E.; Head-Gordon, M. Coupled-Cluster Valence-Bond Singles and Doubles for Strongly Correlated Systems: Block-Tensor Based Implementation and Application to Oligoacenes. *J. Chem. Theory Comput.* **2017**, *13*, 602–615.

(951) Bettinger, H. F.; Tönshoff, C.; Doerr, M.; Sanchez-Garcia, E. Electronically Excited States of Higher Acenes up to Nonacene: A Density Functional Theory/Multireference Configuration Interaction Study. *J. Chem. Theory Comput.* **2016**, *12*, 305–312.

(952) Bettanin, F.; Ferrão, L. F. A.; Pinheiro, M.; Aquino, A. J. A.; Lischka, H.; Machado, F. B. C.; Nachtigallova, D. Singlet L_a and L_b Bands for N-Acenes (N = 2–7): A CASSCF/CASPT2 Study. *J. Chem. Theory Comput.* **2017**, *13*, 4297–4306.

(953) Korytár, R.; Xenioti, D.; Schmitteckert, P.; Alouani, M.; Evers, F. Signature of the Dirac Cone in the Properties of Linear Oligoacenes. *Nat. Commun.* **2014**, *5*, 5000.

(954) Horn, S.; Lischka, H. A Comparison of Neutral and Charged Species of One- and Two-Dimensional Models of Graphene Nanoribbons Using Multireference Theory. *J. Chem. Phys.* **2015**, *142*, 054302.

(955) Pelzer, K.; Greenman, L.; Gidofalvi, G.; Mazziotti, D. a. Strong Correlation in Acene Sheets from the Active-Space Variational Two-Electron Reduced Density Matrix Method: Effects

of Symmetry and Size. *J. Phys. Chem. A* **2011**, *115*, 5632–5640.

(956) Das, A.; Müller, T.; Plasser, F.; Lischka, H. Polyradical Character of Triangular Non-Kekulé Structures, Zethrenes, p-Quinodimethane-Linked Bisphenalenyl, and the Clar Goblet in Comparison: An Extended Multireference Study. *J. Phys. Chem. A* **2016**, *120*, 1625–1636.

(957) Melle-Franco, M. Uthrene, a Radically New Molecule? *Chem. Commun.* **2015**, *51*, 5387–5390.

(958) Yeh, C.-N.; Chai, J.-D. Role of Kekulé and Non-Kekulé Structures in the Radical Character of Alternant Polycyclic Aromatic Hydrocarbons: A TAO-DFT Study. *Sci. Rep.* **2016**, *6*, 30562.

(959) Flores, R.; Torres, A. E.; Fomine, S. Substituent Effect on the Spin State of the Graphene Nanoflakes. *RSC Adv.* **2016**, *6*, 64285–64296.

(960) Torres, A. E.; Fomine, S. Electronic Structure of Graphene Nanoribbons Doped with Nitrogen Atoms: A Theoretical Insight. *Phys. Chem. Chem. Phys.* **2015**, *17*, 10608–10614.

(961) Machado, F. B. C.; Aquino, A. J. A.; Lischka, H. The Diverse Manifold of Electronic States Generated by a Single Carbon Defect in a Graphene Sheet: Multireference Calculations Using a Pyrene Defect Model. *ChemPhysChem* **2014**, *15*, 3334–3341.

(962) Pinheiro, M.; Ferrão, L. F. A.; Bettanin, F.; Aquino, A. J. A.; Machado, F. B. C.; Lischka, H. How to Efficiently Tune the Biradicaloid Nature of Acenes by Chemical Doping with Boron and Nitrogen. *Phys. Chem. Chem. Phys.* **2017**, *19*, 19225–19233.

(963) Deshmukh, S. C.; Rana, S.; Shinde, S. V.; Dhara, B.; Ballav, N.; Talukdar, P. Selective Sensing of Metal Ions and Nitro Explosives by Efficient Switching of Excimer-to-Monomer

Emission of an Amphiphilic Pyrene Derivative. *ACS Omega* **2016**, *1*, 371–377.

(964) Häner, R.; Biner, S. M.; Langenegger, S. M.; Meng, T.; Malinovskii, V. L. A Highly Sensitive, Excimer-Controlled Molecular Beacon. *Angew. Chemie Int. Ed.* **2010**, *49*, 1227–1230.

(965) Inagaki, S.; Ohtani, O.; Goto, Y.; Okamoto, K.; Ikai, M.; Yamanaka, K.; Tani, T.; Okada, T. Light Harvesting by a Periodic Mesoporous Organosilica Chromophore. *Angew. Chemie Int. Ed.* **2009**, *48*, 4042–4046.

(966) Shirai, S.; Iwata, S.; Tani, T.; Inagaki, S. Ab Initio Studies of Aromatic Excimers Using Multiconfiguration Quasi-Degenerate Perturbation Theory. *J. Phys. Chem. A* **2011**, *115*, 7687–7699.

(967) Förster, T.; Kasper, K. Ein Konzentrationsumschlag der Fluoreszenz des Pyrens. *Z. Elektrochem.* **1955**, *59*, 976–980.

(968) Figueira-Duarte, T. M.; Müllen, K. Pyrene-Based Materials for Organic Electronics. *Chem. Rev.* **2011**, *111*, 7260–7314.

(969) Förster, T. Elektronenspektren gekoppelter Moleküle. *Pure Appl. Chem.* **1962**, *4*, 121–134.

(970) Stevens, B. Evidence for the Photo-Association of Aromatic Hydrocarbons in Fluid Media. *Nature* **1961**, *192*, 725–727.

(971) Scholes, G. D.; Ghiggino, K. P. Electronic Interactions and Interchromophore Excitation Transfer. *J. Phys. Chem.* **1994**, *98*, 4580–4590.

(972) East, A. L. L.; Lim, E. C. Naphthalene Dimer: Electronic States, Excimers, and Triplet Decay. *J. Chem. Phys.* **2000**, *113*, 8981–8994.

(973) Montero-Alejo, A. L.; Fuentes, M. E.; Montero, L. A.; de la Vega, J. M. G. Coulomb and Exchange Contributions to Electronic Excitations of Benzene Aggregates. *Chem. Phys. Lett.* **2011**, *502*, 271–276.

(974) Huenerbein, R.; Grimme, S. Time-Dependent Density Functional Study of Excimers and Exciplexes of Organic Molecules. *Chem. Phys.* **2008**, *343*, 362–371.

(975) Amicangelo, J. C. Theoretical Study of the Benzene Excimer Using Time-Dependent Density Functional Theory. *J. Phys. Chem. A* **2005**, *109*, 9174–9182.

(976) García-Fernández, P.; Andjelković, L.; Zlatar, M.; Gruden-Pavlović, M.; Dreuw, A. A Simple Monomer-Based Model-Hamiltonian Approach to Combine Excitonic Coupling and Jahn-Teller Theory. *J. Chem. Phys.* **2013**, *139*, 174101.

(977) Dubinets, N. O.; Safonov, A. A.; Bagaturyants, A. A. Structures and Binding Energies of the Naphthalene Dimer in Its Ground and Excited States. *J. Phys. Chem. A* **2016**, *120*, 2779–2782.

(978) Velardez, G. F.; Lemke, H. T.; Breiby, D. W.; Nielsen, M. M.; Møller, K. B.; Henriksen, N. E. Theoretical Investigation of Perylene Dimers and Excimers and Their Signatures in X-Ray Diffraction. *J. Phys. Chem. A* **2008**, *112*, 8179–8187.

(979) Casanova, D. Theoretical Investigations of the Perylene Electronic Structure: Monomer, Dimers, and Excimers. *Int. J. Quantum Chem.* **2015**, *115*, 442–452.

(980) Sadygov, R. G.; Lim, E. C. A Theoretical Study of the Structure and Energetics of Stacked Dimers of Polycyclic Aromatic Hydrocarbons. Application of INDO 1/S Method to Singlet Excimers of Naphthalene and Phenanthrene. *Chem. Phys. Lett.* **1994**, *225*, 441–447.

(981) Kołaski, M.; Arunkumar, C. R.; Kim, K. S. Aromatic Excimers: Ab Initio and TD-DFT

Study. *J. Chem. Theory Comput.* **2013**, *9*, 847–856.

(982) Kuhlman, T. S.; Lemke, H. T.; Sølling, T. I.; Velardez, G. F.; Henriksen, N. E.; Møller, K. B. Comment on "Theoretical Investigation of Perylene Dimers and Excimers and Their Signatures in X-Ray Diffraction." *J. Phys. Chem. A* **2009**, *113*, 6849–6850.

(983) Hoche, J.; Schmitt, H.-C.; Humeniuk, A.; Fischer, I.; Mitric, R.; Rohr, M. I. S. The Mechanism of Excimer Formation: An Experimental and Theoretical Study on the Pyrene Dimer. *Phys. Chem. Chem. Phys.* **2017**, *19*, 25002–25015.

(984) Rocha-Rinza, T.; Christiansen, O. Linear Response Coupled Cluster Study of the Benzene Excimer. *Chem. Phys. Lett.* **2009**, *482*, 44–49.

(985) Balmer, F. A.; Trachsel, M. A.; van der Avoird, A.; Leutwyler, S. The Elusive S_2 State, the S_1/S_2 Splitting, and the Excimer States of the Benzene Dimer. *J. Chem. Phys.* **2015**, *142*, 234306.

(986) Diri, K.; Krylov, A. I. Electronic States of the Benzene Dimer: A Simple Case of Complexity. *J. Phys. Chem. A* **2012**, *116*, 653–662.

(987) Rocha-Rinza, T.; De Vico, L.; Veryazov, V.; Roos, B. O. A Theoretical Study of Singlet Low-Energy Excited States of the Benzene Dimer. *Chem. Phys. Lett.* **2006**, *426*, 268–272.

(988) Jara-Cortés, J.; Rocha-Rinza, T.; Hernández-Trujillo, J. Electron Density Analysis of Aromatic Complexes in Excited Electronic States: The Benzene and Naphthalene Excimers. *Comput. Theor. Chem.* **2015**, *1053*, 220–228.

(989) de Sainte Claire, P. Molecular Simulation of Excimer Fluorescence in Polystyrene and Poly(Vinylcarbazole). *J. Phys. Chem. B* **2006**, *110*, 7334–7343.

(990) Hirayama, F.; Lipsky, S. Excimer Fluorescence of Benzene and Its Alkyl Derivatives—

Concentration and Temperature Dependence. *J. Chem. Phys.* **1969**, *51*, 1939–1951.

(991) Cundall, R. B.; Robinson, D. A. Primary Photophysical Processes in Benzene. Part 2.—Monomer Studies. *J. Chem. Soc., Faraday Trans. 2* **1972**, *68*, 1145–1151.

(992) Fink, R. F.; Pfister, J.; Zhao, H. M.; Engels, B. Assessment of Quantum Chemical Methods and Basis Sets for Excitation Energy Transfer. *Chem. Phys.* **2008**, *346*, 275–285.

(993) Shirai, S.; Iwata, S.; Maegawa, Y.; Tani, T.; Inagaki, S. Ab Initio Molecular Orbital Study on the Excited States of [2.2]-, [3.3]-, and Siloxane-Bridged Paracyclophanes. *J. Phys. Chem. A* **2012**, *116*, 10194–10202.

(994) Bader, R. F. W. *Atoms in Molecules. A Quantum Theory*; Oxford University Press: New York, 1994.

(995) Zimmerman, P. M.; Zhang, Z.; Musgrave, C. B. Singlet Fission in Pentacene through Multi-Exciton Quantum States. *Nat. Chem.* **2010**, *2*, 648–652.

(996) Casanova, D.; Slipchenko, L. V; Krylov, A. I.; Head-Gordon, M. Double Spin-Flip Approach within Equation-of-Motion Coupled Cluster and Configuration Interaction Formalisms: Theory, Implementation, and Examples. *J. Chem. Phys.* **2009**, *130*, 44103.

(997) Casanova, D.; Head-Gordon, M. Restricted Active Space Spin-Flip Configuration Interaction Approach: Theory, Implementation and Examples. *Phys. Chem. Chem. Phys.* **2009**, *11*, 9779–9790.

(998) Zimmerman, P. M.; Bell, F.; Casanova, D.; Head-Gordon, M. Mechanism for Singlet Fission in Pentacene and Tetracene: From Single Exciton to Two Triplets. *J. Am. Chem. Soc.* **2011**, *133*, 19944–19952.

(999) Petelenz, P.; Pac, B. Is Dipole Moment a Valid Descriptor of Excited State's Charge-

Transfer Character? *J. Am. Chem. Soc.* **2013**, *135*, 17379–17386.

(1000) Zeng, T.; Hoffmann, R.; Ananth, N. The Low-Lying Electronic States of Pentacene and Their Roles in Singlet Fission. *J. Am. Chem. Soc.* **2014**, *136*, 5755–5764.

(1001) Smith, M. B.; Michl, J. Recent Advances in Singlet Fission. *Annu. Rev. Phys. Chem.* **2013**, *64*, 361–386.

(1002) Chan, W.-L.; Ligges, M.; Jailaubekov, A.; Kaake, L.; Miaja-Avila, L.; Zhu, X.-Y. Observing the Multiexciton State in Singlet Fission and Ensuing Ultrafast Multielectron Transfer. *Science* **2011**, *334*, 1541–1545.

(1003) Meunier, B.; Visser, S. P. de; Shaik, S. Mechanism of Oxidation Reactions Catalyzed by Cytochrome P450 Enzymes. *Chem. Rev.* **2004**, *104*, 3947–3980.

(1004) Shaik, S.; Chen, H. Lessons on O_2 and NO Bonding to Heme from Ab Initio Multireference/Multiconfiguration and DFT Calculations. *JBIC J. Biol. Inorg. Chem.* **2011**, *16*, 841–855.

(1005) de Visser, S.; Stillman, M. Challenging Density Functional Theory Calculations with Hemes and Porphyrins. *Int. J. Mol. Sci.* **2016**, *17*, 519.

(1006) Ali, M. E.; Sanyal, B.; Oppeneer, P. M. Electronic Structure, Spin-States, and Spin-Crossover Reaction of Heme-Related Fe-Porphyrins: A Theoretical Perspective. *J. Phys. Chem. B* **2012**, *116*, 5849–5859.

(1007) Kepenekian, M.; Calborean, A.; Vetere, V.; Le Guennic, B.; Robert, V.; Maldivi, P. Toward Reliable DFT Investigations of Mn-Porphyrins through CASPT2/DFT Comparison. *J. Chem. Theory Comput.* **2011**, *7*, 3532–3539.

(1008) Pierloot, K.; Zhao, H.; Vancoillie, S. Copper Corroles: The Question of Noninnocence.

Inorg. Chem. **2010**, *49*, 10316–10329.

(1009) Vancoillie, S.; Zhao, H.; Radoń, M.; Pierloot, K. Performance of CASPT2 and DFT for Relative Spin-State Energetics of Heme Models. *J. Chem. Theory Comput.* **2010**, *6*, 576–582.

(1010) Roos, B. O.; Veryazov, V.; Conradie, J.; Taylor, P. R.; Ghosh, A. Not Innocent: Verdict from Ab Initio Multiconfigurational Second-Order Perturbation Theory on the Electronic Structure of Chloroiron Corrole. *J. Phys. Chem. B* **2008**, *112*, 14099–14102.

(1011) Ben Amor, N.; Soupart, A.; Heitz, M.-C. Methodological CASPT2 Study of the Valence Excited States of an Iron-Porphyrin Complex. *J. Mol. Model.* **2017**, *23*, 53.

(1012) Kerridge, A. A RASSCF Study of Free Base, Magnesium and Zinc Porphyrins: Accuracy versus Efficiency. *Phys. Chem. Chem. Phys.* **2013**, *15*, 2197.

(1013) Kitagawa, Y.; Chen, Y.; Nakatani, N.; Nakayama, A.; Hasegawa, J. A DFT and Multi-Configurational Perturbation Theory Study on O_2 Binding to a Model Heme Compound via the Spin-Change Barrier. *Phys. Chem. Chem. Phys.* **2016**, *18*, 18137–18144.

(1014) Vancoillie, S.; Zhao, H.; Tran, V. T.; Hendrickx, M. F. A.; Pierloot, K. Multiconfigurational Second-Order Perturbation Theory Restricted Active Space (RASPT2) Studies on Mononuclear First-Row Transition-Metal Systems. *J. Chem. Theory Comput.* **2011**, *7*, 3961–3977.

(1015) Vlaisavljevich, B.; Shiozaki, T. Nuclear Energy Gradients for Internally Contracted Complete Active Space Second-Order Perturbation Theory: Multistate Extensions. *J. Chem. Theory Comput.* **2016**, *12*, 3781–3787.

(1016) Chalupský, J.; Rokob, T. A.; Kurashige, Y.; Yanai, T.; Solomon, E. I.; Rulíšek, L.; Srnec,

M. Reactivity of the Binuclear Non-Heme Iron Active Site of Δ^9 Desaturase Studied by Large-Scale Multireference Ab Initio Calculations. *J. Am. Chem. Soc.* **2014**, *136*, 15977–15991.

(1017) Phung, Q. M.; Wouters, S.; Pierloot, K. Cumulant Approximated Second-Order Perturbation Theory Based on the Density Matrix Renormalization Group for Transition Metal Complexes: A Benchmark Study. *J. Chem. Theory Comput.* **2016**, *12*, 4352–4361.

(1018) Stein, C. J.; Reiher, M. Automated Selection of Active Orbital Spaces. *J. Chem. Theory Comput.* **2016**, *12*, 1760–1771.

AUTHOR INFORMATION

Corresponding Author

*Email: hans.lischka@univie.ac.at

Notes

The authors declare no competing financial interest.

Biographies

Hans Lischka received his Ph.D. degree at the University of Vienna in 1969. In the years 1972–73 he worked as a postdoctoral researcher with Professor Kutzelnigg at the University of Karlsruhe. After finishing his habilitation in 1976 he became Professor of Theoretical Chemistry at the University of Vienna in 1980. In the same year, during his stay as Visiting Professor at the Ohio State University the development of the COLUMBUS program system was started in cooperation with Professor Shavitt and Dr Ron Shepard. After the retirement at the University of Vienna in 2008 he spent two years in the time from 2008 - 2010 as visiting professor at the Institute of Organic Chemistry of the Czech Academy of Sciences, Prague, Czech Republic. From 2011 – 2015 he was Research Professor at the Texas Tech University, Texas, USA and became since 2011 professor at the Tianjin University, P. R. China and Adjunct Professor at the Department of Chemistry and Biochemistry of the Texas Tech University, Texas, USA. Research interests focus on multireference calculations of polyradicaloid character in polycyclic aromatic hydrocarbons, on program developments in the program system COLUMBUS and on simulations of nonadiabatic photodynamical processes.

Dana Nachtigallová was born and raised in the Czech Republic. In 1995 she earned her Ph.D. at the University of Pittsburgh, Pittsburgh, United States working in the group of Kenneth D. Jordan on theoretical modelling of the excited states. From 1995 to 1997 she was a postdoc fellow at J. Heyrovský institute of Physical Chemistry of the CAS in Prague working under supervision of Rudolf Zahradník, and from 1997 to 2003 she was working as a researcher at the same Institute. In 2004 she moved to the Institute of Chemistry and Biochemistry of the CAS in Prague, where she is working as a senior researcher in the group of Pavel Hobza. Her current research interests focus on simulations of nonadiabatic photodynamical processes, modeling of non-covalent interactions of the excited state associates and on multireference calculations of the excited states of polycyclic aromatic hydrocarbons.

Adelia Aquino was born and educated in Brazil and received her Ph.D. from the University of São Paulo, São Paulo, Brazil in 1991. From 1994 to 1997 she was a postdoc fellow at the University of California, San Diego, and San Diego Super Computer Center. From 1999 to 2013 she joined the Institute of Theoretical Chemistry, University of Vienna as a senior scientist with the research concentrated in modeling soil interactions with different compounds and environments. From 2011 to 2015 she was a research professor at the Department of Chemistry and Biochemistry, Texas Tech University (TTU). In TTU she cooperated with several colleagues in the Department of Chemistry and Biochemistry and other departments in which she contributed with electronic structure and dynamics calculations. Presently, she is a professor at the School of Pharmaceutical Science and Technology, Tianjin University, Tianjin, China where she received the Thousand Talents award. At the moment her research focuses on the following topics: i) reactions and interaction on Al_2O_3 and MnO_2 mineral surfaces; ii) water molecular bridges in humic substances; ii) electronic spectra, charge transfer in natural pigments; iv) charge transfer in organic photovoltaic systems.

Péter G. Szalay was born in Szentes, Hungary, in 1962. He received his M.Sc. degree in 1986 at ELTE Eötvös Loránd University in Budapest under the supervision of Prof. Fogarasi and in 1989 his Ph.D. at the University of Vienna under the supervision of Prof. Lischka. The latter work consisted of MR-CI calculations on the ground and excited states of conjugated molecules. At the same time, he joined the COLUMBUS community and worked on improvements of the MR-CI code, including the first analytic derivative code for this type of wavefunction. Between 1991 and 1993 he was postdoc at the University of Florida with Prof. Bartlett, where he worked on the development of coupled-cluster methods, including the MR-AQCC method. His research, besides method development, concentrates on excited states and corresponding spectroscopy. Prof. Szalay published more than 100 papers, and he is the co-author and co-editor of several books. These publications resulted in almost 5000 independent citations. Currently, he is a professor of chemistry at ELTE and Vice-Rector for Research. In 2017, together with G. Fogarasi and A.G. Császár, he has been awarded the Széchenyi Prize, the most prestigious scholarly award in Hungary.

Felix Plasser was born and raised in Vienna, Austria. In 2012 he earned his Ph.D. at the University of Vienna working in the group of Hans Lischka on the photophysics of interacting nucleobases. In 2013 he moved to Heidelberg to spend two years at Ruprecht-Karls University in the group of Andreas Dreuw to study phosphorescent iridium complexes. He returned to Vienna in 2015 to join the group of Leticia González. In February 2018, he started as a Lecturer at the University of Loughborough, UK. Felix Plasser has worked on a wide range of topics in computational photochemistry regarding questions of biological and technological interest. His expertise lies in high-level electronic structure computations combined with detailed wavefunction analysis protocols and dynamics simulations. He has designed and developed the excited-state wavefunction analysis package TheoDORE. Furthermore, he has made significant contributions to the electronic structure packages COLUMBUS, Q-Chem, and MOLCAS as well as the nonadiabatic dynamics packages Newton-X and SHARC. To this date, he has published 47 peer-reviewed articles.

Francisco B. C. Machado was born and raised in Brazil. In 1990 he earned his Ph.D. at the University of Sao Paulo, Sao Paulo, Brazil working in the group of Fernando R. Ornellas studying electronic and rovibrational spectra in diatomic molecules using MRCI methodology. From 1991 to 1993, he was a postdoc fellow at the Indiana University, USA, working under the supervision of Ernest Davidson. After finishing his master degree at the University of Sao Paulo, in 1986 he became an associate researcher at the Instituto de Estudos Avancados, Sao Jose dos Campos, Brazil. In 1995 he moved to Instituto Tecnologico de Aeronautica, Sao Jose dos Campos, Brazil where he is working as a senior researcher. Recently, from 2013-2014, he finished one year as a visiting researcher at Texas Tech University working with Hans Lischka. He has been working on the computational theoretical chemistry, mostly using MRCI to characterize excited states of molecules. Also, his research focuses on chemical reaction, clusters, and electronic properties of polycyclic aromatic hydrocarbons (PAHs). To this date, he has published 100 peer-reviewed articles. Also, he is a level II CNPq researcher in Brazil.

Mario Barbatti was born and raised in Brazil. In 2001, he earned a Ph.D. in physics at the Federal University of Rio de Janeiro. In 2004, he moved to Vienna, where he was a postdoctoral fellow in the group of Hans Lischka. In 2008, he earned a Habilitation to teach theoretical chemistry from the University of Vienna. In 2010, he became an independent group leader at the Max Planck Institut für Kohlenforschung in Mülheim an der Ruhr, Germany. Since 2015, he is a professor of the chair of excellence AMIDEX at the University of Aix-Marseille, in Marseille, France. For over fifteen years, Mario Barbatti has been working on the computational theoretical chemistry of molecular excited states. He is the designer and one of the main developers of the Newton-X program package for nonadiabatic dynamics, whose first release completed ten years in 2017. To this date, he has published more than 120 articles. Among his main scientific contributions are the first complete mapping of the deactivation pathways of UV-excited nucleobases using ab initio dynamics, the discovery of a new internal-conversion mechanism through electron transfer between solvent and chromophore, and the determination of the photochemical mechanism of a key prebiotic reaction.

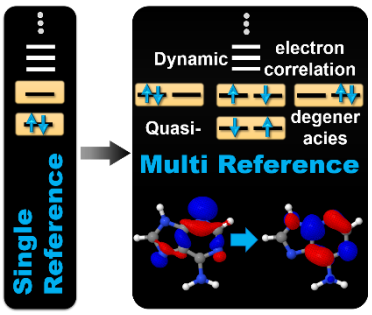

Table of Contents Graph